A CONTACT ELEMENT APPROACH WITH HYSTERESIS DAMPING FOR THE
ANALYSIS AND DESIGN OF POUNDING IN BRIDGES

A Thesis
Presented to
The Academic Faculty

By

Susendar Muthukumar

In Partial Fulfillment
of the Requirements for the Degree
Doctor of Philosophy in
Civil and Environmental Engineering

Georgia Institute of Technology
November 2003

A CONTACT ELEMENT APPROACH WITH HYSTERESIS DAMPING FOR THE ANALYSIS AND DESIGN OF POUNDING IN BRIDGES

Approved by:

Reginald DesRoches, CEE, Chairman

Barry J. Goodno, CEE

Laurence J. Jacobs, CEE

Donald W. White, CEE

Jeffrey L. Streator, ME

Date Approved 11/14/03

To the memory of my grandmother, Malligeswari

ACKNOWLEDGEMENT

TABLE OF CONTENTS

LIST OF TABLES

LIST OF FIGURES

inelastic truss-link model

NOMENCLATURE

a Yield parameter for simplified contact models

A Area of crossection

c_i Damping coefficient of system "i"

c_k Damping coefficient for the Kelvin model

d_d Residual strength reduction displacement in pivot model

d_f Failure displacements

d_t Strength degradation displacement in pivot model

D_t Time step of record

e Coefficient of restitution

E Young's modulus

ΔE Energy loss during impact

F_{Ai} Force in abutment "i"

F_{Bi} Force in bearing "i"

F_d Residual strength in pivot model

F_{Fi} Restoring force from frame "i"

$\tilde{F}_{F_i}$ Normalized frame force-deformation relation

F_{Ii} Impact force due to pounding

F_{Ri} Force in restrainer "i"

F_y Yield strength of system

G Shear modulus of elastomer

g_p Hinge gap

h Time step used in the Runge-Kutta solution algorithm

I	Moment of inertia of cross section
k_h	Impact stiffness of Hertz model
k_k	Impact stiffness in the Kelvin model
k_l	Impact stiffness of linear spring element
K_i	Stiffness of frame "i"
K_L	Stiffness of elastic link in higher order element
K_{mod}	Modified frame stiffness
K_p	Reloading stiffness for Q-Hyst model
K_q	Unloading stiffness for Q-Hyst model
K_r	Restrainer stiffness
K_T	Initial stiffness of truss in higher order element
K_{tl}	Initial stiffness of truss contact element
K_{t2}	Strain hardening stiffness of truss contact element
K_{TH}	Strain hardening stiffness of truss in higher order element
L	Length of bridge deck
m_i	Mass of frame "i"
n	Hertz coefficient
P_i	Primary pivot point
PP_i	Pinching pivot point
R_y	Response modification or strength reduction factor
s	Restrainer slack
T_d	Frame design period
T_g	Characteristic period of earthquake ground motion

T_i Individual frame period (elastic)

u_i Displacement of frame "i" relative to the ground

$\dot{u}_i$ Velocity of frame "i" relative to the ground

$\ddot{u}_i$ Acceleration of frame "i" relative to the ground

$\ddot{u}_g$ Horizontal ground motion input

$\tilde{\ddot{u}}_g$ Normalized ground acceleration

v_i velocity of colliding body "i" before impact

v_i' velocity of colliding body "i" after impact

Greek Symbols

α Pivot parameter

β Pinching pivot parameter

γ Displacement amplification ratio

γ^* Strain hardening ratio

δ Local deformation at contact surface

δ_m Maximum penetration during impact

δ_y Yield deformation of truss contact element

$\dot{\delta}$ Penetration velocity

ζ Damping coefficient for nonlinear hysteresis damper

η_i Frame strength ratio

$\tilde{\eta}$ Ratio of frame strength ratios (η_1/η_2)

κ Restrainer stiffness ratio (K_r/K_{mod})

λ	Frame mass ratio (m_1/m_2)
μ	Ductility ratio
ξ_i	Damping ratio of system "i"
χ	Gap ratio parameter
ω_i	Natural frequency of frame "i"
Φ	Component of ground motion record
Ω	Frequency ratio (ω_2/ω_1)

Acronyms

Caltrans	California Department of Transportation
AASHTO	American Association of State Highway and Transportation Officials
DOF	Degree of Freedom
SDOF	Single Degree of Freedom
PGA	Peak Ground Acceleration
COV	Coefficient of Variation
Hertzdamp	Hertz model with nonlinear hysteresis damper
EPD	Epicentral Distance
PGV	Peak Ground Velocity
PGD	Peak Ground Displacement

SUMMARY

Earthquake ground motion can induce out-of-phase vibrations between adjacent structures due to differences in dynamic characteristics, which can result in impact or pounding of the structures if the at-rest separation is insufficient to accommodate the relative displacements. In bridges, seismic pounding between adjacent decks or between deck and abutment can result in localized deck damage, bearing failure, damage to shear keys and abutments, and even contribute to the collapse of bridge spans.

This study investigates pounding in bridges from an analytical perspective. A simplified nonlinear model of a multiple-frame bridge is developed in MATLAB incorporating the effects of inelastic frame action, nonlinear hinge behavior and abutments. The equations of motion of the bridge response to longitudinal ground excitation are assembled and solved using the fourth-order Runge-Kutta method. Pounding is simulated using contact force-based models such as the linear spring, Kelvin and Hertz models, as well as the momentum-based stereomechanical method. In addition, a Hertz contact model with nonlinear damping (Hertzdamp model) is also introduced to model impact.

The primary factors controlling the pounding response are identified as the frame period ratio, ground motion effective period ratio, restrainer stiffness ratio and frame ductility ratio. Pounding is most critical for highly out-of-phase frames. Impact models without energy dissipation overestimate the stiff system displacements by 15%-25% for highly out-of-phase, elastic systems experiencing moderate to strong ground excitation. The Hertzdamp model is found to be the most effective in representing impact.

Traditional column hysteresis models such as the elasto-plastic and bilinear models underestimate the stiff system amplification and overestimate the flexible system amplification due to impact, when compared with stiffness and strength degrading models. Strength degradation and pounding are critical on the stiff system response to near field ground motions, for highly out-of-phase systems. Current design procedures are adequate in capturing the nonlinear hinge response when the bridge columns are elastic, but require revisions such as the introduction of time dependent reduction factors, and a frame design period to work for inelastic situations. Finally, a bilinear truss element with a gap is proposed for implementing energy dissipating impact models in commercial structural software.

CHAPTER 1

INTRODUCTION

1.1 Problem Description

Bridges are the lifeline of a highway transportation network and past earthquakes have illustrated that they are vulnerable to severe damage and/or collapse during moderate to strong ground motion. Among the possible structural damages, seismic-induced pounding has been commonly observed in several earthquakes. Seismic pounding is the impact between bridge decks, between deck and abutment in the longitudinal direction, or transverse collision between two closely spaced superstructures during an earthquake. Impact occurs when the relative displacement between adjacent decks or deck and abutment exceeds the gap between them. Pounding is a result of out-of-phase motion between adjacent components in a bridge having different dynamic characteristics.

The multiple-frame bridge and the multi-span simply supported bridge are most susceptible to pounding damage due to numerous independent components and lack of continuity in the structure. In a multiple-frame bridge, the interaction between adjacent frames can result in pounding at the intermediate hinge locations or at the abutments. Pounding of girder ends at the pier locations and end abutments can occur in a multi-span simply supported bridge.

The 1994 Northridge earthquake revealed substantial impact damage at the expansion hinges and abutments of standing portions of the connectors at the Interstate 5/State Road 14 interchange which were located at close proximity to the epicenter (EERI, 1995a).

Reconnaissance reports from the 1995 Kobe earthquake identify pounding as a major cause of fracture of the bearing supports and potential contributor to the collapse of the bridge decks (EERI, 1995b). Hammering at the expansion joints in some bridges resulted in damage to shear keys, bearings and anchor bolts during the 1999 Chi-Chi earthquake in Taiwan (EERI 2001a). Cracking and spalling at expansion joints of concrete bridges were observed during the 2001 Nisqually, Washington earthquake (EERI 2001b). More recently, pounding of adjacent simply supported spans resulting in failure of girder ends and bearing damage was observed during the 2001 Bhuj earthquake in Gujarat, India (EERI 2002).

Seismic pounding is known to cause localized deck damage, bearing failure, damage to shear keys and abutments, and even contribute to the collapse of bridge spans. Current design specifications may not adequately account for the large forces generated during bridge deck impact. This study investigates the pounding phenomenon in bridges from an analytical perspective by identifying the bridge parameters controlling impact, determines effective ways to model impact and evaluates the adequacy of code specifications in representing the distribution of forces and deformations due to bridge deck impact.

1.2 Objectives and Scope of Research

The goal of this study is to determine the effect of pounding on the global response of bridges through the development of various analytical models. The multiple frame bridge is considered as the representative bridge structure and a simplified analytical model is developed in MATLAB including the effects of inelastic frame action, nonlinear hinge behavior and abutment action. Pounding is simulated using various impact models. Soil-

structure interaction, non-uniform support motion and traveling wave effects are not investigated in this study. Effects of vertical ground motion and torsion due to curvilinear bridge geometry are not examined.

The specific objectives of this research are:

- Investigate the critical factors affecting the longitudinal pounding response.

- Explore the pounding response of the bridge using several existing impact models.

- Evaluate the performance of a Hertz contact model with nonlinear damping (typically used in robotics) in predicting deck impact.

- Determine the effect of column hysteretic behavior on the pounding response of the bridge.

- Determine the efficacy of code specifications in accounting for pounding.

- Develop a simplified contact model for impact simulation and use in bridge analysis programs.

1.3 Outline of Dissertation

This dissertation is organized into 9 chapters with the following contents:

Chapter 2 presents an overview of seismic pounding. Various analytical models used to simulate impact are presented. The capability of current design specifications in representing bridge deck impact is discussed. Past research on seismic pounding is also summarized.

The development of a numerical, analytical model of a multiple-frame bridge in MATLAB, including the effects of column behavior, restrainers, bearings, abutments and

pounding is presented in Chapter 3. The model is verified by benchmarking the results against those from DRAIN-2DX wherever possible.

Chapter 4 investigates the critical factors affecting the pounding response of bridges. Results from parameter studies on effects of frame period ratio, frame yielding, restrainers, and ground motion characteristics on the pounding response are presented.

The limitations of existing impact models are discussed and a Hertz contact model with hysteresis damping for pounding simulation is introduced in Chapter 5. A parameter study comparing the model response with existing impact models is performed for a suite of ground motions.

Chapter 6 investigates the effect of frame restoring force characteristics on the pounding response of the bridge. Several hysteretic models are considered for the bridge columns including the bilinear, Q-Hyst (stiffness degrading) and pivot hysteresis (strength degrading) models. The effect of near field ground motions is examined through a case study.

Chapter 7 evaluates the adequacy of current design procedures in representing the distribution of forces and deformations due to bridge deck impact. Deficiencies in the current guidelines are identified and recommendations suggested.

Simplified contact models for simulating pounding in bridges are proposed in Chapter 8. Gap elements with piecewise linear springs that can account for energy loss during impact are presented. The contact models are verified by comparing their response with those from the Hertz contact model with nonlinear damping.

The findings from the study are summarized and areas of future research suggested in Chapter 9.

CHAPTER 2

OVERVIEW OF SEISMIC POUNDING

The advent of an earthquake can induce out-of-phase vibrations in adjacent structures due to differences in dynamic characteristics, which can result in impact if the at-rest separation is insufficient to accommodate the relative displacements. This impact, commonly referred to as seismic pounding, generates high magnitude and short duration acceleration pulses that can cause structural damage. Furthermore, seismic pounding can amplify the global response of the participating structural systems. The highly congested building system in many metropolitan cities constitutes a major concern for seismic pounding damage. In the case of bridge structures, impact can occur between bridge decks or between deck and abutment in the longitudinal direction. There is also a possibility of transverse impact between narrowly separated bridge superstructures.

2.1 Observed pounding damage in past earthquakes

Earthquakes during the past four decades have illustrated several instances of pounding damage in both building and bridge structures. During the 1964 Great Alaskan earthquake, parts of the Anchorage Westward hotel were damaged due to pounding with the adjoining three-storey ballroom (National Academy of Sciences, 1964). Severe structural damage was observed due to impact between the outside towers and the main building of the Olive View Hospital, during the 1971 San Fernando earthquake (Mahin et al., 1976). Impact between bridge deck and abutments caused extensive damage to highway bridges with seat type abutments, during the same earthquake (Jennings, 1971).

After the 1985 Mexico City earthquake, pounding damage was reported in over 40% of the collapsed or severely damaged buildings. In at least 15% of the damaged buildings, pounding was the primary cause of collapse (Bertero, 1987).

During the 1989 Loma Prieta earthquake, pounding of adjacent unreinforced masonry (URM) buildings resulted in shear failure of the brickwork leading to partial collapse of the wall. Cases of veneer spalling were also reported from buildings in downtown San Francisco (EERI, 1990). Pounding of the lower roadway and columns supporting the upper deck of the Southern viaduct section at the China Basin, California occurred due to the height differences between the neighboring bridge members (Priestly et al., 1996). After the 1994 Northridge earthquake, significant pounding damage was observed at the expansion hinges and abutments of standing portions of the connectors at the I-5/SR-14 interchange which were located at close proximity to the epicenter (EERI, 1995a). Pounding at expansion hinges of the San Fernando-Simi Valley Freeway (SR118) and the Santa Clara River Bridge was also observed during the same earthquake.

Reconnaissance reports from the 1995 Kobe earthquake identify pounding as a major cause of fracture of the bearing supports and potential contributor to the collapse of several bridge decks (EERI, 1995b). Impact between a six-story building and two-story building in Golcuk, Turkey during the 1999 Kocaeli earthquake contributed to column failure above the third floor slab in the taller building and shear failure of two second-floor piers in the smaller building (EERI, 2000). In other cases, columns were lost completely due to impact with adjacent buildings. Pounding of abutments and deck joints were also observed in several of the highway bridges during the same earthquake. The

1999 Chi-Chi earthquake in Taiwan revealed hammering at the expansion joints in some bridges which resulted in damage to shear keys, bearings and anchor bolts (EERI, 2001a).

Masonry wall damage in buildings and concrete spalling damage at the expansion joints of concrete bridges were reported after the 2001 Nisqually, Washington earthquake (EERI 2001b). Pounding of adjacent simply supported spans was observed in the Old Surajbadi highway bridge, India Bridge and several other bridges on National Highway 8A during the 2001 Bhuj (Gujarat, India) earthquake (EERI, 2002). Structural damage included the failure of girder ends, superstructure dislocation and bearing damage.

Based on the observations from past earthquakes, closely spaced buildings can experience infill wall damage, column shear failure and possible column collapse due to pounding. Pounding in bridges can lead to local crushing and spalling of concrete, damage to column bents, abutments, shear keys, bearing pads and restrainers and possible deck collapse. Figures 2.1 and 2.2 illustrate some instances of pounding damage, ranging from the superficial to complete collapse.
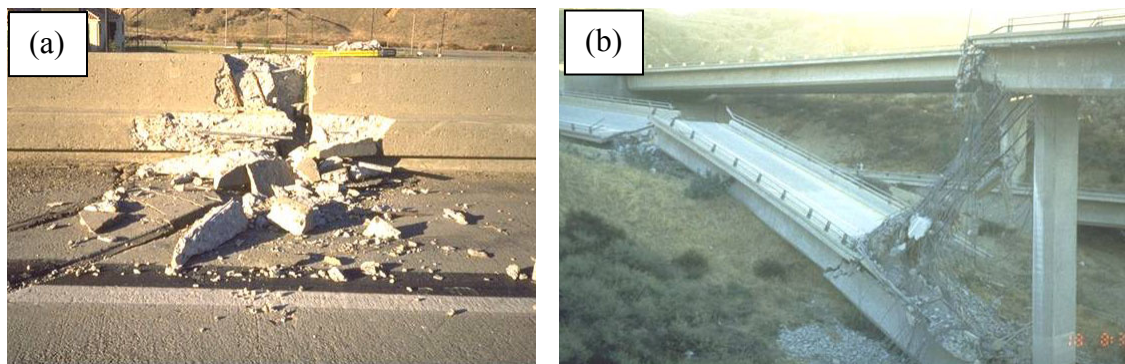
Figure 2.1: Pounding damage in bridges: (a) barrier rail damage during the 1994 Northridge earthquake; (b) connector collapse during the 1994 Northridge earthquake.
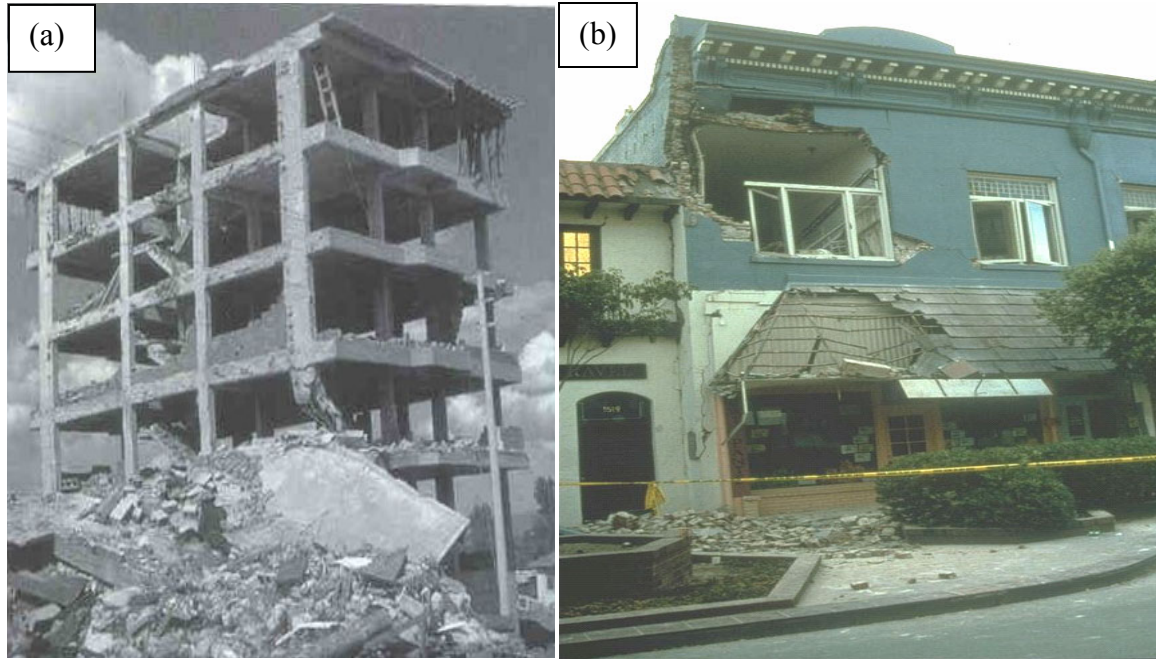
Figure 2.2: Pounding damage in buildings: (a) loss of column from impact during the 1999 Kocaeli earthquake; (b) wall collapse during the 1989 Loma Prieta earthquake.

2.2 Analytical models for impact

Pounding is a highly nonlinear phenomenon, which leads to several uncertainties in its mathematical modeling. Researchers have primarily used two approaches to model dynamic impact; namely the contact element approach and the stereomechanical approach. A brief summary of the various modeling techniques is presented below.

2.2.1 Contact element approach

The contact element approach is a very widely used formulation because of its easy adaptability and logical nature to model impact. The impact forces generated during the collision of two adjacent structures can readily be thought as being provided by a contact

element, which is activated only when the structures come into contact. The collision forces are assumed to act in a continuous manner. The contact element is usually a spring of very high stiffness, which may be used in conjunction with a damping element. The high spring stiffness is necessary to provide a realistic estimate of the impact force, ensure small impact duration and limit the penetration or overlapping of the colliding structures. Various contact elements have been used in the past including the linear spring element, Kelvin-Voigt element and the Hertz contact element.

The linear spring element illustrated in Figure 2.3(a) is the simplest contact element used to model impact. The spring comes into effect when the gap between the adjacent bodies closes and is representative of the force developed during impact. Maison & Kasai (1990a, 1992a) have extensively used this model to study pounding between adjacent buildings. However, the linear spring cannot account for the energy loss during impact.

The Kelvin-Voigt element represented by a linear spring in parallel with a damper, as shown in Figure 2.3(b) has been used in some studies (Wolf and Skrikerud, 1980; Anagnostopoulos, 1988; Anagnostopoulos and Spiliopoulos, 1992; Jankowski et al., 1998). The linear spring represents the force during impact and the damper accounts for the energy loss during impact. The damping coefficient (c_k) can be related to the coefficient of restitution (e), by equating the energy losses during impact.

$$c_k = 2\xi \sqrt{k_k \left(\frac{m_1 m_2}{m_1 + m_2} \right)} \tag{2.1}$$

$$\xi = -\frac{\ln e}{\sqrt{\pi^2 + (\ln e)^2}} \tag{2.2}$$
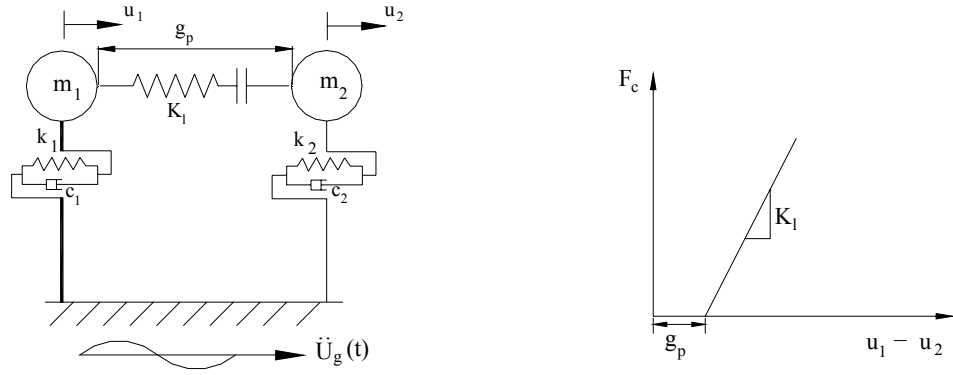
(a) Linear spring element
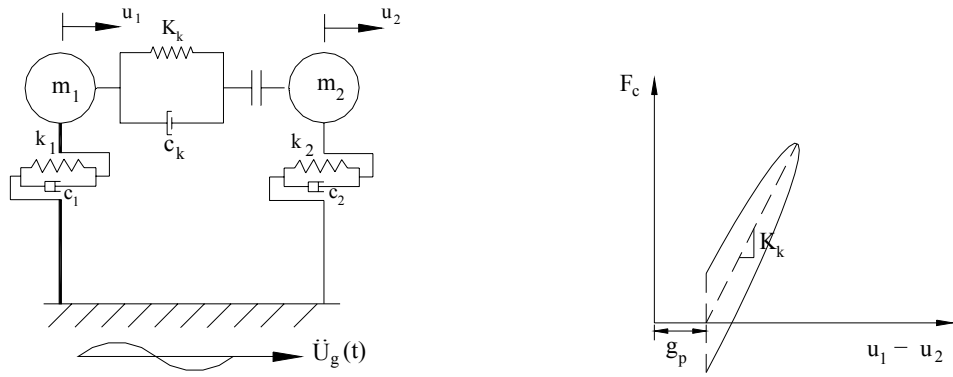
(b) Kelvin-Voigt element
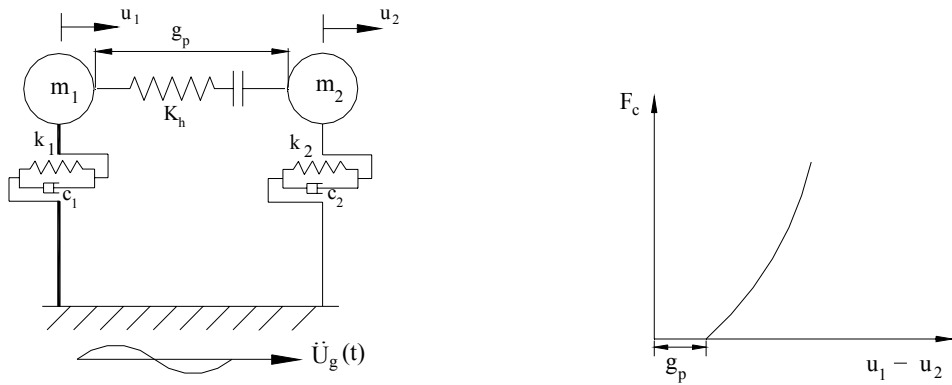
(c) Hertz nonlinear spring element

Figure 2.3: Various impact models and their contact force relations.

where k_k is the stiffness of the contact spring and m_1, m_2 are the masses of the colliding bodies.

Alternatively, a nonlinear spring based on the Hertz contact law can be used to model impact, as depicted in Figure 2.3(c). The impact force can be expressed as

$$F(t) = R[x(t) - g]^n \qquad ; x(t) \geq g$$

$$= 0 \qquad\qquad ; x(t) < g \qquad\qquad (2.3)$$

where R is the impact stiffness parameter that depends on the material properties of the colliding structures and the contact surface geometry, g is the at-rest separation and n is the Hertz coefficient, typically taken as 1.5. Several analysts have adopted this approach, including Davis (1992), Jing and Young (1991), Pantelides and Ma (1998), Chau and Wei (2001) and Chau et al. (2003). However, the Hertz contact law is representative of static contact between elastic bodies and fails to include energy dissipation during impact.

The contact element approach has its limitations, with the exact value of spring stiffness to be used, being unclear. Uncertainty in the impact stiffness arises from the unknown geometry of the impact surfaces, uncertain material properties under loading and variable impact velocities. The contact spring stiffness is typically taken as the in-plane axial stiffness of the colliding structure (Maison and Kasai, 1990a). Another reasonable estimate is twenty times the stiffness of the stiffer structure (Anagnostopoulos, 1988). However, using a very stiff spring can lead to numerical convergence difficulties and unrealistically high impact forces. The solution difficulties arise from the large

changes in stiffness upon impact or contact loss, thus resulting in large unbalanced forces affecting the stability of the assembled equations of motion.

2.2.2 Stereomechanical approach

The stereomechanical approach, also known as the coefficient of restitution approach, is a macroscopic attempt to model dynamic impact. Impact is assumed to be instantaneous. The principle of momentum balance and the coefficient of restitution are applied to modify the velocities of the colliding bodies after impact. The coefficient of restitution (e) is defined as the ratio of the separation velocities of the bodies after impact to their approaching velocities before impact (Goldsmith, 1960).

$$e = \frac{v_2' - v_1'}{v_1 - v_2} \tag{2.4}$$

where v_1', v_2' are the velocities after impact and v_1, v_2 are the velocities before impact, as shown in Figure 2.4. The value of e ranges from 0 (for perfectly plastic impact) to 1.0 (for elastic impact). The coefficient of restitution depends on the material properties of the colliding structures and their relative shapes and masses. Equations (2.5) and (2.6) give the velocities of the colliding bodies after impact.

$$v_1' = v_1 - (1 + e)\frac{m_2(v_1 - v_2)}{m_1 + m_2} \tag{2.5}$$

$$v_2' = v_2 + (1 + e)\frac{m_1(v_1 - v_2)}{m_1 + m_2} \tag{2.6}$$
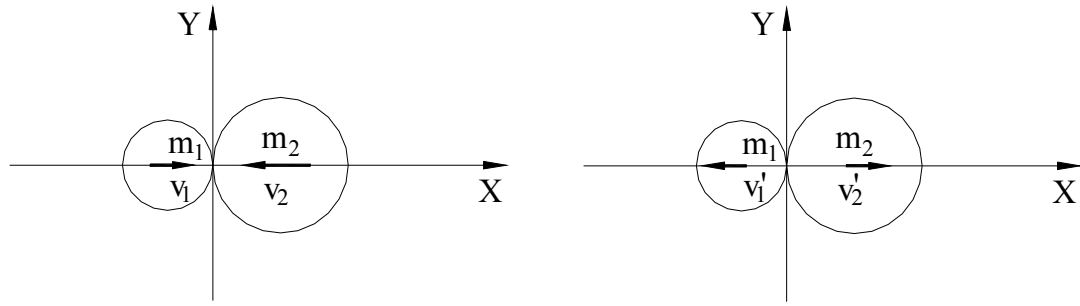
Figure 2.4: Stereomechanical impact: (a) Pre-impact state; (b) Post-impact state.

This approach has been used to model impact by several researchers including Papadrakakis et al. (1991), Athanassiadou et al. (1994), DesRoches and Fenves (1997a) and Malhotra (1998). It has been shown that the variation in (*e*) has a relatively minor effect on the structural response due to pounding (Athanassiadou et al., 1994; DesRoches and Fenves, 1997a).

The stereomechanical approach though relatively efficient is limited in its application because of the unknown duration of contact. If the impact duration is large enough so that significant changes occur in the configuration of the system, the assumption of instantaneous impact is no longer valid. The theory assumes a direct, central impact and does not consider transient stresses and deformations in the impacting bodies. Furthermore, this approach cannot be implemented in commercially available software.

2.3 Design methods and tools

The response of a bridge retrofitted with restrainers is nonlinear, even if the columns and foundations remain elastic. This is because the restrainers are tension-only devices

with an initial slack, which engage only after the slack is exhausted. Furthermore, bridge deck impact is a highly nonlinear phenomenon that cannot be rigorously solved through simplified means.

In order to permit equivalent elastic solutions to the bridge response, several assumptions are necessary. Typically two linear, dynamic models are used to bound the nonlinear response of the bridge – a *tension model* and a *compression model* (Caltrans, 1990; FHWA 1995). The tension model reflects the response of the bridge when the superstructure joint elements, including the abutments are released longitudinally. There is no restraint in the longitudinal direction except for that provided by restrainers. A compression model represents the state when impact occurs and the superstructure joints are closed. The restrainers are inactivated and a rigid element connects the impacting structures, mobilizing the abutments if needed. An illustrative sketch of the two linear models is shown in Figure 2.5.
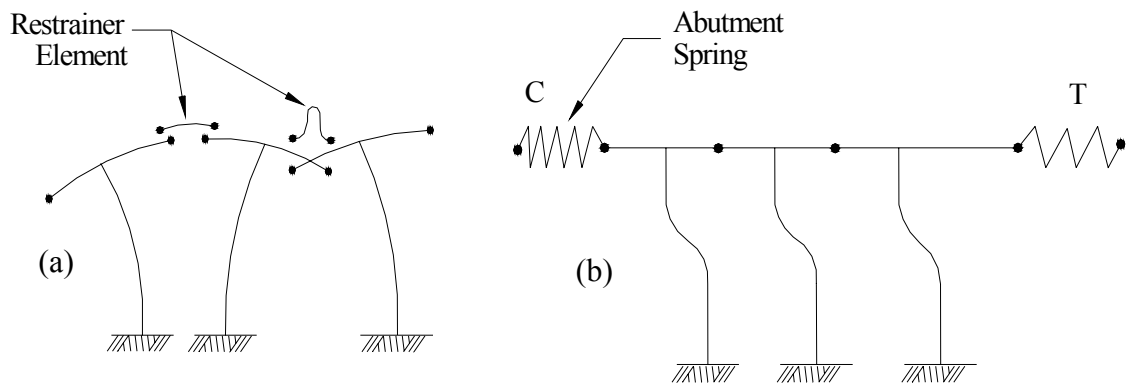
Figure 2.5: Linear bounding models: (a) Tension model; (b) Compression model.

The maximum of the component forces obtained from either model is taken as the bounding force for that component. For a strength-based design, the component yield forces are determined by dividing the elastic forces with response modification factors. The American Association of State Highway and Transportation Officials (AASHTO) provides response modification factors based on the general framing types and component location and/or function, which are independent of the period of the system (AASHTO, 1995). For instance, the response modification factor is 2 for wall-type piers and 3 single columns. Caltrans provides period-dependent Z factors to account for ductility and risk (Caltrans, 1993), as shown in Figure 2.6. However, the Caltrans Z factors decrease with increasing period, while studies have shown that reduction factors increase with increasing period (Miranda and Bertero, 1994; Cuesta et al., 2003). The application of the design yield forces is expected to limit the bridge ductility demands to designer specified values.
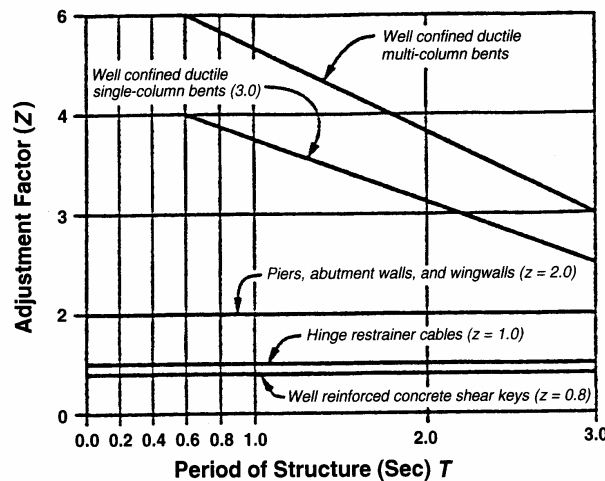
Figure 2.6: Caltrans Z factors to account for ductility and risk (Caltrans, 1993)

The inelastic demand is known to be sensitive to the period. The use of pre-set, period-independent reduction factors may not provide a correct estimate of the bridge ductility demands, especially for short periods. Several studies have shown that the response modification factor is a function of the period and the target demand (μ) for a particular frame force-deformation relationship (Krawinkler and Nassar, 1992; Vidic et al., 1994; Miranda, 2000). Preliminary investigations reveal that although the bounding models provide adequate bounds for the element forces in the bridge, they are unable to provide bounds for the bridge ductility demands (DesRoches and Fenves, 1997a).

2.4 Review of previous studies

Impact between adjacent structures during an earthquake is a phenomenon that has attracted considerable research interest in the recent past. The following sections summarize some of the important contributions in seismic pounding research.

2.4.1 Analytical studies

Several analytical studies have focused on pounding between inadequately separated buildings. Anagnostopoulos (1988) studied the effects of seismic pounding in a continuous building system, by idealizing each building as a single degree-of-freedom (SDOF) structure with a bilinear force-deformation relationship. Pounding was modeled using the Kelvin element with an impact stiffness of twenty times the stiffness of the stiffest adjacent structure. The coefficient of restitution (e) was taken as 0.65. The initial gap size was taken as 10 mm. Different configurations of buildings in a row were

considered and the effect of gap size, relative mass and impact spring stiffness on the system response were studied.

The results indicated that exterior systems exhibited mean displacement amplifications due to pounding greater than one for all period ratios, while the interior systems exhibited substantially lower amplifications. Furthermore, an increase in the gap size resulted in a decrease in displacement amplifications due to impact. A larger mass ratio between adjacent systems produced greater displacement amplification. The effects of changes in system damping and the impact spring stiffness were not significant.

Maison and Kasai (1992) investigated the pounding response of two flexible, high rise buildings using the contact element approach. The buildings (15 storey and 8 storey steel moment resisting frames) were modeled as linear elastic, with 3 degrees-of freedom at each level. Pounding was assumed to occur only at the floor level between the roof of the shorter building and Level 8 of the taller building. A linear spring of stiffness 50,000 kip/in was used to model impact. The response quantities of interest were story deflections, drifts, shears and overturning moments.

A preliminary study revealed that pounding increased the peak responses of the taller, lighter building and decreased the peak responses of the shorter, heavier building. Further parametric studies indicated that an increase in the mass ratio between the taller and shorter buildings resulted in increases of all the lighter building responses with impact. A building separation based on the square root of the sum of squares (SRSS) combination of the no-pounding peak building responses at the pounding location was found effective in reducing the likelihood of impact. The study concluded that the pounding responses were invariant to the impact spring stiffness provided a high stiffness value was used.

Pantelides and Ma (1998) studied the effects of one-sided pounding between a flexible, damped single degree of freedom structure and an adjacent rigid structure, due to earthquake motion. Both elastic and inelastic behaviors of the SDOF structure were considered. For the inelastic system, an elasto-plastic shear displacement relationship was used. Pounding was modeled using a Hertz contact element, with an impact stiffness parameter (R) of 80 kN mm$^{-3/2}$. The gap was taken as 25 mm.

The authors observed that the level of pounding damage in the elastic system was dependent on the period of the flexible structure. For the inelastic structure with a ductility of 4, pounding increased the peak displacement by 16% and increased the peak acceleration four fold, when compared to the no-pounding case. A comparison of the elastic and inelastic system for the same set of parameters revealed that the maximum displacement of the inelastic structure was greater than that of the elastic structure. But the maximum acceleration, pounding force and number of impacts were considerably less for the inelastic case.

Papadrakakis et al. (1991) treated pounding as a frictionless contact without sliding and proposed a Lagrange multiplier method, based on a variational formulation. The basic condition of contact that no material overlap occurs was treated as a geometric compatibility condition. The static equilibrium equations were derived by invoking the stationarity of the total potential function subject to the no penetration geometric constraint, which was then transformed to an unconstrained optimization problem of a Lagrangian functional. The dynamic formulation was obtained by using the procedure for static analysis and including the effects of inertia and damping forces.

The integration of the equations in the time domain was carried out using the Newmark method (Newmark, 1959). For the case of elastic impact, the values of the Newmark parameters $\beta = \gamma = \frac{1}{2}$ exactly correlated with the momentum balance and energy dissipation criteria of the stereomechanical method. However, it was difficult to correlate the values of β, γ with the post-impact conditions for inelastic contact. Hence, the compatibility of displacements during contact was enforced using Lagrange multipliers and the post-impact velocities were modified using the stereomechanical approach.

The Lagrange multiplier method was then applied to a three-dimensional simulation of pounding between adjacent two-storey buildings (Papadrakakis et al., 1996). Different building configurations were considered including combinations of a stiff and a flexible building adjacent to each other and three buildings in orthogonal directions in plan with the stiff building at the corner. Elastic analyses performed using the El Centro and Kalamata motions revealed that pounding had an amplification effect on the response of the stiff structure for all cases and a mitigation effect on the flexible building in most cases.

Valles and Reinhorn (1995) introduced the concept of Pseudo Energy Radius (PER) to study the effect of pounding in buildings. The response of a single degree of freedom system in the state space plane, subjected to seismic input was related to the elastic structural energy (E_e) of the system through the Pseudo Energy Radius as follows.

$$r_{PER} = \sqrt{\frac{2E_{e_{max}}}{mw^2}} \qquad (2.7)$$

where m is the mass of the structure, w is the frequency of the ground motion, E_{emax} is the maximum elastic structural energy of the system (P.E + K.E) and r_{PER} is the pseudo energy radius (PER). The Pseudo Energy Radius being expressed as units of displacement could be used to determine the critical gap to preclude pounding (g_{cr}) between adjacent structures, as shown below.

$$g_{cr} = \sqrt{r_1^2 + r_2^2 - 2r_1r_2\rho} \qquad (2.8)$$

where ρ is the correlation coefficient, and r1, r2 is are the pseudo energy radii corresponding to the energy levels of the two structures. Pounding occurred when the pseudo energy radii overlap and the initial separation between the structures (g_p) was less than the critical gap (g_{cr}). The impact of the structures was assumed to occur at their respective maximum energy levels imposed by the earthquake. The stereomechanical approach was then used to determine the post impact states of the colliding masses. The ratio of post impact PER to pre impact PER was an estimate of the amplification effects due to pounding.

However, the concept of PER is based on the maximum elastic structural energy (E_e) of the system. No adjustments are made to include the effects of yielding, which may alter the structural energy of the system considerably, depending on the period of the system and characteristics of the input motion.

Other studies have investigated the effects of dynamic impact in bridge structures. Jankowski at al. (1998) performed an analysis of pounding in an isolated bridge superstructure subject to a propagating seismic wave. High Damping Rubber Bearings (HDRBs) modeled in a nonlinear fashion based on the shear strain and shear strain rate were used for seismic isolation purposes. The bridge model consisted of five

superstructure segments, with the neglected segments being simulated using spring dashpots. Impact between the superstructure segments was simulated using the Kelvin element. The stiffness and damping of the impact element were 3.5 x 10^9 N/m and 1.8 x 10^7 kg/s respectively.

A response analysis revealed that pounding patterns significantly altered the bridge behavior. Two gap sizes of 10 mm and 110 mm were studied. The largest deformations, shear and pounding forces were observed for the larger gap, even though there were fewer collisions. The displacement response for the smaller gap was smaller than the bridge response without pounding. The authors concluded that the optimal separation gap between the superstructure segments should be either too small (less than 10 mm, in which case internal forces due to thermal expansion might occur) or large enough to avoid collisions.

Malhotra (1998) investigated seismic pounding at the expansion joints of multispan concrete bridges by formulating the problem as collinear impact between concrete rods of the same cross section but different lengths. A free vibration analysis of the axial responses of the rods was performed using the mode superposition method and frequency-independent damping. The force during impact was shown to be directly proportional to the compression wave velocity of concrete and the approach velocity of the impacting rods. The duration of impact was found to equal the fundamental period of axial vibration of the shorter rod. The coefficient of restitution that accounts for energy loss was determined as a function of the length of the rods and the damping ratio.

The results of the analysis were used to study the impact response of a 300m long multi-span concrete box girder bridge modeled as a two degree-of-freedom system with

linear, elastic columns. The findings indicated that pounding reduced the column deformations and impact forces generated in the superstructure were not transmitted to the columns and foundations.

Maragakis et al. (1991) studied the effect of impact between the bridge deck and abutments on the dynamic response of the bridge during strong ground motion. A simplified model of the bridge was developed with appropriate mass and stiffness values for the deck and abutment. All the springs were assumed as linear and impact was modeled using the stereomechanical approach. Since, the stereomechanical approach is difficult to implement in bridge analysis software, another model of the bridge was developed with the abutments represented as spring-damper systems with no mass. A reasonable estimate of the abutment damping was obtained by equating the energy loss from the stereomechanical method with the energy loss in the damper. The authors concluded that the important parameters affecting the impact response were the abutment gap, mass ratio between bridge deck and abutment, abutment stiffness and the coefficient of restitution.

Zhu et al. (2002) developed a three-dimensional contact friction model for studying arbitrary impact between bridge deck girders. Pounding was visualized as an impact between a contactor node *k* and a rigid, plane contact surface *abcd* as shown in Figure 2.7. Point *p* was the physical contact position on the target surface. The Kelvin model with dashpots in both normal and tangential directions to the target surface was utilized. The nature of contact could be either *stick* or *slide* depending on the following conditions

$$Stick : \left| F_k \mid_t \right| < \mu_s \left| F_k \mid_n \right| \tag{2.9}$$

$$Slide : \left| F_k \mid_t \right| \geq \mu_s \left| F_k \mid_n \right| \tag{2.10}$$

where $F_k|_n$, $F_k|_t$ are the normal and tangential components of the contact force, F_k to the target surface, respectively and μ_s is the coefficient of static friction. The contact forces at node k were determined separately for stick and slide conditions and were then interpolated to the four nodes (a, b, c, d) of the target surface using a linear interpolation matrix.

Shaking table experiments were conducted to verify the pounding model by studying impact between a model girder and an abutment, and two model girders. Sinusoidal input with varying angles of excitation was used. Good agreement was observed between the experimental and analytical results of displacement responses in both the longitudinal and transverse directions. The experiments helped identify the restitution coefficients in the normal and tangential directions as 0.4 and 0.9, respectively. The static and kinetic friction coefficients were found to be 0.2 and 0.15, respectively.
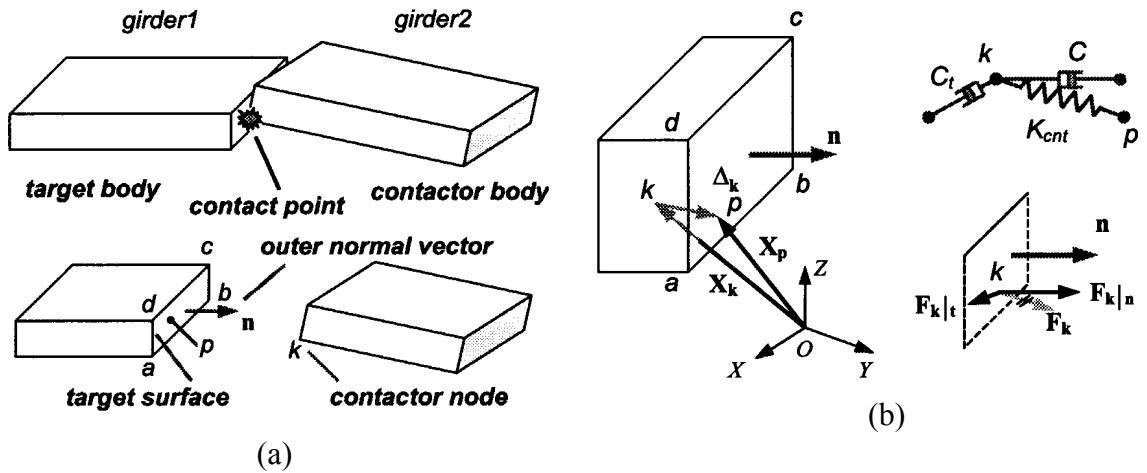
Figure 2.7: (a) Arbitrary contact between adjacent girders; (b) 3D contact friction model

(Zhu et al., 2002)

23

The three-dimensional model was then adapted to model pounding in a three-span simply supported steel bridge, with rubber bearings used for base isolation in both longitudinal and transverse directions. The Takatori record from the 1995 Kobe earthquake was used in the analysis. Pounding reduced the longitudinal displacement, increased the rotational response and did not affect the transverse displacements of the center span. The effects of tangential friction on the girder response were found to be negligible and the responses in the main directions were not sensitive to variation in the friction coefficients.

2.4.2 Experimental studies

Although several theoretical studies have been performed on seismic pounding, very few experiments have been conducted to investigate the effects of impact. van Mier et al. (1991) studied the concrete-to-concrete impacts between breakwater armor elements through a series of dynamic experiments on various contact surface geometries. The test apparatus consisted of a prestressed concrete pile with crossection 250 mm x 250 mm and length 20 m, and a concrete striker of variable mass (290 kg, 570 kg) hung in an overall frame, as shown in Figure 2.8. The concrete pile served as a measuring device and a prismatic concrete specimen was attached to the top of the pile. The striker was raised to a certain height (to ensure a specified velocity at impact) and then released. A total of 24 dynamic tests were conducted with the impact velocity and mass of the striker, concrete strength and contact surface geometry as the variables. The surface of the target specimens was either planar or corrugated and the striker surface geometries were either spherical, conical or truncated conical.
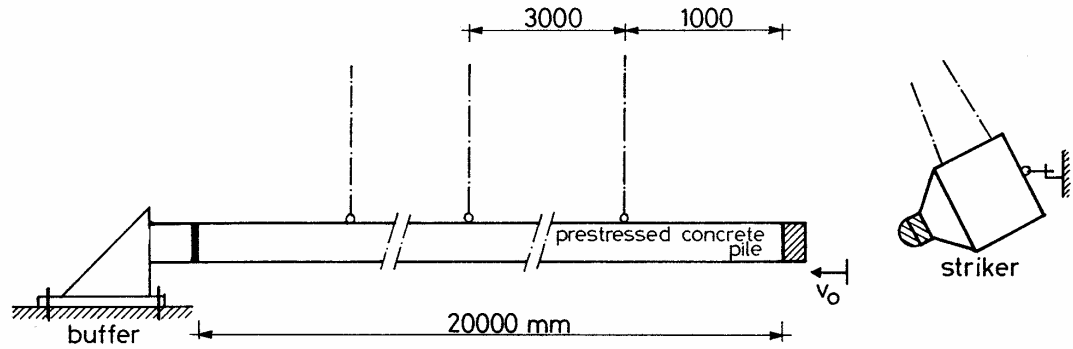
Figure 2.8: Apparatus for dynamic impact experiments (van Mier et al., 1991)

The load-time histories during contact were determined from the experiments and an impact stiffness parameter (K_e) was calculated using the Hertz law (Goldsmith, 1960). The impact stiffness ranged from 2 kN/mm$^{3/2}$ to 80 kN/mm$^{3/2}$. The choice of contact surface geometry had a significant influence on the load-time response, with the largest stiffness being observed when a truncated conical specimen collided with a planar target.

A decreasing stiffness and a longer impact time were observed for the spherical/planar, spherical corrugated and conical/planar contact surfaces. The pressure-time history of the contact zone was also fitted to a simple elastoplastic model with input parameters based on the contact stiffness K_e, critical stress and size of the contact surface and the unloading stiffness, which were determined from the dynamic tests. However, the experiments were performed on relatively small specimens and translation to large-scale situations is subject to further research.

Papadrakakis et al. (1995) performed shaking table experiments on pounding between two-storey reinforced concrete buildings with zero gap separation, subject to sinusoidal

25

excitation. The test structures were designed to remain elastic under an excitation with an acceleration design spectrum of 1.0 g. A plan view of the test set up is shown in Figure 2.9. A shaking table test was conducted with a ramped sinusoidal displacement signal having a peak displacement of 0.13 cm and at resonance with the fundamental frequency of the flexible structure (f = 4.1 Hz). Both pounding and no-pounding cases were studied.

The results indicated that pounding amplified the displacement responses of the stiffer structure and reduced the responses of the flexible structure. A six fold increase in the acceleration peaks due to impact was recorded. A consistent penetration at the contact locations was also observed. Comparison of the experimental results with analytical predictions using the Lagrange multiplier method showed good agreement.
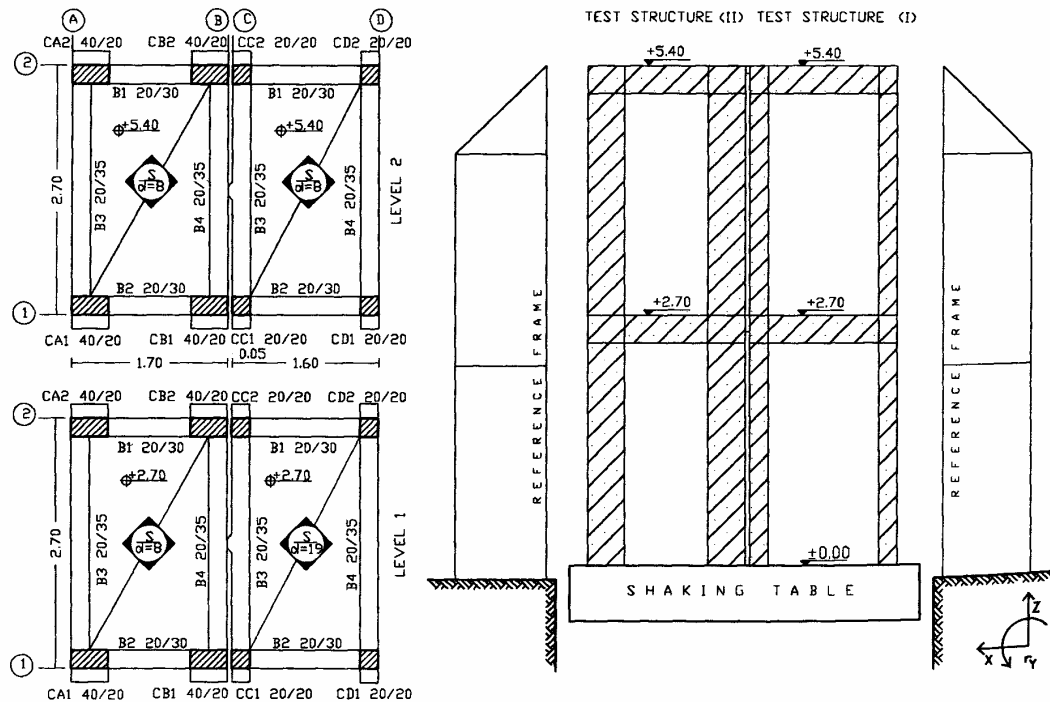
Figure 2.9: Test set up for investigations into seismic pounding (Papadrakakis et al. 1995)

Filiatrault et al. (1995) conducted shaking table tests on dynamic impact between adjacent three and eight storey steel frames (1/8 scale model), with 0 mm and 15 mm gap separations, subject to the 1940 El Centro earthquake. The structures remained elastic during the ground shaking. Both floor-to-floor impact and floor-to-column impact were considered and the results showed significant acceleration levels at the roof of the three storey frame, sometimes as high as 30g for the floor-to-column pounding.

The experimental results were then compared with analytical results from two pounding analysis programs – SLAM-2 (Maison and Kasai, 1990b) and PC-ANSR (Maison, 1992), where impact was modeled using a linear spring element. The amplitude and phase of the displacement and impact forces obtained from the experiment were well predicted by the analytical models. However, the accelerations at the contact locations were not well predicted.

Kajita (2000) performed collision tests on steel girders to assess the pounding behavior in bridges and to examine the effectiveness of laminated fiber reinforced rubber over natural rubber as a shock absorbing device. The collision test was performed using a horizontal hydraulic high-speed loading machine with a loading capacity of 1000 kN and a maximum speed of 3 m/s. The test set-up is illustrated in Figure 2.10. Initial velocities of 1 m/s, 2 m/s and 3 m/s were applied to the *colliding* specimen, which then impacted with the stationary *collided* specimen.

Steel H-beams with a length of 1000 mm, width of 200 mm, height of 200 mm, web thickness of 8 mm and flange thickness of 12 mm were used to study the pounding behavior. Rectangular solid steel bars 1000 mm long, 200 mm wide and 200mm high

were employed to assess the performance of the shock absorber. The impact force during collision and the velocities of the bodies before and after collision were measured.
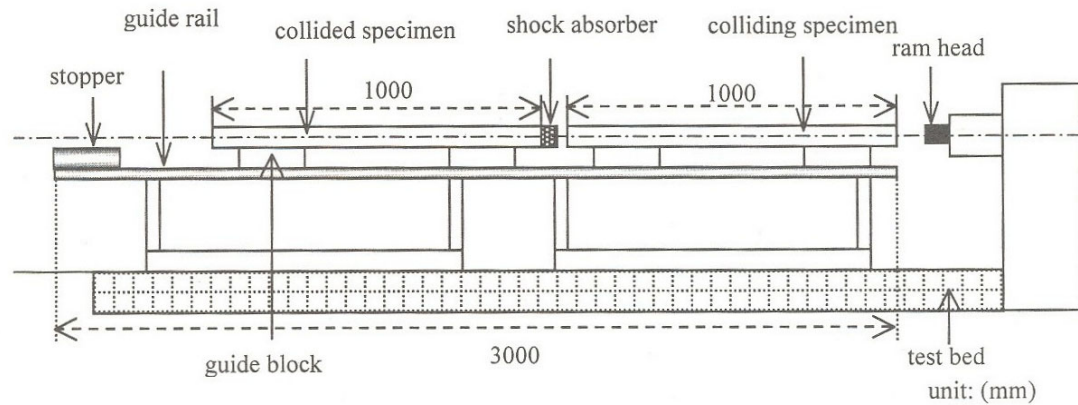
Figure 2.10: Experimental set-up to study pounding behavior (Kajita, 2000)

The test results showed that the law of conservation of momentum was satisfied in all cases. For the test with no shock absorber, 30% to 40% of the energy was lost during collision. The maximum impact force during impact increased with an increase in the collision velocity. The test also demonstrated that for collision velocities greater than 0.7 m/s, the maximum impact load on the laminated reinforced rubber was half of the impact load on natural rubber.

The experimental results were then compared with results from a one-dimensional spring-mass-dashpot model with impact modeled using a linear spring, and a three-dimensional finite element model. The finite element model was able to account for the stress wave during collision and was used to evaluate the impact load precisely. The

study concluded that the simplified analysis using the spring-mass-dashpot model was effective in capturing the motion of the bodies before and after collision.

Chau et al. (2003) performed shake table tests on pounding between two steel towers subject to sinusoidal ground motions, as illustrate in Figure 2.11. The natural frequency, damping, the stand-off distance between the towers and the forcing frequency were varied during the experiment. The steel towers remained elastic during the duration of shaking. Under sinusoidal excitations, impacts were either periodic (one impact within each excitation cycle or within every other excitation cycle) or chaotic. A group of non-periodic impacts repeating themselves periodically were also observed in some cases. Chaotic motions dominated when there was a large difference in the natural frequencies of the two towers. It was observed that pounding amplified the response of the stiffer structure and reduced the flexible tower response. The maximum relative impact velocity was found to occur at an excitation frequency between the natural frequencies of the two towers.

The experimental findings were then compared with results from an analytical model where impact was modeled using the Hertz contact law (Chau and Wei, 2001). The region of excitation frequency within which impact occurred was well predicted by the analytical model. The estimated relative impact velocity and the maximum stand-off distance to prevent pounding agreed qualitatively with the experiments. However, discrepancies did exist in many cases.
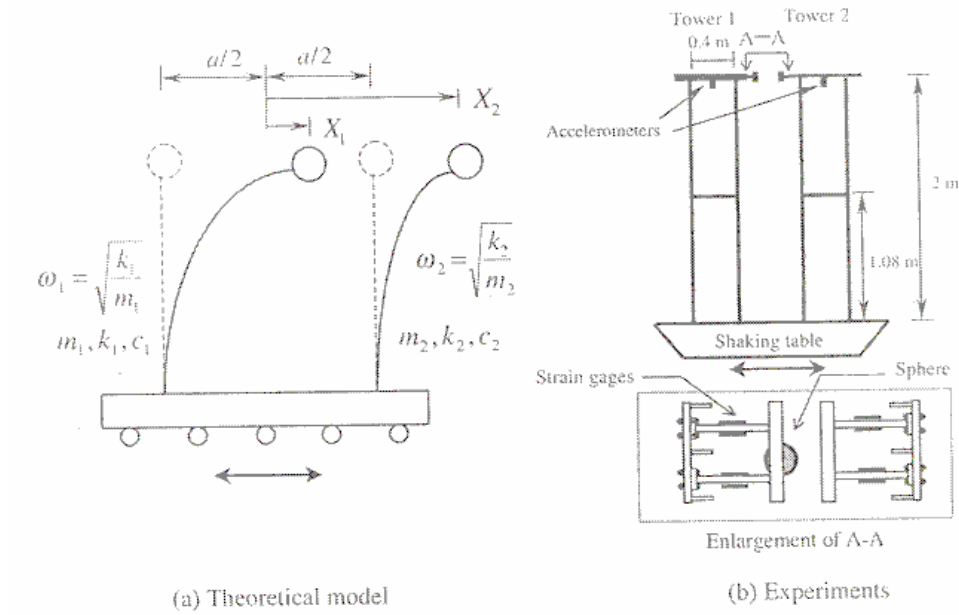
Figure 2.11: Theoretical model and experimental setup to study pounding between two steel towers (Chau et al., 2003)

2.5 Conclusions

Recent earthquakes have indicated that seismic pounding can cause infill wall damage and column failure in buildings and result in damage to piers, abutments and possible span collapse in bridges. Based on a review of the literature, the critical parameters affecting seismic pounding include the relative stiffness of the participating systems, gap between adjacent structures and ground motion characteristics. Typically, bilinear or stiffness degrading models have been used to describe the behavior of the participating systems. Impact has been modeled using contact based elements such as a linear spring, Kelvin-Voigt element and Hertz nonlinear spring, or a stereomechanical

approach based on momentum balance and energy dissipation using the coefficient of restitution.

The general trend is amplification in the stiffer structure response and de-amplification in the flexible structure response, as a result of pounding. To better understand the parameters affecting seismic pounding in bridges, a simplified bridge model needs to be developed and parameter studies conducted. The effectiveness of various analytical models used to simulate impact also needs to be examined, since the linear spring and Hertz contact elements cannot account for energy dissipation and the Kelvin-Voigt model results in sticky tensile forces acting on the bodies during separation. Moreover, the nature of impact (linear or nonlinear) is not well understood. Some analytical models like the stereomechanical method and the Kelvin model are difficult to incorporate in standard analysis software. Strength degradation in the participating systems could prove to be a critical factor in the system response and needs to be investigated. The adequacy of current design procedures in accounting for bridge deck impact also needs scrutiny.

The following chapters of this dissertation focus on the development of a simplified analytical model for a multiple-frame bridge with impact modeled using a Hertz nonlinear spring with a nonlinear hysteresis damper for energy dissipation. Parameter studies on the effects of various impact models and strength degrading columns on the bridge response are presented. Design guidelines that account for seismic pounding in bridges are reviewed and revisions recommended. Finally, a simplified contact model that accounts for energy loss during impact and which can be easily incorporated in bridge analysis software is discussed.

CHAPTER 3

SIMPLIFIED NUMERICAL MODEL FOR THE ANALYSIS OF MULTIPLE-FRAME BRIDGES

A multiple-frame bridge is a widely used bridge form in the United States, often favored for freeway connectors and highway interchange structures. A typical multiple-frame bridge consists of deck elements separated by expansion joints (intermediate hinges) and supported on columns and end abutments, as illustrated in Figure 3.1. Intermediate hinges allow for post tensioning the superstructure, facilitate the construction process and accommodate stress-free thermal expansion. Elastomeric bearing pads support the decks at the intermediate hinge and shear keys limit transverse displacement. For bridges with short hinge seats, tension-only cable restrainers tie the decks together and prevent excessive longitudinal displacement.

Past earthquakes have shown that the multiple-frame bridge is very susceptible to seismic pounding damage at the abutments and intermediate hinge locations. In this study, the multiple-frame bridge is considered as the representative bridge structure to study the effects of pounding. The opening and closing of intermediate hinges, yielding of bridge frames and engaging of cable restrainers, bearings and abutments constitute nonlinearities inherent with the interaction of adjacent bridge frames during strong ground motion. A nonlinear model incorporating these effects needs to be developed to adequately study the response of the bridge subject to longitudinal ground motion. Since the primary goal is to focus on the pounding effects and conduct parameter studies, a simplified numerical bridge model is developed in this study.
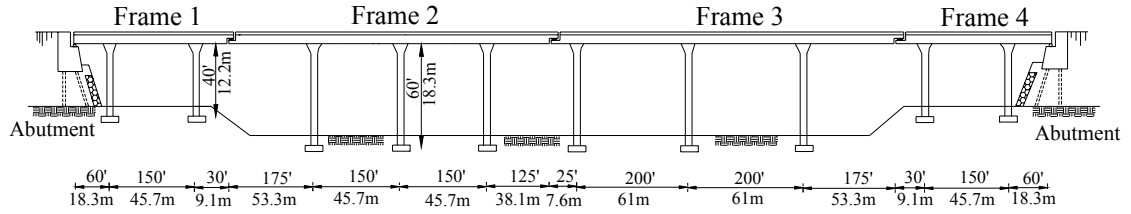
(a) General elevation
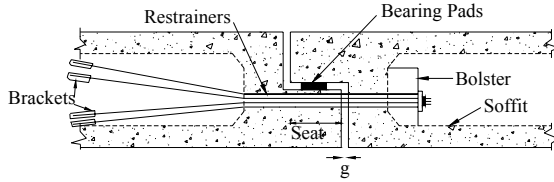
(b) Longitudinal section at hinge
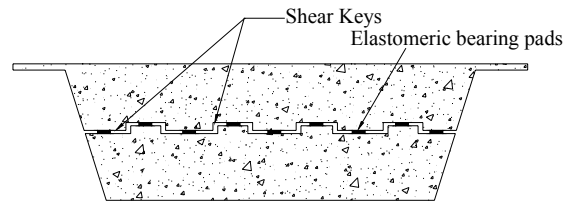
(b) Transverse section at hinge

Figure 3.1: Typical multiple-frame bridge – general elevation and hinge detail

3.1 Problem formulation and solution strategy

The objective of this study is to develop a better understanding of the effects of pounding on the global response of the bridge when subjected to a suite of ground motions. A compromise between accuracy and efficiency is necessary given the scope of the problem being addressed. The crux of the analytical model is to focus on the impact phenomenon while representing all major behavioral characteristics of the bridge. Hence, a simplified planar nonlinear analytical model of a multiple-frame bridge is developed, as shown in Figure 3.2. The modeling of the various components of the bridge will be discussed in the next section. The equations of motion for the bridge system consisting of n frames subject to horizontal ground motion can be expressed as:

$$
\begin{bmatrix} m_1 & & \\ & \ddots & \\ & & m_n \end{bmatrix} \begin{Bmatrix} \ddot{u}_1 \\ \vdots \\ \ddot{u}_n \end{Bmatrix} + \begin{bmatrix} c_1 & & \\ & \ddots & \\ & & c_n \end{bmatrix} \begin{Bmatrix} \dot{u}_1 \\ \vdots \\ \dot{u}_n \end{Bmatrix} + \begin{Bmatrix} F_{F_1}(u_1) \\ \vdots \\ F_{F_n}(u_n) \end{Bmatrix} - \begin{Bmatrix} F_{R_1}(u_2 - u_1) \\ F_{R_2}(u_3 - u_2) - F_{R_1}(u_2 - u_1) \\ \vdots \\ -F_{R_{n-1}}(u_n - u_{n-1}) \end{Bmatrix}
$$

$$
- \begin{Bmatrix} F_{B_1}(u_2 - u_1) - F_{B_0}(u_1 - u_0) \\ F_{B_2}(u_3 - u_2) - F_{B_1}(u_2 - u_1) \\ \vdots \\ F_{B_n}(u_{n+1} - u_n) - F_{B_{n-1}}(u_n - u_{n-1}) \end{Bmatrix} + \begin{Bmatrix} F_{I_1}(u_2 - u_1) \\ F_{I_2}(u_3 - u_2) - F_{I_1}(u_2 - u_1) \\ \vdots \\ -F_{I_{n-1}}(u_n - u_{n-1}) \end{Bmatrix} = - \begin{bmatrix} m_1 & & \\ & \ddots & \\ & & m_n \end{bmatrix} \begin{Bmatrix} 1 \\ \vdots \\ 1 \end{Bmatrix} \ddot{u}_g \qquad (3.1a)
$$

$$
\begin{Bmatrix} F_{A_1}(u_0) \\ F_{A_2}(-u_{n+1}) \end{Bmatrix} = \begin{Bmatrix} F_{B_0}(u_1 - u_0) \\ F_{B_n}(u_{n+1} - u_n) \end{Bmatrix} \qquad (3.1b)
$$

where m_i is the mass of each frame, c_i is the frame damping coefficient, F_{Fi} is the inelastic restoring force for each frame based on the hysteretic relation chosen, F_{Ri} is the force from restrainer R_i, F_{Bi} is the force in bearing B_i, F_{Ii} is the force due to impact between frames i and $i+1$ and F_{Ai} is the force in abutment A_i; $\ddot{u}_i$, $\dot{u}_i$ and u_i (i = 1 to 4) represent the frame acceleration, velocity and displacement relative to the ground; u_0, u_{n+1} are abutment displacements obtained using static condensation and $\ddot{u}_g$ represents the horizontal ground motion applied to the bridge.
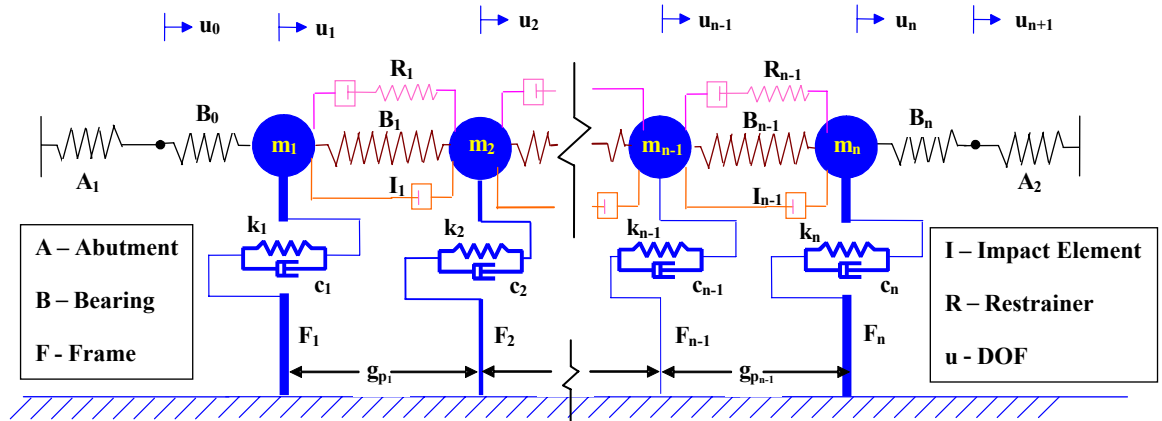
Figure 3.2: Analytical bridge model used in the study

Since several studies have shown that damping is not a significant factor in the pounding response, modal damping of 5% is assigned to each frame. The solution for equation 3.1 can be obtained in the time domain using a numerical time stepping algorithm. Several algorithms are available such as the Newmark, Wilson-Theta and Runge-Kutta methods. The Newmark and Wilson-Theta methods are popular for single degree-of-freedom systems. However, these are computationally demanding for inelastic, higher degree-of-freedom systems, as they involve iteration at every time step. Moreover, they are difficult to implement for nonlinear and coupled system of equations.

On the other hand, the classical fourth-order Runge-Kutta method for solving first-order differential equations is well suited for computational solution. It needs no special starting procedure, makes light demand on storage, and repeatedly uses the same straightforward computational procedure. It is also numerically stable and can be easily extended to systems with higher order differential equations. Hence, the classical fourth-order Runge-Kutta method is adopted as the equation solver in this study.

The numerical solution of a simple first-order differential equation shown in equation 3.2 is obtained by applying equations 3.3-3.8 over the number of time steps, N-1.

$$\frac{dy}{dt} = f(t, y); y(x_0) = y_0 \tag{3.2}$$

$$k_1 = hf(t_n, y_n) \tag{3.3}$$

$$k_2 = hf\left(t_n + \frac{1}{2}h, y_n + \frac{1}{2}k_1\right) \tag{3.4}$$

$$k_3 = hf\left(t_n + \frac{1}{2}h, y_n + \frac{1}{2}k_2\right) \tag{3.5}$$

$$k_4 = hf(t_n + h, y_n + k_3) \tag{3.6}$$

$$t_{n+1} = t_n + h \tag{3.7}$$

$$y_{n+1} = y_n + \frac{1}{6}\left(k_1 + 2k_2 + 2k_3 + k_4\right) \tag{3.8}$$

where x_0, y_0 are the initial conditions, h is the time step and k_1, k_2, k_3, k_4 are evaluations used to determine the final function value (y_{n+1}) at each time step. In each step, the derivative is evaluated four times: once at the initial point (y_n), twice at trial midpoints, and once at a trial end point. The final function value (y_{n+1}) shown as a filled dot in Figure 3.3 is then calculated, based on an effective slope. The effective slope is the weighted mean of the four derivatives, with the two midpoint values being the dominant contributors.

However, Equation 3.1(a) is a second-order differential equation system, which needs to be reduced to a first-order system by writing vector functions {y} and {f}, whereas t remains a scalar variable. Equation 3.1(a) can be rewritten in matrix form as follows:

$$[M]\{\ddot{u}(t)\} + [C]\{\dot{u}(t)\} + \{F_F(u(t))\} - \{F_R(u_j(t) - u_i(t))\}$$
$$- \{F_B(u_j(t) - u_i(t))\} + \{F_I(u_j(t) - u_i(t))\} = -[M]\{1\}\ddot{u}_g(t) \tag{3.9}$$

where [.] denotes a matrix, {.} denotes a vector and i, j represent adjacent degrees-of-freedom. Making the substitutions, (3.10), (3.11), (3.12), equation 3.9 can be written as a first-order system given by (3.13).

$$\{y_1\} = \{u\} \tag{3.10}$$

$$\{y_2\} = \{\dot{y}_1\} = \{\dot{u}\} \tag{3.11}$$

$$\{y_3\} = \{\dot{y}_2\} = \{\ddot{u}\} \tag{3.12}$$

36
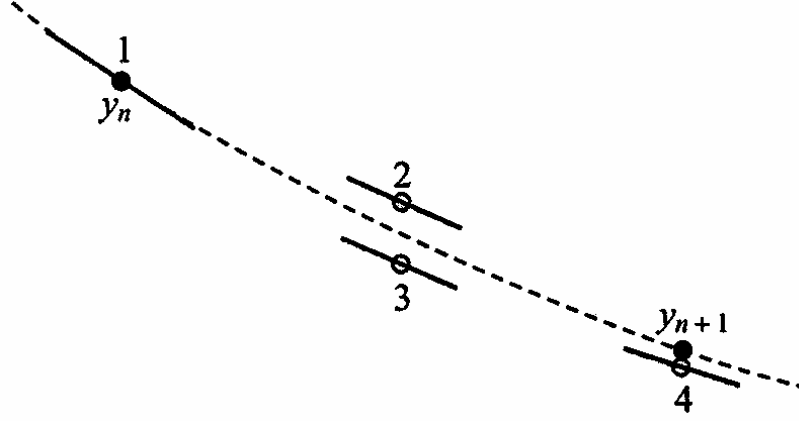
Figure 3.3: Fourth order Runge-Kutta method – function evaluation

$$\{\dot{y}_1\} = \{y_2\}$$
$$\{\dot{y}_2\} = -\{1\}\ddot{u}_g - [M]^{-1}[C]\{y_2\} - [M]^{-1}\{F_F\} + [M]^{-1}\{F_R\}$$
$$+ [M]^{-1}\{F_B\} - [M]^{-1}\{F_I\}$$
(3.13)

The Runge-Kutta method can now be applied to the above set of equations to get a numerical solution. Pounding occurs when the gap between the adjacent masses (i, j) closes, as given by (3.14).

$$u_i - u_j - g_p > 0$$
(3.14)

The contact force (F_I) depends on the choice of the impact element selected. The contact force for the linear spring, Kelvin solid and Hertz models are given by equations (3.15), (3.16) and (3.17) respectively.

$$F_I = k_l \left(u_i - u_j - g_p \right) \quad ; \quad u_i - u_j - g_p \geq 0$$
(3.15a)

$$F_I = 0 \quad ; \quad u_i - u_j - g_p < 0$$
(3.15b)

$$F_I = k_k \left(u_i - u_j - g_p \right) + c_k \left(\dot{u}_i - \dot{u}_j \right) \quad ; \quad u_i - u_j - g_p \geq 0$$
(3.16a)

37

$$F_I = 0 \qquad\qquad ; \quad u_i - u_j - g_p < 0 \qquad\qquad (3.16b)$$

$$F_I = k_h \left(u_i - u_j - g_p \right)^{3/2} \qquad ; \quad u_i - u_j - g_p \geq 0 \qquad (3.17a)$$

$$F_I = 0 \qquad\qquad ; \quad u_i - u_j - g_p < 0 \qquad\qquad (3.17b)$$

where k_l, k_k, and k_h are the impact stiffness parameters and c_k is the damping coefficient for the Kelvin model that is given by equations (2.1), (2.2). The contact force (F_I) for the stereomechanical model is taken as zero, since it is not a force based approach. However, the velocities of the colliding masses are adjusted after impact, as shown in equations (2.5) and (2.6).

The system of equations is implemented in MATLAB[1] based on the above discussions. Using MATLAB as a platform for implementation offers the advantages of simplicity in coding a variety of inbuilt functions for matrix analysis and graphical functions for the visualization of results. However, the analysis would be inefficient time-wise as the resulting code is not pre-compiled.

The program uses an input file "bridge.inp" which contains information on the number of bridge frames, properties of frames, restrainers, bearings, abutments and impact elements, ground motion details and time interval for analysis. From this information, the bridge model is created and the system matrices are assembled as described in (3.1). A nonlinear time history analysis is performed using the Runge-Kutta routine illustrated earlier. The output of the time-history analysis is vectors containing the structure states at every time step specified. Post processing of the results includes plots of element deformations and force-displacement relations.

---

[1] MATLAB is a registered trademark of The Mathworks Inc., 24 Prime Park Way, Natic, MA 01760-1415

3.2 Structural bridge modeling

This section provides a description of the various bridge components and discusses the development of analytical models for these components.

3.2.1   Bridge frames

Bridge frames consist of the deck slab supported by piers. In general, piers are designed to sustain superstructure dead and live loads and transmit all loads to the foundation. For most piers, concrete is the material of choice. However, steel and to a lesser extent timber have also been used. The basic types of piers popular in highway bridges are shown in Figure 3.4. In the case of multiple-frame bridges, single column bents support the superstructure as illustrated in Figure 3.5.
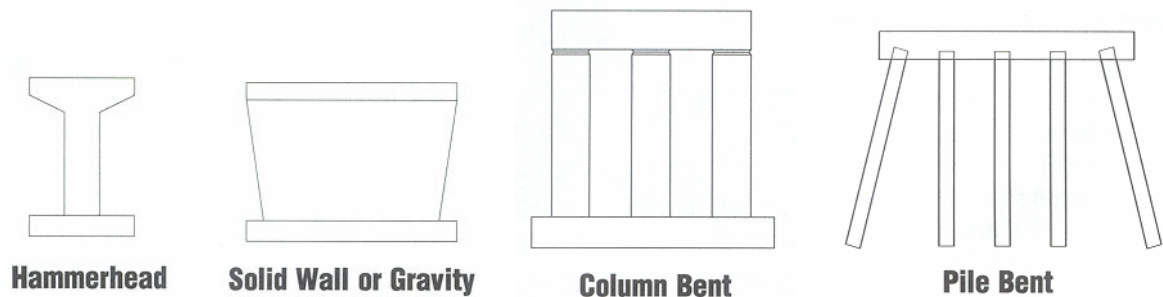
Figure 3.4: Basic types of highway bridge piers (Tonias, 1995)
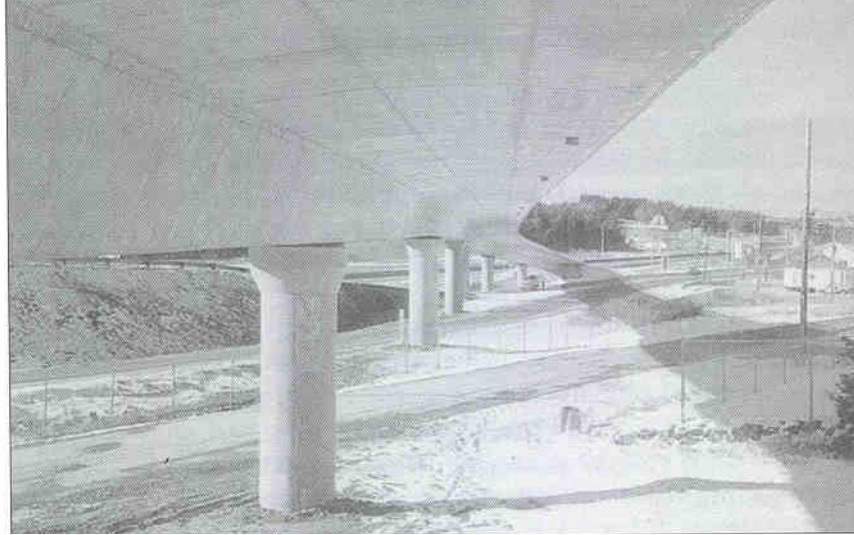
Figure 3.5: Single column bents in a multiple-frame bridge (Tonias, 1995)

The response of bridge columns during intense ground shaking can deform into the inelastic range and exhibit nonlinear behavior. Experimental studies on column specimens have shown that the cyclic behavior of reinforced concrete is characterized by constantly changing stiffness, strength degradation and a reduction in the energy absorption capacity (Takeda et al., 1970; Saatciaoglu and Ozcebe, 1989; Dowell et al., 1998). Several analytical models have been developed to capture the nonlinear dynamic response of a reinforced concrete column subjected to base excitation (Clough and Johnston, 1966; Takeda et al., 1970; Saiidi and Sozen, 1979; Dowell et al., 1998).

For this study, each bridge frame is idealized as a single degree-of-freedom yielding system with an assumed frame force-deformation relationship. The hysteretic models considered include the bilinear, stiffness degrading (Q-Hyst) and strength degrading (pivot hysteresis) models shown in Figures 3.6 and 3.7. A description of the properties of the various models can be found in Chapter 6.
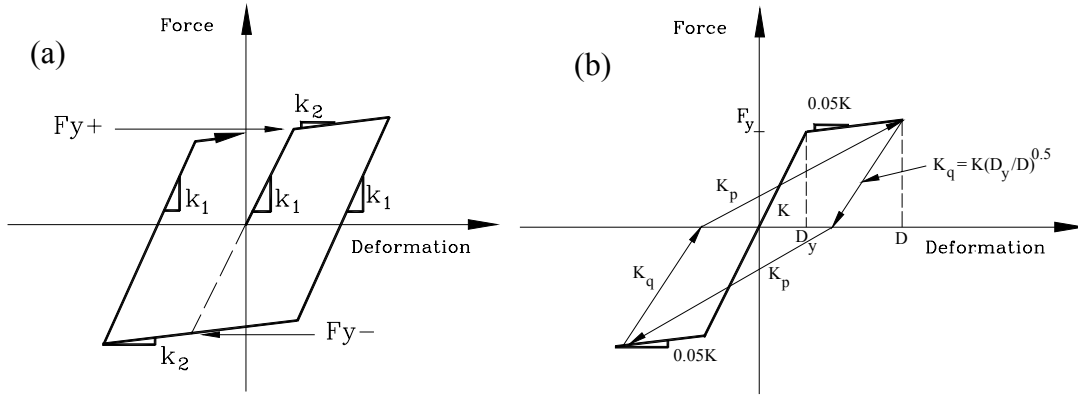
Figure 3.6: Frame force-deformation relations (a) Bilinear; (b) Q-Hyst
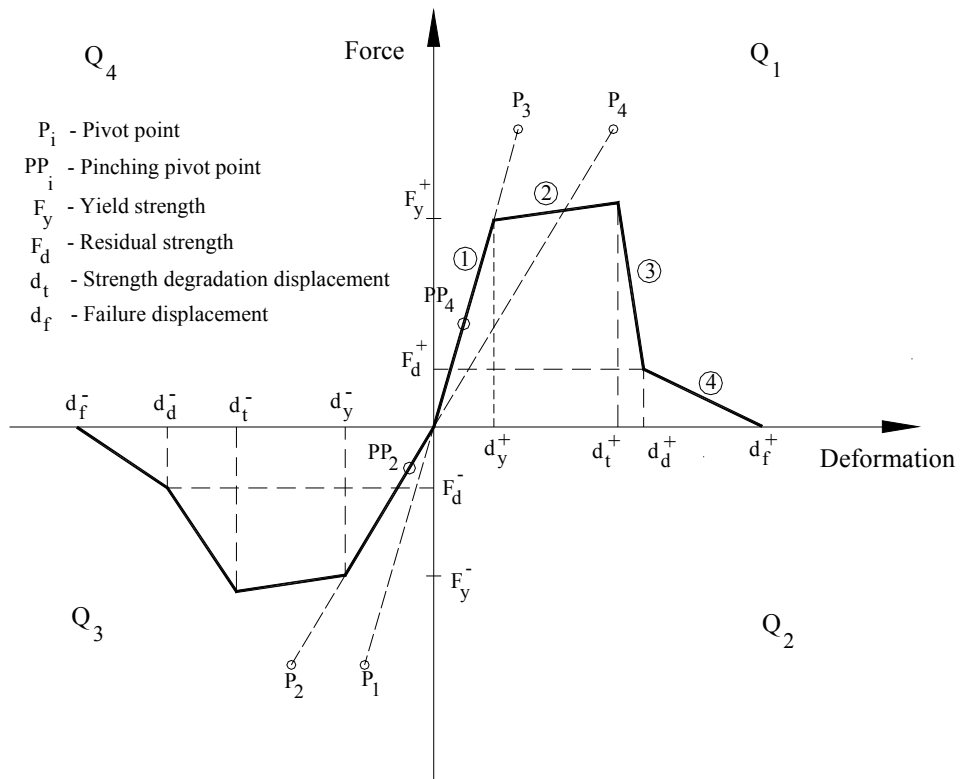
Figure 3.7: Strength envelope for the Pivot hysteresis model (Dowell et al., 1998)

3.2.2 Restrainers

The 1971 San Fernando earthquake led to a re-evaluation of the design procedures for bridges, after a number of bridge collapses were observed (Murphy, 1973). Following the earthquake, the California Department of Transportation suggested a retrofit scheme, whereby steel cable or bar restrainers were provided between adjacent spans to prevent excessive relative displacement and unseating of the spans. The spans were either tied together or tied to the substructure. Although several restrainer failures were observed during the 1994 Northridge earthquake, restrainers had some success in controlling large movements of the spans (Schiff, 1995).

Typical restrainers used in California are ¾ inch (19 mm) diameter steel cables with an area of 0.22 square inch (143 mm^2) made of 6x19 strands, galvanized with a wire strand core, a right regular lay and made of improved plow steel (Scalzi and McGrath, 1971; Section 83-2.02A, Standard Specifications). The restrainer assembly is composed of cables with swagged fittings, studs, nuts and turnbuckles, all of which should be 25% stronger than the cable (Yashinsky, 1992). Figure 3.8 illustrates a typical restrainer unit assembly. Under cyclic loading, the cables have a yield strength of 39.1 kips (174 kN), which corresponds to a yield stress of 176 ksi (1210 MPa) and an initial modulus of elasticity of 10,000 ksi (69,000 MPa). The ultimate strength per cable is 53 kips (235 kN). The force deformation relationship for a typical cable restrainer is shown in Figure 3.9. Figures 3.10 and 3.11 illustrate the various ways of connecting restrainer rods or cables to the pier.

In this study, twenty foot long, ¾ inch diameter cables that stretch approximately 4.22 inches at yield are considered. The slack of the cables is assumed to be ½ inch as

specified for typical bridges. Restrainers are modeled at the intermediate hinge locations

only, using a bilinear spring element with a slack that resists only tensile forces. A strain

hardening ratio of 5% is assumed as shown in Figure 3.12.
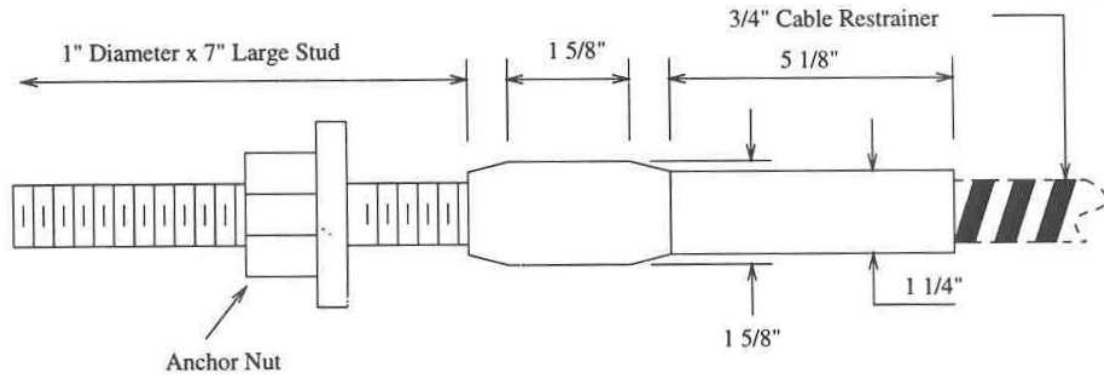
Figure 3.8: Typical cable restrainer assembly
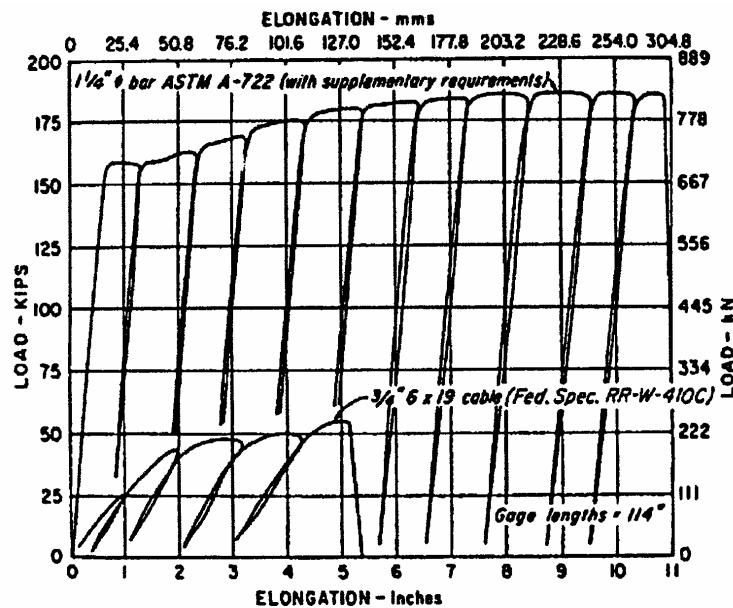
Figure 3.9: Load deformation relationship for restrainers (Caltrans, 1990)

(a)

(b)

Restrainer cables

Restrainer Rod

Gap Allowing Normal Service Motions

Bent
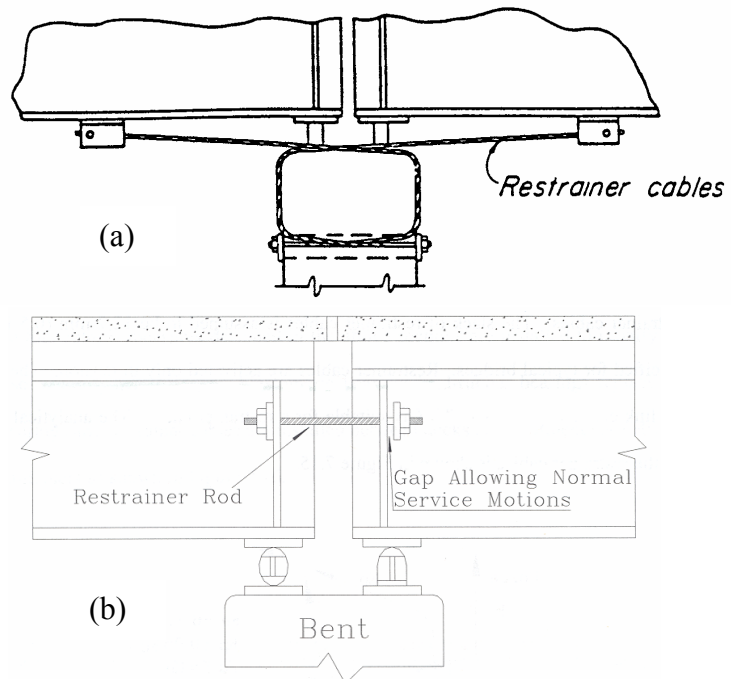
Figure 3.10: Restrainer connection in steel bridges: (a) between deck and pier; (b) deck to

deck
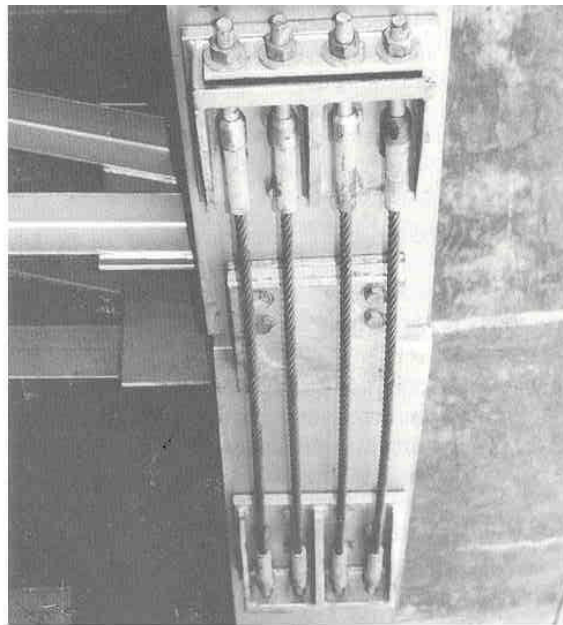
Figure 3.11: Restrainer connection between decks in concrete bridge
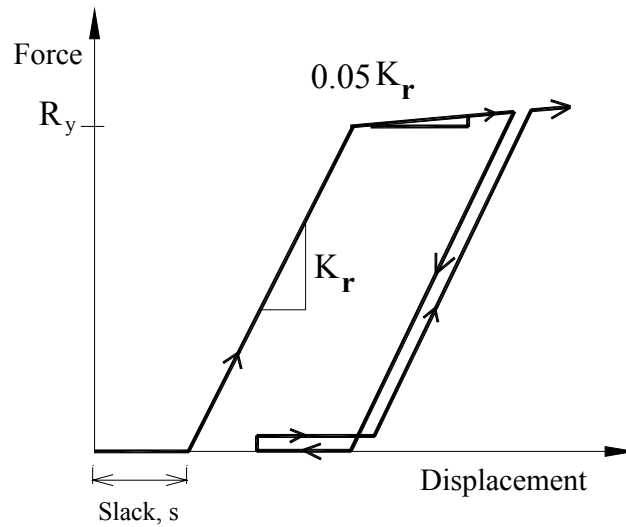
Figure 3.12: Analytical model for cable restrainer

3.2.3 Elastomeric Bearings

Bridge bearings are mechanical devices that transmit loads from the superstructure to the substructure and allow thermal expansion, contraction and rotational movement of the superstructure. Bearings are grouped in two types; fixed bearings and expansion bearings. Fixed bearings resist translation but permit rotation of the superstructure, while expansion bearings allow both rotation and translation. Most bearings are constructed of either steel, neoprene, PFTE (Teflon), bronze or a combination of these materials.

Elastomeric bearings have been used in highway bridge superstructures that undergo large deformations due to thermal expansion. They are made of elastomer (synthetic rubber) that develops adequate strength to support bridge loads. Two types are available as shown in Figure 3.13; plane pads consisting of elastomer only and reinforced bearings that have layers of elastomer and carbon steel molded into a solid void-free mass. When the bearing is loaded under compression, the elastomeric material tends to bulge as

illustrated in Figure 3.14 (a). For unreinforced pads, the bulging restraint is provided by friction between the pad and the bearing surface. In the case of the steel reinforced bearing, the steel laminates provide the bulging restraint under large compressive loads.

Shear deformation of the bearing can also occur as shown in Figure 3.14 (b) due to creep, shrinkage or thermal expansion of the bridge superstructure. The rotation from the girder ends can cause an uneven bulge as depicted in Figure 3.14 (c) that can lead to stability problems if excessive rotations occur. Elastomeric bearings present an attractive alternative to traditional steel bearings, as they limit forces to the substructure, are less susceptible to corrosion and provide more flexibility in terms of both functionality and maintenance. However, the shear stiffness of elastomeric bearings is a function of temperature, with higher stiffness at extremely low temperatures (Roeder et al., 1990). This could potentially lead to a brittle failure when installed in bridges exposed to cold winters.
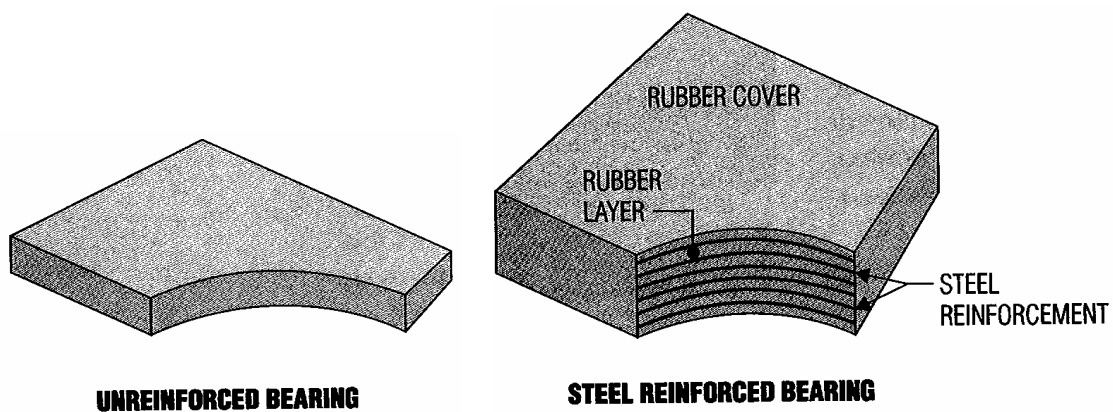
Figure 3.13: Typical elastomeric bearings (Roeder et al., 1991)
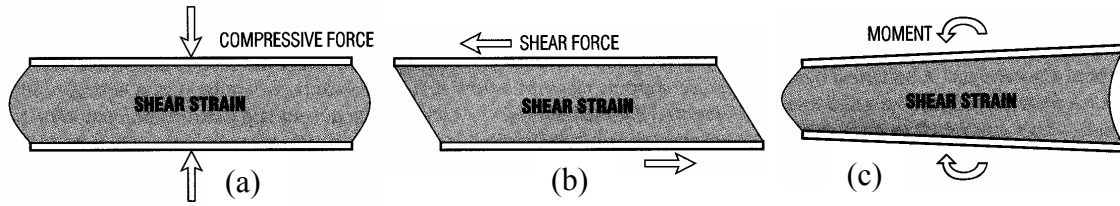
Figure 3.14: Deformation of elastomeric bearings (Roeder et al., 1991)

The elastomeric bearings are modeled using a bilinear element based on Kelly's model with three parameters, the elastic stiffness (K_1), strain hardening stiffness (K_2) and the characteristic strength (Q) as shown in Figure 3.15(a) (Naeim and Kelly, 1999). Experimental tests on elastomeric bearings produced a shear force-deformation relationship as shown in Figure 3.15 (b) (Roeder et al., 1987). From the graph, it can be seen that the ratio of K_1/K_2 is around 3.0.
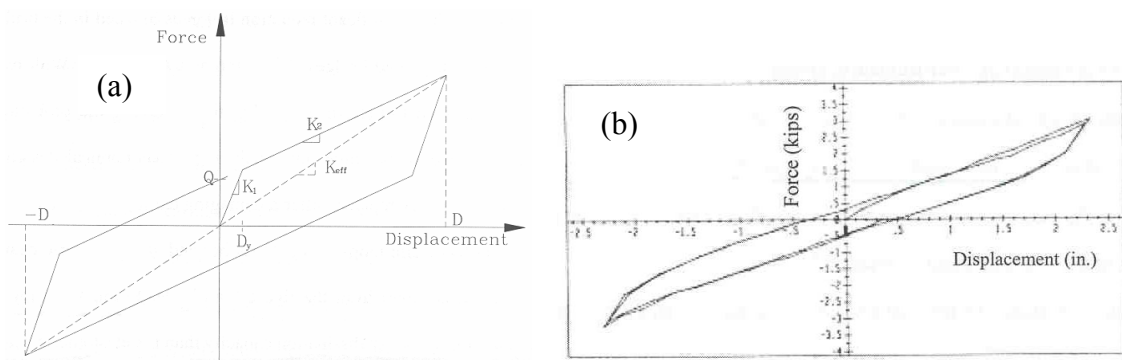
Figure 3.15: (a) Bilinear model for elastomeric bearings; (b) Experimental shear force-displacement relation (Roeder et al., 1987)

The effective stiffness of the bearings can be calculated as:

$$K_{eff} = \frac{GA}{h}$$ (3.18)

where A is the area of the elastomeric bearing, G is the shear modulus of the elastomer, taken as 100 psi (Skinner et al., 1993), and h is the height of the elastomer. The effective stiffness can be related to other parameters, as shown below

$$K_{eff} = K_2 + \frac{Q}{D}$$ (3.19)

where D is the maximum design deformation in the bearing, typically taken equal to the height of the elastomer. The yield displacement can be expressed in terms of the primary parameters as,

$$D_y = \frac{Q}{K_1 - K_2}$$ (3.20)

The yield displacement is typically taken to be one-tenth the maximum deformation (D). Thus, all the primary parameters can be calculated from Equations 3.18-3.20 given the bearing dimensions. In this study, elastomeric bearings are modeled at the intermediate hinge and abutment locations. Table 3.1 presents the properties of elastomeric bearings used herein.

Table 3.1: Properties of elastomeric bearings considered in study

Dimensions (in)	D (in)	D_y (in)	K_{eff} (kip/in)	K_1 (kip/in)	K_2 (kip/in)
12 x 8 x 4	4	0.4	2.4	6.0	2.0
18 x 12 x 6	6	0.6	3.6	9.0	3.0

3.2.4 Abutments

Abutments are the end supports of a bridge whose function is to transfer the reactions from the superstructure to the foundation and to retain the earth embankment of the approach roadway. Abutments consist of a back wall that serves as the principal retaining component, a bridge seat composed of either free-standing pedestals or a continuous breastwall and wingwalls that confine the earth behind. Figure 3.16 illustrates the various types of abutments.
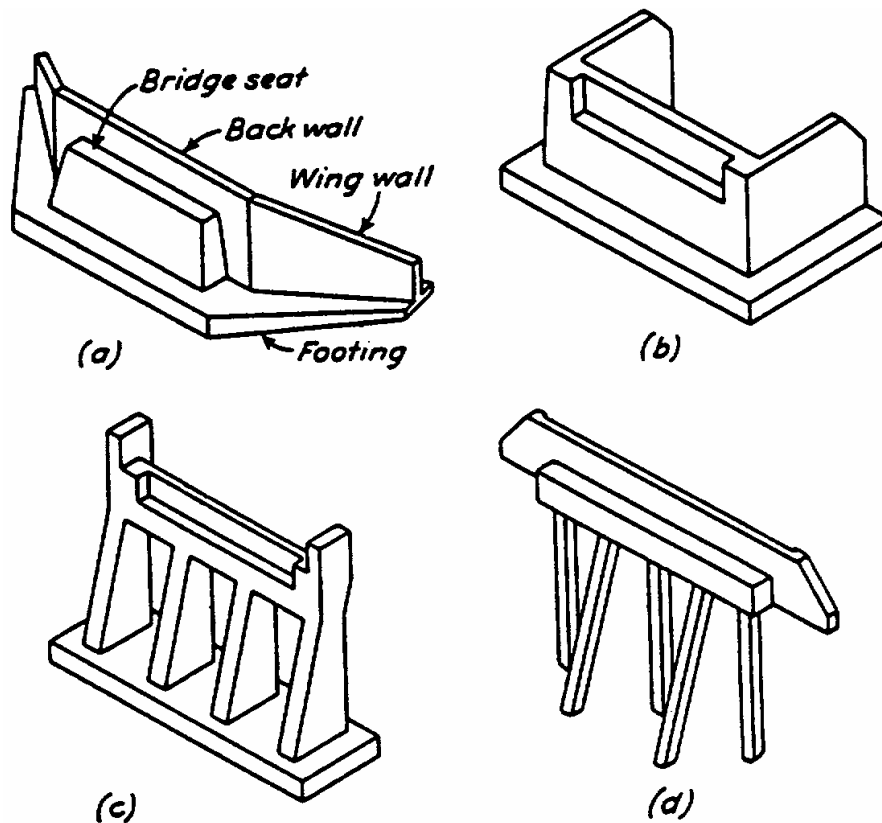
Figure 3.16: Various types of abutments: (a) gravity abutment; (b) U-abutment; (c) spill-through abutment; (d) pile bent abutment (Xanthakos, 1996)

A gravity abutment is constructed of concrete or stone masonry and resists the horizontal earth pressure with its own dead weight. The U-type abutment has wingwalls perpendicular to the backwall, an arrangement that improves overall stability. A spill-through abutment consists of two or more vertical columns with a cap beam on top that supports the bridge seat. The soil is allowed to spill through the open spaces between the columns so that only a portion of the embankment is retained by the abutment. The pile bent abutment consists of a pile cap that acts as the bridge seat, supported by rows of piles. Batter piles are provided to prevent overturning.

Abutments play an important role in the seismic response of a bridge, as they attract a large portion of the earthquake loads and many design guidelines require their inclusion as equivalent linear springs (Caltrans, 1999; AASHTO-83, 1988). Pile bent abutments are considered in this study. The resistance in the passive direction (compression) is provided by both the soil and piles but the resistance in the active direction (tension) is provided by the piles alone. The stiffness of the piles is taken as 40 kips/in/pile based on the Caltrans recommendation. The analytical model for abutments developed in this study is shown in Figure 3.17. Linearized springs are employed with different stiffness in the active and passive directions. Inertial effects due to the abutment mass are not considered.
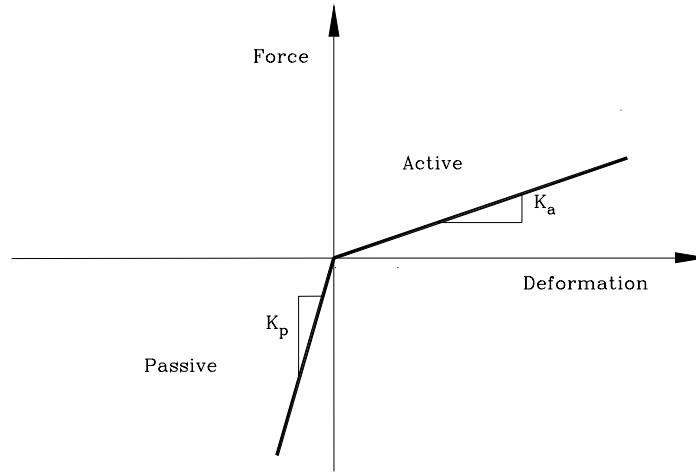
Figure 3.17: Analytical model for abutment action

3.2.5 Impact elements

Seismic pounding of bridge decks at the intermediate hinges and abutments can alter the response of the bridge significantly. The various analytical models used to account for bridge deck impact were discussed in Section 2.2. All the analytical models described therein are considered for modeling impact, including the linear spring, Kelvin model, Hertz nonlinear spring and the stereomechanical approach. A Hertz spring with hysteresis damper introduced in Chapter 4 is also evaluated.

In this study, seismic pounding is accounted for at the intermediate hinge locations only. Impact between the bridge deck and abutments is not explicitly considered. This is because, several of the impact models including the stereomechanical approach and Kelvin-Voigt solid need to know the masses of the colliding bodies. In this work, abutments are modeled as linearized springs with no mass. Since, pounding at the

abutment will induce high passive pressures, the effect of deck impact is considered indirectly by including a high passive stiffness in the abutment model.

3.3 Validation of the numerical MATLAB model

In this section, the numerical model is validated by comparing its responses with those from DRAIN-2DX (Prakash et al., 1992), a popular software for planar nonlinear dynamic analysis of structures. A multiple-frame bridge with two frames is considered, as depicted by Figure 3.18 with frame weights of 2880 k and 7080 k. The properties of the various bridge components are listed in Table 3.2. To enable comparison with DRAIN-2DX, a bilinear force-deformation relation, with 5% strain hardening is chosen for the frames and Rayleigh damping is used with a damping ratio of 5%. The restrainers are designed according to the design procedure suggested by DesRoches and Fenves (DesRoches and Fenves, 2001). The restrainer slack is assumed as ½ in.
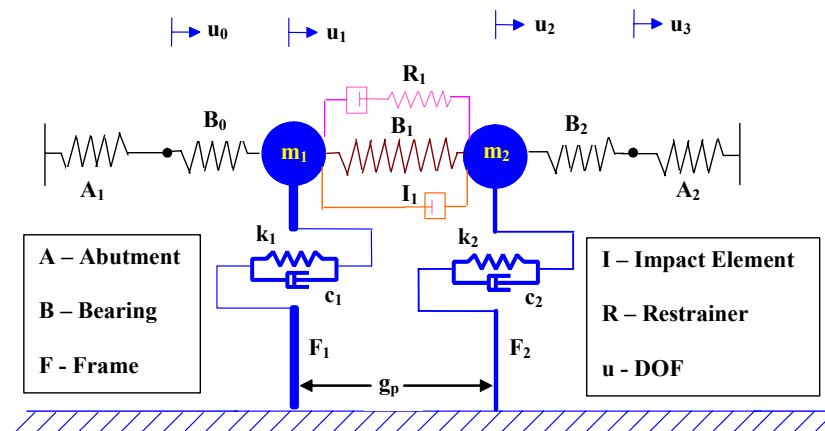
Figure 3.18: Multiple-frame bridge used in test case study

Table 3.2: Properties of various elements in the bridge model

Element	Component	Initial stiffness (kips/in)	Yield strength (kips)	Period (s)
Frame	F_1	1333	814	0.47
	F_2	577	853	1.12

Element	Component	Initial stiffness (kips/in)	Yield strength (kips)	Strain hardening (%)
Restrainer	R_1	850	935	5
Bearing	B_1	6	2.4	33
	B_0, B_2	2600	1560	33

Element	Component	Active stiffness (kips/in)	Passive stiffness (kips/in)
Abutment	A_1, A_2	10	2600

The bearings at the abutment locations are designed to have a stiffness proportional to the passive stiffness of the abutment. The active stiffness of the abutment is taken proportional to the typical hinge bearing stiffness. Pounding is modeled using a linear spring with a stiffness, $K_l = 25,000$ kip/in. Two cases are considered for comparison; Case 1, where the hinge gap is set large so that pounding does not occur and Case 2, where the hinge gap is taken as ½ inch and pounding occurs. The bridge is subjected to the 1940 El Centro record, which has a peak ground acceleration of 0.35 g.

Figures 3.19-3.21 present the comparison of results from the numerical procedure with DRAIN-2DX, for the no-pounding case. The comparisons for the pounding case (Case 2) are presented in Figures 3.22-3.24. All the responses show excellent agreement, thus validating the solution strategy of the numerical model.
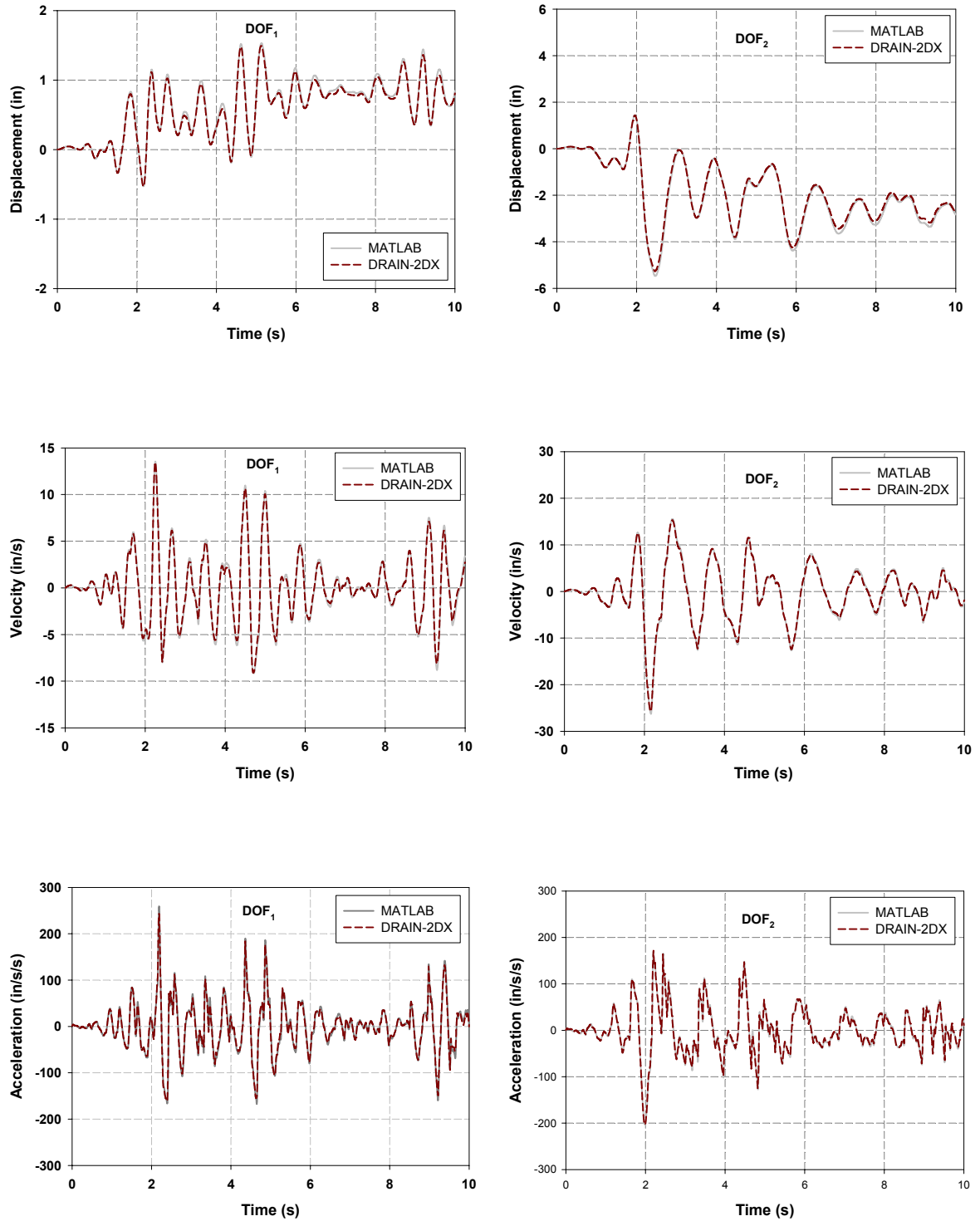
Figure 3.19: Comparison of numerical model results with DRAIN-2DX for inelastic two-frame bridge; Case 1 (no pounding) – 1940 El Centro record
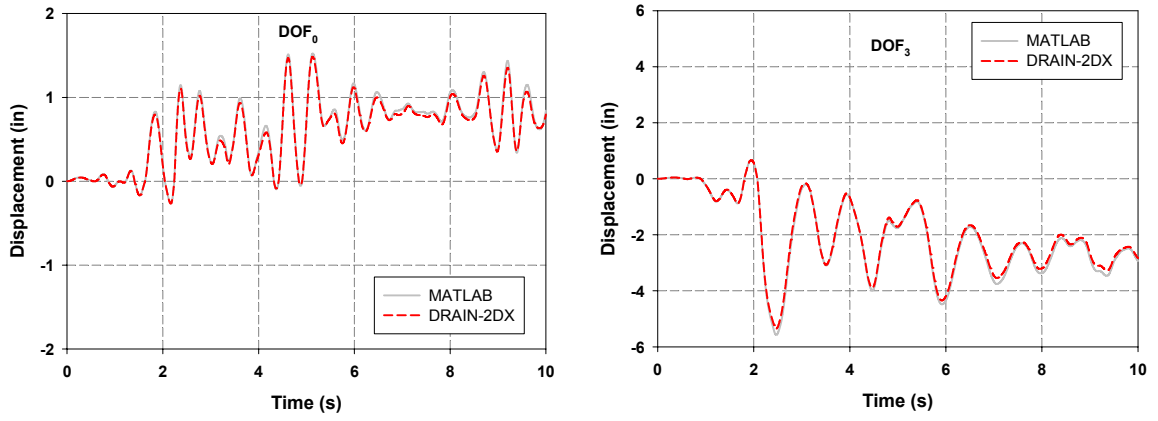
Figure 3.20: Comparison of displacements at DOFs 0, 3 for inelastic two-frame bridge;

Case 1 (no pounding); 1940 El Centro record
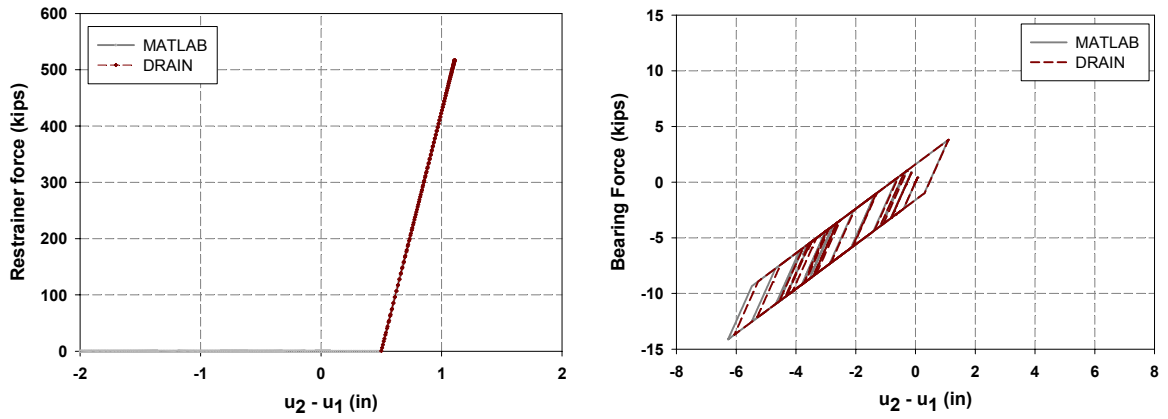
Figure 3.21: Comparison of restrainer and bearing (B_1) force-deformation relationships

for inelastic two-frame bridge; Case 1 (no pounding) - 1940 El Centro record
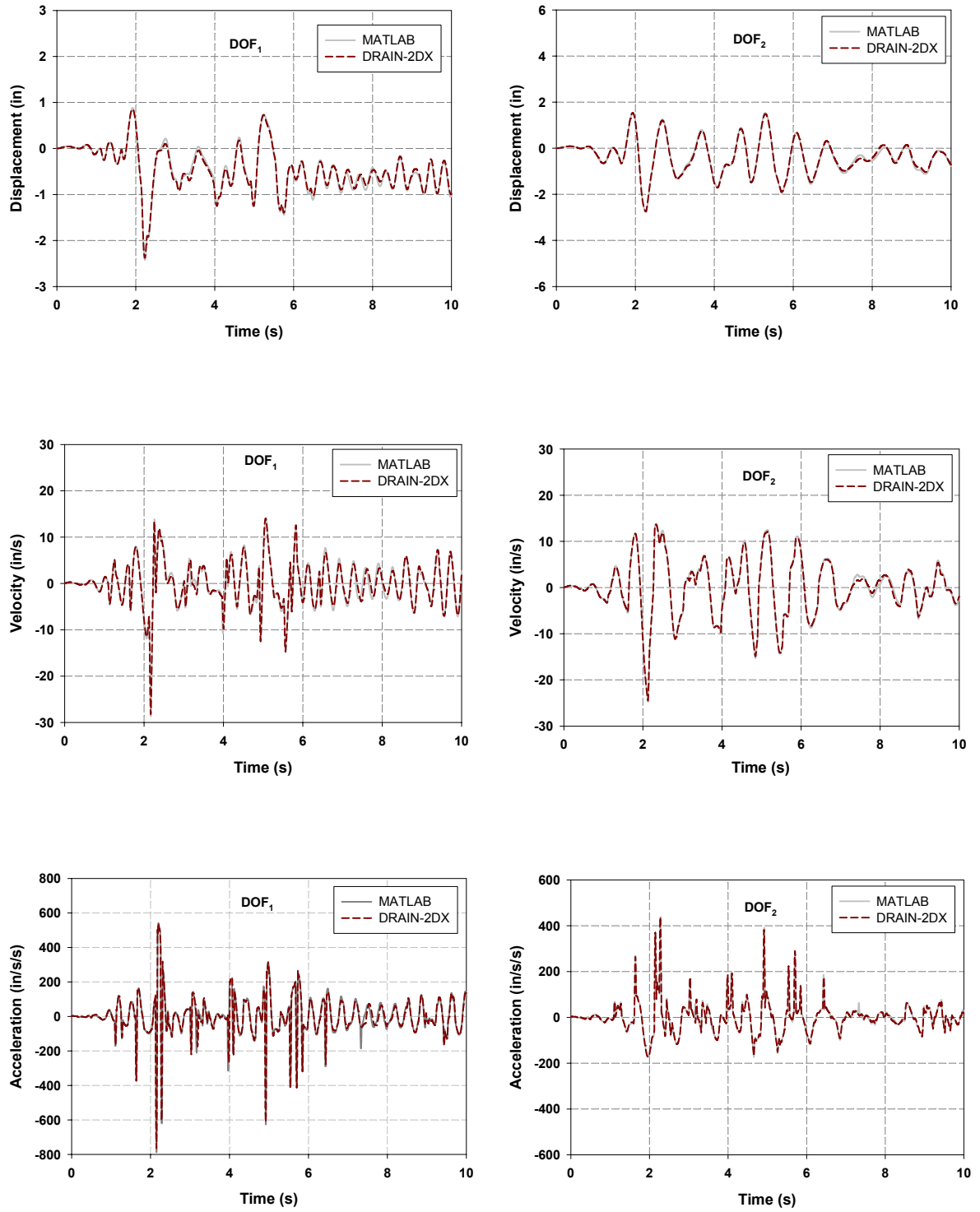
Figure 3.22: Comparison of numerical model results with DRAIN-2DX for inelastic two-

frame bridge; Case 2 (with pounding) – 1940 El Centro record
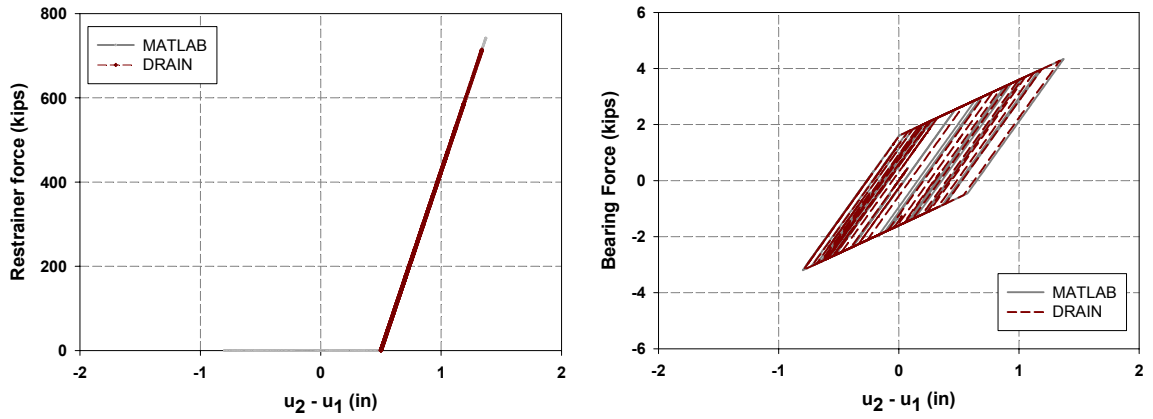
Figure 3.23: Comparison of restrainer and bearing (B$_1$) force-deformation relationships

for inelastic two-frame bridge; Case 2 (with pounding) - 1940 El Centro record
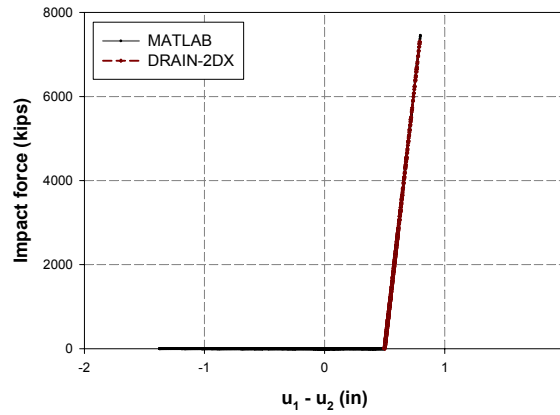
Figure 3.24: Comparison of impact element force-deformation relation for inelastic two-

frame bridge; Case 2 (with pounding) – 1940 El Centro record

CHAPTER 4

PARAMETERS AFFECTING THE BRIDGE POUNDING RESPONSE

In order to mitigate pounding damage in bridges, it is important to determine the factors affecting the pounding response. Past research has shown that the forces acting on the piers and deck deformations increase as a result of pounding (Jankowski et al., 1998; Pantelides and Ma, 1998). However, a study by Malhotra (1998) showed that a multi-span concrete box girder bridge with an adjacent frame stiffness ratio of 1.14 had a reduction in response due to pounding. Other researchers have suggested that pounding generally reduces the response of the bridge frames because of the energy dissipated during pounding and because pounding disrupts the buildup of resonance (Priestly et al., 1996).

Other studies have evaluated mitigation strategies for pounding in bridges. Kim et al. (2000) found that restrainers reduce the relative displacements between pounding frames and prevent the collapse of spans. Several researchers have shown that shock absorbers, connectors with high damping or stiffness and energy dissipation devices are effective in mitigating the pounding effects in bridges (Kawashima & Yabe, 1996; Jankowski et al., 1999; Kawashima and Shoji, 2000).

As mentioned, the effect of pounding on bridge response has led to conflicting results. A comprehensive study is performed in this chapter to better understand the parameters affecting pounding, and to investigate the effects of restrainers and yielding frames on the demands in bridges. The stereomechanical approach is used to simulate impact, with the coefficient of restitution (e) being taken as 0.8.

4.1. Preliminary investigations into dynamic impact

A sample pounding analysis is performed to comprehend the effects of deck impact on the bridge response. The seismic response of adjacent frames in a typical multiple-frame bridge shown in Figure 4.1 is considered. The bridge is subjected to the 1940 El Centro earthquake, scaled to 0.70g to coincide with typical design response spectra. To simplify the analysis and better understand the factors affecting pounding, only single-sided pounding is considered (i.e., effects of abutments or adjacent frames are ignored). The effects of bearings and restrainers are also not considered.
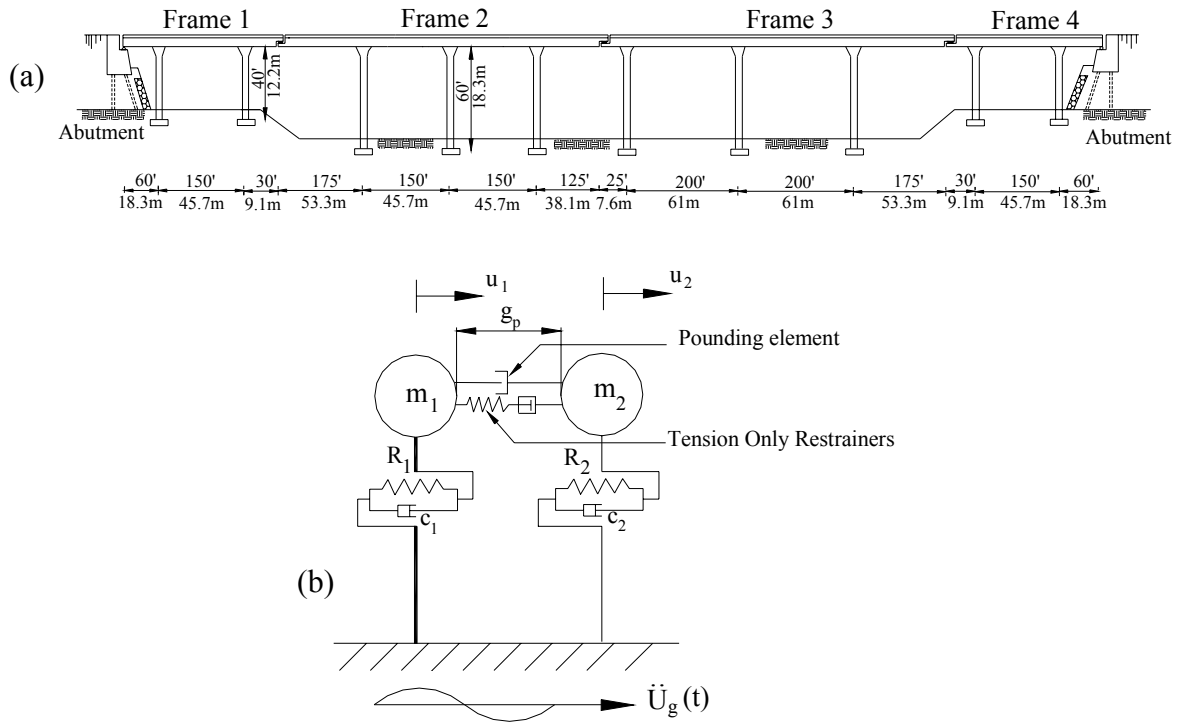
Figure 4.1: (a) Typical multiple-frame bridge; (b) model idealization

Two cases are evaluated: a case with a frame period ratio of $T_1/T_2 = 0.32$, and a case with a frame period ratio of $T_1/T_2 = 0.71$. Case 1 represents the response of highly out-of-phase frames, and case 2 represents the response of slightly out-of-phase frames. In both cases, the modes are assigned 5% critical damping, and the frames have a gap of 12.5 mm (½ in). The frames are designed to have an individual displacement ductility demand of $\mu = 4.0$, for the scaled 1940 El Centro record.

Figure 4.2 presents the time history of frame displacements for the no-pounding and pounding studies for case 1 ($T_1/T_2 = 0.32$). The comparison shows that pounding significantly increases the maximum displacement of the stiff frame from 15 mm for the no-pounding case, to over 40 mm for the case when the frames are pounding. Conversely, for the flexible frame, pounding reduces the displacement from 130 mm in the no-pounding case to 90 mm when the frames pound. The flexible frame, which has a larger displacement, pounds the stiff frame increasing its response. Similarly, the stiff frame acts as a barrier to the flexible frame, thereby limiting the flexible frame response.

Figure 4.3 shows the same analysis, except the stiffness of frame 1 has been modified such that the frames now have a frame period ratio of $T_1/T_2 = 0.71$. A comparison of the pounding and no-pounding response shows that the effect of pounding is considerably reduced in this case. For the stiff frame, pounding increases the response from 72 mm to 100 mm. For the flexible frame, the pounding and no-pounding maximum absolute displacements are nearly identical (approximately 125 mm).
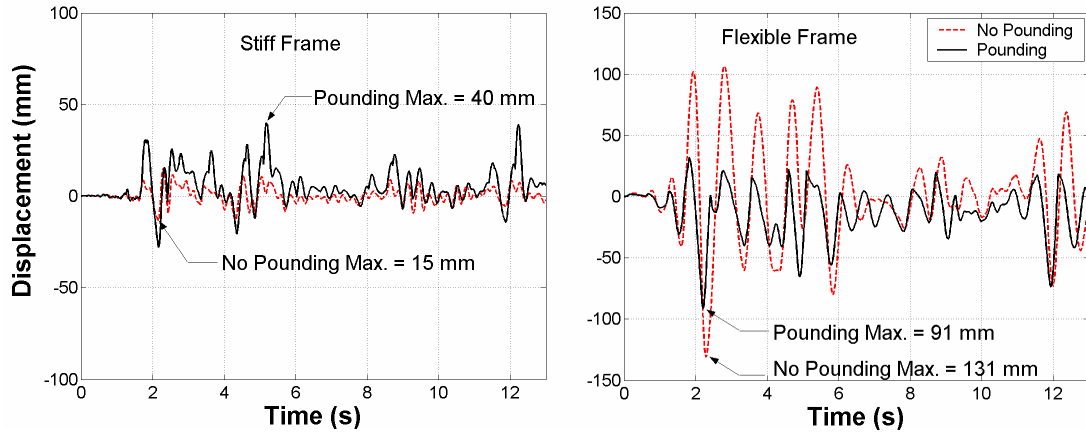
Figure 4.2: Time history of frame displacements for the pounding and no-pounding studies. Inelastic frames ($T_1/T_2 = 0.32$); El Centro record scaled to 0.7 g
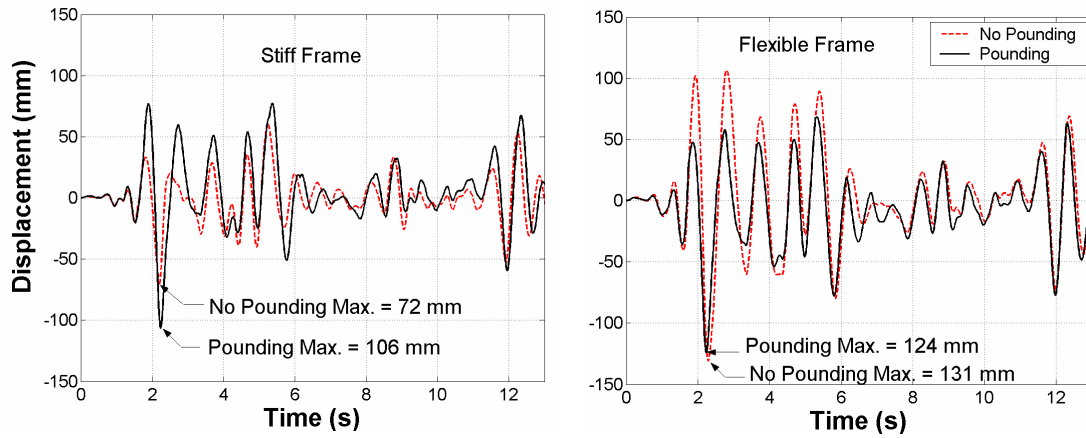
Figure 4.3: Time history of frame displacements for the pounding and no-pounding studies. Inelastic frames ($T_1/T_2 = 0.71$); El Centro record scaled to 0.7 g

4.2. Identification of the parameters affecting seismic pounding

The case study performed in the previous section illustrated the dramatic effect of frame period ratio on the response of pounding bridge frames. However, it is not clear what effect other parameters, such as ground motion characteristics, have on the response of pounding frames. In addition, bridges that have been retrofitted with restrainers may have a different pounding response than those without restrainers. Past research has shown that frame stiffness ratios, earthquake loading, hinge gap, frame yield strength and restrainer stiffness are important factors in determining the effects of pounding in bridges (DesRoches and Fenves, 1997a). Secondary factors that affect the pounding response include the coefficient of restitution, relative masses of impacting structures and the impact spring stiffness. It has been shown that the relative mass does not play a significant role as long as the differences in the structure periods result from the differences in stiffness (Athaniassiadou et al., 1994; Trochalakis, 1997).

In order to identify the primary factors affecting the pounding response of adjacent bridge frames, a two degree-of-freedom system with frame stiffnesses, K_1, K_2 and restrainers is considered, as shown in Figure 4.1(b). The equations of motion governing the system response due to seismic input can be written as:

$$\begin{bmatrix} m_1 & 0 \\ 0 & m_2 \end{bmatrix} \begin{Bmatrix} \ddot{u}_1 \\ \ddot{u}_2 \end{Bmatrix} + \begin{bmatrix} c_1 & 0 \\ 0 & c_2 \end{bmatrix} \begin{Bmatrix} \dot{u}_1 \\ \dot{u}_2 \end{Bmatrix} + \begin{Bmatrix} F_{F_1}(u_1) \\ F_{F_2}(u_2) \end{Bmatrix} - \begin{Bmatrix} F_{R_1}(u_2 - u_1) \\ -F_{R_1}(u_2 - u_1) \end{Bmatrix} = - \begin{bmatrix} m_1 \\ m_2 \end{bmatrix} \ddot{u}_g \qquad (4.1)$$

where m_i is the mass of each frame, c_i is the frame damping coefficient, F_{Fi} is the frame restoring force, F_{R1} is the force in the restrainer and $\ddot{u}_g$ is ground acceleration. Pounding is modeled using the stereomechanical approach, with e = 0.8. Dividing each equation by the respective frame yield displacement, $u_{y_i} = F_{F_{y_i}}/K_i$ gives

$$\begin{bmatrix} m_1 & 0 \\ 0 & m_2 \end{bmatrix} \begin{Bmatrix} \ddot{\mu}_1 \\ \ddot{\mu}_2 \end{Bmatrix} + \begin{bmatrix} c_1 & 0 \\ 0 & c_2 \end{bmatrix} \begin{Bmatrix} \dot{\mu}_1 \\ \dot{\mu}_2 \end{Bmatrix} + \begin{Bmatrix} \dfrac{F_{F_1}(u_1)}{u_{y_1}} \\ \dfrac{F_{F_2}(u_2)}{u_{y2}} \end{Bmatrix} - \begin{Bmatrix} \dfrac{F_{R_1}(u_2-u_1)}{u_{y_1}} \\ \dfrac{-F_{R_1}(u_2-u_1)}{u_{y2}} \end{Bmatrix} = - \begin{bmatrix} \dfrac{m_1}{u_{y_1}} \\ \dfrac{m_2}{u_{y2}} \end{bmatrix} \ddot{u}_g \quad (4.2)$$

where $\mu_i = u_i/u_{y_i}$ is the frame displacement ductility factor. Equation 4.2 is divided by m_2 and the following terms are defined: mass ratio, $\lambda = m_1/m_2$; frequency ratio, $\Omega = \omega_2/\omega_1$; normalized force-deformation relation, $\tilde{F}_{F_i}(\mu_i) = F_{F_i}(u_i)/F_{F_{y_i}}$; frame strength ratio, $\eta_i = F_{F_{y_i}}/m_i \ddot{u}_{g_{max}}$; and the normalized ground acceleration, $\tilde{\ddot{u}}_g(t) = \ddot{u}_g/\ddot{u}_{g_{max}}$. Using the standard expressions, $\omega_i = \sqrt{K_i/m_i}$, and $c_i = 2\xi_i m_i \omega_i$, equation (4.2) becomes:

$$\begin{bmatrix} \lambda & 0 \\ 0 & 1 \end{bmatrix} \begin{Bmatrix} \ddot{\mu}_1 \\ \ddot{\mu}_2 \end{Bmatrix} + \begin{bmatrix} \dfrac{2\lambda\xi_1\omega_2}{\Omega} & 0 \\ 0 & 2\xi_2\omega_2 \end{bmatrix} \begin{Bmatrix} \dot{\mu}_1 \\ \dot{\mu}_2 \end{Bmatrix} + \begin{Bmatrix} \dfrac{\tilde{F}_{F_1}(\mu_1)\omega_2^2\lambda}{\Omega^2} \\ \tilde{F}_{F_2}(\mu_2)\omega_2^2 \end{Bmatrix} - \begin{Bmatrix} \dfrac{F_{R_1}(u_2-u_1)}{m_2 u_{y_1}} \\ \dfrac{-F_{R_1}(u_2-u_1)}{m_2 u_{y2}} \end{Bmatrix} = - \begin{bmatrix} \dfrac{\lambda\omega_1^2}{\eta_1} \\ \dfrac{\omega_2^2}{\eta_2} \end{bmatrix} \tilde{\ddot{u}}_g \quad (4.3)$$

To simplify the normalized restrainer term in the above equation, the restrainers are assumed to be elastic. This simplification is justified because design procedures require the restrainers to remain elastic. The restrainers engage after the slack, s, is exhausted and the restrainer force can be expressed as:

$$F_{R_1} = K_r \left[(u_2 - u_1) - s \right] \quad (4.4)$$

where K_r is the restrainer stiffness. Substituting equation 4.4 into (4.3) and isolating the restrainer term in the normalization, the normalized restrainer force is given by,

$$F_{R_{norm}} = \frac{K_r}{m_2 u_{y_1}} \left[(u_2 - u_1) - s \right] \quad (4.5)$$

Further normalization of (4.5) results in:

$$F_{R_{norm}} = \frac{K_r}{K_2} \omega_2^2 \left[\left(\frac{\mu_2}{\Omega^2 \tilde{\eta}} - \mu_1 \right) - \frac{s}{u_{y_1}} \right]$$ (4.6)

where $\tilde{\eta} = \eta_1 / \eta_2$ is the ratio of the frame strength ratios. In order to involve both the frame stiffnesses in the above equation, the numerator and denominator are divided by the flexibilities of the two frames, $\dfrac{1}{K_{mod}} = \dfrac{1}{K_1} + \dfrac{1}{K_2}$ which results in the following:

$$F_{R_{norm}} = \omega_2^2 \kappa \left(\frac{1}{1 + \dfrac{\Omega^2}{\lambda}} \right) \left[\left(\frac{\mu_2}{\Omega^2 \tilde{\eta}} - \mu_1 \right) - \frac{s}{u_{y_1}} \right]$$ (4.7)

where $\kappa = K_r / K_{mod}$.

From equations 4.3 and 4.7, it can be observed that the frequency of frame 2, ω_2, is the only term that is not normalized. This is rectified by relating ω_2 (or T_2) to the characteristic period of the ground motion, T_g. The characteristic period of a ground motion is defined as the period at which the input energy of a 5% damped linear elastic system is a maximum (Miranda and Bertero, 1994). Based on the above normalizations, the primary parameters affecting the pounding response are identified as the mass ratio, λ, the frame period ratio, T_1/T_2 (or frequency ratio ω_2/ω_1), ground motion period ratio, T_2/T_g, restrainer stiffness ratio, κ, and the frame ductility ratio, μ. The ratio of frame strength ratios ($\tilde{\eta}$) can be related to the frame ductility ratios, μ_1, μ_2, as shown below.

$$\tilde{\eta} = \frac{u_1}{u_2} \frac{\mu_2}{\mu_1} \frac{1}{\Omega^2}$$ (4.8)

In addition, the hinge gap is also considered and is expressed in terms of a gap ratio parameter, χ, as given in equation 4.9.

$$g_p = \chi * D_{np}$$ (4.9)

64

where D_{np} is the relative displacement of the hinge when pounding of the frames does not occur. $\chi = 1.0$ corresponds to the critical gap; i.e. the gap which is just sufficient to preclude pounding.

4.2.1. Effect of principal parameters on the pounding response – A case study

Having determined the factors affecting pounding, a case study is conducted with the simplified model shown in Figure 4.1(b), to evaluate the effect of various parameters on the system response. The mass ratio of the frames (λ) is taken as unity and elastic frames are considered ($\mu = 1$). Restrainers are not included ($\kappa= 0$). Table 4.1 lists the values of all parameters used in this case study.

Previous earthquakes have shown the relative hinge displacement in bridges subject to strong ground motion ranges from 5 in. to 15 in. (DesRoches and Fenves, 1997a). Since typical hinge gaps are approximately ¼ - ½ in., this results in a range of gap ratios from 0.02 to 0.10. Preliminary studies showed small differences in bridge response for gap ratios in this range. Therefore, to simplify the analysis, the gap parameter, χ, is set at 0.02 for further investigations.

Table 4.1: Pounding parameters and range of values for case study

Parameter	Values
Frame mass ratio, λ	1.0
Frame stiffness ratio, K_1/K_2	1.05, 2.0, 3.0, 4.0, 5.0, 6.0, 7.0, 8.0, 9.0, 10.0
Ground motion period ratio, T_2/T_g	0.25, 0.35, 0.5, 0.75, 1.0, 1.25, 1.5, 1.75, 2.0, 2.25, 2.5, 2.75, 3.0, 3.25, 3.5, 4.0, 4.5, 5.0
Gap ratio, χ	0.02
Frame ductility ratio, μ	1.0
Coefficient of restitution, e	0.8

The frames are subjected to the set of ground motions listed in Table 4.2. All the records are scaled to 0.7g peak ground acceleration, to coincide with typical design response spectra. The input records cover a wide range of characteristic periods (T_g), and peak ground accelerations (PGA), and are of magnitude six or greater. The effect of pounding is expressed in terms of the displacement amplification (γ), which is the ratio of the maximum pounding frame displacement to the maximum frame displacement if pounding does not occur.

Table 4.2 Free-field ground motions used in study

No.	Earthquake record	Location	M_s[a]	PGA[b] (g)	T_g[c] (sec)
(1)	(2)	(3)	(4)	(5)	(6)
1	1940 Imperial Valley	El Centro*	6.9	0.35	1.00
2	1989 Loma Prieta	Saratoga	7.1	0.47	0.40
3	1989 Loma Prieta	Holister*	7.1	0.37	1.03
4	1992 Landers	Baker Fire	7.5	0.11	1.70
5	1994 Northridge	Sylmar*	6.7	0.83	1.60
6	1994 Northridge	Taff	6.7	0.22	0.90
7	1994 Northridge	Pacoima Dam*	6.7	0.50	0.42
8	1994 Northridge	Lake Hughes	6.7	0.27	0.50
9	1994 Northridge	Lake Obrego Pk.	6.7	0.45	0.41
10	1995 Kobe	Kobe*	6.9	0.85	0.88
11	1995 Kobe	Osaka	6.9	0.08	1.17

[a]Magnitude; [b]Peak Ground Acceleration; [c]Characteristic Period; * - used in inelastic analyses

Figure 4.4 presents the average amplification in frame displacements, as a function of the stiffness ratio (K_1/K_2) and the ground motion period ratio (T_2/T_g), for the ground motions records specified in Table 4.2. For lower T_2/T_g ratios ($T_2/T_g < 1$), the stiff frame

response is amplified due to pounding and flexible frame response is reduced. However, for higher T_2/T_g ratios, the flexible frame amplification is greater than one. Furthermore, seismic pounding amplifies both the frame responses when T_2/T_g is around 1.5 and K_1/K_2 is greater than 3. These observations are in contradiction with the general trend that pounding amplifies the stiff frame response and reduces the flexible frame response, and needs further investigation.
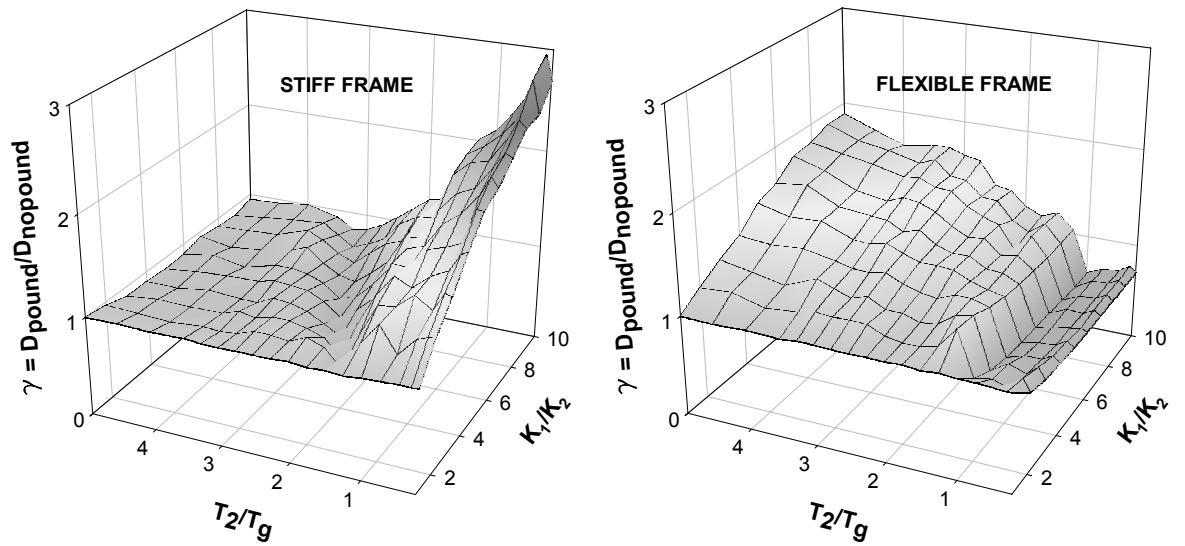
Figure 4.4: Average amplification in the frame response due to pounding; $\chi = 0.02$; 11 ground motion records

4.3. Parameter study

The earlier section identified the important parameters affecting the bridge pounding response as the frame stiffness ratio (K_1/K_2) or period ratio (T_1/T_2), the ground motion period ratio (T_2/T_g), restrainer stiffness ratio, κ, and the frame ductility ratio, μ. To the

author's knowledge, this is the first study that recognizes the ground motion period ratio as a significant pounding parameter. A case study conducted earlier with K_1/K_2 and T_2/T_g as parameters, illustrated pounding trends that are contrary to the general expectations. Hence, a thorough parameter study is conducted herein, to better understand the effects of the various parameters on the pounding response. Both elastic and inelastic systems are considered, with the Q-Hyst model being used for the frame force-deformation relation. The following values are used for the various parameters: $\lambda = 1$, $K_1/K_2 = 2, 4, 8, 10$, $T_2/T_g = 0.25 - 5.00$ with 0.05 increments, $\chi = 0.02$, $\mu = 1, 4$, $\kappa = 0, 0.5$, and 1.0, e = 0.8. The ground motion records listed in Table 4.2 are used for analyses.

4.3.1. Elastic response

The pounding response of elastic systems with no restrainers is considered first. The displacement amplification due to pounding as a function of T_1/T_2 and T_2/T_g is investigated. Figure 4.5 shows a plot of the mean displacement amplification as a function of T_1/T_g and T_2/T_g for four values of T_1/T_2. Thin dashed lines indicate the variability in response, in terms of mean $\pm$ 1 standard deviation.

Pounding reduces the frame response when vibrating at a period near the characteristic period of the ground motion record (T_g). For example, when $T_2/T_g = 1$, the response of the flexible frame is reduced, while the response of the stiff frame is amplified. The significant reduction is observed since pounding prevents the build-up of resonance energy in the frame subjected to input at its resonant frequency. Similarly, at $T_1/T_g = 1$, the response of the stiff frame (Frame 1) is reduced while that of the flexible frame (Frame 2) is amplified.
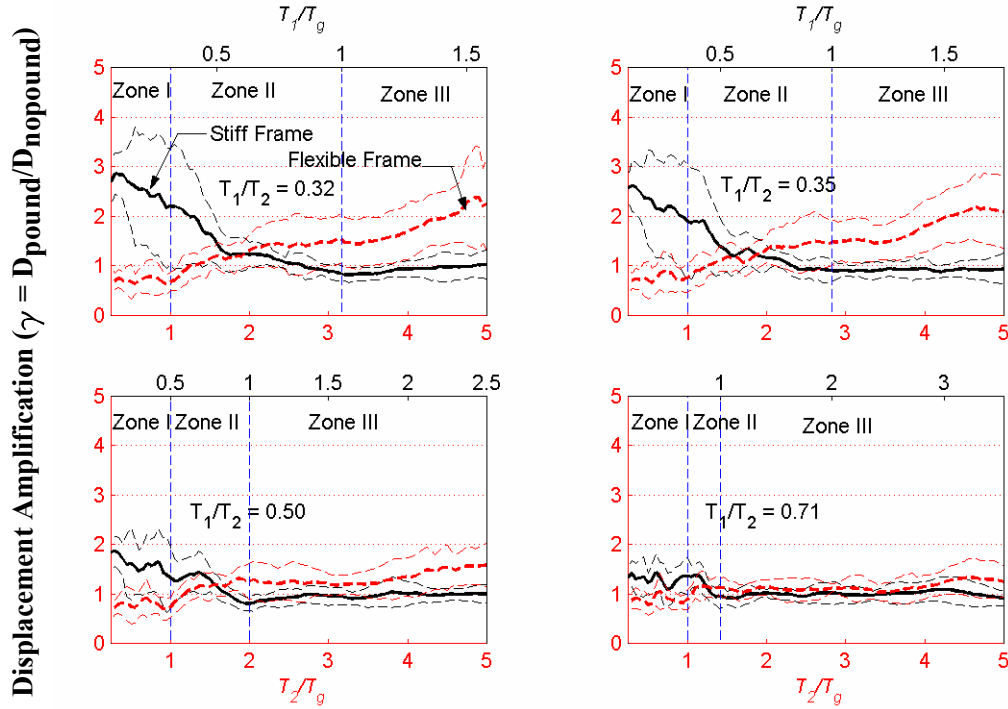
Figure 4.5: Mean ± 1 standard deviation displacement amplification for elastic frames –

11 earthquake records scaled to 0.7g.

The displacement amplification plot has three distinct zones. In Zone I, where $T_2/T_g <$ 1, the stiff frame amplification is greater than one and the flexible frame amplification is less than one. The mean response of the stiff frame is increased by as much as 180% and the flexible frame's mean response is reduced by 30% in Zone I, for $T_1/T_2 = 0.32$. In Zone III, when $T_1/T_g > 1$, the flexible frame response increases and the stiff frame response is reduced. In Zone II, $T_1/T_g < 1 < T_2/T_g$ the frame displacement amplification is slightly greater than one for both the frames. The coefficient of variation (COV) defined as the ratio of the standard deviation to the mean can be as high as 57% for the stiff frame and 52% for the flexible frame when $T_1/T_2 = 0.32$. In general, the displacement amplification decreases as the frame period ratio approaches unity, for all values of T_2/T_g,

as shown in Figure 4.5. For the case with $T_1/T_2 = 0.71$ ($K_1/K_2 = 2.0$), only slight displacement amplifications of the stiff frame are observed for the entire range of T_2/T_g values. The maximum increase in the stiff frame's mean response is 43% which is much less than that observed for $T_1/T_2 = 0.32$.

4.3.2. Effect of frame yielding

The response of any structure subjected to strong ground shaking often extends into the inelastic range and can be significantly different from the corresponding linear response. The inelastic behavior of the frame is characterized by a force-deformation relationship, which is an idealization of the actual behavior of the frame during cyclic load. The yield force of the frame (F_y) is established by dividing the elastic force demand (F_e) by a yield reduction factor R_y, in order to obtain a specified target ductility (μ), using a constant ductility spectrum.

To adequately represent the frame period ratio for all the yielding frames, the frame period is written using the effective stiffness, K_{eff}, where $K_{eff} = K/\mu$. Therefore, the effective frame period ratio, T_{2eff} can be written as:

$$T_{2_{eff}} = 2\pi\sqrt{\frac{m}{K_{eff}}} = 2\pi\sqrt{\frac{m}{K/\mu}} = T_2\sqrt{\mu} \tag{4.10}$$

where T_2 is the period of the flexible frame in the elastic range. In order to enable comparison with the linear behavior of the frames, both the frames are designed for the same target ductility of $\mu = 4$. Thus, the frame period ratio remains as T_1/T_2 and is varied as done in the linear study. The ground motion effective period ratio T_{2eff}/T_g is varied from 0.25 to 5.0 s in increments of 0.05 s. The reduction factors necessary to maintain a

constant frame ductility depend on the frame period. An iterative procedure is used to determine the reduction factors required to give $\mu = 4$ for the individual frame response. The frames are subjected to five ground motion records, as indicated in Table 4.2. Figure 4.6 presents the pounding and no-pounding responses for inelastic frames with no restrainers, bearings or abutments. Displacement amplification and ductility demand are presented.
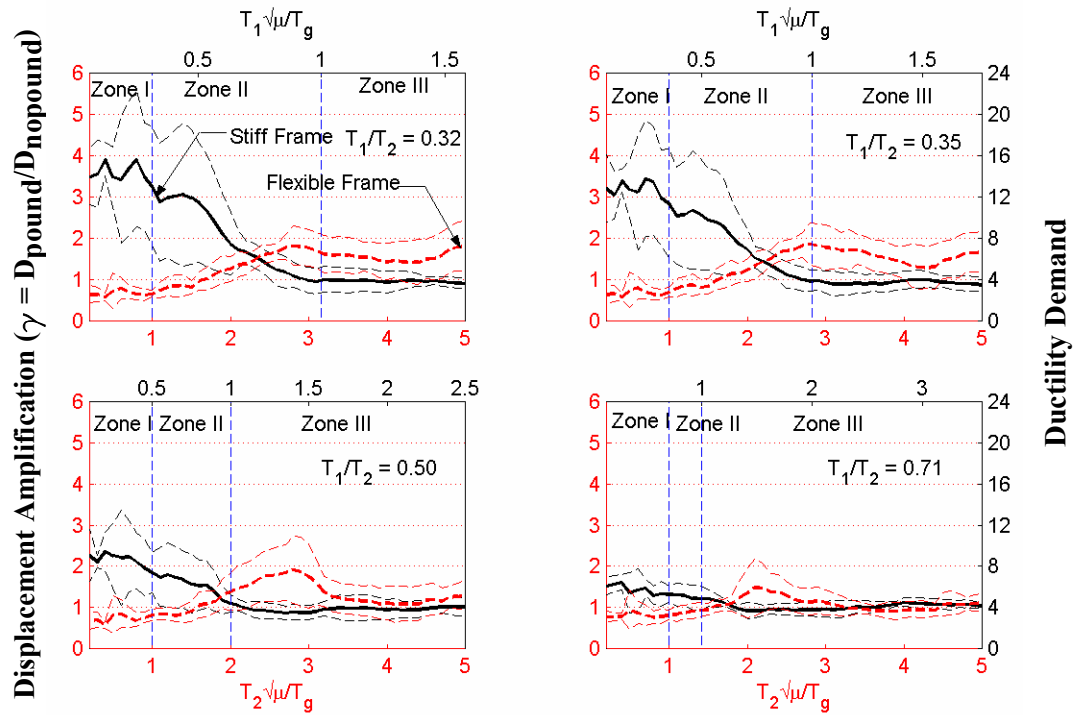
Figure 4.6: Mean and variation in displacement demand for inelastic frames; five earthquake records scaled to 0.7g.

As observed in the linear case, pounding is more critical for highly out-of-phase frames. Pounding reduces the frame response when the effective frame period (T_{eff}) is close to the characteristic period of the earthquake (T_g). The displacement amplification curves due to pounding can once again be classified into three zones depending on the effective ground motion period ratio.

Zone I covers the region where $T_{2eff}/T_g \leq 1.0$. The stiff frame ductility demand is increased by as much as 300% and the flexible frame ductility demand is reduced by approximately 40% in Zone I, for $T_1/T_2 = 0.32$ ($K_1/K_2 = 10$). The maximum COVs for the stiff and flexible frames are 57% and 58% respectively. The elastic frames had a corresponding Zone I displacement increase of 180% for the stiff frame and a reduction of 30% for the flexible frame.

Zone II exhibits an increase in both frame ductility demands, as observed for the displacement amplification in the linear study. Zone III shows similar behavior to the elastic cases. However, the increase in the flexible frame demand is slightly less in the inelastic behavior of the frames than exhibited in the corresponding linear study. This effect is attributed to yielding and hysteretic damping. The yielding of the frames results in a smaller relative velocity before impact than if they were elastic, and thus the pounding response is reduced. The hysteretic behavior of the frames in the nonlinear range results in significant energy dissipation that could also affect the pounding response. The effects of pounding are less pronounced when $K_1/K_2 = 2.0$ ($T_1/T_2 = 0.71$), similar to the elastic case.

4.3.3. Effect of restrainers

Cable restrainers are often used at intermediate hinges as a retrofit measure to limit relative hinge displacement and prevent unseating during an earthquake. However, the presence of restrainers alters the behavior of adjacent frames by transferring forces as the frame opening exceeds the slack in the cable. While it has been shown that pounding can increase the linear and nonlinear response of the frames, it is not clear how the restrainers affect pounding in nonlinear frames. Hence, the effect of restrainers on pounding is also evaluated for yielding frames.

In the earlier section, the restrainer stiffness (K_r) was normalized by K_{mod}, the sum of flexibilities of the adjacent frames, based on effective stiffness properties. Thus, the normalized stiffness (κ) was given as $\kappa = K_r/K_{mod}$. For yielding frames, K_{mod} can be expressed as:

$$K_{mod} = \frac{K_1 K_2}{\mu(K_1 + K_2)}$$

(4.3)

where K_1 and K_2 are the elastic stiffnesses of the frames and μ is the design ductility demand. Values of $\kappa = 0$, 0.5 and 1.0 are considered for this study, where $\kappa = 0$ corresponds to the case with no hinge restrainers. The restrainer slack is assumed to equal the hinge gap g_p. The frames are subject to the suite of 5 ground motion records used in the inelastic study.

The effect of restrainers on the frame pounding response is illustrated in Figure 4.7. The addition of restrainers helps in reducing the frame response in Zone I but increases the stiff frame demand in Zone II. Overall, the effect of restrainers on the frame response is observed only for highly out-of-phase frames and is marginal for other stiffness ratios.

For $T_1/T_2 = 0.32$, the addition of restrainers reduces the stiff frame response by approximately 25% in Zone I for $\kappa = 1.0$ and $T_{2eff}/T_g = 0.2$. The flexible frame response is reduced by 23% in Zone III for $\kappa = 1.0$ and $T_{2eff}/T_g = 5$. However, the presence of restrainers does not alter the general frame displacement trends due to pounding, thus underlining the importance of the pounding effect over the restrainer effect in the response of bridge frames.
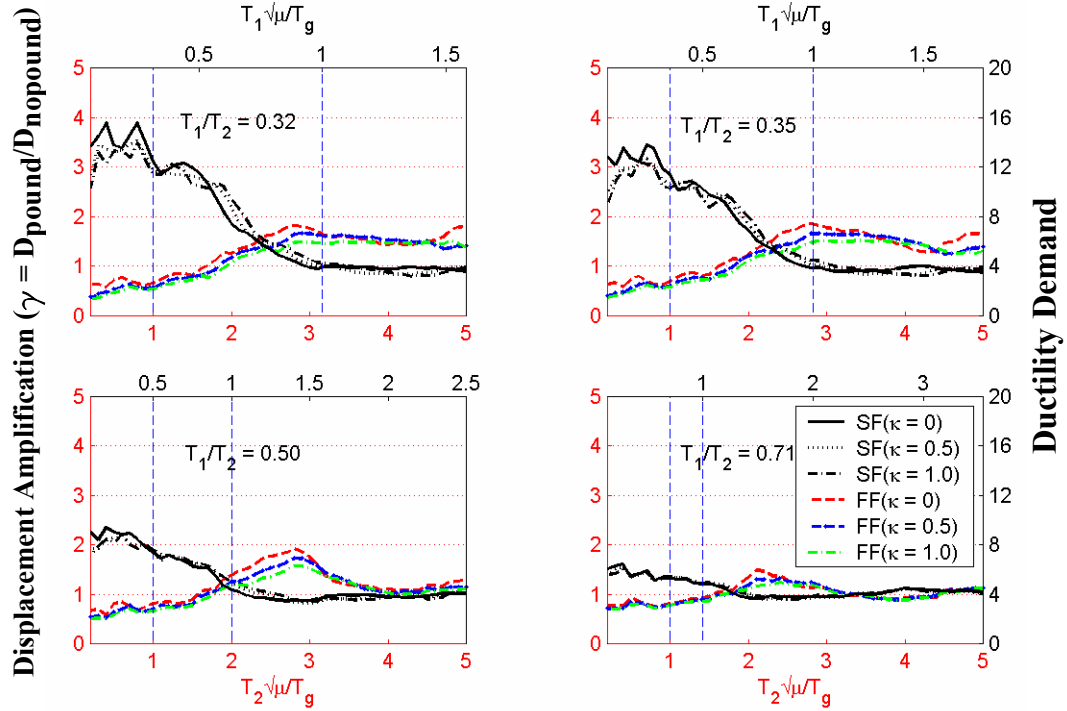
Figure 4.7: Mean amplification in displacement demand for 5 earthquake records: inelastic frames with and without restrainers; target ductility $\mu = 4$; SF – Stiff Frame; FF – Flexible Frame; Restrainer stiffness ratio, $\kappa = 0, 0.5, 1.0$.

4.4. Conclusions

This chapter investigates the effects of pounding and restrainers on the global demand of bridge frames in a multi-frame bridge. The primary factors affecting the pounding response are identified as the frame stiffness ratio (K_1/K_2) or period ratio (T_1/T_2), ground motion effective period ratio (T_{2eff}/T_g), restrainer stiffness ratio, κ, and the frame ductility ratio, μ. Unlike earlier studies which only accounted for the system period ratio in studying the pounding response, this is the first study that identifies T_{2eff}/T_g as an important pounding parameter.

Parametric studies using simplified 2-DOF models show that pounding is most critical for highly out-of-phase frames. Pounding reduces the frame response when vibrating near the characteristic period of the ground motion (T_g). The amplification in frame response as a function of T_{2eff}/T_g, and T_1/T_2 falls into three regions. In Zone I ($T_{2eff}/T_g < 1$), the stiff frame demand increases and the flexible frame demand decreases due to pounding. In Zone III ($T_{1eff}/T_g > 1$), the flexible frame pounding response is increased while the stiff frame pounding response is reduced. In Zone II ($T_{1eff}/T_g < 1$ & $T_{2eff}/T_g > 1$), pounding slightly increases both frame responses.

Inelastic behavior (frame design ductility, $\mu = 4$) shows greater stiff frame amplification in Zone I when compared to the linear case. The yielding of frames also results in smaller response amplification for the flexible frame in Zone III, when compared to elastic behavior. It can be concluded that the response of bridge frames due to pounding is much less pronounced for $K_1/K_2 = 2.0$ ($T_1/T_2 = 0.71$) irrespective of the ground motion period ratio. The effect of restrainers on the pounding response of bridge

frames is also evaluated, for inelastic frames. The results show that restrainers have very

little effect on the demands on bridge frames compared with pounding.

CHAPTER 5

HERTZ MODEL WITH HYSTERESIS DAMPING FOR DYNAMIC IMPACT

The aspect of seismic pounding in bridges is essentially a problem of dynamic impact. A clear understanding of the impact phenomenon is intrinsic for the analysis and design of bridge structures. The forces created by collision act over a short period of time, where energy is dissipated as heat due to random molecular vibrations and the internal friction of the colliding bodies. Usually, contact is modeled using either a continuous force model or via a stereomechanical (coefficient of restitution) approach, as described in Chapter 2. With several models available for the investigation of dynamic impact, there is a need to perform an evaluation and comparison of all the models to determine their applicability and efficacy in accurately capturing the pounding phenomenon. More importantly, the stereoemechanical model needs to be compared with other contact force-based models, to ascertain the effect of impact modeling methodology on the response of participating systems.

In this chapter, the limitations of the various impact models are discussed and a contact force model based on the Hertz law, with hysteresis damping is introduced to simulate impact. The performance of the new contact model in comparison with the existing impact models is evaluated. Parameter studies are then conducted with two degree-of-freedom linear and nonlinear models to ascertain which pounding models are effective in simulating bridge deck impact. Finally, a case study is performed on a multiple-frame bridge with restrainers, bearings and abutments to determine the differences in the global bridge response, when impact is simulated using various models.

5.1. Limitations of existing impact models

Past research has shown that the linear spring element is a popular choice for modeling impact. This contact-based approach is relatively straightforward and can be easily implemented in commercial software. However, the linear spring element is incapable of modeling energy loss during impact, as observed by the absence of a hysteretic loop in Figure 5.1(a). Hence, the Kelvin-Voigt solid consisting of a linear spring in parallel with a damper has been used in some studies (Wolf and Skrikerud, 1980; Anagnostopoulos, 1988; Jankowski et al., 1998).

In the Kelvin model, the relative motion during impact is represented as a half damped sine wave. The force during contact is given by a half-ellipse as illustrated in Figure 5.2(a). However, this is contrary to the expected shape of the hysteresis loop due to a compressive load that is applied to and removed from a body within its elastic range at a slow rate, as shown in Figure 5.2(b).
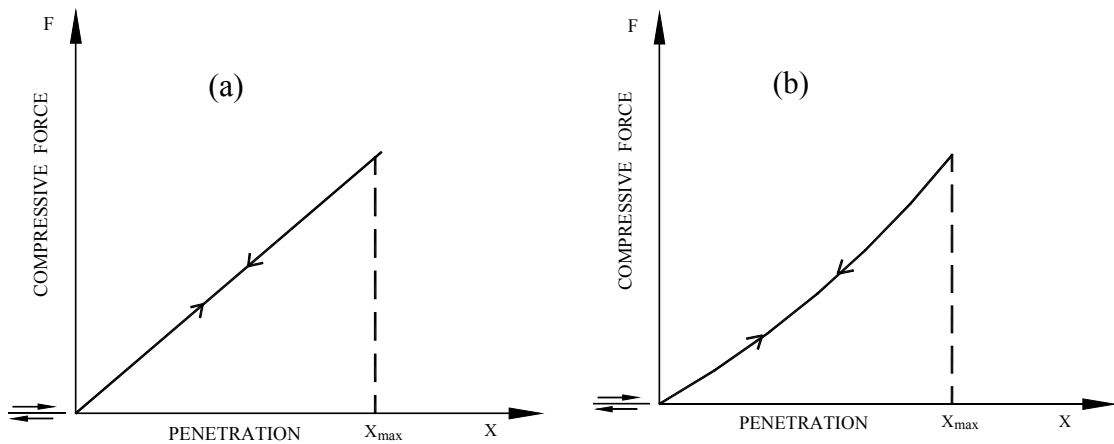
Figure 5.1: Impact-penetration relation for (a) Linear spring; (b) Hertz contact element
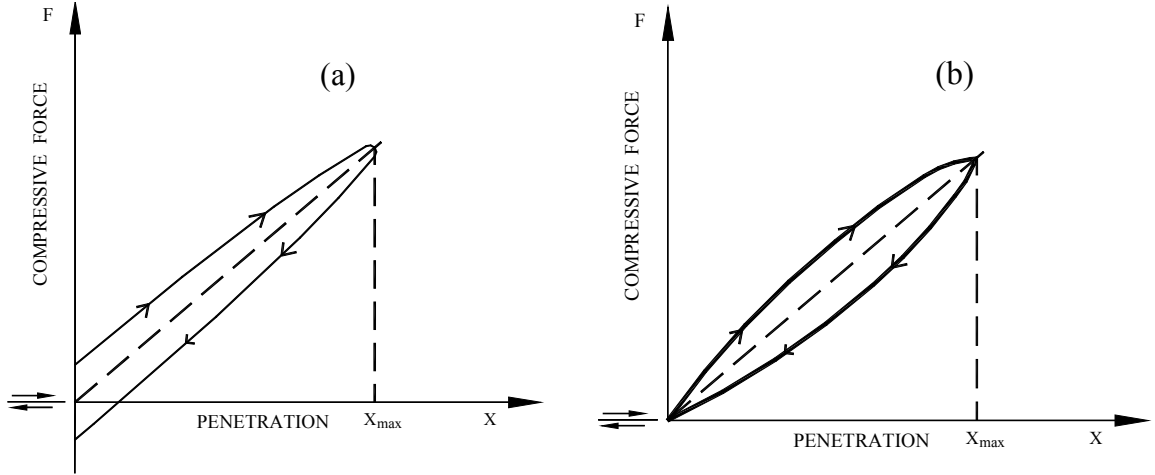
Figure 5.2: (a) Hysteresis loop from the Kelvin-Voigt model; (b) Hysteresis loop for the application and removal of compressive load.

Hunt and Crossley (1975) have shown the Kelvin-Voigt model to be unrepresentative of the physical nature of energy transfer. It results in "sticky" tensile forces acting on the bodies just before separation that lengthen the period of contact and reduce the separation velocities of the colliding bodies. The Kelvin-Voigt model also results in a coefficient of restitution that is independent of the impact velocity (Marhefka and Orin, 1999). However, Goldsmith (1960) has shown that for most materials in the linear elastic range and for low values of the impact velocity, v, the coefficient of restitution can be expressed as:

$$e = 1 - \alpha v \tag{5.1}$$

where α is a constant that depends on the type of material. It can be shown that the energy loss during impact (ΔE) is proportional to the cube of the impact velocity v (Hunt and Crossley, 1975). However, the half-ellipse loop from the Kelvin-Voigt model results

in an energy loss that is proportional to the square of the impact velocity *v*, thus making it untenable.

Other studies have used the Hertz contact model, which uses a nonlinear spring, as illustrated in Figure 5.1(b) to represent impact (Davis, 1992; Pantelides and Ma, 1998; Chau et al., 2003). However, the Hertz model fails to account for energy dissipation during impact. The stereomechanical method is limited in its application because of the unknown duration of contact, as noted in Chapter 2. Furthermore, since it involves modification of the velocities of the colliding bodies at the instant of impact, the stereomechanical method cannot be implemented in existing bridge analysis programs. Hence, a comprehensive impact model needs to be developed which is representative of the nature of impact and can be easily incorporated in commercial structural software.

5.2. Proposed contact model

The contact forces during direct central impact of two isotropic elastic bodies with perfectly smooth surfaces can be described using the Hertz law of contact (Goldsmith 1960). In general, an impact can be considered to occur in two phases – the compression phase and the restitution phase, as shown in Figure 5.3. The colliding bodies undergo local deformation in the direction normal to the impact surface during the compression phase. The relative velocity of the centers of mass reduces to zero at the end of the compression phase. The restitution phase begins after the compression phase and lasts until the separation of the colliding masses. When the curvatures of the contacting surfaces are large, the contact becomes concentrated at a point and Hertzian theory predicts a nonlinear contact spring as shown below (Goldsmith, 1960):
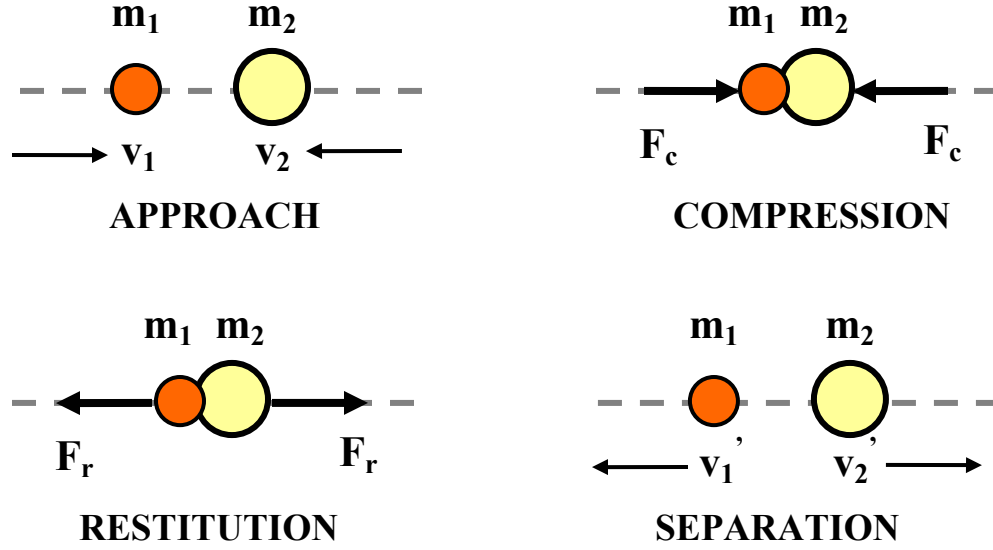
Figure 5.3: Stages of Impact – Poisson's Hypothesis

$$f_c = k_h \delta^n \qquad (5.2)$$

where f_c is the contact force, δ is the local relative penetration between the center of masses of the two bodies, k_h is the spring constant which depends on the material properties and radii of curvature of the bodies and n is taken as 3/2.

The Hertz model suffers from the limitation that it cannot represent the energy loss during contact. Hence, an improved version of the Hertz model is proposed, whereby a hysteresis damper is used in parallel with the nonlinear spring element. The contact model can be represented as:

$$f_c = k_h \delta^n + c_h \dot{\delta} \qquad (5.3)$$

where c_h is the damping coefficient of the hysteresis damper, δ is the local deformation and $\dot{\delta}$ is the penetration velocity. A nonlinear damping coefficient is proposed so that the

hysteresis loop of the damper matches the one shown in Figure 5.2(b). The damping coefficient is taken as:

$$c_h = \zeta \delta^n \tag{5.4}$$

where ζ is the damping constant. The hysteresis loop for the Hertz model with nonlinear damping can be represented as shown in Figure 5.4(a).
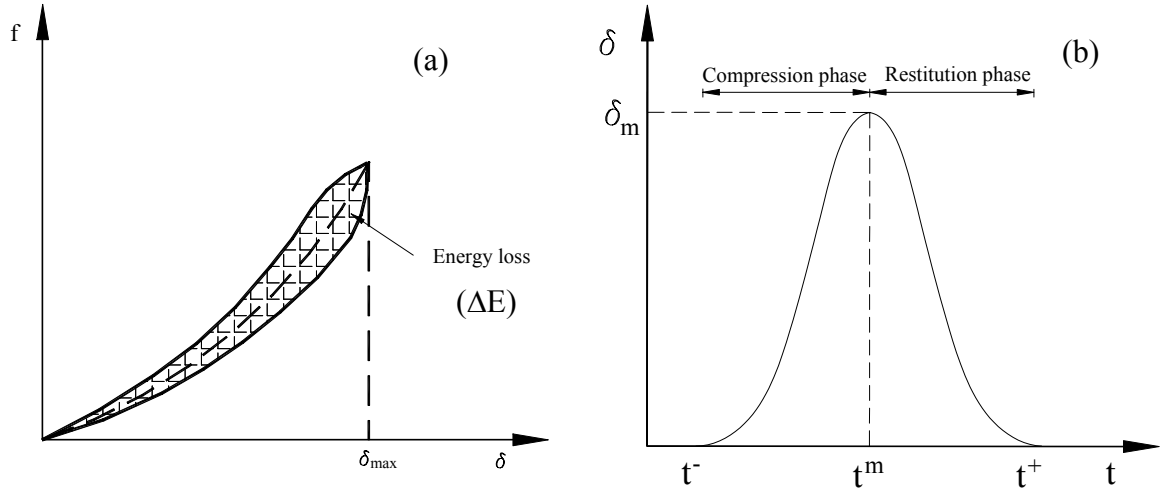
Figure 5.4: (a) Hysteresis loop for Hertz contact model with nonlinear damping; (b) penetration versus time for proposed model.

Using the stereomechanical approach, the energy loss as a result of impact (ΔE) can be expressed in terms of the coefficient of restitution and the approach velocities of the colliding bodies, as follows:

$$\Delta E = \frac{1}{2} \frac{m_1 m_2}{m_1 + m_2} \left(1 - e^2\right)\left(v_1 - v_2\right)^2 \tag{5.5}$$

where m_1, m_2 are the masses of the colliding bodies, e is the coefficient of restitution and v_1, v_2 are the approaching velocities of the masses. The energy dissipated by the damper is the shaded area shown in Figure 5.4(a) and can be evaluated as:

$$\Delta E = \oiint c_h \dot{\delta} d\delta = \oiint \zeta \delta^n \dot{\delta} d\delta \tag{5.6}$$

In order to evaluate the energy loss from Equation 5.6, the penetration velocity $\dot{\delta}$ must be expressed as a function of the penetration δ at any time t during the period of contact. The variation of penetration with time is illustrated in Figure 5.4(b), where t^-, t^m and t^+ denote the initial time of contact, time of maximum penetration and the time of separation of the colliding bodies. At the end of the compression phase, the two bodies move with a common velocity V_{12}. Assuming the energy dissipated during impact to be small compared to the maximum absorbed elastic energy, an energy balance between the start and end of the compression phase gives:

$$\frac{1}{2}m_1 v_1^2 + \frac{1}{2}m_2 v_2^2 = \frac{1}{2}(m_1 + m_2)V_{12}^2 + U_m \tag{5.7}$$

where U_m is the maximum strain energy stored. A momentum balance during the same period results in the following:

$$m_1 v_1 + m_2 v_2 = (m_1 + m_2)V_{12} \tag{5.8}$$

Based on (5.7) and (5.8), the maximum strain energy stored can be expressed as:

$$U_m = \frac{1}{2}\frac{m_1 m_2}{(m_1 + m_2)}(v_1 - v_2)^2 \tag{5.9}$$

The elastic strain energy absorbed equals the work done by the Hertz contact force from the instant of impact ($\delta = 0$) to the state of maximum penetration ($\delta = \delta_m$) and can be evaluated as:

$$U_m = \int_0^{\delta_m} f d\delta = \frac{k_h \delta_m^{n+1}}{n+1} \qquad (5.10)$$

Equating (5.9) and (5.10) results in an expression for the relative velocity at the onset of impact (v_1-v_2), in terms of the maximum penetration (δ_m).

$$(v_1 - v_2)^2 = \left[\frac{2(m_1 + m_2)}{m_1 m_2}\right]\left[\frac{k_h \delta_m^{n+1}}{n+1}\right] \qquad (5.11)$$

By repeating the preceding steps between the onset of impact (t^i) and an intermediate time t ($t^i \le t \le t^m$), the penetration velocity $\dot{\delta}$ can be related to the penetration, δ, at any time t, as follows:

$$\dot{\delta} = \sqrt{(v_1 - v_2)^2 - 2\left[\frac{m_1 + m_2}{m_1 m_2}\right]\left[\frac{k_h \delta^{n+1}}{n+1}\right]} \qquad (5.12)$$

The above expression is for penetration velocity during the compression phase. If we assume that the penetration velocities during the compression and restitution phases are approximately equal, the energy loss expression in (5.6) reduces to:

$$\Delta E = \frac{4\zeta}{3(n+1)}\left[\frac{2(m_1 + m_2)k_h}{m_1 m_2 (n+1)}\right]^{1/2} (\delta_m)^{3(n+1)/2} \qquad (5.13)$$

Substituting for δ_m from (5.11) and equating the energy losses from (5.13) and (5.5), an expression for the damping factor (ζ) can be found in terms of the spring stiffness (k_h), the coefficient of restitution (e) and the relative approaching velocity ($v_1 - v_2$) as follows:

$$\zeta = \frac{3k_h (1 - e^2)}{4(v_1 - v_2)} \qquad (5.14)$$

Hence, the force during contact in (5.3) can be expressed as:

$$f_c = k_h \delta^n \left[1 + \frac{3(1-e^2)}{4(v_1 - v_2)} \dot{\delta} \right]$$

(5.15)

Now, all the parameters of the model are known and the Hertz model with nonlinear damping can now be used in impact analysis. Similar models have been used in other areas such as robotics and multi-body systems (slider-crank mechanisms) to analyze contact (Lankarani and Nikravesh, 1990; Marhefka and Orin, 1999; Hunt and Crossley, 1975). The nonlinearity associated with impact and the energy losses are both accounted for in the proposed model. The use of the elastic Hertz law beyond the limits of its validity is justified as it appears to predict with reasonable accuracy most of the impact parameters that can be experimentally verified (Goldsmith, 1960).

5.3. Comparison with existing impact models

The efficacy of the proposed model in predicting the pounding response of adjacent structures needs investigation. In this regard, the two-DOF system shown in Figure 5.5 is subjected to the El Centro record (N-S component) from the 1940 Imperial Valley earthquake. The record has a Peak Ground Acceleration (PGA) of 0.35g. The properties of the system are assumed to be elastic, as specified in Table 5.1. With a view of focusing solely on the pounding response, the presence of restrainers, bearings and abutments is ignored. Two cases are evaluated; Case 1, where the separation between the models (g_p) is very large to preclude pounding and Case 2, where g_p is small so that pounding can occur. The gap between the models in Case 2 is taken as:

$$g_{p_{Case2}} = \chi D_{np} = \chi \max \{ u_1(t) - u_2(t) \}_{Case1}$$

(5.16)
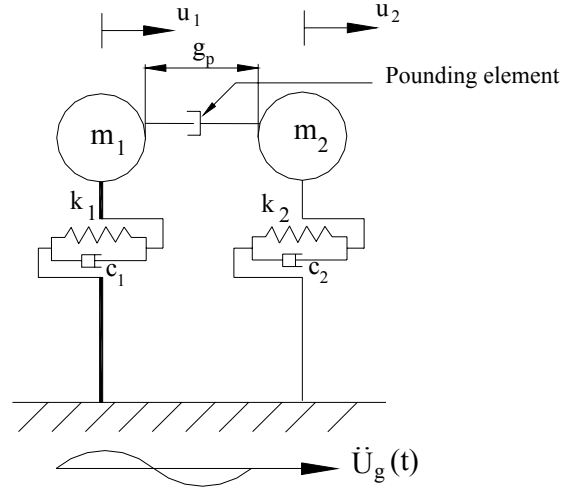
Figure 5.5: Simplified model used to test the proposed impact model

Table 5.1: Properties of two-DOF system used for impact model comparisons

Parameter	Value
m_1, m_2	3.6 kip-s^2/in
c_1, c_2	based on 5% damping ratio
T_1, T_2	0.25 s, 0.50 s
Force-deformation	Elastic
k_l, k_k	25000 kip/in
k_h	25000 kipin$^{-3/2}$
e	0.6
c_k	68 kip-s/in
χ	0.5

where χ is the gap ratio parameter and D_{np} is the maximum relative displacement from Case 1.

Pounding is implemented using the proposed Hertz contact model with nonlinear damping. The proposed contact model will be referred to as the Hertzdamp model throughout the rest of the dissertation. The contact force for the Hertzdamp model is given by Equation 5.17.

$$F_c = k_h \left(u_1 - u_2 - g_p \right)^{\frac{3}{2}} \left[1 + \frac{3(1 - e^2)}{4 \left(v_1 - v_2 \right)} \left(\dot{u}_1 - \dot{u}_2 \right) \right] \qquad ; u_1 - u_2 - g_p \geq 0 \qquad (5.17a)$$

$$F_c = 0 \qquad\qquad\qquad\qquad ; u_1 - u_2 - g_p < 0 \qquad (5.17b)$$

where $u_1 - u_2 - g_p$ is the relative penetration and $\dot{u}_1 - \dot{u}_2$ is the penetration velocity. For comparison, the linear spring, Kelvin, Hertz and stereomechanical models are also evaluated for this particular record. The coefficient of restitution is assumed as 0.6, where applicable. The stiffness parameters of the various impact models are assumed to be the same for consistency, as listed in Table 5.1. The gap ratio parameter is taken as 0.5, which results in a gap of 0.85" for Case 2. Figure 5.6 presents the responses when pounding is represented using the Hertzdamp model.

The time history of displacements for the pounding and no pounding cases shows that pounding increases the maximum displacement of DOF$_1$ (stiffer system) from 0.58 in to 0.71 in. Conversely, for DOF$_2$ (flexible system), impact reduces the maximum displacement from 2.04 in to 1.65 in. The nonlinearity and energy loss associated with impact are clearly illustrated by the impact force vs. relative displacement plot in Figure 5.6. For completeness, the variation of impact force as a function of time is also presented for one instance of impact.
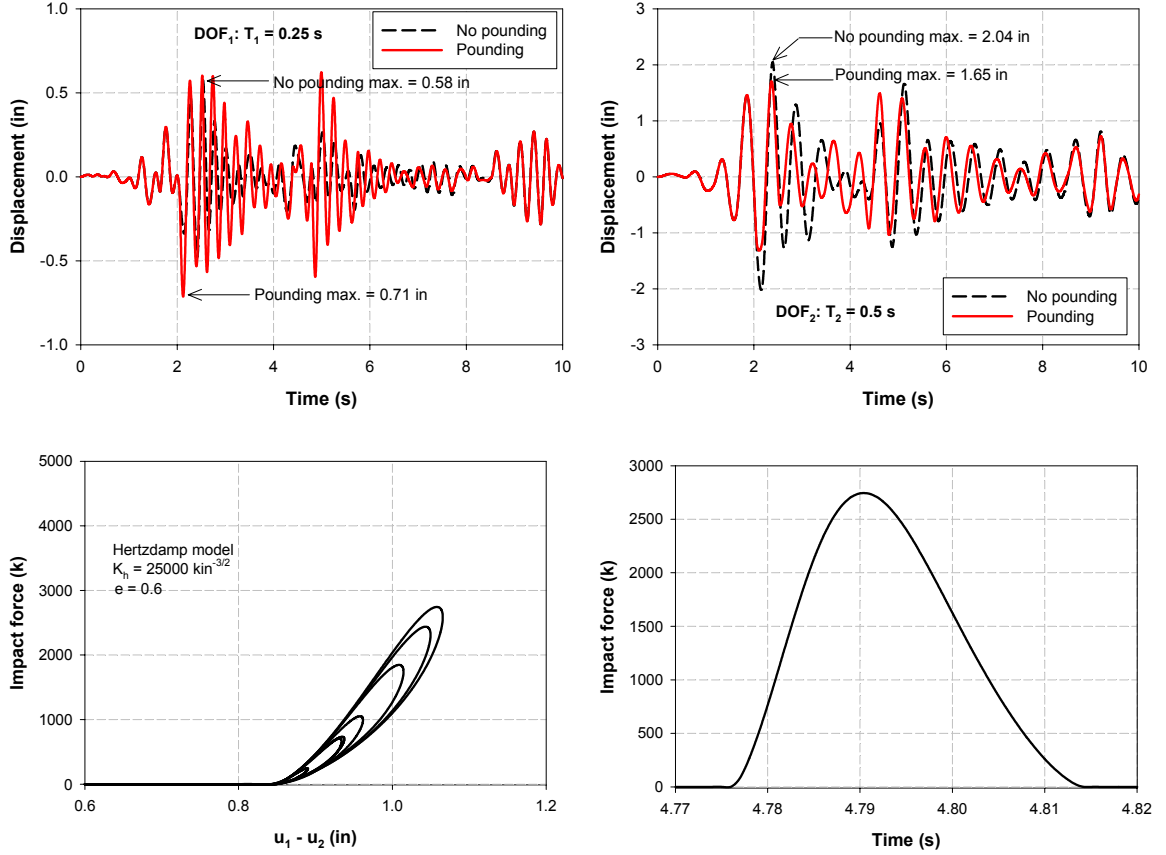
Figure 5.6: Effect of pounding on two-DOF linear system with $T_1/T_2 = 0.5$; $e = 0.6$; El Centro record (10 seconds); clockwise from top – time history of displacements (DOF_1), time history of displacements (DOF_2), hertzdamp impact force vs. time (one instance), hertzdamp impact force vs. relative displacement.

To compare the performance of the Hertzdamp model, the maximum pounding responses of the two-DOF system using the other impact models are normalized with respect to the no-pounding response. Figure 5.7 presents the amplification in displacement and acceleration relative to the ground for DOF_1 (stiffer system), and the maximum impact force from the various models. The hysteresis loops during impact for

the force-based models are presented in Figure 5.8. Clearly, the models which cannot represent energy loss (linear spring and hertz models) overestimate the displacement amplification due to pounding. The hertzdamp and stereomechanical model displacement amplification are very similar. The displacement amplification from the Kelvin model is the smallest. This can be attributed to a larger hysteretic loop and the presence of some impact force even as the bodies just touch each other (relative displacement = g_{pCase2}), as illustrated in Figure 5.8.

The amplification in the acceleration response of DOF_1 and the maximum impact force is much higher for models based on a linear spring. The hertzdamp model provides the lowest impact force among force-based models. The stereomechanical model is not a force-based model. Hence, there is no impact force and consequently, no amplification in the acceleration response.
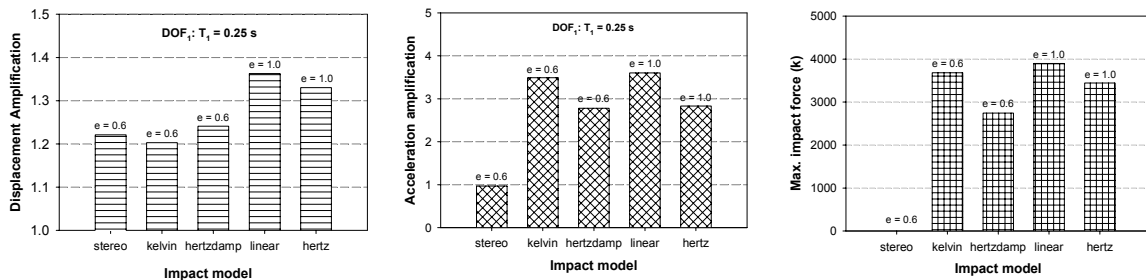
Figure 5.7: Comparison between various impact models; L-R displacement amplification – DOF_1, acceleration amplification – DOF_1, maximum impact force.
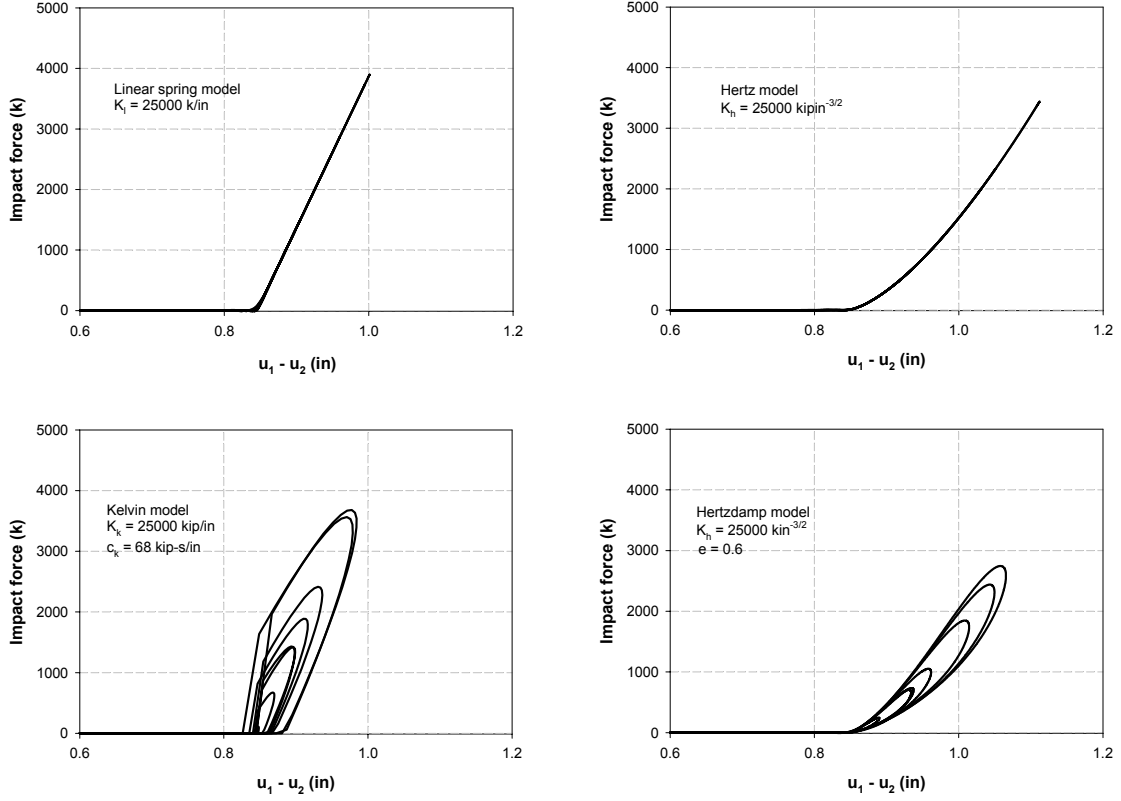
Figure 5.8: Comparison of contact models – impact force vs. relative displacement.

This case study illustrates the effects of energy loss, nonlinearity in impact stiffness and compares the performance of the various impact models, for one ground motion record. However, the effects of ground motion characteristics, system period ratio and system inelastic behavior on the pounding response using the various impact models need to be studied. In the following section, a parameter study investigating these effects is presented.

5.4. Parameter study to assess the performance of various impact models

With several analytical methods available to investigate seismic pounding, it is important to address the limitations of various models and identify effective ways to model impact. The two degree-of-freedom model shown in Figure 5.5 is selected for study, with equal masses of 7.8 kip-s^2/in and 5% modal damping. Both elastic and inelastic systems are considered. Pounding is analyzed using several impact models, such as the linear spring, Kelvin, Hertz, stereomechanical and Hertzdamp models. The impact parameters are tabulated in Table 5.2.

The stiffness of the linear contact spring is chosen proportional to the axial stiffness of the deck (EA/L). Typical values of E, A and L for bridge decks range from 3000 to 4500 ksi, 70 to 100 sq. ft, and 200 to 500 ft, respectively. This results in a deck axial stiffness of 5040 kip/in to 27,000 kip/in. Several studies have shown the system response to be insensitive to changes in the impact spring stiffness by one order of magnitude (Anagnostopoulos, 1988; Maison and Kasai, 1992). Hence, a value of 25,000 kip/in is chosen as the impact spring stiffness in this study. The effects of restrainers, bearings and abutments are not considered so that the differences in system responses can be directly attributed to the impact models.

The system period ratio and ground motion characteristics were recognized as critical parameters affecting the pounding response, in Chapter 4. In this section, three cases are considered with system periods of (0.18 s, 0.60 s), (0.30 s, 0.60 s) and (0.42 s, 0.60 s) corresponding to period ratios (T_1/T_2) of 0.3, 0.5 and 0.7, respectively. A suite of thirty ground motion records with peak ground accelerations (PGAs) varying from 0.1g to 1.0g are selected, as listed in Table 5.3. The characteristic periods of the records are carefully

chosen such that the ground motion period ratio (T_2/T_g) falls within Zone I (see Chapter 4). The effect of pounding is expressed in terms of response amplification, which is the ratio of the maximum response when pounding occurs to the maximum response when there is no pounding. The hinge gap in the simplified model is set very large for the no-pounding analysis and assumed as ½ inch for the pounding analysis.

Table 5.2: Impact parameters selected for the various models

Impact Model	Parameters
Linear spring	K_l = 25,000 kip/in
Kelvin-Voigt	K_k = 25,000 kip/in; e = 0.6. 1.0[*]
Hertz	K_h = 25,000 kipin$^{-3/2}$
Stereomechanical	e = 0.6, 1.0
Hertzdamp	K_h = 25,000 kipin$^{-3/2}$; e = 0.6. 1.0[*]

* - when e = 1.0, the Kelvin-Voigt reduces to the linear spring model and the Hertzdamp reduces to the Hertz model.

Table 5.3: Suite of thirty earthquake ground motion records used in parameter study

PGA bin (g)	PGA (g)	Earthquake	M_w	Station	$\Phi°$	EPD (km)	PGV (cm/s)	PGD (cm)	Soil Class	T_g (s)	D_t (s)
0.1	0.11	Northridge, 1994	6.7	Wonderland Ave	095	22.7	8.7	1.8	A,A	0.80	0.010
	0.10	Imperial Valley, 1979	5.2	5054 Bonds Corner	230	15.6	8.2	1.4	D,C	0.75	0.005
	0.09	San Fernando, 1971	6.6	Pasadena	000	25.7	6.4	1.4	D,B	0.85	0.010
0.2	0.19	Loma Prieta, 1989	6.9	Fremont	090	43.4	12.7	5.5	B,-	0.70	0.005
	0.19	Morgan Hill, 1984	6.2	Gilroy Array #3	000	14.6	11.2	2.4	D,C	1.10	0.005
	0.21	N. Palm Springs, 1986	6.0	Morongo Valley	135	10.1	40.9	15.0	C,B	1.90	0.005
0.3	0.30	Whittier Narrows, 1987	6.0	E Grand Ave	180	9.0	23.0	3.3	A,A	0.70	0.020
	0.28	Landers, 1992	7.3	Joshua Tree	090	11.3	43.2	14.5	C,B	0.70	0.020
	0.29	Morgan Hill, 1984	6.2	Gilroy Array #6	090	11.8	36.7	6.1	B,B	1.20	0.005
0.4	0.37	Loma Prieta, 1989	6.9	WAHO	000	16.9	27.2	3.8	D,-	0.85	0.005
	0.42	Northridge, 1994	6.7	Mulhol	009	19.6	62.8	11.1	C,B	0.85	0.010
	0.39	Cape Mendocino, 1992	7.1	Rio Dell Overpass	270	12.3	43.9	22.0	C,B	0.65	0.020
0.5	0.51	Northridge, 1994	6.7	Old Ridge Route	360	22.6	52.2	2.4	B,B	0.95	0.020
	0.48	Loma Prieta, 1989	6.9	Coyote Lake Dam	285	21.8	39.7	15.2	A,-	0.65	0.005
	0.48	Northridge, 1994	6.7	W Lost Cany	270	12.2	45.1	12.6	D,C	0.70	0.010
0.6	0.51	Loma Prieta, 1989	6.9	Saratoga – Aloha Ave	000	11.7	41.2	16.2	D,B	1.80	0.005
	0.59	N Palm Springs, 1986	6.0	5070 N Palm Springs	210	8.2	73.3	11.5	D,B	1.10	0.005
	0.59	Cape Mendocino, 1992	7.1	Petrolia	000	9.5	48.4	21.7	D,C	0.75	0.020
0.7	0.61	Loma Prieta, 1989	6.9	16 LGPC	000	6.1	51.0	11.5	A,-	0.80	0.005
	0.60	Coalinga, 1983	5.8	Pleasant Valley P.P.	045	17.4	34.8	8.1	D,-	0.65	0.005
	0.57	Northridge, 1994	6.7	Old Ridge Route	090	22.6	52.1	4.2	B,B	0.80	0.020
0.8	0.66	Cape Mendocino, 1992	7.1	Petrolia	090	9.5	89.7	29.6	D,C	0.70	0.020
	0.82	Duzce, 1999	7.1	Bolu	090	17.6	62.1	13.6	D,C	0.90	0.010
	0.84	Coalinga, 1983	5.8	Transmitter Hill	270	9.2	44.1	6.8	A,-	0.75	0.005
0.9	0.84	Northridge, 1994	6.7	Rinaldi	228	7.1	166.1	28.8	C,C	1.05	0.005
	0.89	Superstition Hills, 1987	6.7	286 Superstition Mtn	135	4.3	42.2	7.3	A,B	0.70	0.010
	1.04	Cape Mendocino, 1992	7.1	Cape Mendocino	090	8.5	42.0	12.4	A,A	2.00	0.020
1.0	1.08	Coalinga, 1983	5.8	Transmitter Hill	360	9.2	39.7	5.4	A,-	0.70	0.005
	0.90	Chi-Chi, 1999	7.6	CHY080N	080	6.8	102.4	34	-,B	1.00	0.005
	1.29	Northridge, 1994	6.7	Pacoima Dam	194	8.0	103.9	23.8	A,A	0.75	0.020

PGA - Peak Ground Acceleration; M_w – Moment magnitude; $\Phi°$ - Component; EPD – Epicentral distance; PGV – Peak Ground Velocity; PGD – Peak Ground Displacement; Soil Class – Geomatrix soil class, USGS; T_g – Characteristic period; D_t – time step of record.

5.4.1. Two degree-of-freedom elastic system

The effects of various pounding models on the elastic system response are discussed in this section. Mean values of displacement amplification and acceleration amplification due to pounding, as a function of the peak ground acceleration (PGA) are presented in Figures 5.9 – 5.12, for different values of the coefficient of restitution (e). Three ground motion records are used at each PGA level. The expected Zone I trend of increase in the displacement response of the stiff structure and decrease in the flexible structure response, as a result of impact is clearly observed. The displacement amplifications get closer to one with an increase in the period ratio, as observed in Chapter 4.

The stereomechanical and contact force-based models predict similar displacement responses, even though they use different methodologies to account for impact. Differences in displacement amplifications between various impact models are larger for highly out-of-phase frames ($T_1/T_2 = 0.3$) and more pronounced for lower values of e (e = 0.6). For instance, when $T_1/T_2 = 0.3$ and e = 1.0, the differences in stiff frame displacement amplifications between the Kelvin and stereomechanical models are 17% and 18% for PGAs of 0.7g and 0.9g, respectively. The differences between the Hertzdamp and stereomechanical models for the same set of parameters are 21% and 17%. For the flexible frame, with $T_1/T_2 = 0.3$ and e = 1.0, the differences between the Kelvin and stereomechanical models are 11% and 16% for PGAs of 0.5g and 0.9g, respectively. The differences between the Hertzdamp and stereomechanical models for the same set of parameters are 20% and 16%.

Differences in displacement amplifications between the Kelvin and Hertzdamp models are under 10% for all values of PGA and both values of e. The variation of

displacement amplification with PGA shows no clear trend, for any impact model. Lowering the coefficient of restitution (e) from 1.0 to 0.6 reduces displacement amplifications of both systems, on the average.

Pounding amplifies the acceleration response of both systems, when simulated using contact force-based methods such as the Kelvin and Hertzdamp models. The acceleration amplifications from the stereomechanical model follow the corresponding displacement trends, and are much smaller than those from the contact force-based models. The contact force models predict acceleration amplifications as high as 5 for the stiff frame, when $T_1/T_2 = 0.5$ and PGA = 0.8g. This corresponds to an acceleration pulse of nearly 5g that can potentially damage sensitive equipment placed on the structure.

Contrary to the displacement amplification trends, the acceleration amplifications from the contact models increase as the period ratio approaches unity. This is because higher period ratios (T_1/T_2) are achieved by increasing T_1, while keeping T_2 constant and for stiff system periods considered herein ($T_1 = 0.18$, 0.30 and 0.42 seconds), the spectral acceleration values typically increase with increasing period. The acceleration amplifications are reduced significantly when e is lowered from 1.0 to 0.6. On the average, the Hertzdamp model provides the least acceleration amplification among the contact force based models.

To more closely examine the effect of energy loss on the system response, the percent difference in response between the Hertz (e = 1.0) and Hertzdamp (e = 0.6), the linear spring (e = 1.0) and Kelvin (e = 0.6) and the stereomechanical (e = 1.0) and stereomechanical (e = 0.6) models are expressed as a function of PGA. Figures 5.13 and 5.14 present the results. The Hertzdamp model shows the least variation with respect to

changes in the coefficient of restitution (e). Differences in response between the Hertz and Hertzdamp models are under 20% for displacements and less than 35% for accelerations, when e is changed from 1.0 to 0.6. This indicates that using a spring with nonlinear stiffness might be the most effective way to represent impact.

The models without energy dissipation such as the linear spring, stereomechanical (e = 1.0) and the Hertz models are ill-suited to represent impact, as they overestimate the response amplifications due to impact. It is surprising to note the large differences in the stereomechanical model response with respect to changes in e, for some PGA values. This could be attributed to the fact that at lower values of e, the bodies tend to "stick" resulting in several impacts within a short period of time as opposed to one impact.

Overall, the Hertzdamp model appears to be the most effective in modeling pounding, as it exhibits the least variation with changes in the coefficient of restitution and also predicts lower acceleration amplifications when compared to other contact models. However, for a period ratio (T_1/T_2) of 0.7, the contact models provide high acceleration amplifications and hence the stereomechanical model is better suited to model impact.
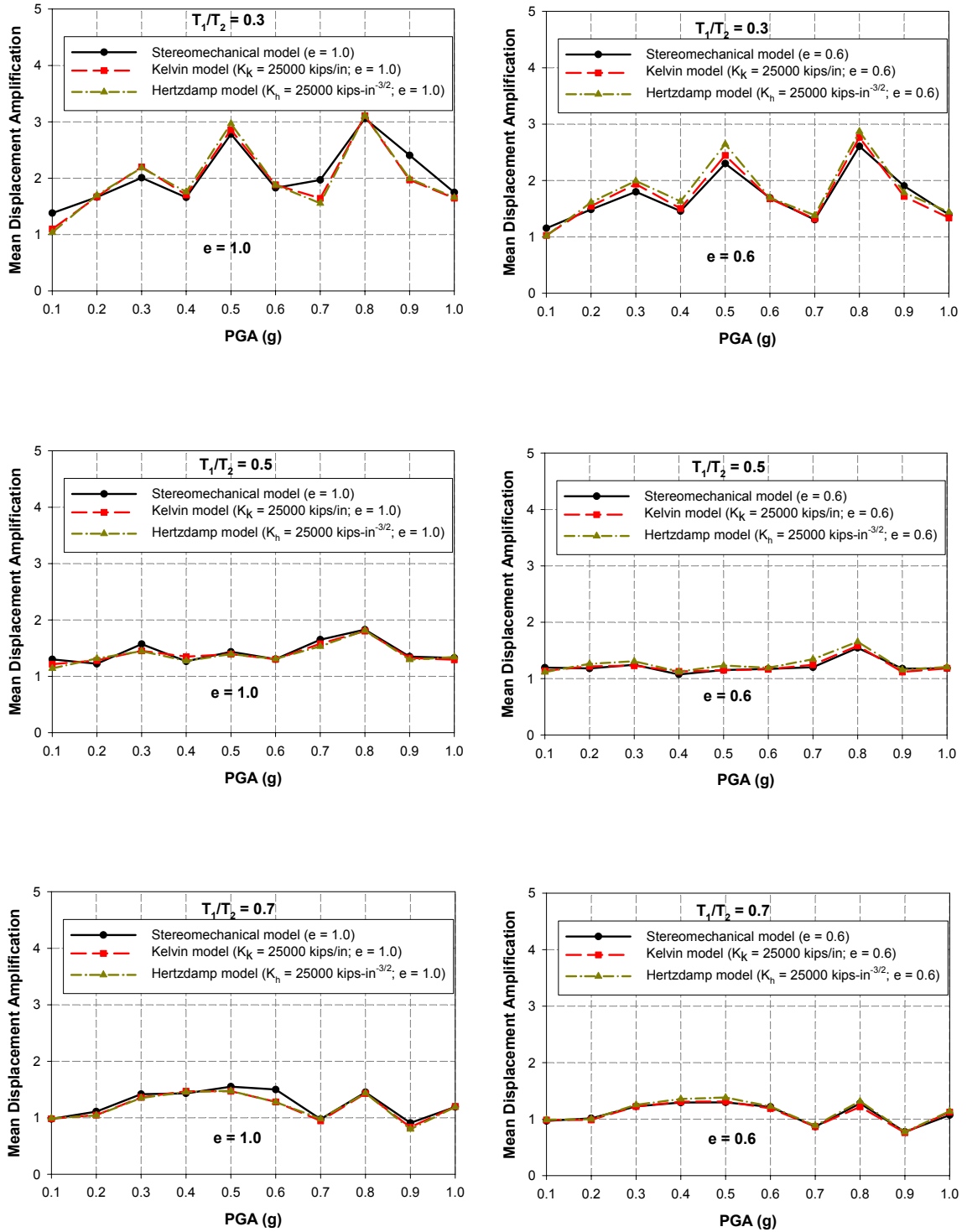
Figure 5.9: Mean displacement amplification due to pounding – DOF_1 – elastic systems;

T_1/T_2 = 0.3, 0.5, 0.7; e = 1.0, 0.6; 30 ground motions
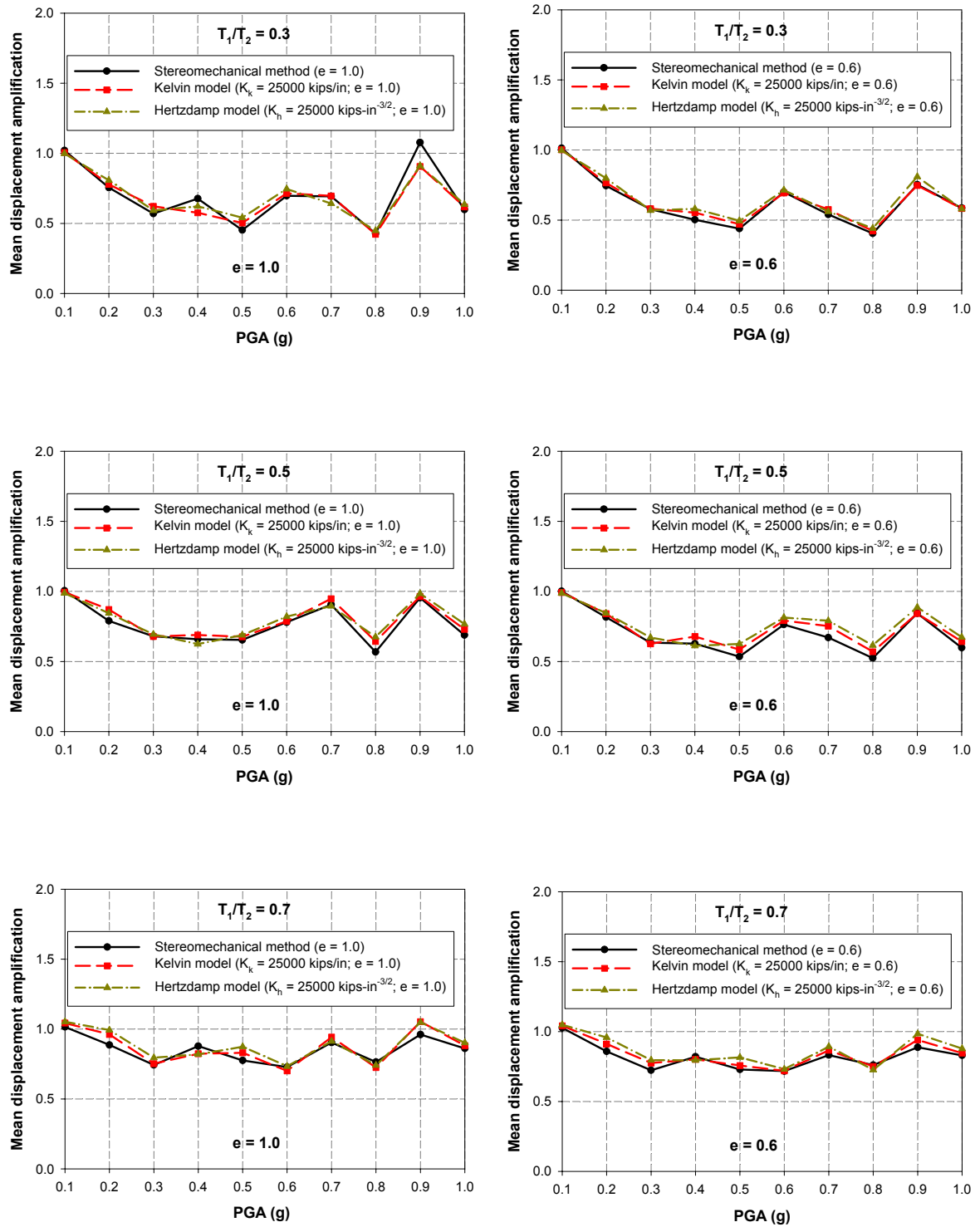
Figure 5.10: Mean displacement amplification due to pounding – DOF$_2$ – elastic systems;

T$_1$/T$_2$ = 0.3, 0.5, 0.7; e = 1.0, 0.6; 30 ground motions
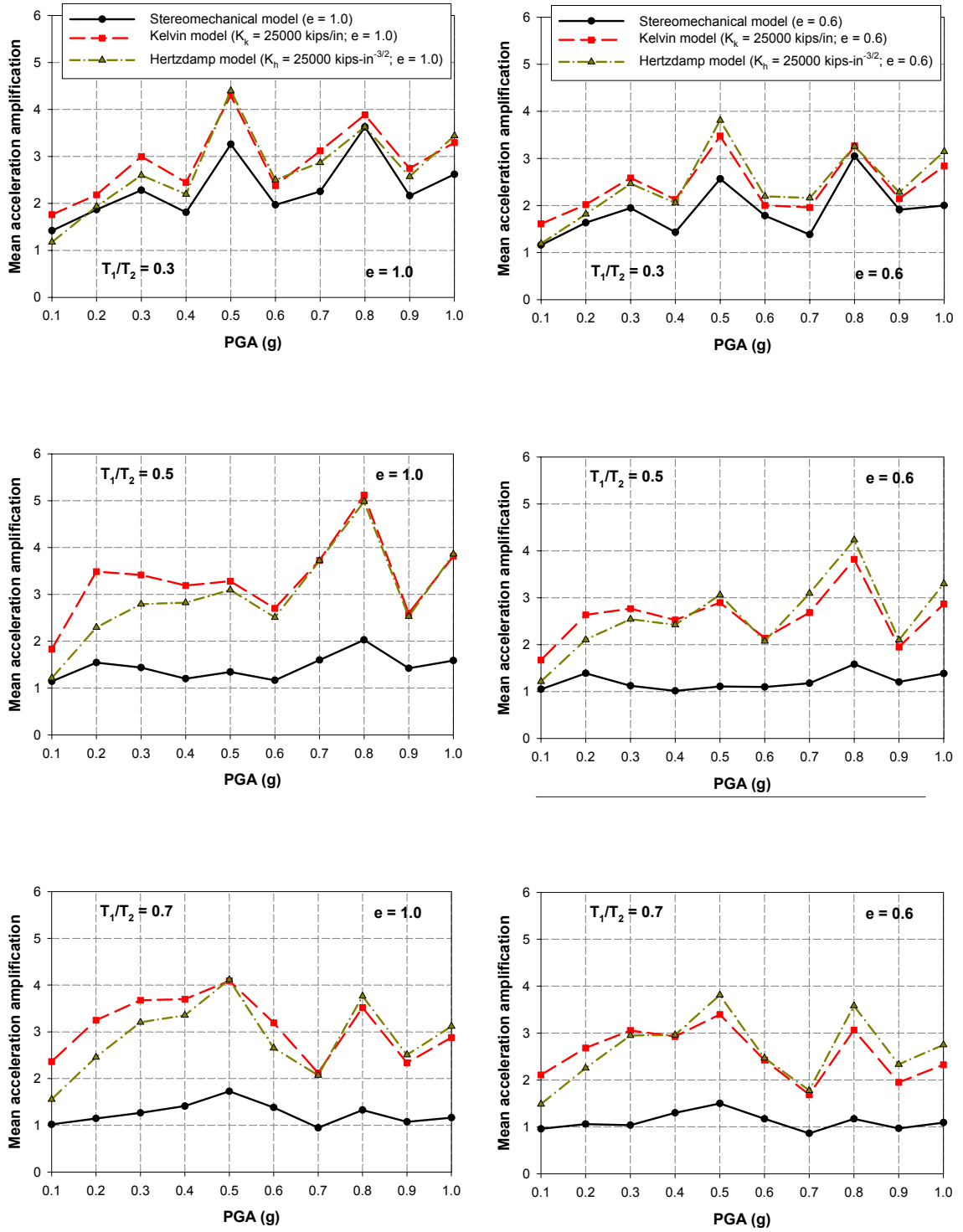
Figure 5.11: Mean acceleration amplification due to pounding – DOF$_1$ – elastic systems;

T$_1$/T$_2$ = 0.3, 0.5, 0.7; e = 1.0, 0.6; 30 ground motions
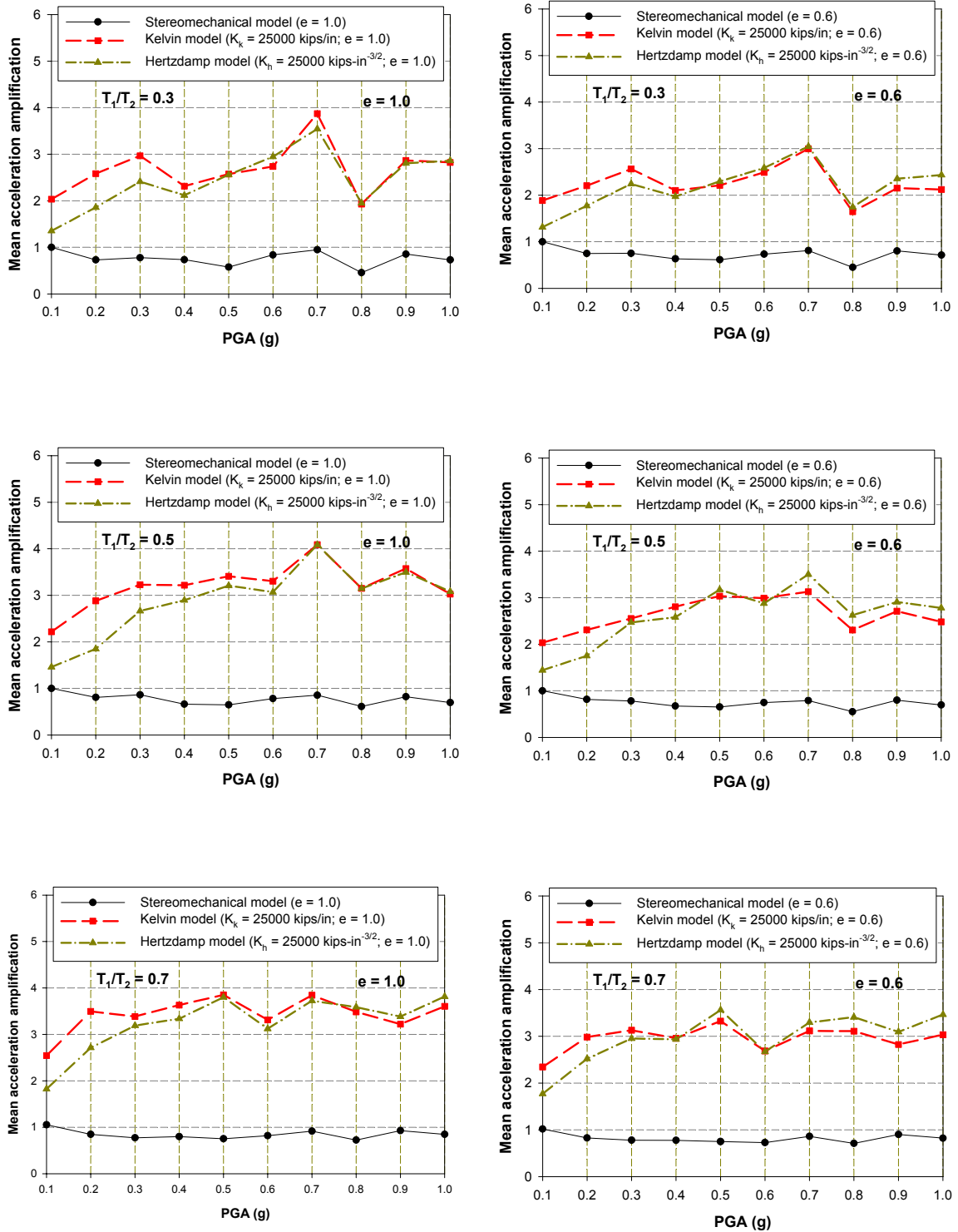
Figure 5.12: Mean acceleration amplification due to pounding – DOF$_2$ – elastic systems;

T$_1$/T$_2$ = 0.3, 0.5, 0.7; e = 1.0, 0.6; 30 ground motions
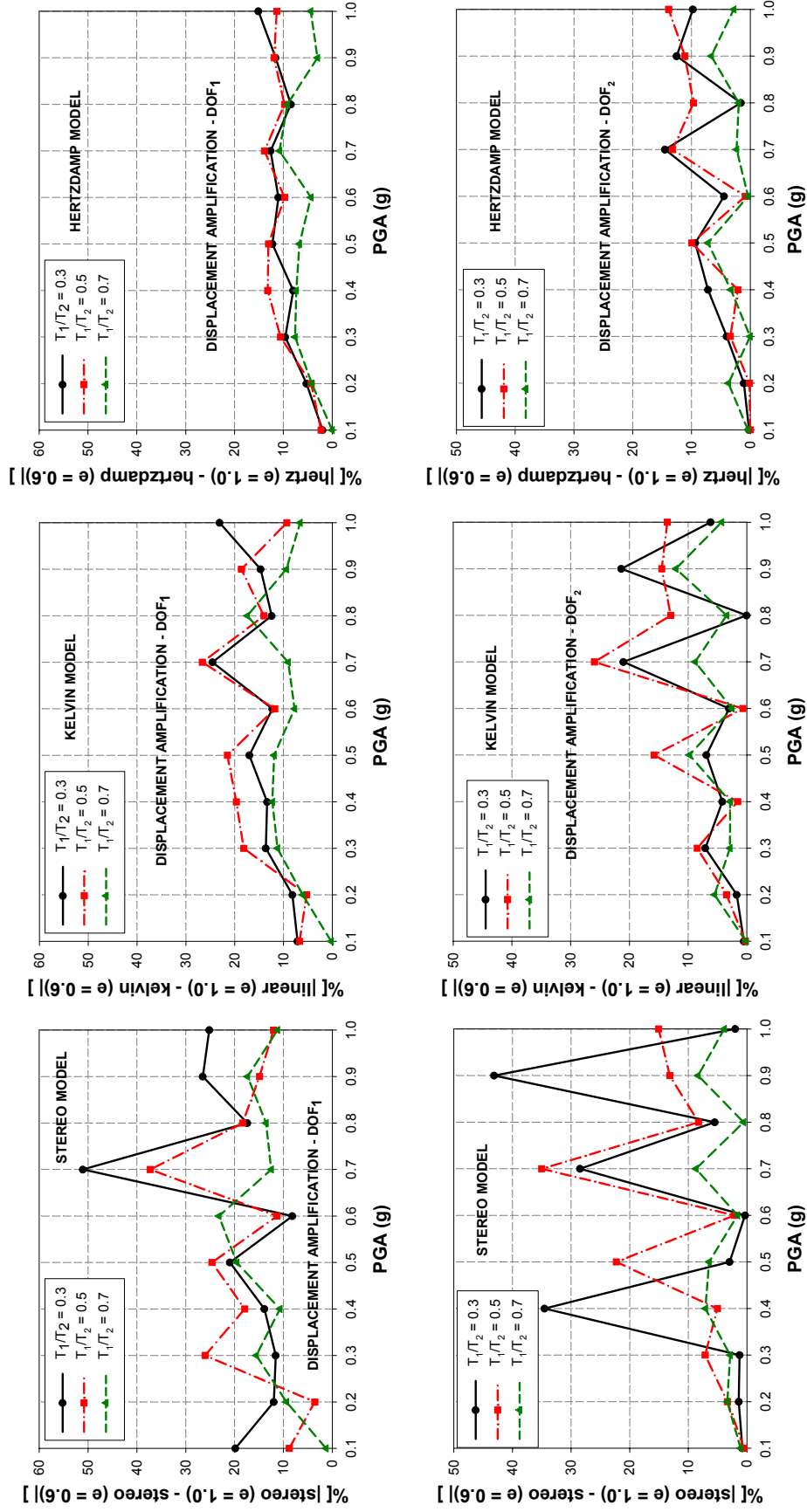
Figure 5.13: Difference in displacement amplifications due to change in the coefficient of restitution from 1.0 to 0.6; elastic systems;

top – DOF$_1$; bottom – DOF$_2$
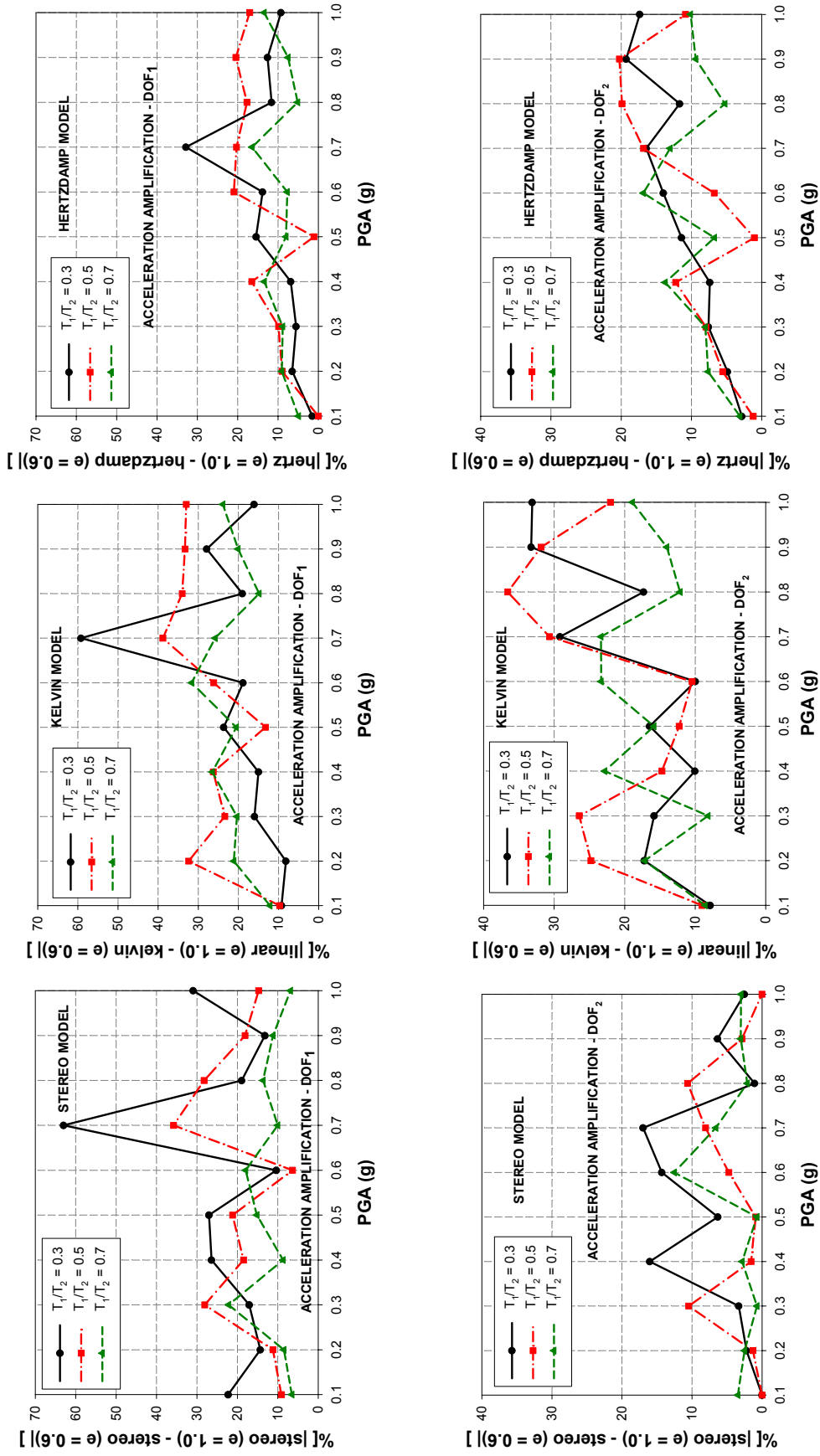
Figure 5.14: Difference in acceleration amplifications due to change in the coefficient of restitution from 1.0 to 0.6; elastic systems;
top – DOF$_1$; bottom – DOF$_2$

5.4.2. Two degree-of-freedom inelastic system

To determine if the observed trends of impact model performance are the same for yielding systems, the two degree-of-freedom system shown in Figure 5.5 is re-considered with the Q-Hyst model used for the inelastic response. The suite of earthquake records listed in Table 5.3 is used for analysis. The system yield forces for each ground motion record are obtained by dividing the maximum elastic forces by a constant reduction factor, $R_y = 3$. Figures 5.15-5.18 present the displacement and acceleration amplification for various values of PGA and e. The displacement amplifications get closer to one with increasing period ratio, as observed for linear systems. The stereomechanical and contact force models predict similar displacement amplifications, for all cases considered.

Linear systems exhibited larger differences in displacement amplifications for highly out-of-phase frames, which became marginal with increasing period ratio. However, the differences in displacement amplifications between various impact models are smaller for yielding systems. This can be explained by observing that the period ratio for the yielding system is actually, $T_1\sqrt{\mu_1}/T_2\sqrt{\mu_2}$, where μ_1, μ_2 are the ductility demands of system 1 and 2, respectively. The ductility demand for both systems will be different even though the same reduction factor is used for both. With T_1 being less than T_2, μ_1 will be greater than μ_2, for any given earthquake record. This implies that the yielding system is essentially more in-phase than its linear counterpart. Thus, the differences in displacements between the various models are less for yielding systems.

As observed for the linear case, variation of displacement amplification with PGA shows no clear trend for all the impact models. Lowering the coefficient of restitution, once again reduces the displacement amplification of both systems. The acceleration

amplifications are smaller compared to the linear case but exhibit similar trends to those observed in the linear study. The contact force models predict large acceleration amplifications, with the Hertzdamp model having lower amplifications than the Kelvin model. But now, there is a difference in how the acceleration amplifications vary as a function of T_1/T_2. The acceleration amplifications reduce with increasing period ratio, as yielding lowers the acceleration spectrum values and also increases the system period, thereby shifting the acceleration response on the spectrum more to the right. In fact, for $T_1/T_2 = 0.7$, the acceleration amplifications from the Hertzdamp model are comparable to those from the stereomechanical model for $e = 0.6$.

The effect of energy loss is presented in Figures 5.19 and 5.20. Once again, the Hertzdamp model displays the least variation to changes in e, with differences in displacements under 15% and differences in acceleration under 20%, for all period ratios. For a period ratio of 0.7, the stereomechanical and Hertzdamp models are the most effective and energy loss is not significant.
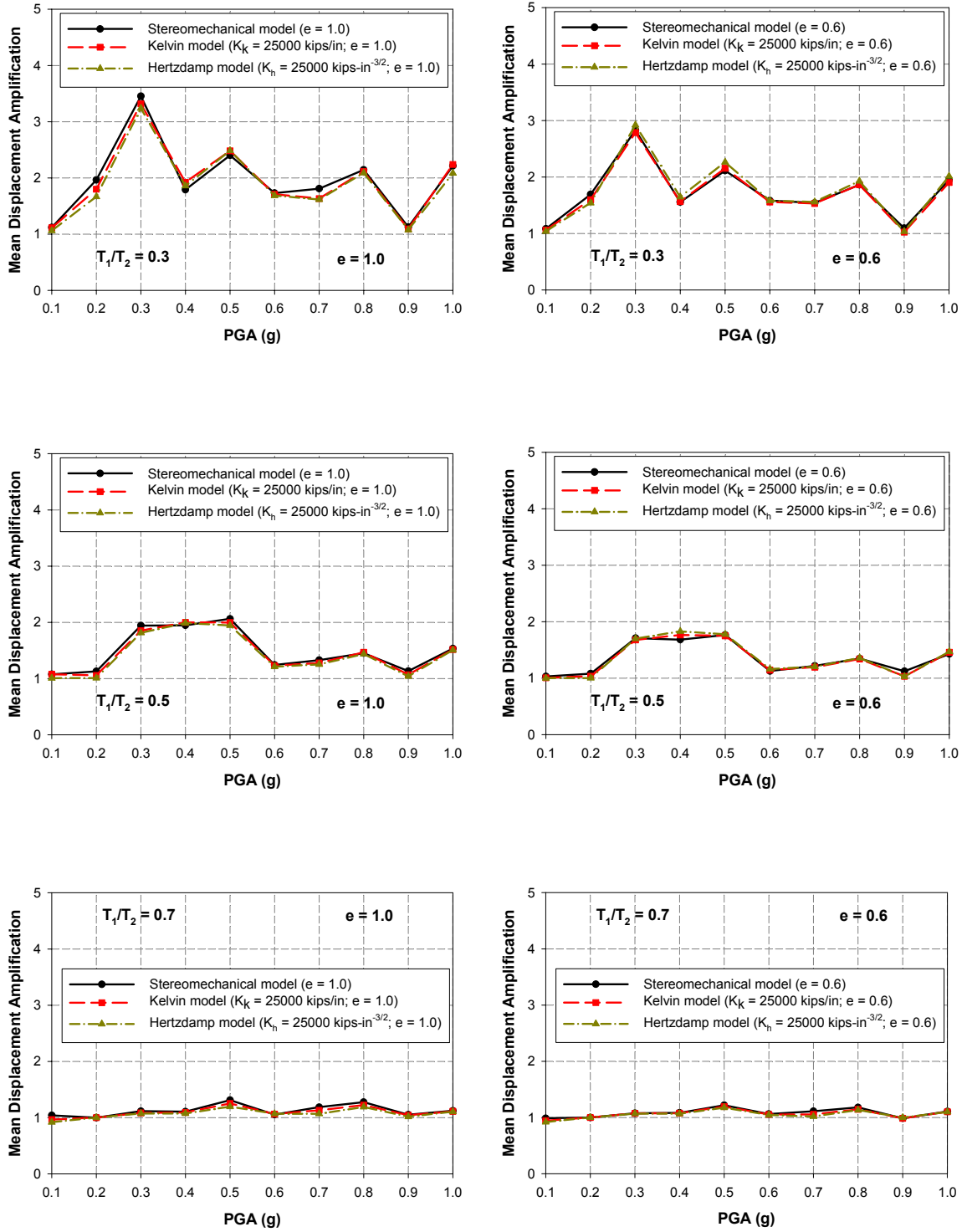
Figure 5.15: Mean displacement amplification due to pounding – DOF$_1$ – inelastic

systems – Qhyst (R_y = 3); T$_1$/T$_2$ = 0.3, 0.5, 0.7; e = 1.0, 0.6; 30 ground motions
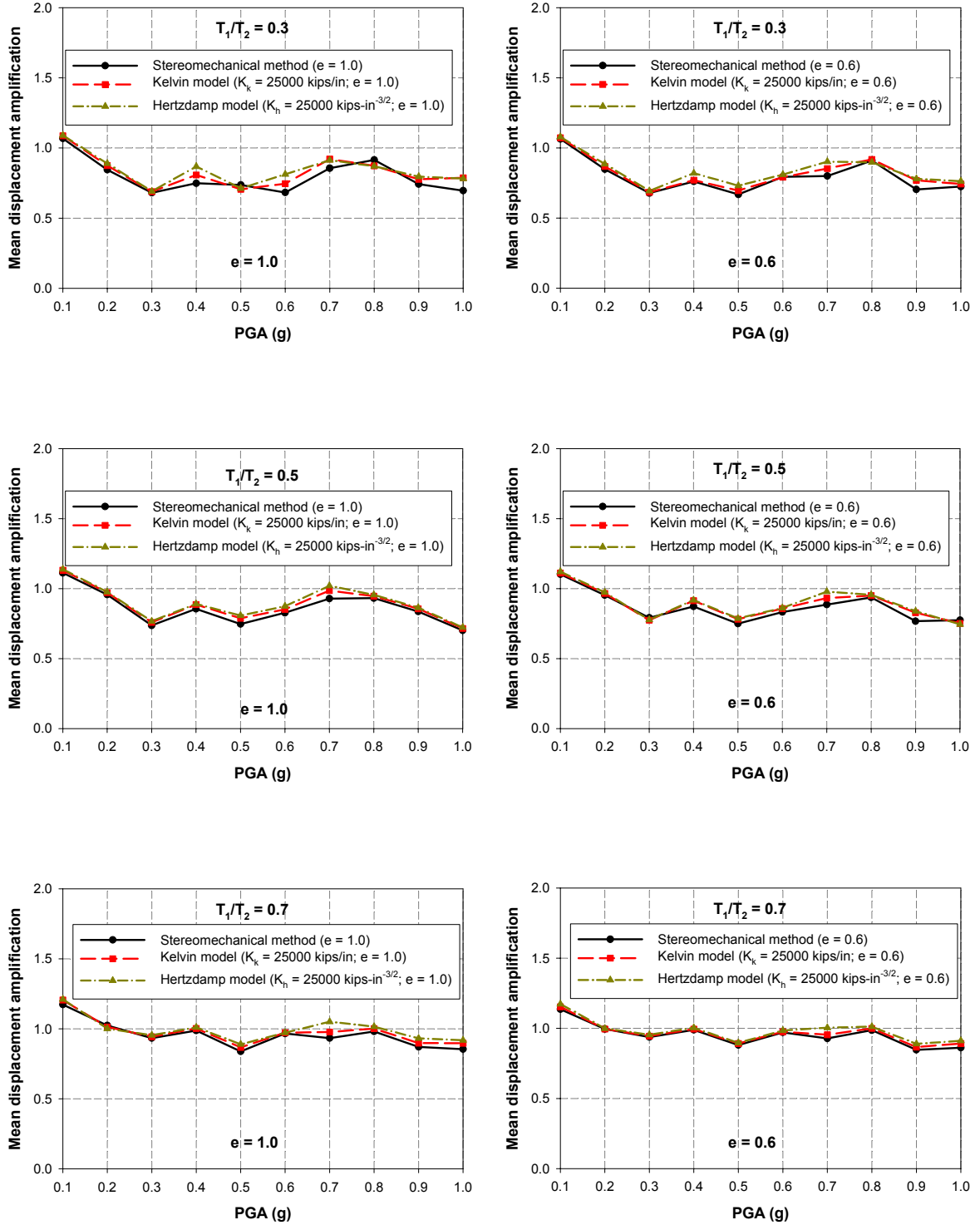
Figure 5.16: Mean displacement amplification due to pounding – DOF$_2$ – inelastic

systems – Qhyst (R$_y$ = 3); T$_1$/T$_2$ = 0.3, 0.5, 0.7; e = 1.0, 0.6; 30 ground motions
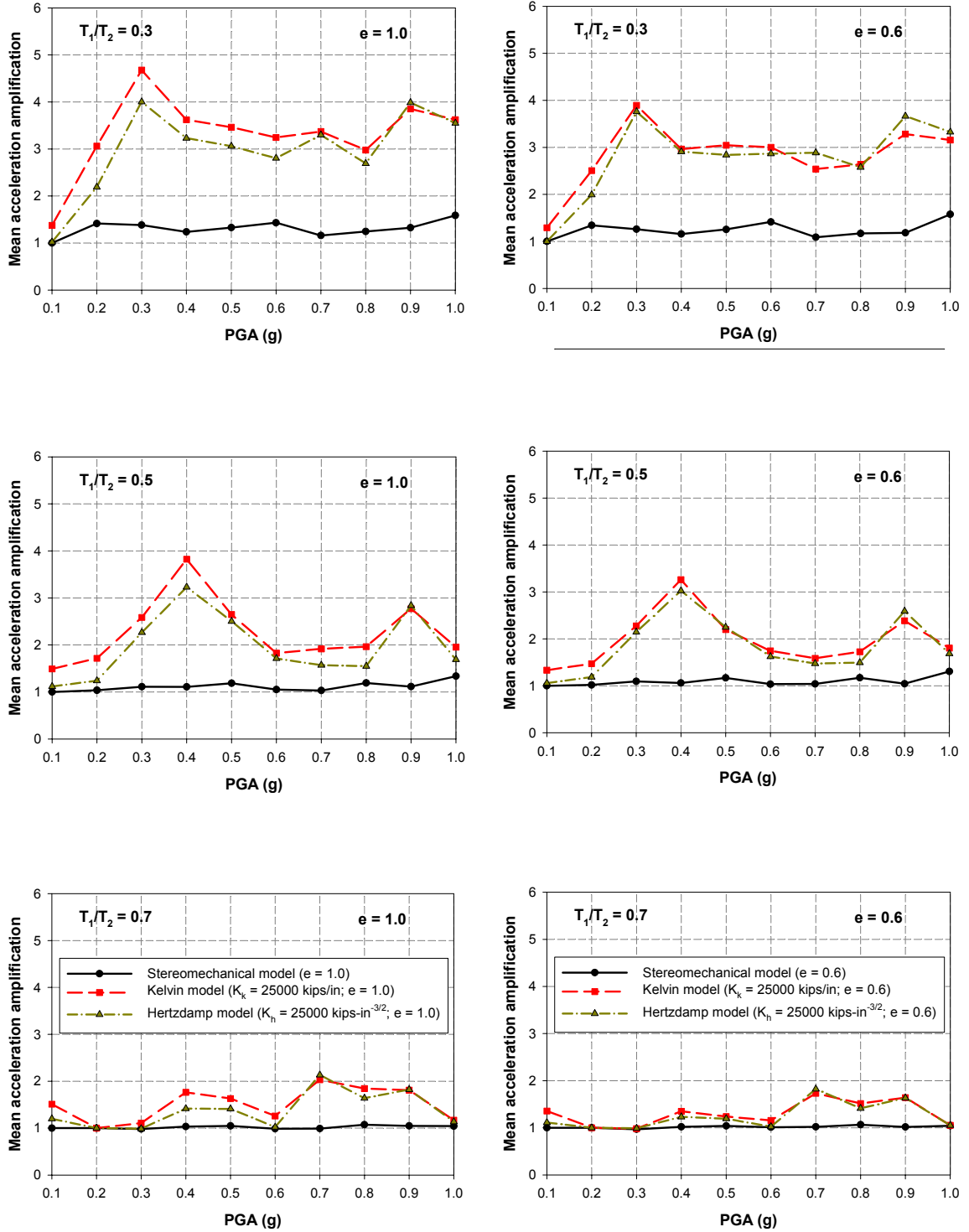
Figure 5.17: Mean acceleration amplification due to pounding – DOF_1 – inelastic systems

– Qhyst ($R_y = 3$); $T_1/T_2 = 0.3, 0.5, 0.7$; $e = 1.0, 0.6$; 30 ground motions
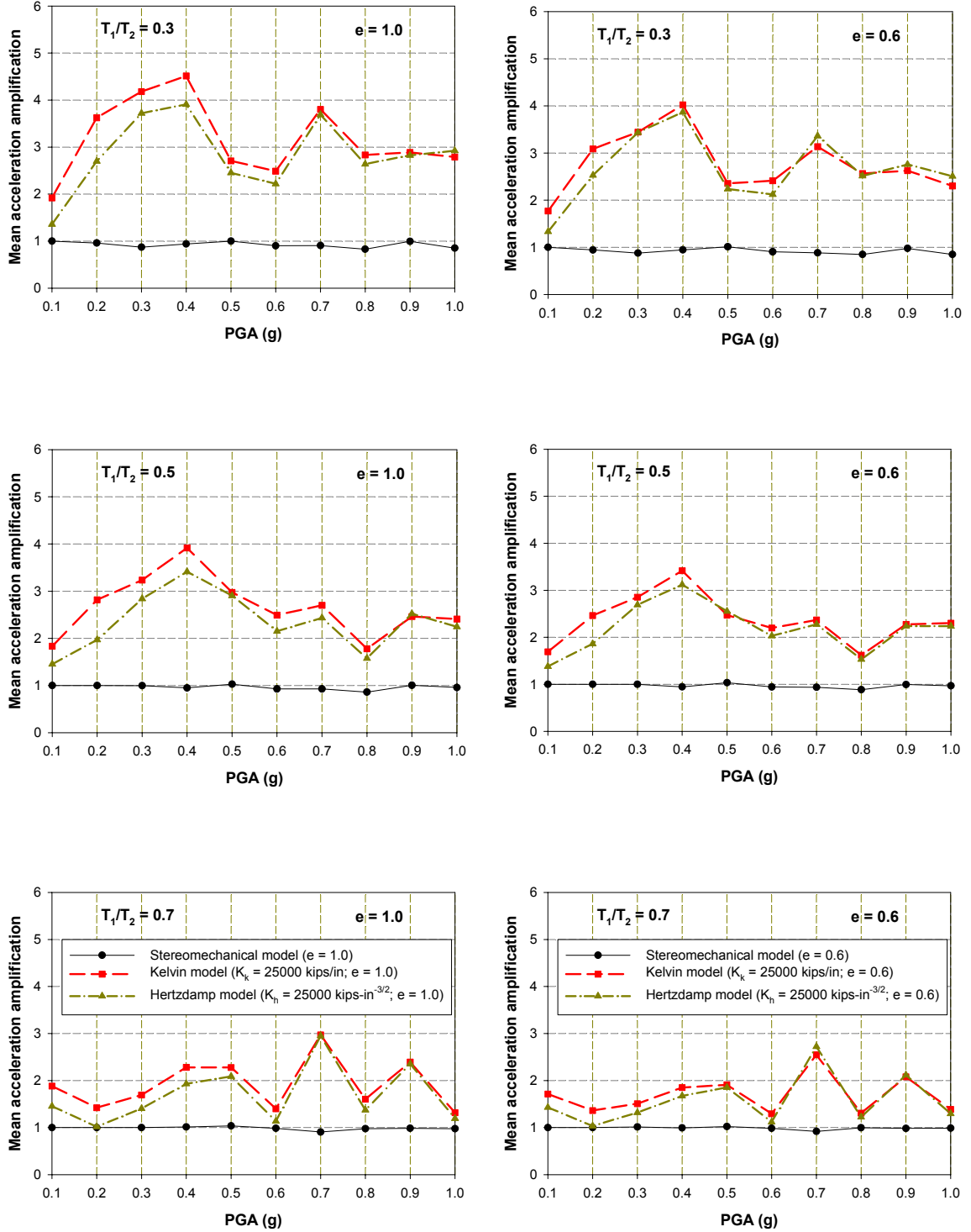
Figure 5.18: Mean acceleration amplification due to pounding – DOF$_2$ – inelastic systems

– Qhyst (R$_y$ = 3); T$_1$/T$_2$ = 0.3, 0.5, 0.7; e = 1.0, 0.6; 30 ground motions
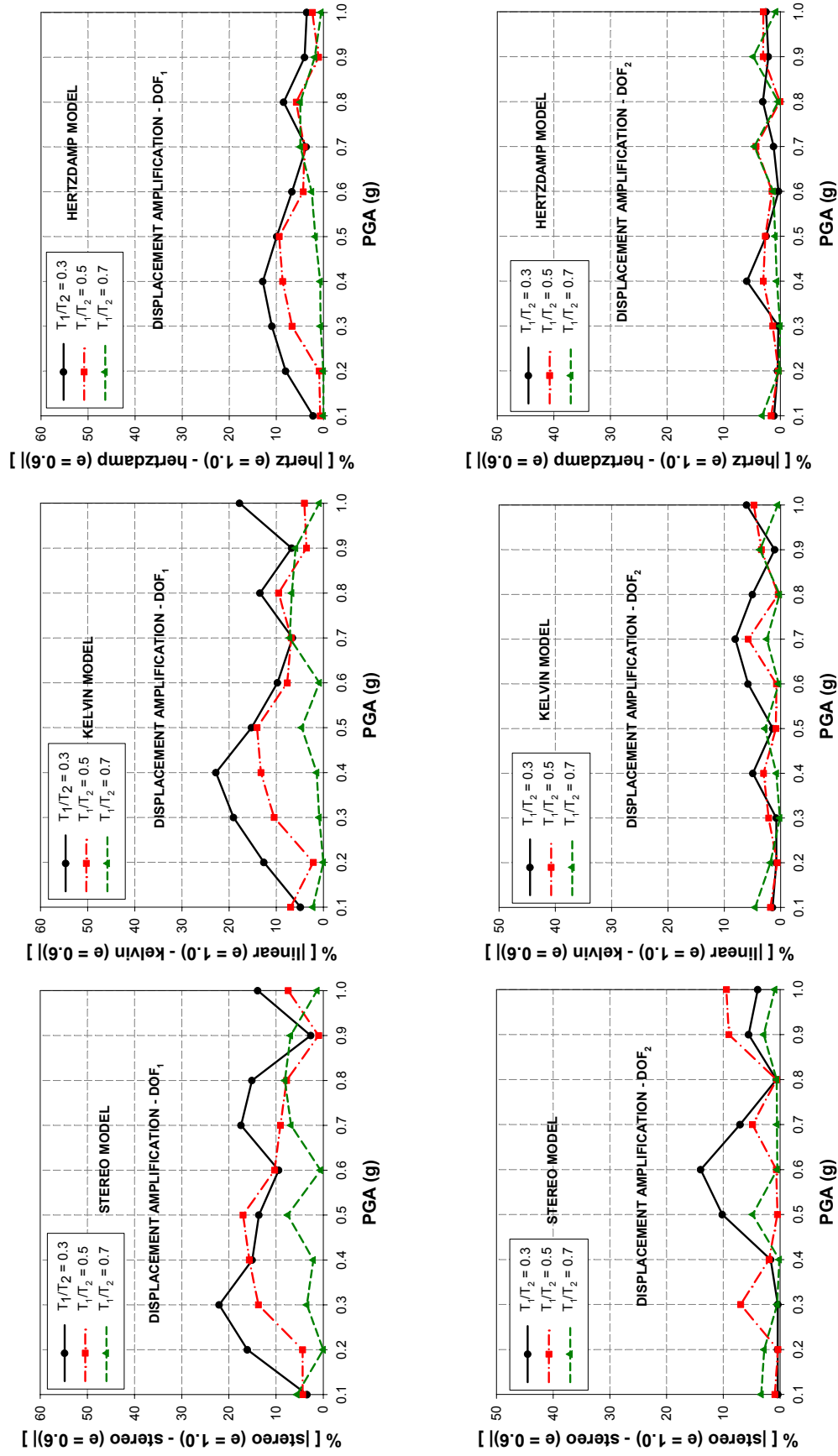
Figure 5.19: Difference in displacement amplifications due to change in the coefficient of restitution from 1.0 to 0.6; inelastic systems; top – DOF_1; bottom – DOF_2
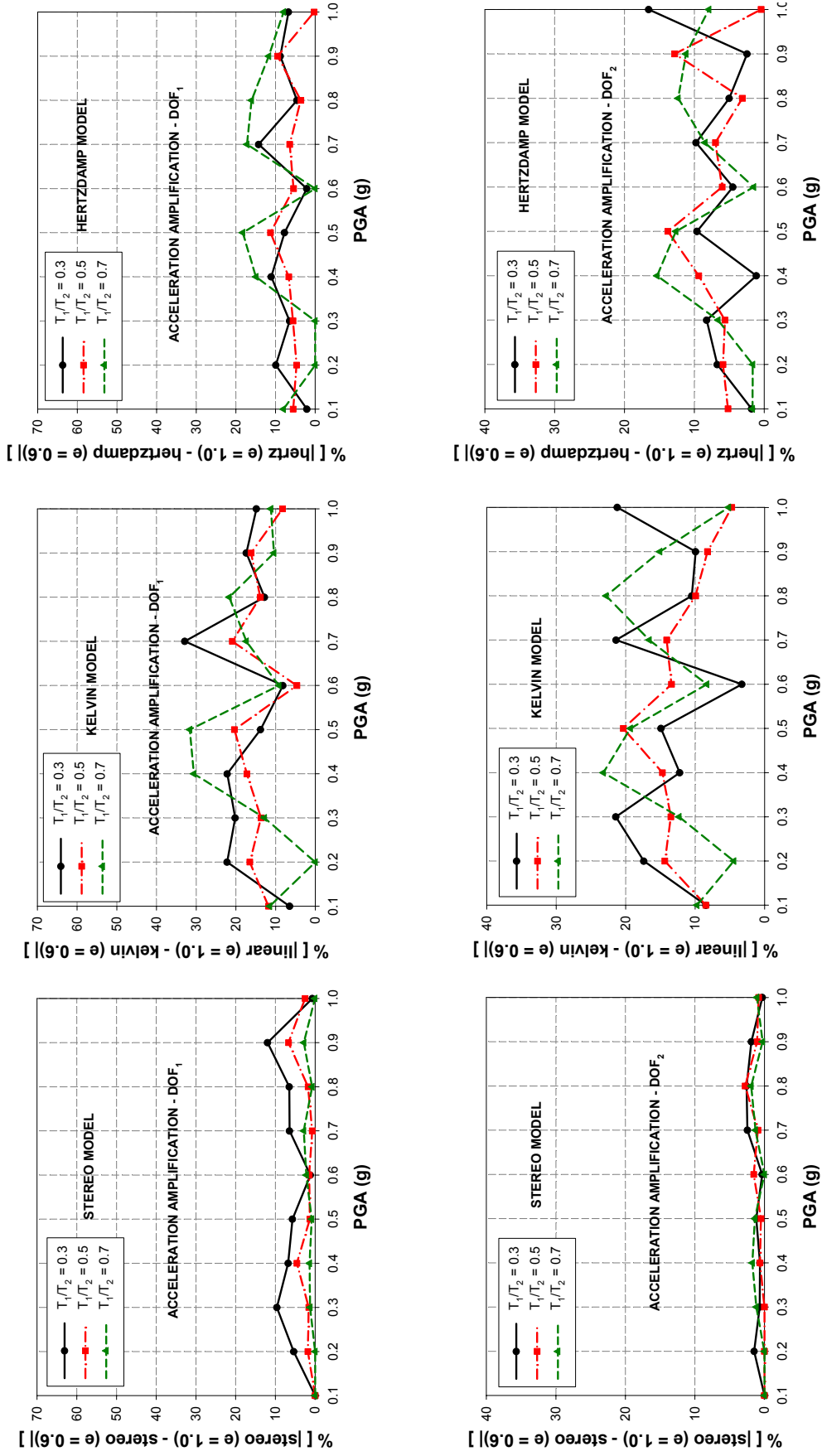
Figure 5.20: Difference in acceleration amplifications due to change in the coefficient of restitution from 1.0 to 0.6; inelastic systems;

$top - DOF_1$; $bottom - DOF_2$

5.5. Effect of impact models on the global bridge response – A case study

The previous section performed a comparison of various pounding models for a two degree-of-freedom system without restrainers, bearings and abutments. The system responses using various impact models were fairly similar, for a given coefficient of restitution (e). However, the addition of bearings, restrainers and abutments could induce greater differences in the pounding response of the bridge, through interaction of the various components. Hence, a case study is performed with a four-frame bridge model shown in Figure 5.21. Frame weights of 2880 k, 7080 k, 7080 k and 2880 k are selected for frames 1 through 4 and 5 % modal damping is assigned to the individual frames. The properties of various bridge components are listed in Table 5.4. The Q-Hyst model is selected as the frame-force deformation relation. The hinge gap is taken as ½ inch at all intermediate hinge locations. The Saratoga record from the 1989 Loma Prieta earthquake, having a PGA of 0.5g is chosen for analysis.
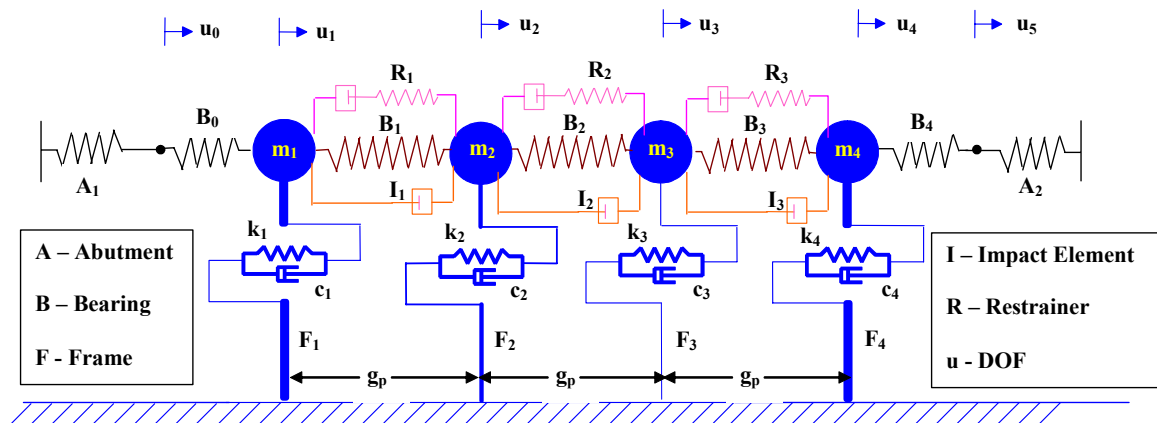
Figure 5.21: Four-frame bridge used in case study comparing various impact models

Table 5.4: Properties of various bridge components

Element	Component	Initial stiffness (kips/in)	Yield strength (kips)	Period (s)
Frame	F_1, F_4	1333	774	0.47
	F_2, F_3	577	1824	1.12

Element	Component	Initial stiffness (kips/in)	Yield strength (kips)	Strain hardening (%)
Restrainer	R_1, R_3	200	840	5
	R_2	100	420	5
Bearing	B_1, B_2, B_3	6	2.4	33
	B_0, B_4	2600	1560	33

Element	Component	Active stiffness (kips/in)	Passive stiffness (kips/in)
Abutment	A_1, A_2	10	2600

The maximum frame displacements and accelerations when pounding is simulated using various models are presented in Figures 5.22 and 5.23. The models without energy dissipation such as the stereomechanical (e = 1), linear and hertz models overestimate the stiff frame displacement (Frames 1 and 4), as observed in the parameter studies. Differences can be as large as 25% for Frame 1 when the Hertzdamp model is used.

However, the energy dissipating models predict higher flexible frame displacements than the models without energy dissipation, contrary to what was observed earlier. This is because the flexible frame undergoes two-sided impact in this case and also interacts with restrainers and bearings. The contact force-based models – Kelvin and Hertzdamp predict high frame accelerations due to pounding with larger accelerations for e = 1. The impact acceleration can reach as high as 2.8g for Frame 4, when the Kelvin model is used and e = 1.0. The Hertzdamp model predicts the least impact accelerations among the contact models.
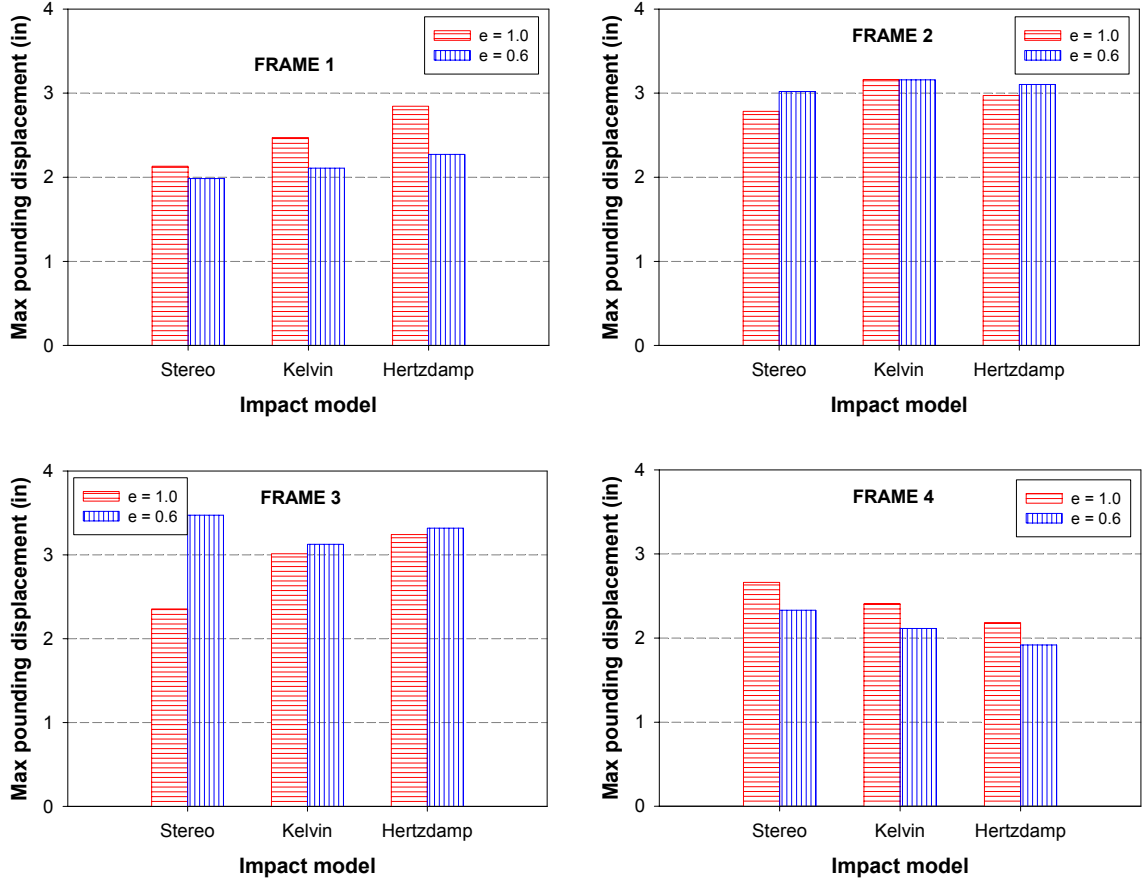
Figure 5.22: Maximum frame displacements using various impact models – Coyote Lake

Dam record, 1989 Loma Prieta earthquake (PGA = 0.5 g)

The Kelvin model shows the least variation in the displacement response due to changes in e. However, the Hertzdamp model shows smaller variation for differences in accelerations. Moreover, the Hertzdamp model provides the least impact forces among contact models as illustrated in Figure 5.24, because the penetration is less than one inch and impact is modeled using a nonlinear spring. Thus, it can be concluded that the Hertzdamp model is the most effective contact-based model.
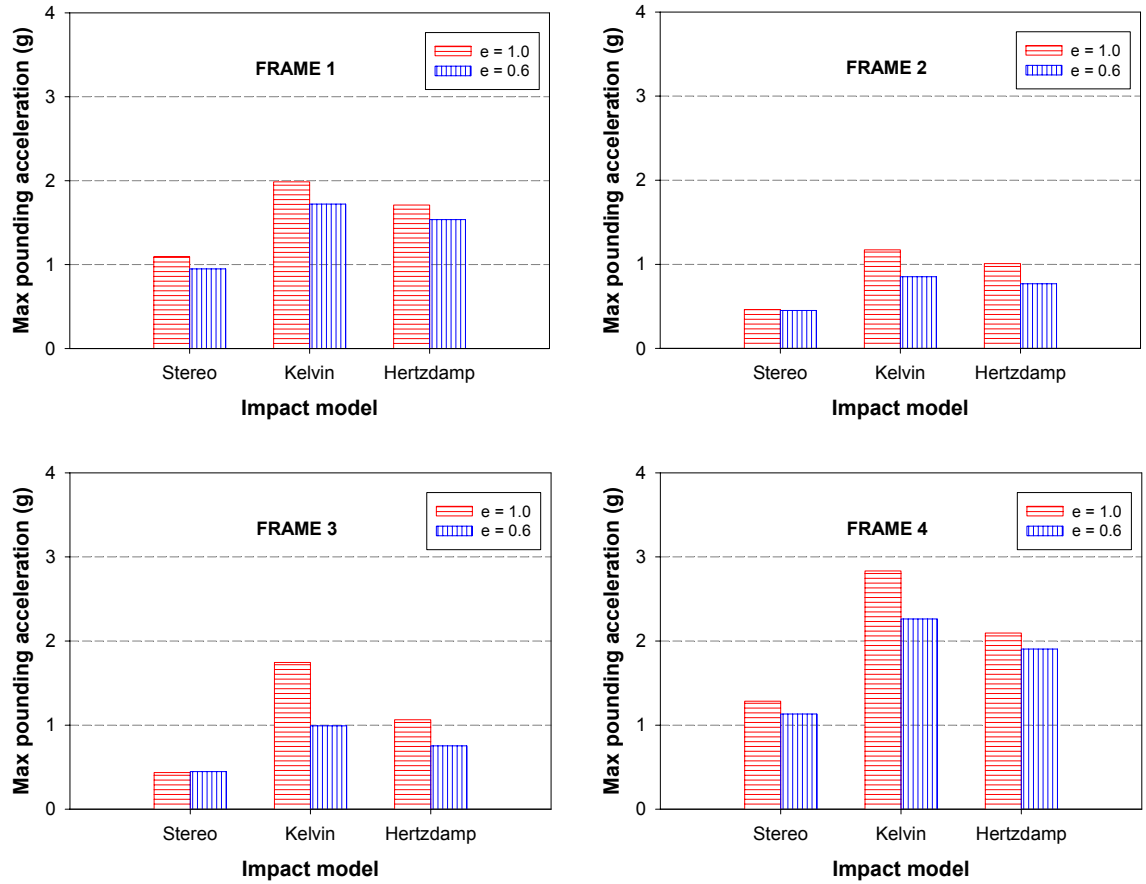
Figure 5.23 Maximum frame accelerations using various impact models – Coyote Lake

Dam record, 1989 Loma Prieta earthquake (PGA = 0.5 g)
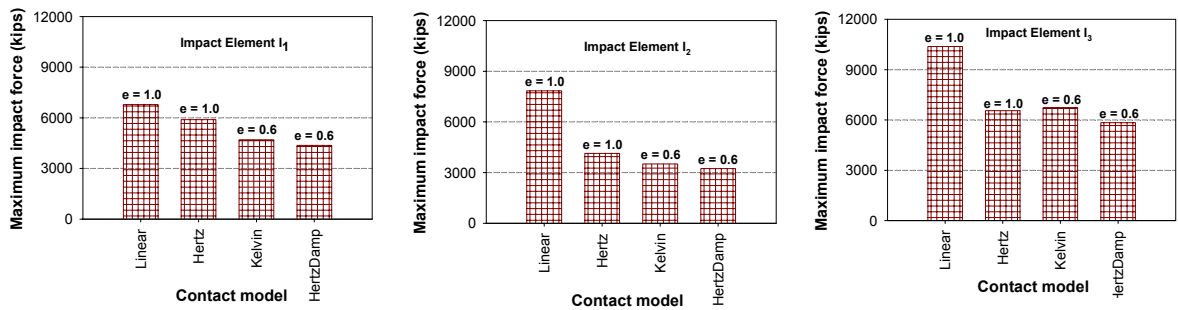
Figure 5.24: Maximum impact forces from various contact models

5.6. Conclusions

The cogency of various impact models in representing the pounding response of closely spaced structures is investigated in this chapter. Existing impact models such as the linear spring, Kelvin, Hertz and stereomechanical models are considered for analysis. In addition, a contact model based on the Hertz law and using a nonlinear hysteresis damper (Hertzdamp model) is introduced for pounding simulation. A case study is conducted to compare the performance of the impact models in simulating dynamic impact between two closely spaced adjacent structures modeled as a two degree-of-freedom elastic system. The results indicate that the pounding models without energy dissipation overestimate the stiff system response by as much 15%, when impact is modeled using a linear spring.

A parameter study is then performed using two degree-of-freedom linear and nonlinear systems to study the efficacy of various impact models for three system period ratios $(T_1/T_2) - 0.3, 0.5, 0.7$ and two values of the coefficient of restitution, e = 0.6, 1.0. Thirty ground motion records with PGAs varying from 0.1g to 1.0g are used in the analysis. The displacement results indicate that the stereomechanical and contact force-based models show similar trends, even though they use different methodologies to represent impact. For linear systems, the differences in displacement amplifications between various impact models are larger (up to 20%) for highly out-of-phase frames. Smaller differences (up to 10%) are exhibited for nonlinear frames.

Lowering the coefficient of restitution from 1.0 to 0.6, reduces both the displacement and acceleration amplifications due to impact. For linear systems with $T_1/T_2 = 0.3$ and PGA = 0.7g, the stiff frame displacement amplification is reduced by 50% for the

stereomechanical model and 25% for the Kelvin model, when e changes from 1.0 to 0.6. The corresponding reduction in acceleration amplifications is around 60% for both models. The Hertzdamp model appears to be the most effective contact-based model as it shows the least variation due to changes in e and also provides the lowest acceleration amplification and impact force, for both linear and nonlinear systems.

The results from the parameter study confirm that energy loss during impact is not significant for systems with a period ratio of 0.7. At a period ratio of 0.7, the stereomechanical model is found to be the most effective for linear systems and the stereomechanical and hertzdamp models provide better results, for nonlinear systems. Finally, a case study is conducted with a four-frame bridge to investigate the differences in bridge response when impact is represented using various models. The results show good agreement with the findings from the parameter study.

CHAPTER 6

EFFECT OF FRAME RESTORING FORCE CHARACTERISTICS ON THE

POUNDING RESPONSE

Past research into seismic pounding has primarily focused on determining the factors affecting pounding (DesRoches and Fenves, 1997a), modeling the impact phenomenon (Jankowski et al., 1998; Malhotra, 1998), and developing mitigation strategies for pounding hazard reduction (Kawashima and Shoji, 2000). Typically, the participating structural systems have been modeled using bilinear or stiffness degrading models. However, experimental tests on concrete columns have shown that strength degradation occurs under increased cycles of loading, which is accelerated under the presence of axial compressive loads (Saaticioglu and Ozcebe, 1989). To the author's knowledge, no study has yet considered the effects of strength degradation on the pounding response of bridge frames.

In this chapter, the influence of column hysteretic characteristics, such as stiffness degradation, strength deterioration and pinching on the pounding response is studied. Several analytical models are considered including the bilinear, Q-Hyst (stiffness degrading) and pivot hysteresis (strength degrading) models. Parameter studies are performed using two degree-of-freedom systems with varying period ratios subject to a suite of far-field ground motion records, to ascertain if the pounding trends observed in Chapter 4 are valid for all hysteretic models. A case study is then conducted to assess the pounding response of the various hysteretic models in the presence of near-field

earthquakes. Finally, the effect of hysteretic model type on the global responses of a multiple-frame bridge system is highlighted through an example.

6.1. Hysteretic models for reinforced concrete columns

Reinforced concrete bridge columns can develop inelastic deformations and exhibit nonlinear behavior under moderate to strong base excitation. In the past, elasto-plastic and bilinear models were used due to their simplicity in concept and numerical implementation. Stiffness degradation in concrete was first accounted for with the introduction of a degrading stiffness approach (Clough and Johnston, 1966). Subsequent experimental tests on both small-scale and full-scale column specimens have shown that cyclic behavior of reinforced concrete is characterized by constantly changing stiffness, strength degradation and a reduction in energy absorption capacity (Takeda et al., 1970; Saatcioglu and Ozcebe, 1989; Dowell et al., 1998).

A typical lateral load-deflection hysteretic relationship for a reinforced concrete column is shown in Figure 6.1. The general hysteretic characteristics can be summarized as follows:

➢ Reduction in stiffness occurs due to the increased loading cycles, which can be attributed to the flexural cracking in concrete and the Bauschinger effect in steel.

➢ The peak strength attained in each cycle decreases with increased loading cycles. This strength degradation is a result of the disintegration of core concrete.

➢ The hysteretic loop exhibits pronounced pinching effects, which can be attributed to high shear stress reversals and slippage of the longitudinal reinforcement within the anchorage area.

118
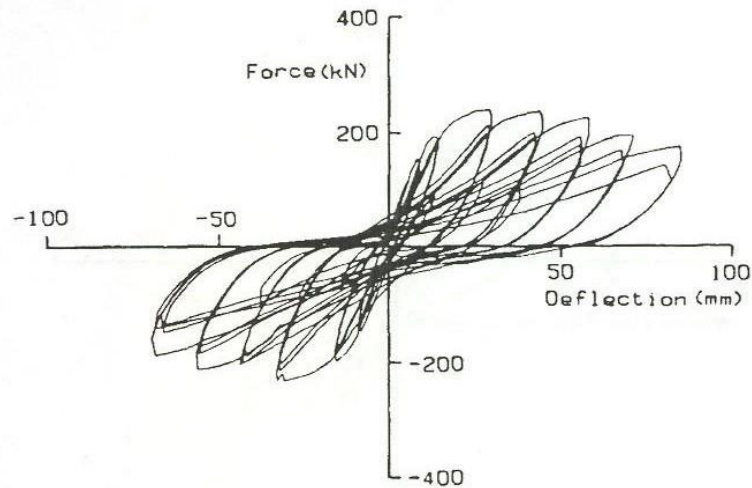
Figure 6.1: Lateral load-deflection relation for a reinforced concrete column obtained

from experiment (Saatcioglu and Ozcebe, 1989)

> ➢ The hysteretic characteristics of reinforced concrete are dependent on the loading
>
>   history.

Several hysteresis models have been developed to capture the nonlinear dynamic response of reinforced concrete columns subjected to base excitation. These range from relatively simplistic models such as the elasto-plastic and bilinear models, to more rigorous models, such as the Takeda (Takeda et al., 1970), Park (Kunnath et. al., 1990) and the Pivot hysteresis models (Dowell et al., 1998). Other models such as the Clough model (Clough and Johnston, 1966) and the Q-Hyst model (Saiidi and Sozen, 1979) have also been popular. A brief discussion of the hysteretic models considered in this study is outlined below.

Elasto-plastic model

This is a simple model defined by three rules. The backbone curve is defined by an elastic stiffness (k) which represents cracked-section behavior and a post-yield portion with zero stiffness, as shown in Figure 6.2. The unloading stiffness is taken to be the same as the elastic loading stiffness. This model is a very poor representation of the hysteretic behavior of concrete as it does not represent stiffness deterioration with increasing displacement amplitude reversals. However, it has been extensively used because of its simplicity in modeling.
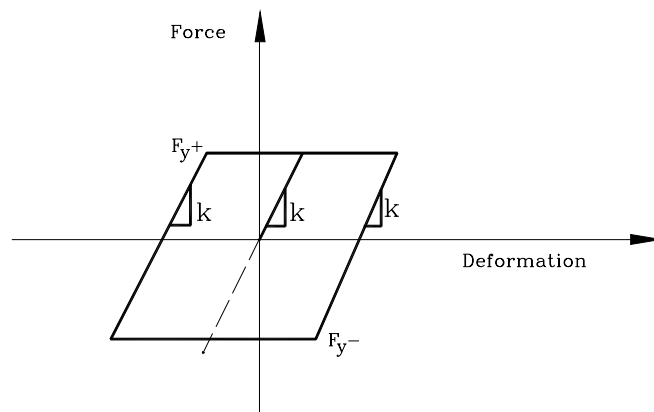
Figure 6.2: Elasto-plastic hysteresis model

Bilinear model

This is very similar to the elasto-plastic model, but it also accounts for the strain hardening effect in steel using a non-zero post yield stiffness, as shown in Figure 6.3. Stiffness and strength degradation effects cannot be represented. Both the elasto-plastic

and bilinear models do not consider hysteretic energy dissipation for small displacements. Many studies evaluating the effects of pounding have used bilinear models to represent the behavior of adjacent structures (Anagnostopoulos, 1988; Pantelides and Ma, 1998; Kim et al., 2000).
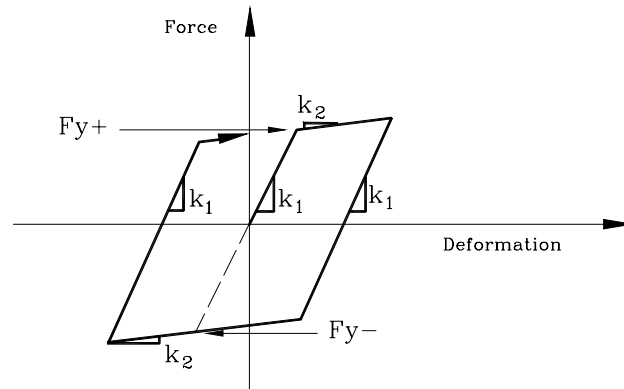
Figure 6.3: Bilinear hysteresis model

Q-Hyst model (Saiidi and Sozen, 1979)

The Q-hyst model is defined by four rules and closely represents the response from a Takeda model, which is a more realistic representation of the cyclic behavior of reinforced concrete columns. The backbone curve used is bilinear with strain hardening as shown in Figure 6.4. Stiffness degradation is accounted for at unloading and load reversal. The unloading stiffness is defined by $K_q = K(D_y/D)^{0.5}$, where K is the initial elastic slope, D is the largest absolute deformation and D_y is the yield deformation. The re-loading stiffness, K_p, is defined as the slope of the line connecting the intersection of

the latest unloading branch with the displacement axis (point A) to the maximum

absolute displacement (point B), as shown in Figure 6.4. The Q-Hyst model is much

simpler than the Takeda model. However, both the Q-Hyst and Takeda models do not

account for the effect of column axial loads and strength degradation in concrete.
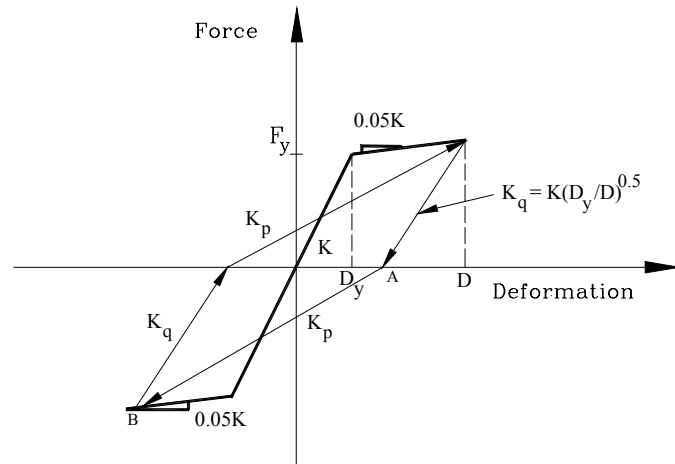
Figure 6.4: Q-Hyst model for reinforced concrete

Pivot hysteresis model (Dowell et al., 1998)

This model is governed by three simple rules and has the ability to capture the

dominant nonlinear characteristics of concrete under cyclic load. The backbone curve

used for positive and negative loading is shown in Figure 6.5. The first and second

branches of the strength envelope represent cracked-section stiffness and strain hardening

stiffness, respectively. Strength degradation from shear failure or confinement failure is

represented by the third branch. The fourth branch allows for a linearly decreasing

residual strength.
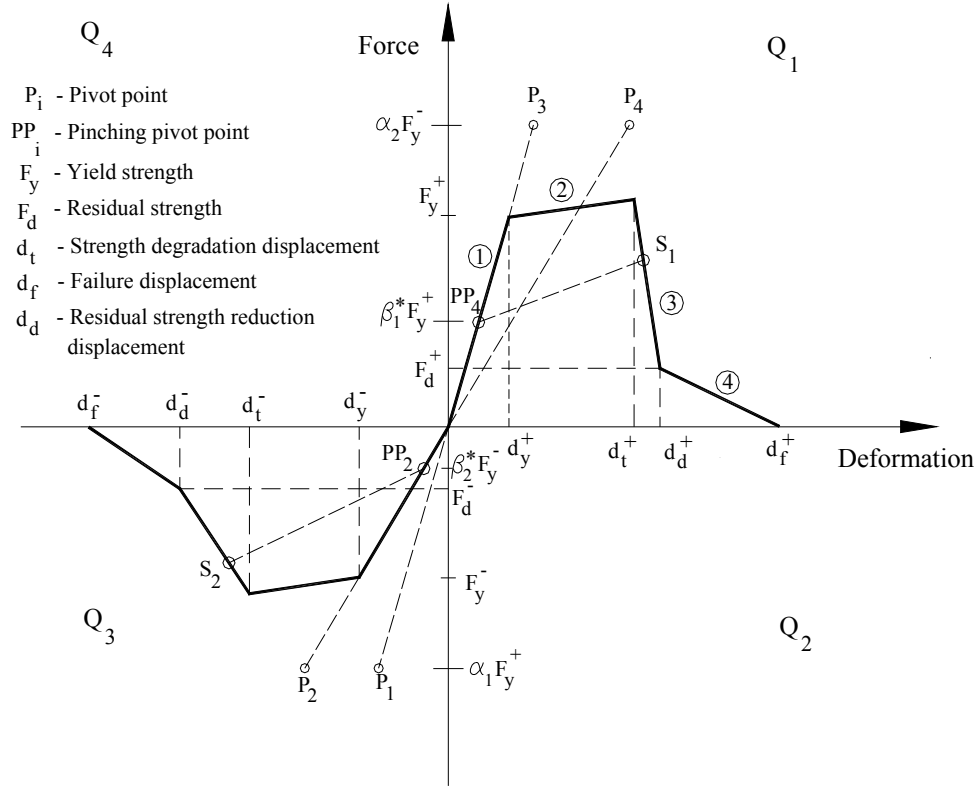
Figure 6.5: Strength envelope for the pivot hysteresis model

Primary pivot points P_1 through P_4 control the amount of softening expected with increasing displacement, using parameters α_1, α_2 as shown in Figure 6.5. Pinching pivot points PP_2 and PP_4 fix the degree of pinching following a load reversal, through parameters β_1^*, β_2^*. The response follows the strength envelope as long as no displacement reversal occurs. Once the yield displacement is exceeded in either direction, a modified strength envelope is defined by the lines joining PP_4 to S_1 and PP_2 to S_2, as illustrated in Figure 6.5. The pinching pivot points start moving toward the origin of the force-deformation relation, once strength degradation occurs. The pinching parameters, β_1^*, β_2^* are given by following equations.

$$\beta_i^* = \beta_i \; ; d_{i_{max}} \leq d_{t_i} \qquad\qquad (6.1)$$

$$\beta_i^* = \frac{F_{i_{max}}}{F_{t_i}} \beta_i \; ; d_{i_{max}} > d_{t_i} \qquad\qquad (6.2)$$

where β_1, β_2 define the degree of pinching for a ductile flexural response before strength degradation occurs. Displacements d_{imax} and d_{ti} represent the maximum displacement and strength degradation displacement, respectively, in the "i" direction of loading. F_{imax} and F_{ti} represent the force levels corresponding to d_{imax} and d_{ti}, respectively.

The set of rules defining loading and unloading in the various quadrants are graphically portrayed in Figure 6.6. The four quadrants are demarcated by the deformation axis and the elastic loading lines as indicated by the bold lines in Figure 6.6.
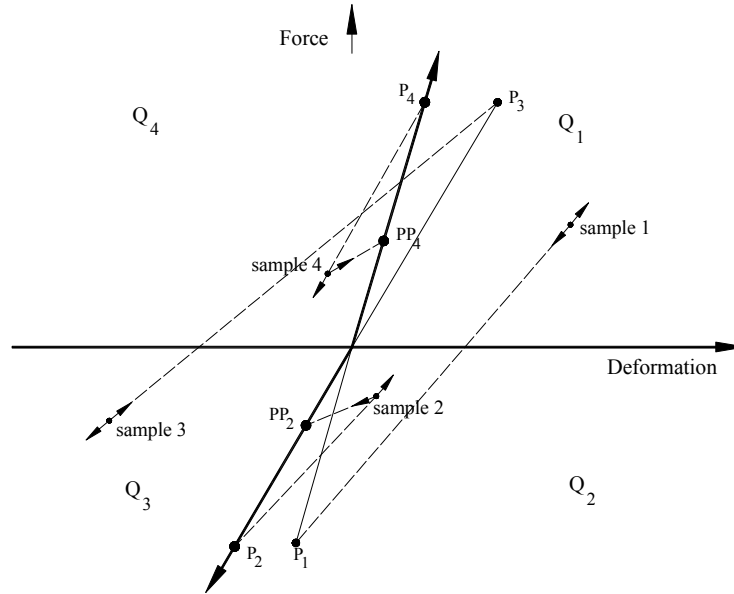
Figure 6.6: Graphical representation of loading/unloading rules for pivot model

Loading is defined as $+\varDelta d$ for quadrants Q_1, Q_4, and $-\varDelta d$ for quadrants Q_2, Q_3. Unloading is defined as $-\varDelta d$ for quadrants Q_1, Q_4, and $+\varDelta d$ for quadrants Q_2, Q_3. The condensed set of rules can be expressed as follows

1. For quadrants 1 and 3, loading and unloading are directed away from or toward point P_n, respectively.

2. For quadrants 2 and 4, loading is directed toward point PP_n.

3. For quadrants 2 and 4, unloading is directed away from point P_n.

The loading and unloading rules are followed only when the force-deformation path leaves the strength envelope.

The primary advantage of the pivot hysteresis model compared to the other models is its ability to represent effects of cyclic axial load, unsymmetrical sections and strength degradation. Unlike other models, the pivot model recognizes that yielding in one direction does not soften the member in the opposite loading direction. For instance, if the yield strength is exceeded in the positive loading direction, unloading occurs and the member reloads in quadrant Q_2 towards PP_2, the response will follow the initial elastic loading line if yielding has not yet occurred in the negative loading direction.

6.2. Comparison of hysteretic model response

A single degree-of-freedom (SDOF) system shown in Figure 6.7 is considered to study the differences in frame response when various hysteretic models are used. The system has an initial stiffness, $k = 295$ kips/in, damping ratio, $\xi = 5\%$ and a period, $T = 1$ second. The Saratoga – Aloha Avenue record with a peak ground acceleration (PGA) of 0.51g, from the 1989 Loma Prieta earthquake is chosen for analysis. The yield strength

for the system is selected such that the target ductility, μ equals 4, when the Q-Hyst model is used as the force-deformation relation. Five percent strain hardening is used wherever applicable.
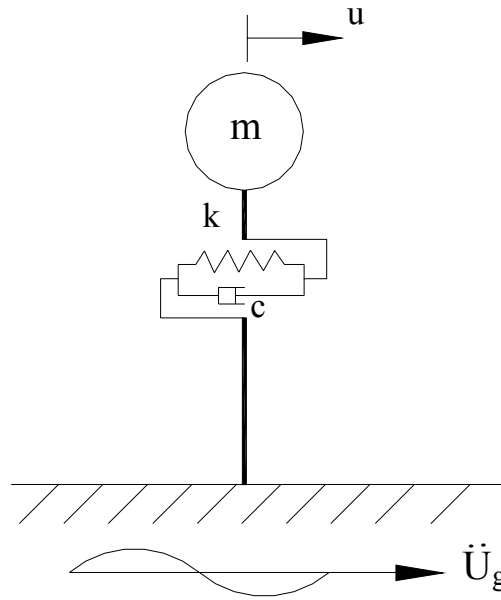
Figure 6.7: Single degree-of-freedom system used to compare hysteretic model responses

The pivot hysteresis model is considered with and without strength degradation. The case without strength degradation will be compared with the Q-Hyst model results. The parameters of the pivot model used in analysis are tabulated in Table 6.1. Parameters, α and β are selected from the recommended values for flexure dominant columns (Dowell et al., 1998).

Table 6.1: Hysteresis parameters for the pivot model

Parameter	No strength degradation	With strength degradation
Pivot parameters, α_1, α_2	4.00	4.00
Pinching pivot parameters, β_1, β_2	0.55	0.55
Yield strengths (kips), F_y^+, $\|F_y^-\|$	459	459
Yield displacements (in), d_y^+, $\|d_y^-\|$	1.56	1.56
Strength degradation displacements (in), d_t^+, $\|d_t^-\|$	$5* d_y^+$	$2* d_y^+$
Residual strength (kips), F_d^+, $\|F_d^-\|$	N/A	$0.5* F_y^+$
Residual strength reduction displacements (in), d_d^+, $\|d_d^-\|$	$7* d_y^+$	$4* d_y^+$
Failure displacements (in), d_f^+, $\|d_f^-\|$	$10* d_y^+$	$10* d_y^+$

Figure 6.8 presents the time history of displacement responses for the various hysteresis models. The responses from all the models are identical for the first 6.2 sec, as nonlinear deformations have not yet occurred. However, once the yield force has been exceeded, the elasto-plastic and bilinear model responses exhibit more permanent deformations, with a pronounced shift in the equilibrium position. This is because neither of the two models considers hysteretic energy dissipation for small displacements. The absolute maximum displacements and ductility ratios from the various models are listed in Table 6.2. Figure 6.9 presents the hysteresis loops for the various models.

The Q-Hyst response is larger than the bilinear response, as stiffness degradation in the Q-Hyst model produces less damping per cycle. However, despite major differences in the force-deformation relations, the absolute peak responses are similar for the Q-Hyst
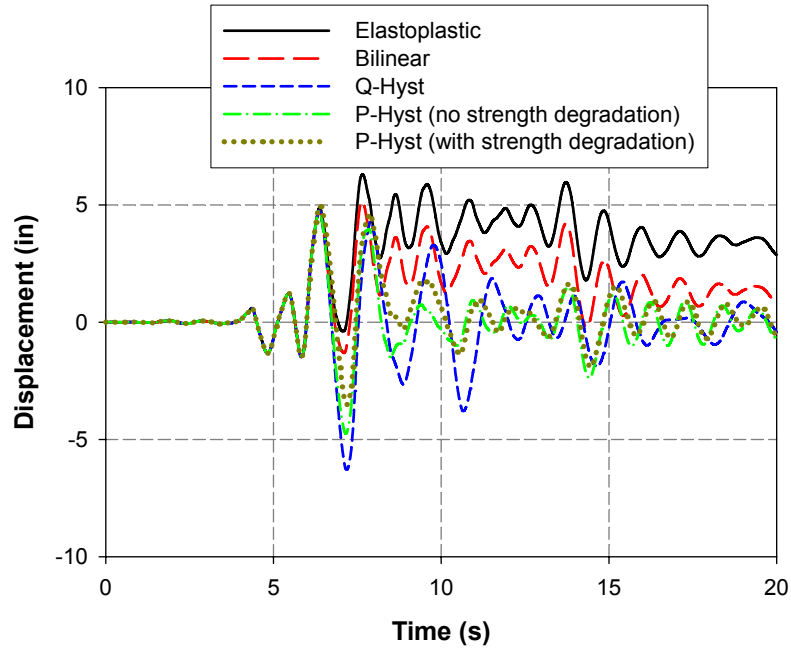
Figure 6.8: Time history displacements from various hysteresis models – 1989 Saratoga-

Aloha Avenue record

Table 6.2: Maximum displacement responses from various hysteretic models

Hysteretic model	U_{max} (in)[a]	μ[b]
Elastoplastic	6.30	4.0
Bilinear	5.15	3.3
Q-Hyst	6.29	4.0
Pivot hysteresis (no strength degradation)	4.76	3.0
Pivot hysteresis (with strength degradation)	4.97	3.2

a – maximum absolute displacement; b – displacement ductility (μ) = u_{max}/u_y
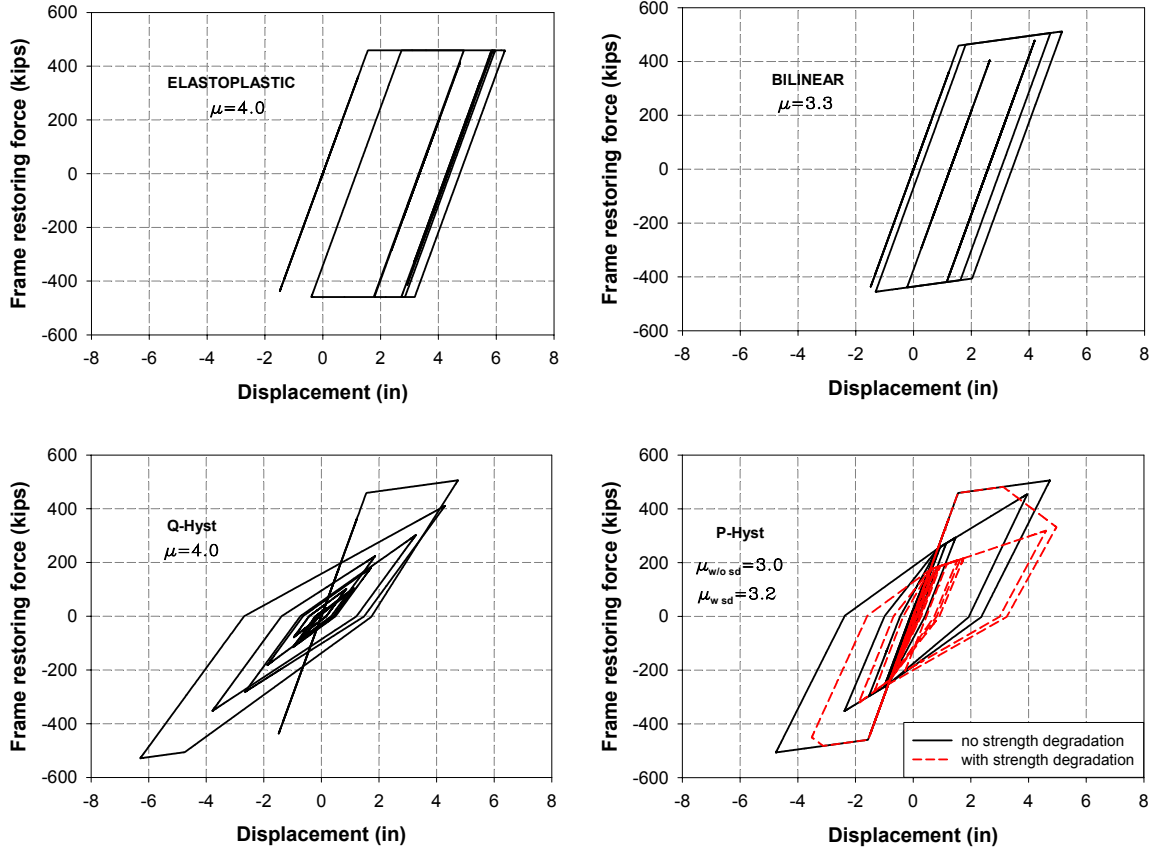
Figure 6.9: Hysteresis loops for SDOF system - 1989 Saratoga- Aloha Avenue record

and elasto-plastic models. Typically, the Q-Hyst response is expected to be larger than the elasto-plastic response due to a smaller hysteretic loop for the Q-Hyst model. But for this particular ground motion, the elasto-plastic model shows large excursions along the post yielding branch, which could account for the peak responses being identical. The lack of strain hardening in the elasto-plastic model could be a factor as well.

The pivot (without strength degradation) and Q-Hyst models exhibit similar peak responses in the positive loading direction (4.75 inches), but the peak response in the negative loading direction is 6.29 inches for the Q-Hyst model and 4.75 inches for the

pivot model. One reason for the discrepancy is that the hysteretic parameters for the pivot model (α_1, α_2, β_1, β_2) have not been matched with the Q-Hyst model parameters, which results in the pivot model having a slightly larger hysteretic loop than the Q-Hyst model. However, the major contributor to the difference in response is the assumption in the pivot model that yielding in one direction does not soften the member in the opposite loading direction. After the maximum displacement in the positive direction (u_{max}^+) is reached, the member unloads and reloads in the negative direction. The Q-Hyst response then proceeds toward $-u_{max}^+$ in the negative direction, but the pivot model follows the elastic loading line in the negative direction after crossing PP_2. The effect of strength degradation appears to increase the system ductility ratio, as evident in Figure 6.9.

The results of this comparison confirm that the elasto-plastic and bilinear models show poor correlation with more complex models like the Q-Hyst and pivot models. The force-deformation relations for the traditional models exhibit major differences with respect to shape and the amount of energy dissipated, and the time history responses show a pronounced shift in the equilibrium position. Next, the hysteretic parameters of the Q-Hyst and pivot models will be matched so that their model responses without strength degradation are similar to one another.

6.2.1. Correlation of Q-Hyst and Pivot model hysteretic parameters

The hysteretic parameters for the Q-Hyst model are the initial stiffness, K, strain hardening ratio, γ^*, yield strength, F_y, unloading stiffness K_q and reloading stiffness, K_p. For the pivot model without strength degradation, the hysteretic parameters include the initial stiffness, K, strain hardening ratio, γ^*, yield strength, F_y, pivot parameters, α_1, α_2

and the pinching pivot parameters, β_1, β_2. For simplicity, let $\alpha_1 = \alpha$, $\alpha_2 = \alpha$ and $\beta_1 = \beta$, β_2 = β. The initial stiffness, strain hardening ratio and the yield strengths for the two models are assumed to be the same.

The unloading stiffnesses of the two models are shown in Figure 6.10. For the Q-Hyst model, the unloading stiffness, K_{qQH} can be expressed as:

$$K_{qQH} = K \sqrt{\frac{D_y}{D_m}} = \frac{K}{\sqrt{\mu}}$$ (6.3)

where μ is the ductility ratio from the Q-Hyst model. From Figure 6.10(b), the unloading stiffness for the pivot model, K_{qPH} can be written as:

$$K_{qPH} = \frac{K}{\mu} \frac{\left(1 - \gamma^* + \gamma^* \mu + \alpha\right)}{\left(1 + \dfrac{\alpha}{\mu}\right)}$$ (6.4)

where α is the pivot parameter. Equating (6.3) and (6.4), an expression for the pivot parameter, α, can be found in terms of the strain hardening ratio, γ^*, and the ductility ratio, μ of the Q-Hyst model, as given below.

$$\alpha = \sqrt{\mu}\left[1 - \gamma^*\left(1 + \sqrt{\mu}\right)\right]$$ (6.5)

Figure 6.11 sketches the reloading stiffnesses for the two models. From the Q-Hyst model, the reloading stiffness, K_p can be written as:

$$K_p = \frac{K}{\mu} \frac{\left[1 - (1 - \mu)\gamma^*\right]}{\left[2 - \gamma^* \sqrt{\mu} - \dfrac{(1 - \gamma^*)}{\sqrt{\mu}}\right]}$$ (6.6)

The pinching pivot parameter, β can be expressed as:

Figure 6.10: Unloading stiffnesses (a) Q-Hyst model (b) Pivot model

Figure 6.11: Reloading stiffnesses (a) Q-Hyst model (b) Pivot model
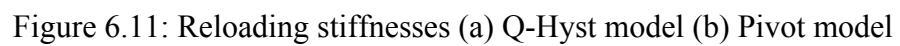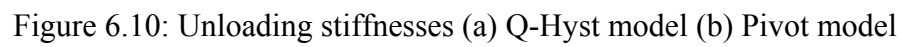
$$\beta = \frac{-K_p X_r}{F_y \left(1 - \dfrac{K_p}{K}\right)} \tag{6.7}$$

where X_r is x-coordinate of point A in Figure 6.11(b), as expressed in (6.8).

$$X_r = \frac{F_y}{K}\left[\left(1 - \gamma^* \sqrt{\mu}\right)\mu - \sqrt{\mu}\left(1 - \mu\right)\right] \tag{6.8}$$

where F_y is the yield strength of the system and K is the initial elastic stiffness. Substituting for K_p from (6.6) and X_r from (6.8) into (6.7), the pinching pivot parameter, β can be simplified to:

$$\beta = \frac{\sqrt{\mu}\left[1 - \gamma^* - \sqrt{\mu} + 2\gamma^* \mu + \gamma^* \mu^{3/2}\left(\dfrac{1 - \gamma^* \sqrt{\mu}}{\gamma^* - 1}\right)\right]}{1 - \mu + \sqrt{\mu} + \mu\left(\dfrac{1 - \gamma^* \sqrt{\mu}}{\gamma^* - 1}\right)} \tag{6.9}$$

It should be noted that the pivot model assumes that yielding in one direction does not soften the member in the opposite direction. Thus, the response proceeds towards point C from point PP$_4$, if the yield deformation has not been exceeded in the negative loading direction, in Figure 6.11(b). On the other hand, the response from the Q-Hyst model will proceed toward point B, the largest absolute displacement. This implies that in most cases, the maximum response from the pivot model will either be equal to or smaller than the maximum Q-Hyst model response.

To confirm the validity of above statement, the hysteretic model comparison performed in the earlier subsection is repeated for the Q-Hyst and pivot models, with correlated hysteretic parameters. For a target ductility of $\mu = 4$, and a strain hardening ratio, $\gamma^* = 5$ %, parameters α and β are determined as 1.70 and 0.43, respectively. The model responses are presented in Figure 6.12. The maximum displacement response from

the Q-Hyst model is found to be greater than the response from the pivot model by around 15%.
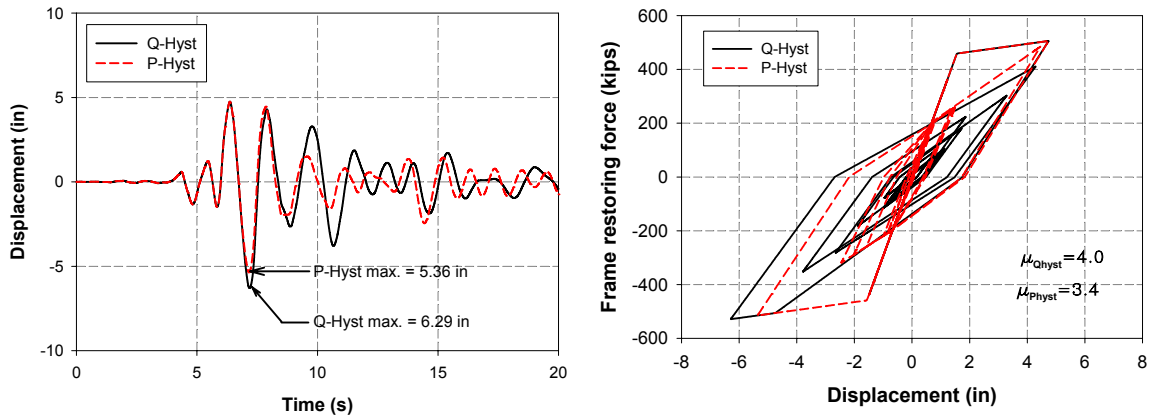
Figure 6.12: Time history responses and hysteretic loops – 1989 Saratoga-Aloha record

Figure 6.13 presents the results when the SDOF system is subjected to the Rio Dell Overpass record (PGA = 0.39g) from the 1992 Cape Mendocino earthquake. The yield strength of the system is taken as 493.5 kips, which results in a ductility, $\mu = 4$ for the Q-Hyst model. Much better correlation between the maximum responses can be observed for this case. The percent difference between the maximum responses of the Q-Hyst and pivot models reduce from 25% when the hysteretic parameters are uncorrelated to 15% when the parameters are correlated. The maximum responses can also be identical depending on the ground motion record. Thus, for the purposes of comparing the maximum displacement response, the correlation of hysteretic parameters between the Q-Hyst and the pivot models given by (6.5) and (6.9) appears to be satisfactory.
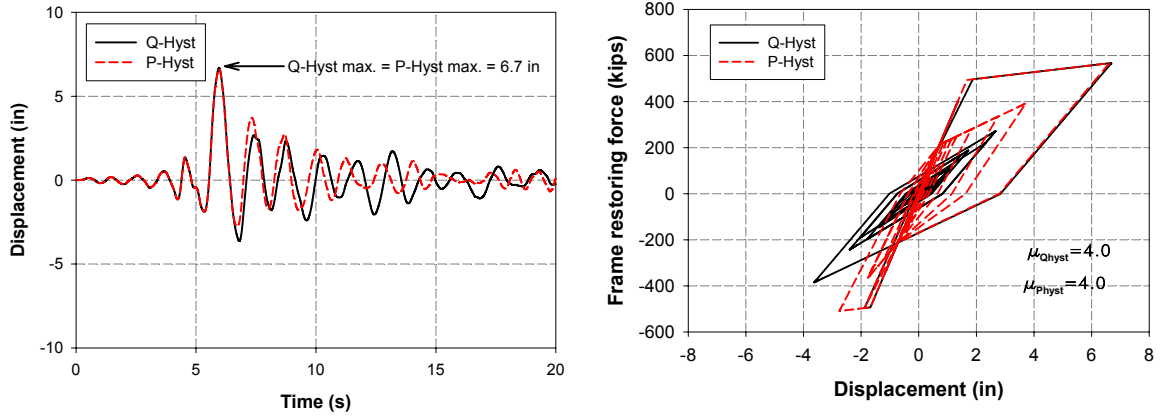
Figure 6.13: Time history responses and hysteretic loops – 1992 Rio Dell overpass record

6.3. Parameter study to compare the impact response of various hysteretic models

The previous section illustrated the effects of various hysteretic models on the column response, using a single degree-of-freedom system. The elasto-plastic and bilinear model responses did not compare very well with the Q-Hyst and pivot model responses. The hysteretic parameters of the Q-Hyst model and pivot model without strength degradation were correlated to get good agreement in their maximum displacement responses. The effect of strength degradation appeared to increase the system's ductility demand. However, the effect of various hysteretic models on the impact response of closely spaced adjacent structures needs to be examined. For instance, strength degradation in bridge columns when combined with pounding could have an adverse effect on the response of adjacent bridge frames. Hence, a parameter study is conducted with the two degree-of-freedom system shown in Figure 6.14, to examine the effects of column restoring force characteristics and pounding, on the displacement response of the system.

135
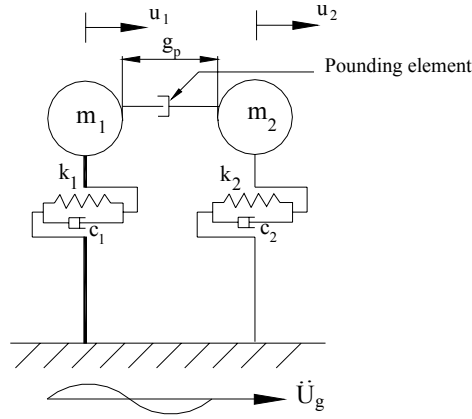
Figure 6.14: Two degree-of-freedom system used for hysteretic model parameter study

The parameter studies conducted in Chapter 4 revealed that the system displacement amplification due to pounding could be classified into three zones depending on the ground motion effective period ratio (T_{2eff}/T_g). Impact was found to be most detrimental in Zone I ($T_{2eff}/T_g < 1$), where the stiff system response was amplified by 300% and flexible system response reduced by 40%, on the average, when the system period ratio (T_1/T_2) was 0.32. Thus, in the following study only Zone I responses from the various hysteretic models are considered, with three values for the system period ratio (T_1/T_2), 0.3, 0.5 and 0.7. The flexible system period is fixed at 0.40 second and the stiff system period is varied to get the desired period ratio. The initial stiffness, yield strength and strain hardening ratio (if applicable) are assumed to be the same for all hysteretic models.

Ten far-field ground motions recorded on medium soil ($T_g = 0.6 - 1.2$ sec) are selected for analysis, as listed in Table 6.3. The pseudo acceleration response spectrum for the suite of ground motion records is illustrated in Figure 6.15. Each record is scaled such that the spectral acceleration at fundamental period equals the mean spectral

acceleration of the suite of records at the fundamental period of the system. The yield strengths of the hysteretic models are selected such that the stand-alone ductility of each degree-of-freedom (μ) equals 4, when the Q-Hyst model is used as the force-deformation relation. An iterative scheme is used to obtain the requisite yield strengths for each ground motion record at the various system periods. The characteristic periods of the records ensure that the effective ground motion period ratio, T_{2eff}/T_g lies in Zone I.

Table 6.3: Suite of far-field records used in parameter study comparing hysteretic models

No	Earthquake	Station	Φ°	PGA (g)	T_g (s)
1	San Fernando, 1971	Pasadena	000	0.09	0.85
2	Morgan Hill, 1984	Gilroy Array #3	000	0.19	1.10
3	Morgan Hill, 1984	Gilroy Array #6	090	0.29	1.20
4	N. Palm Springs, 1986	5070 N Palm Springs	210	0.59	1.10
5	Loma Prieta, 1989	WAHO	000	0.37	0.85
6	Loma Prieta, 1989	Saratoga – W Valley Coll.	270	0.33	1.20
7	Loma Prieta, 1989	16 LGPC	090	0.61	0.80
8	Northridge, 1994	LA - Wonderland Avenue	095	0.11	0.80
9	Northridge, 1994	LA – Hollywood Stor	360	0.36	0.85
10	Northridge, 1994	Old Ridge Route	090	0.57	0.80

Φ° - Component; PGA – Peak Ground Acceleration; T_g – Characteristic period
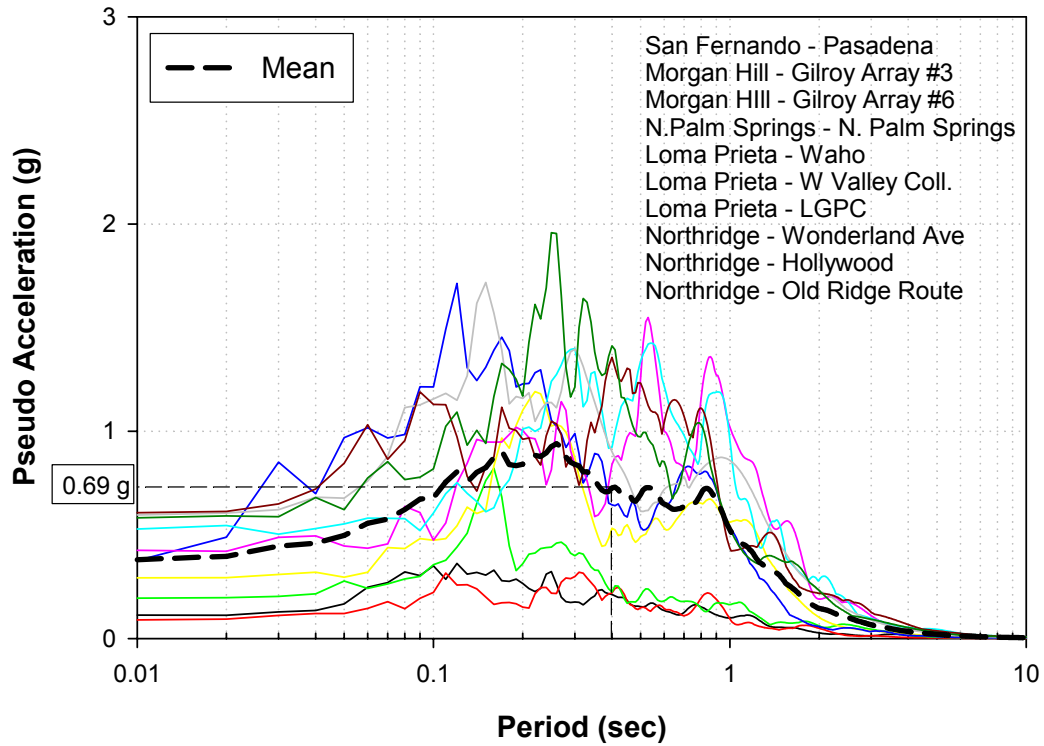
Figure 6.15: Pseudo acceleration spectra of 10 far-field records used in analysis

For consistency with Chapter 4, the stereomechanical method, with a coefficient of restitution, e = 0.8, is used for simulating impact. The effect of pounding is expressed in terms of displacement amplification (γ), which is the ratio of the maximum pounding displacement to the maximum displacement if pounding does not occur. The hinge gap is set very large for the no-pounding analysis, and is assumed as ½ inch for the pounding analysis.

The strength degradation parameters selected for the pivot model are specified in Table 6.4. The parameters are carefully chosen such that strength degradation does not occur during the no-pounding analysis. The correlation of the α and β parameters with the Q-Hyst model parameters, ensures that the ductility of each degree-of-freedom when

the pivot model is used and when no pounding occurs is less than or equal to 4. Thus, differences in displacement amplifications between the Q-Hyst and pivot models can be directly related to the effects of strength degradation.

Table 6.4: Strength degradation parameters for pivot model

Parameter	Value
Pivot parameters, α_1, α_2	1.70
Pinching pivot parameters, β_1, β_2	0.43
Strength degradation ductility, μ_t^+, $|\mu_t^-|$	4
Residual strength ratio, F_{dr}^+, $|F_{dr}^-|$	0.7
Residual strength reduction ductility, μ_d^+, $|\mu_d^-|$	8
Failure ductility, μ_f^+, $|\mu_f^-|$	100

F_{dr} = Residual strength (F_d)/ Yield strength (F_y)

Figure 6.16 presents the mean plus one standard deviation of the displacement amplification due to pounding for the various hysteretic models as a function of the frame period ratio (T_1/T_2), for effective ground motion period ratios in Zone I ($T_{2eff}/T_g < 1$). In general, the elasto-plastic and bilinear models (traditional models) underestimate the stiff system amplification and overestimate the flexible system amplification, when compared to the Q-Hyst and pivot models (sophisticated models). For instance, at $T_1/T_2 = 0.3$, the stiff system mean displacement amplification predicted by the sophisticated models is

30% more than that predicted by the traditional models. The traditional models underestimate the flexible frame displacement amplification by 20%, when $T_1/T_2 = 0.3$. The differences become smaller with increasing period ratio. At $T_1/T_2 = 0.5$, the differences between the traditional and complex model responses are 20% for the stiff system and 10% for the flexible system. For essentially in-phase frames ($T_1/T_2 = 0.7$), the deviations are only 5% and 2% for the stiff and flexible systems, respectively. Moreover, the traditional models predict a higher stiff system amplification at $T_1/T_2 = 0.7$ than at $T_1/T_2 = 0.5$, contrary to the earlier observed trend that displacement amplification decreases with an increase in the system period ratio.

Figure 6.16: Mean plus one standard deviation of displacement amplification due to pounding from various hysteresis models – 10 far-field ground motion records.

While comparing the Q-Hyst and pivot models, the strength degradation effect imposes no additional demands on the response of the system. The pivot model shows

only a 7% increase in the mean displacement amplification when compared to the stiffness degrading only (Q-Hyst) model, for $T_1/T_2 = 0.3$. In fact, at $T_1/T_2 = 0.5$, the stiff system amplification from the pivot model is smaller than the Q-Hyst model response by around 12%. All of the hysteretic models correctly predict the impact response when the system is essentially in-phase ($T_1/T_2 = 0.7$). The coefficient of variation (COV) defined as the ratio of the standard deviation to the mean ranges from 55% at low period ratios ($T_1/T_2 = 0.3$) to 14% at high period ratios, for the pivot hysteresis model. The COVs for the Q-Hyst model range from 34% to 14%, for low to high system period ratios.

This study shows that the effects of pounding are highly dependent on the hysteretic model chosen for the participating systems. The selection of traditional models like elasto-plastic and bilinear models can result in lower impact amplifications for the stiff system and higher impact amplifications for the flexible system when compared to more sophisticated models, especially for highly out-of-phase systems. Including the effects of strength degradation in predicting the pounding response of closely spaced adjacent structures does not produce a significant change in the impact response as long as stiffness-degradation is modeled. A case study is presented in the following subsection, to study the effects of strength degradation and pounding in the presence of near field ground motions.

6.3.1. Effect of near source ground motions

Near field earthquake motions are characterized by high peak ground accelerations and velocity pulses with a long period component (Yang and Agrawal, 2002). Such characteristics may greatly amplify the dynamic response of multiple-frame bridges,

resulting in severe damage. Recent earthquakes such as the 1994 Northridge, 1995 Kobe, 1999 Kocaeli, and 2001 Chi-Chi earthquakes have demonstrated the damage that can be caused by near field ground motions. To study the effects of near field ground motion on the pounding response of strength-degrading systems, ten near source records are selected for analysis, as listed in Table 6.5.

The near field records are chosen such that their characteristic periods are between 0.6 and 1.2 seconds. The parameter study conducted in the earlier section is repeated using the two degree-of-freedom system shown in Figure 6.14. The system yield strengths at various periods for each ground motion record are obtained such that the system ductility demands when using the Q-Hyst model equal four. All records are scaled to the mean spectral acceleration at the fundamental period of the system. Figure 6.17 presents the pseudo acceleration response spectra for the near field records. The mean spectral acceleration at the fundamental period (T = 0.40 s) is 0.83g.

The mean plus one standard deviation of the displacement amplification due to pounding for the various hysteretic models is presented in Figure 6.18. As observed for the far-field records, the traditional models (elasto-plastic and bilinear models) underestimate the stiff system amplification and overestimate the flexible system amplification, when compared to the more sophisticated models (Q-Hyst and pivot models). However, when using near source records, the differences between the traditional and sophisticated models persist even when the system is essentially in-phase, unlike earlier. At $T_1/T_2 = 0.7$, the traditional models underestimate the stiff system displacement amplification by 20% and overestimate the flexible system amplification by 15% when compared to the more rigorous models.

Table 6.5: Suite of ten near-field earthquake records used in case study comparing hysteretic models

No.	Earthquake	M_w	Station	Φ°	EPD (km)	PGA (g)	PGV (cm/s)	PGD (cm)	Soil Class	T_g (s)	D_t (s)
1	Gazli, USSR, 1976	6.8	Karakyr	000	3.0	0.61	65.4	25.3	A,-	1.10	0.005
2	Coyote Lake, 1979	5.7	Gilroy Array #6	230	1.2	0.43	49.2	7.8	B,B	0.85	0.005
3	Imperial Valley, 1979	6.5	El Centro Array #7	140	0.6	0.34	47.6	24.7	D,C	1.10	0.005
4	Imperial Valley, 1979	6.5	Bonds Corner	140	2.5	0.59	45.2	16.8	D,C	0.85	0.005
5	Morgan Hill, 1984	6.2	Halls Valley	240	3.4	0.31	39.4	7.7	C,C	0.85	0.005
6	Northridge, 1994	6.7	Arleta	090	3.9	0.34	40.6	15.0	D,B	0.85	0.020
7	Northridge, 1994	6.7	Sylmar	052	0.2	0.61	117.4	53.5	D,C	1.10	0.005
8	Chi-Chi, Taiwan, 1999	7.6	TCU072	N	0.24	0.40	56.3	41.3	-,C	0.90	0.005
9	Chi-Chi, Taiwan, 1999	7.6	TCU129	N	1.18	0.63	36.1	28.9	-,C	0.80	0.005
10	Chi-Chi, Taiwan, 1999	7.6	TCU076	N	1.95	0.42	64.2	35.4	-,C	0.80	0.005

M_w – Moment magnitude; Φ° - Component; EPD – Epicentral distance; PGA - Peak Ground Acceleration; PGV – Peak Ground Velocity; PGD – Peak Ground Displacement; Soil Class – Geomatrix soil class, USGS; T_g – Characteristic period; D_t – Record time step.

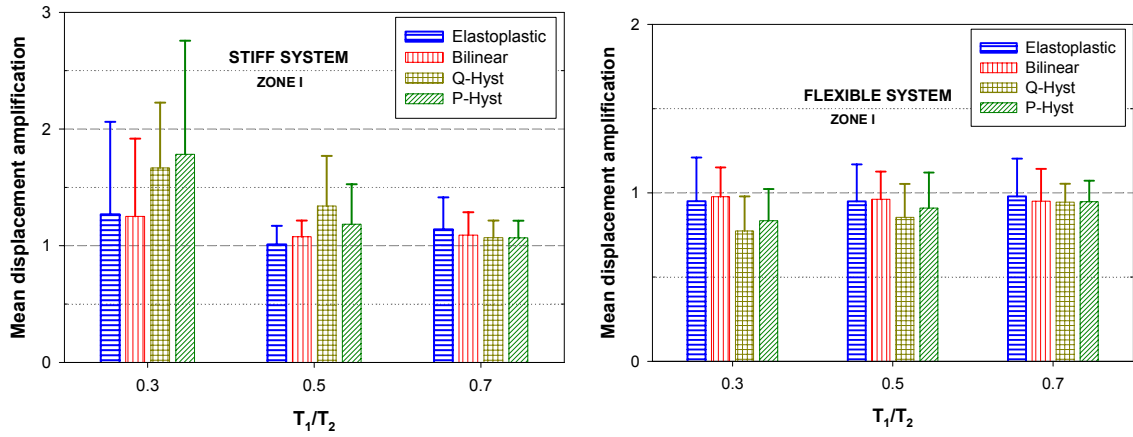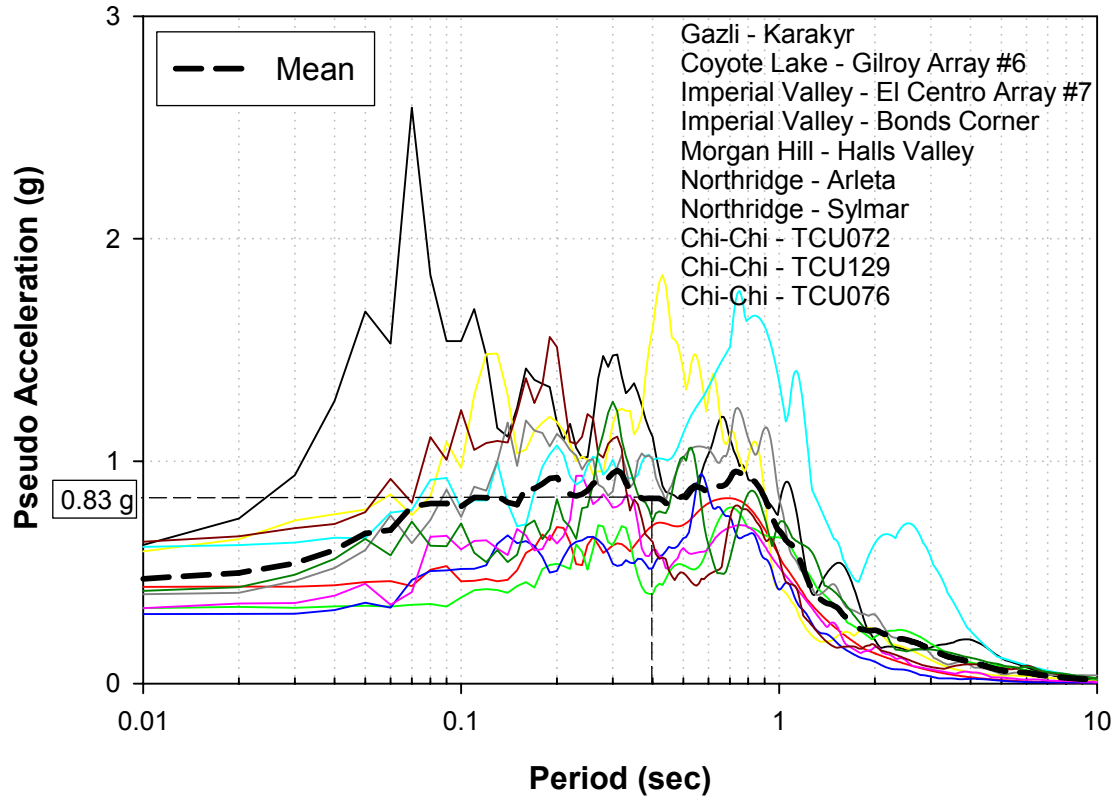Figure 6.17: Pseudo acceleration spectra of 10 near-field records used in analysis
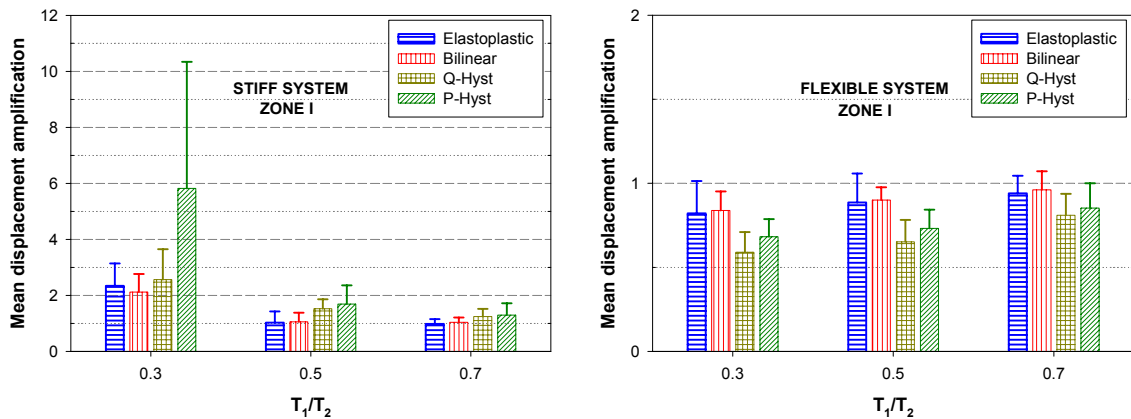
Figure 6.18: Mean plus one standard deviation of displacement amplification due to

pounding from various hysteretic models – 10 near-field records.

The biggest difference in using near-field records is that strength degradation and pounding significantly affect the system response, especially when the system is highly out-of-phase. For example, the pivot model results in a mean stiff system displacement amplification of 5.8 as opposed to 2.6 for the Q-Hyst model. Thus, accounting for strength degradation increases the stiff system demand by 125%. This implies that utilizing a bilinear or stiffness-degrading only model while analyzing pounding effects will grossly underestimate the displacement demands when compared with a strength degrading model, for highly out-of-phase systems.

The earlier study using far-field ground motions indicated that the system amplifications get closer to unity as the period ratio becomes higher. The pivot model showed a stiff system amplification of 1.07 and a flexible system amplification of 0.95, at $T_1/T_2 = 0.7$. However, for near field ground motions, the system amplifications show greater discrepancy from unity. In the latter case, the corresponding pivot model amplifications are 1.3 and 0.85 for the stiff and flexible systems, respectively.

6.4. Effects of strength degradation and pounding on the global bridge response

In this section, the differences in the global responses of a multiple-frame bridge system, due to various hysteretic frame models are investigated. The bridge considered consists of four frames connected at three intermediate hinges. The hinge gap is taken as ½ in. at all intermediate hinge locations. The simplified bridge model, as shown in Figure 6.19 is developed with frame weights of 2880 k, 7080 k, 7080 k and 2880 k, for frames 1 through 4 respectively. The damping ratio for each frame is taken as 5%. The properties of various elements used in the model are listed in Table 6.6.
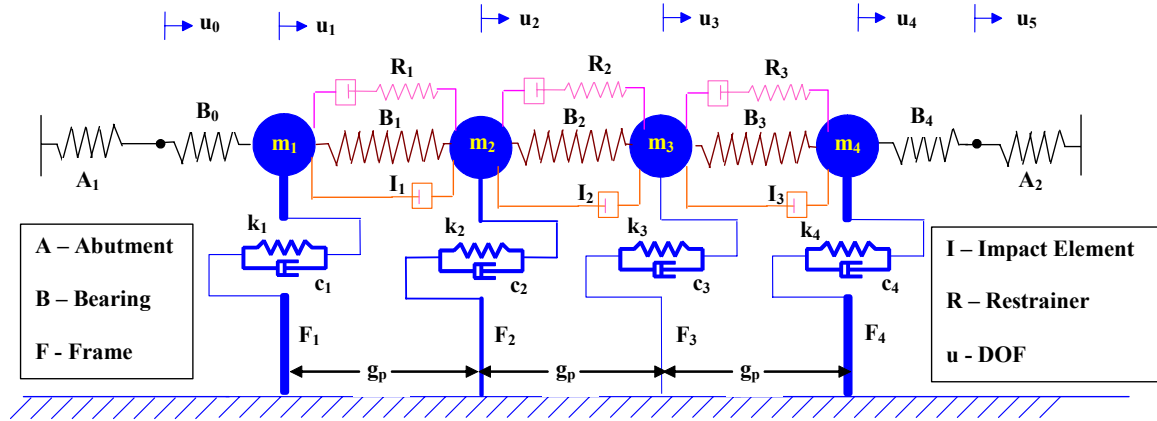
Figure 6.19: Four-frame bridge used in case study comparing various hysteretic models

Table 6.6: Properties of various bridge components

Element	Component	Initial stiffness (kips/in)	Yield strength (kips)	Period (s)
Frame	F_1, F_4	1333	877	0.47
	F_2, F_3	577	750	1.12

Element	Component	Initial stiffness (kips/in)	Yield strength (kips)	Strain hardening (%)
Restrainer	R_1, R_3	200	840	5
	R_2	100	420	5
Bearing	B_1, B_2, B_3	6	2.4	33
	B_0, B_4	2600	1560	33

Element	Component	Active stiffness (kips/in)	Passive stiffness (kips/in)
Abutment	A_1, A_2	10	2600

The hysteretic models discussed earlier namely, the elasto-plastic, bilinear, Q-Hyst and the pivot hysteresis models are used to describe the frame behavior, with all models having the same initial stiffness and yield strength. The bilinear and Q-Hyst models assume a strain hardening ratio of 5%. The pivot hysteresis model is assumed to have the

146

same properties in both loading directions with $d_t = 2*d_y$, $d_d = 4*d_y$ and $d_f = 6*d_y$.

The restrainers are designed according to the design procedure suggested by DesRoches and Fenves (DesRoches and Fenves, 2001). The restrainer slack is assumed as ½ in. The properties for the elastomeric bearings at the hinge locations are calculated based on the bearing dimensions (12 in. X 8 in. X 4 in., LXWXH). The bearings at the abutment locations are designed to have a stiffness proportional to the passive stiffness of the abutment. The active stiffness of the abutment is taken proportional to the stiffness of the hinge bearing. The coefficient of restitution (e) for impact is assumed as 0.8. The bridge is subjected to horizontal ground motion from the 1989 Loma Prieta earthquake. The Saratoga record is used, which has a peak ground acceleration of 0.5g, and a characteristic period (T_g) of 1.8 second.

To study the effect of pounding on the bridge response, two cases are considered; Case 1, where the hinge gap is set very large so that pounding does not occur and Case 2, where the hinge gap is set at ½ inch and pounding occurs. Figure 6.20 presents the displacement time-history of frame 1 for the various hysteresis models. The corresponding hysteresis loops for the pounding and no-pounding cases are shown in Figure 6.21.

The no-pounding responses for the various models are very similar, because there are not too many excursions into the nonlinear range and the displacement ductility (μ) is small ($\mu \approx 2$). However, for Case 2, seismic pounding amplifies the displacement response of frame 1 by 100% to 173% depending on the hysteresis model. The maximum displacement from the Q-Hyst and bilinear models is around 2.0 in, for the pounding case, while the pivot hysteresis model response is 3.0 in.

The results indicate that strength degradation in bridge columns has a significant influence on the pounding response of frame 1. Strength degradation with increased loading cycles combined with the interaction of adjacent frames increases the stiff frame displacement demand by 50%, when compared to other hysteresis models. This example serves to highlight the importance of correct hysteresis modeling in capturing the pounding response of closely spaced adjacent structures. The use of traditional models like the elasto-plastic and bilinear models can underestimate the severity of the pounding effect in a multiple-frame bridge.
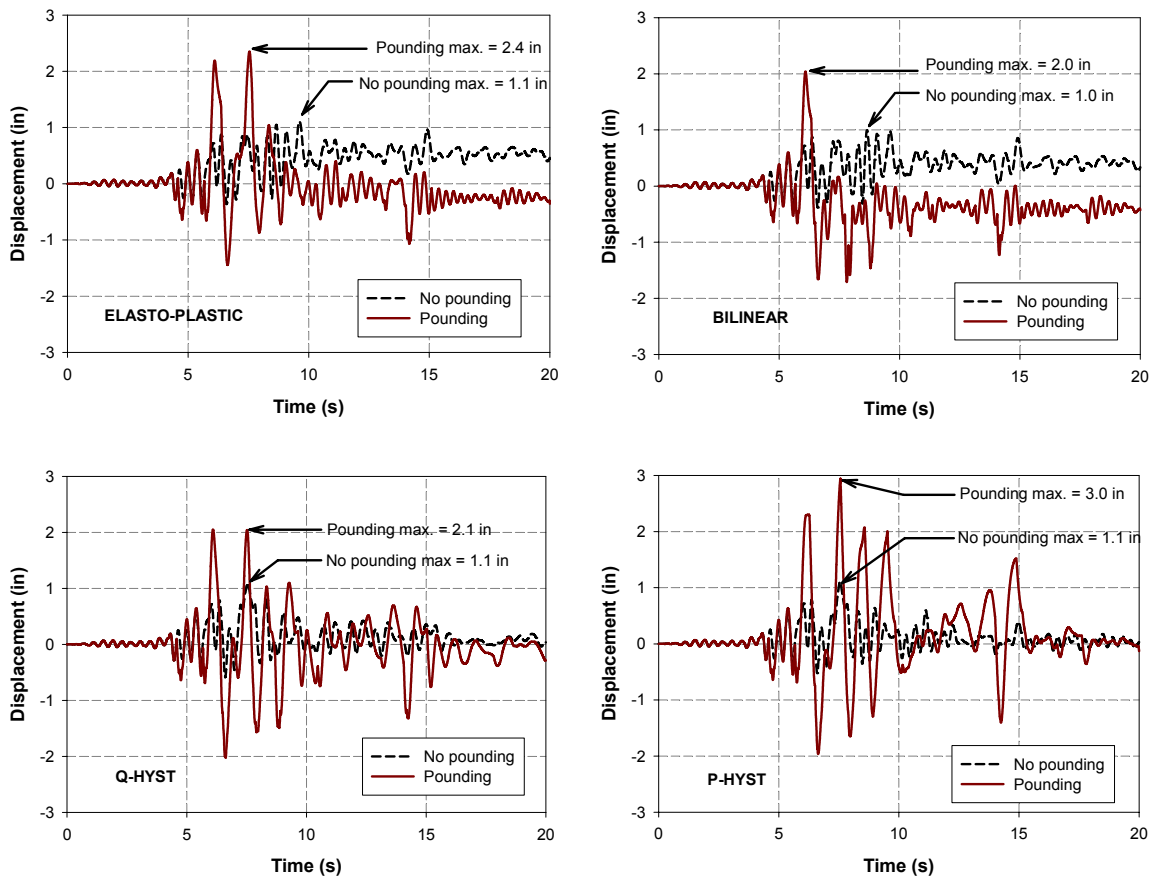
Figure 6.20: Time history of frame 1 displacement– 1989 Saratoga record (PGA = 0.5g)
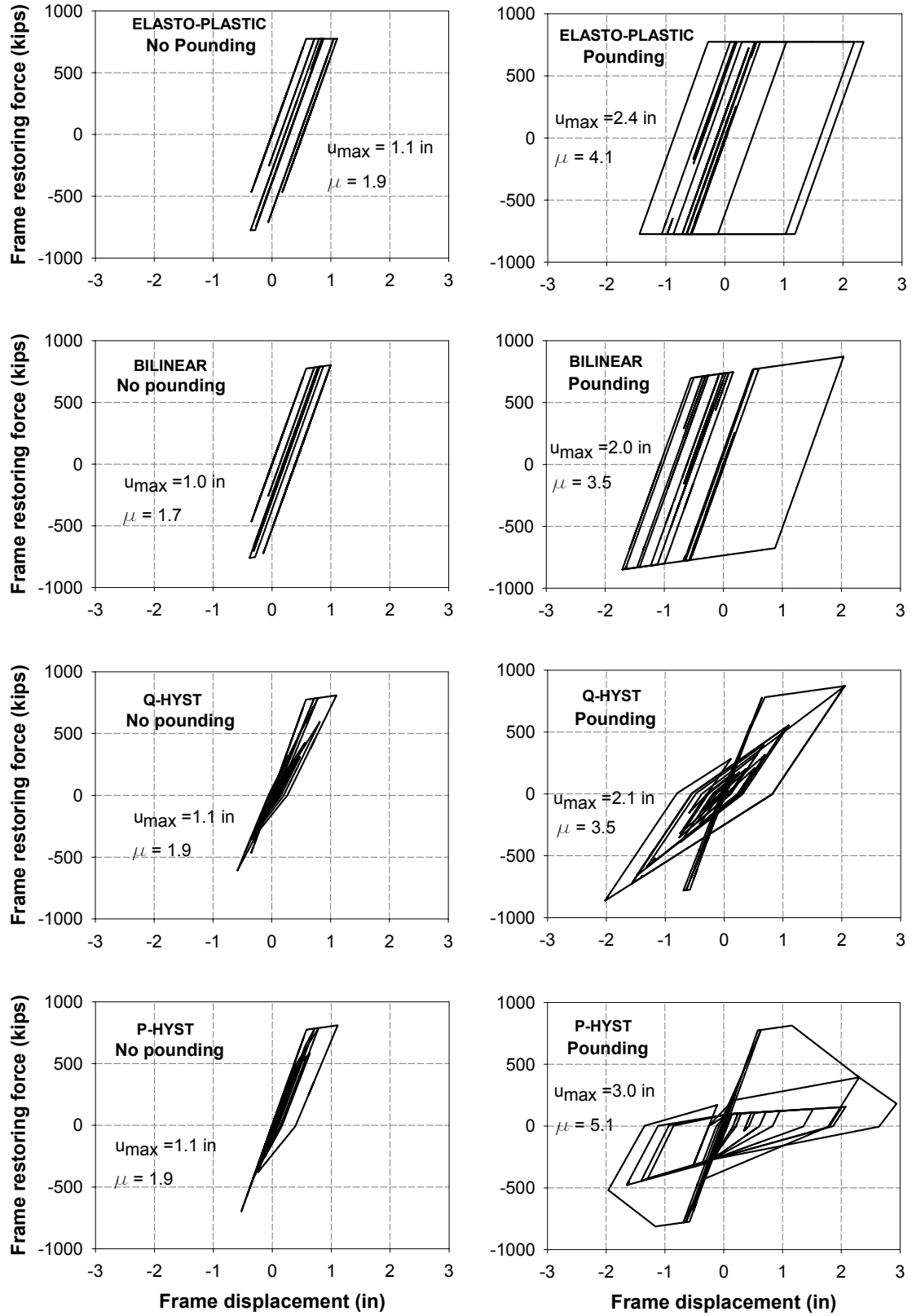
Figure 6.21: Hysteresis loops for Frame 1 – 1989 Saratoga record (PGA = 0.5g)

6.5. Conclusions

The effect of column hysteretic characteristics, such as stiffness degradation, strength deterioration and pinching on the impact response of adjacent frames is studied in this chapter. Traditional analytical models such as the elasto-plastic and bilinear models, and more sophisticated models such as the Q-Hyst and pivot models are considered for analyzing the hysteretic behavior of participating structural systems. A case study performed with a single degree-of-freedom system reveals that the hysteretic responses of the various models are different from one another. The traditional models exhibit markedly different force-deformation loops and show pronounced permanent deformations when compared with more rigorous models. The hysteretic parameters of the Q-Hyst and pivot model without strength degradation are adjusted such that the maximum displacement responses from both the models are similar.

Parameter studies conducted on two degree-of-freedom systems subject to ten far field earthquake records show that the traditional models underestimate the stiff system amplification and overestimate the flexible system amplification, when compared to the sophisticated models, for moderate to highly out-of-phase systems. At $T_1/T_2 = 0.3$, the traditional models under predict the stiff system pounding response by 30% and overestimate the flexible system response by 20%. The effect of various hysteresis models is not significant for in-phase frames ($T_1/T_2 = 0.7$).

For far field ground motions, the strength degradation effect imposes no additional demands on the pounding response as long as stiffness degradation is modeled. However, strength degradation increases the stiff frame displacement demand by 125% when compared to stiffness-degrading only systems, for highly out-of-phase systems, in the

150

presence of near field records. Moreover, the system amplifications show greater discrepancy from unity for near field ground motions, with a stiff frame amplification of 1.3 and a flexible frame de-amplification of 0.85, for $T_1/T_2 = 0.7$.

A case study conducted on a four-frame bridge with the 1989 Saratoga record (PGA = 0.5g) indicates that strength degradation in bridge columns combined with pounding can increase the stiff frame displacement response by 50%, when compared to other hysteresis models. The traditional models underestimate the stiff frame response, in good agreement with the findings from the parameter study using a two degree-of-freedom system.

CHAPTER 7

EVALUATION OF LINEAR BOUNDING MODELS IN CAPTURING THE

POUNDING RESPONSE OF BRIDGES

Impact between bridge decks during seismic loading is a highly nonlinear behavior that is not directly accounted for in the design of bridge structures. The American Association of State Highway and Transportation Officials (AASHTO) and the California Department of Transportation (Caltrans) recommend the use of two linear dynamic models - a tension model and a compression model, to bound the nonlinear response of the bridge (FHWA, 1995; Caltrans, 1990). The application of these linear models is expected to provide reasonable bounds on the pier forces and ductility demands.

A considerable amount of research has been devoted to the analytical modeling of pounding. However, no study has yet concentrated on the implications of seismic pounding on bridge design. In particular, the performance of code-suggested bounding models in capturing the pounding response has not been investigated. This chapter evaluates the efficacy of the bounding models through a comprehensive study. A two-dimensional nonlinear analytical model of a typical multiple-frame bridge is developed using DRAIN-2DX and is used as a benchmark. Pounding is simulated using the linear contact spring element. The bounding models are then developed and their seismic responses compared with those from the nonlinear analytical model for a suite of ground motion records, to determine if they provide adequate bounds.

7.1. Linear bounding models

The interaction of adjacent frames in a multiple-frame bridge plays an important role in its seismic response. During an earthquake, adjacent bridge frames can vibrate out-of-phase resulting in two kinds of interaction, as illustrated in Figure 7.1. The first interaction relates to the opening of the intermediate hinge resulting in the engagement of cable restrainers installed across the joint. The second interaction relates to the closing action of the hinge joint, which results in seismic pounding of the bridge decks. The impact forces from pounding can increase the frame displacement demands, beyond what is typically assumed in design. Moreover, pounding can increase the relative hinge opening, resulting in the requirement of a longer seat length to support the decks (Ruangrassamee and Kawashima, 2001).
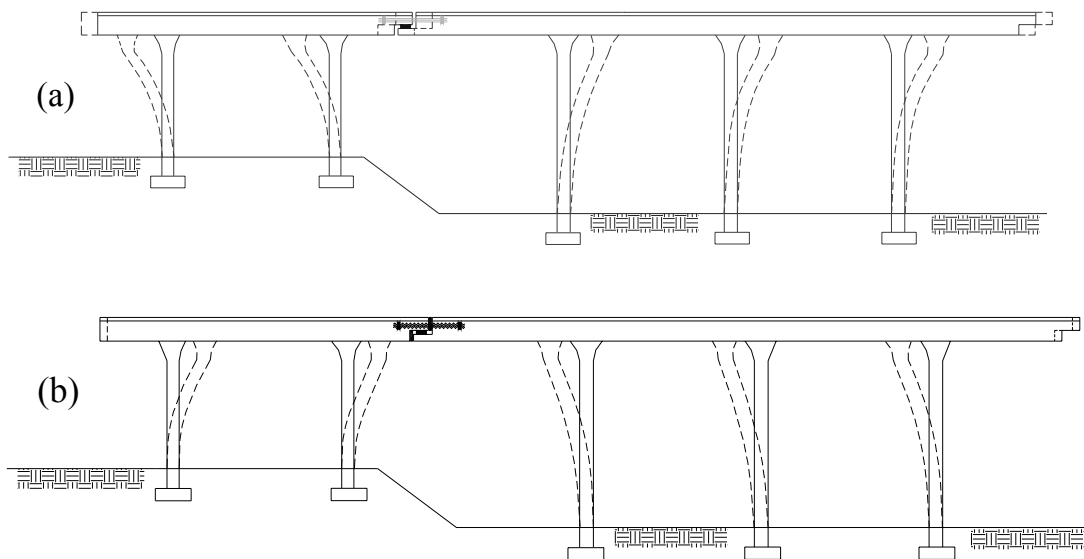
Figure 7.1: Interaction of adjacent frames during an earthquake; (a) Opening action; (b) Closing action (pounding)

Current design practice in the United States advocates the use of two dynamic models to capture the nonlinear hinge response of the bridge. The tension model is assumed to reflect the response of the bridge when the hinges are open. There is no restraint in the longitudinal direction except for that provided by restrainers. A compression model is used to represent the state when impact occurs and the hinges are closed. A rigid element connects the impacting structures and hence prevents any relative displacement at the hinges. An illustrative sketch of the bounding models is shown in Figure 7.2.
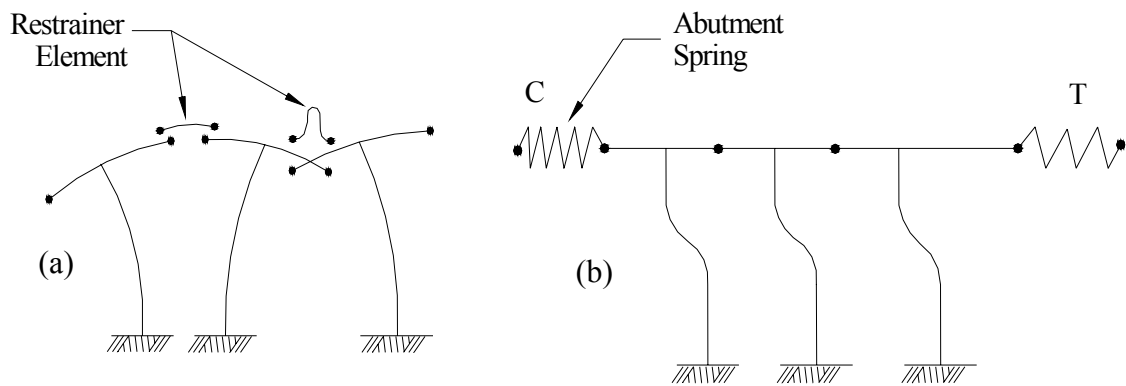
Figure 7.2: Linear bounding models; (a) Tension model (b) compression model

The maximum of the frame forces obtained from either model is taken as the bounding force for a particular frame. Using a strength-based approach, the design yield force for each frame is determined by dividing the bounding force by a response modification factor. The principle of using response modification factors is explained in the following subsection. AASHTO provides response modification factors based on the general framing types, component location and/or function, as detailed in Table 7.1,

which are independent of the period of the system. Caltrans provides period dependent Z factors to account for ductility and risk. The Z factors used in the Caltrans Bridge Design Specifications are illustrated in Figure 7.3. The application of these response modification factors to obtain the design yield forces is expected to limit the frame ductility demands to designer specified values.

Table 7.1: AASHTO (1995) Response Modification Factors (R-Factors)

Substructure	R
Wall-type pier	2
Reinforced concrete pile bents – Vertical piles only	3
Reinforced concrete pile bents – One or more batter piles	2
Single Columns	3
Multiple-column bent	5
Connections of columns or piers to foundations	1
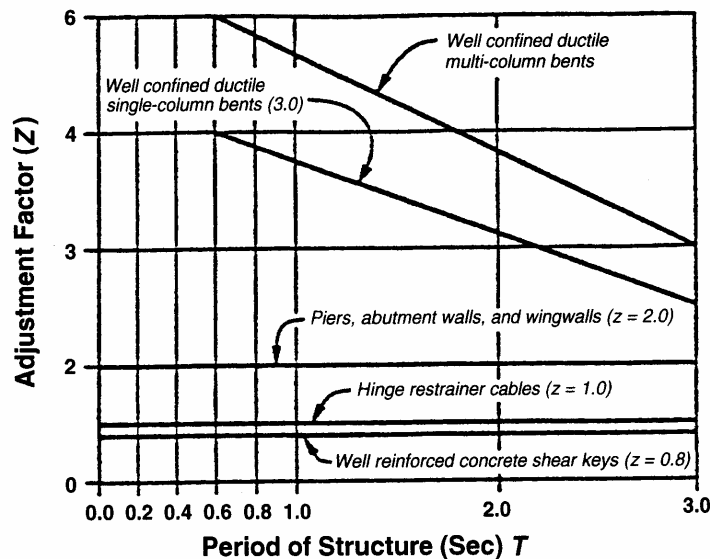
Figure 7.3: Caltrans Z factors to account for ductility and risk (Caltrans, 1993)

7.1.1. Response modifications factors used in strength-based design

The response of any structure during intense ground shaking often deforms into the inelastic range and can be significantly different from the corresponding linear response. The inelastic behaviour of the structure is characterised by a force-deformation relationship, which is an idealisation of the actual behaviour of the structure during cyclic load, as shown in Figure 7.4. The yield force of the idealised representation of the system is F_y and F_e is the elastic force demand. The yield force is established by dividing the elastic force demand by a yield reduction factor R_y, in order to obtain the specified target ductility.

The response modification factor R_y is defined as the ratio of the elastic strength demand to the yield strength required to maintain the displacement ratio below a specified target ductility, as shown below.

$$R_y = \frac{F_e}{F_y\left(\mu = \mu_i\right)} \tag{7.1}$$

The displacement ductility ratio (μ) for any system is given by Equation 7.2.

$$\mu = \frac{D_{max}}{D_y} \tag{7.2}$$

where D_{max} is the maximum deformation of the inelastic system due to ground motion and D_y is the yield displacement as shown in Figure 7.4.

In seismic design, structures are usually designed for a target displacement ductility (μ) ranging from 2 to 8, depending on the performance goal and characteristics of the system. The target ductility ratio depends on the type of material and strength properties of the structure. For design purposes, an inelastic design spectrum is often developed for a specified ductility ratio. The response spectrum is referred to as a constant ductility

response spectrum and is a function of the ground motion, system period, damping ratio and the type of force-deformation relationship used. An interpolative procedure is often necessary to obtain the yield strength of an inelastic system for a specified target ductility, since the response of a system with arbitrarily selected yield strength will seldom correspond to the target ductility (Chopra, 2000).
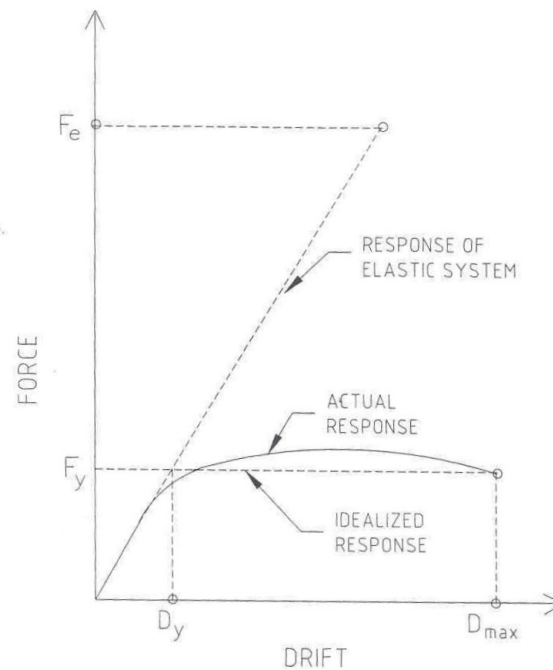
Figure 7.4: Idealized force-deformation relationship for an inelastic system

Several research studies have determined response modification or strength reduction factors (R_ys) for limiting the peak ductility demands of simple single degree-of-freedom (SDOF) systems. The reduction factors are estimated based on the computed responses of a large number of SDOF oscillators, subject to a suite of ground motion records. The

157

results indicate that strength reduction factors are a function of the system period (T) and target ductility (μ), for a given force-deformation relation and structural damping. Several R_y-μ-T relationships have been developed including Ridell and Newmark (1979), Lai and Biggs (1980), Hidalgo and Arias (1990), Krawinkler and Nassar (1992), Vidic et al. (1994), Miranda (1993, 2000) and Cuesta et al. (2003). Some of the relationships are graphically portrayed in Figures 7.5 and 7.6.

Krawinkler and Nassar (1992) proposed the following expression to estimate strength reduction factors.

$$R_\mu = \left[c(\mu - 1) + 1 \right]^{1/c} \tag{7.3}$$

with

$$c(T, \gamma^*) = \frac{T^a}{1 + T^a} + \frac{b}{T} \tag{7.4}$$

where μ is the target ductility demand and γ^* is the strain hardening ratio. The parameters a and b are listed in Table 7.2.

Table 7.2: Parameters used in Krawinkler and Nassar (1992) strength reduction model

γ^*	a	b
0.00	1.00	0.42
0.02	1.00	0.37
0.10	0.80	0.29
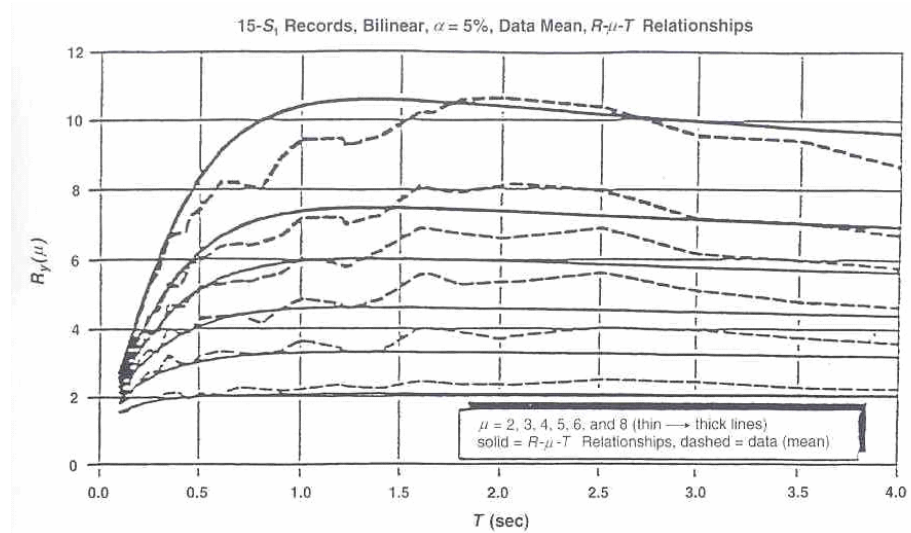
Figure 7.5: Strength reduction factors for SDOF systems (Krawinkler and Nassar, 1992)
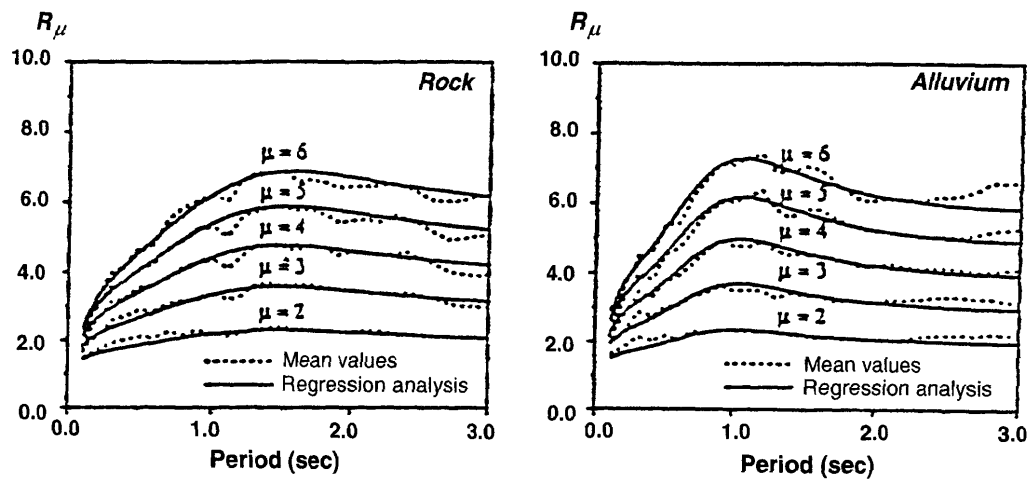
Figure 7.6: Strength reduction factors, R_μ as a function of period (T) for SDOF systems

on rock and alluvium sites (Miranda and Bertero, 1994)

159

Most strength reduction relations do not include the frequency content of the ground motion in their relations. The relation developed by Vidic et al. (1994) and later modified by Cuesta et al. (2003) addresses this deficiency. The simplified expression for R_y outlined by Cuesta et al. is given below:

$$R_y = c_1 (\mu - 1) \frac{T}{T_g} + 1; \frac{T}{T_g} \leq 1 \tag{7.5a}$$

$$R_y = c_1 (\mu - 1) + 1; \frac{T}{T_g} > 1 \tag{7.5b}$$

where μ is the target ductility demand, T_g represents the characteristic period of the ground motion record, and $c_1 = 1.3$ for systems with limited stiffness degradation and $c_1 = 1.0$ for systems with substantial stiffness degradation. The above expressions are based on the response of SDOF systems with $\mu \leq 8$, damping ratio (ζ) between 2% and 10%, strain hardening ratio, $\gamma^* \leq 10$ and system period, $T \leq 3$ seconds.

The Z factors used by Caltrans decrease as the system period increases, as shown in Figure 7.3. This is in contradiction with the findings of research studies which suggest that response modification factors increase with increasing period. The AASHTO response modification factors are independent of the period of the system.

7.2. Nonlinear analytical bridge model used for benchmarking

To evaluate the efficacy of linear bounding models in capturing the pounding response, an eleven span, 1680 ft long bridge with reinforced concrete box girder superstructure is considered, as shown in Figure 7.7. Four frames with single column bents are connected at three intermediate hinges. The spans range from 60 ft to 205 ft and the column heights vary from 40 ft to 60 ft. Some of the section and material properties

of the bridge are taken from the Northwest Connector model developed by DesRoches and Fenves (1997b). Table 7.3 gives the properties of the bridge deck and columns.
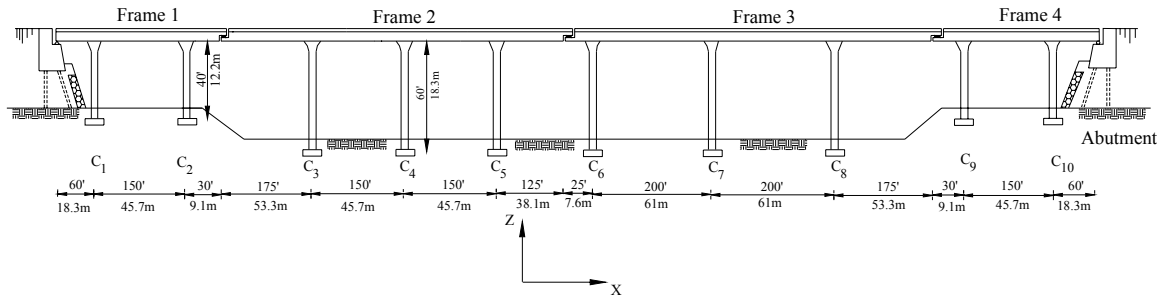
Figure 7.7: Multiple-frame bridge considered for bounding model study

Table 7.3: Section properties for the bridge superstructure and columns.

Deck			Columns					
			C_1, C_2, C_9, C_{10}			$C_3 - C_8$		
E^a (ksi)	I_{dyy}^b (ft^4)	A_{eff}^c (ft^2)	E (ksi)	I_{yy}^d (ft^4)	A_{eff} (ft^2)	E (ksi)	I_{yy}^d (ft^4)	A_{eff} (ft^2)
3420	491	65.5	3420	95	67.5	3420	80	62.4

[a]Modulus of elasticity; [b]Moment of Inertia about transverse axis of deck; [c]Effective Area; [d]Moment of Inertia about weak axis of column.

A two dimensional nonlinear analytical model of the bridge is developed in DRAIN-2DX, as shown in Figure 7.8. The mass of the superstructure and columns is calculated based on the self weight of the various structural members. The model uses 132 frame elements for the deck and columns, 20 elements to represent friction, abutments and rigid
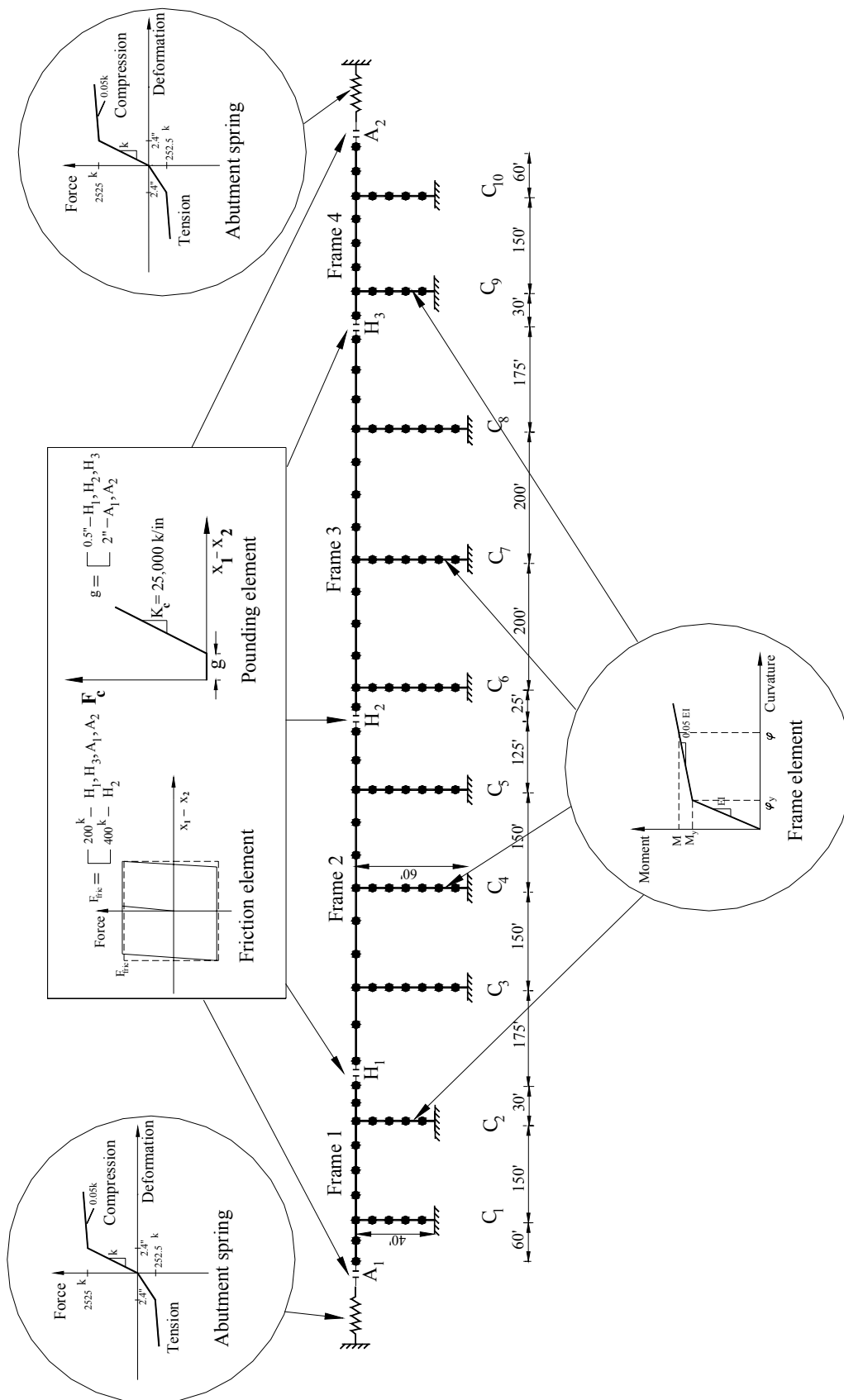
Figure 7.8: Analytical bridge model used in bounding model studies

connection elements between the deck and columns, and 5 nonlinear compression link elements to represent dynamic impact. The superstructure is assumed to be linear, elastic and the columns are modeled using a bilinear moment-curvature relationship, as shown. The gap at the intermediate hinges is taken as ½ inch. The gap between the end deck and abutment is assumed to be 2 inches. Pounding is modeled using a linear impact spring of stiffness, $K_c = 25,000$ kip/in (twice the axial stiffness of the superstructure).

The effects of elastomeric bearing pads are assumed negligible and only the friction developed by the girder as it slides off the bearing is modeled. An elasto-plastic spring with yield force equal to the friction force is used. The friction yield force is estimated to be 200-400 kips based on a gravity load analysis of the bridge and assuming a kinetic coefficient of friction between the bearing pads and concrete surface to be 0.20. The abutments are modeled as link elements, which are capable of resisting only axial forces. The abutment capacity and stiffness are determined using the Caltrans procedure (Caltrans, 1999). Effects of restrainers at the intermediate hinges are not considered, as the focus of the study is on seismic pounding.

The bounding models are developed as per the design specifications with linearized properties for columns and abutments. The abutment stiffness in tension and compression is calculated using a secant stiffness approach. The effects of friction are not considered in the linear models. The hinges remain open in the tension model and the compression model is developed by locking together all the frames and abutments with rigid links. Parameter studies are then conducted to compare bounding model responses with responses from the nonlinear pounding model. The numerical analysis program DRAIN-2DX is used with 5% modal damping assumed in all cases (Prakash et al., 1992).

163

7.3. Results from analytical studies

The adequacy of linear bounding models in capturing the opening and closing of intermediate hinges is evaluated in this section. A suite of 10 ground motion records listed in Table 7.4 is used for the analysis. All records are scaled to 0.7g peak ground acceleration, to coincide with typical design response spectra. The period ratio of adjacent frames in the nonlinear analytical model (pounding model) is 0.40. The compression model period is 0.97 s. The fundamental longitudinal periods of the flexible and stiffer frames in the tension model are 1.68s and 0.66 s, respectively. The first part of the study compares elastic frame responses from the bounding and nonlinear pounding models. The latter part deals with frame ductility demands, where the frame yield forces are calculated from the bounding model forces using a strength-based approach.

The elastic frame overturning moments (sum of the column base moments in each frame) obtained from the various models is shown in Figure 7.9. Figure 7.10 presents the displacements at the top of columns (C_2, C_3, C_6, and C_9) for various models. The bounding model forces are almost always greater than the pounding model forces, except for the response of Frame 1 to the 1995 Osaka record. Similar observations can be made for the column displacements. Furthermore, it can be observed that the compression model provides bounds for the stiffer frame responses (Frames 1 and 4) in all cases. For flexible frames 2 and 3, the governing model depends on the ground motion record. Overall, it can be concluded that the linear bounding models provide reasonable bounds on the elastic column forces and displacements.

Table 7.4: Suite of ground motion records used for evaluating the bounding models

No.	Earthquake record	Location	M_s[a]	PGA[b] (g)	T_g[c] (sec)
1	1940 Imperial Valley	El Centro	6.9	0.35	1.00
2	1989 Loma Prieta	Holister	7.1	0.37	1.03
3	1992 Landers	Amboy	7.5	0.15	2.29
4	1992 Landers	Baker Fire	7.5	0.11	1.70
5	1994 Northridge	Lake Hughes	6.7	0.27	0.50
6	1994 Northridge	Lake Obrego Pk.	6.7	0.45	0.41
7	1994 Northridge	Pacoima Dam	6.7	0.50	0.42
8	1994 Northridge	Sylmar	6.7	0.83	1.60
9	1995 Kobe	Osaka	6.9	0.08	1.17
10	1995 Kobe	Kobe City	6.9	0.85	0.88

[a]Magnitude; [b]Peak Ground Acceleration; [c]Characteristic Period.

In order to estimate the frame ductility demands, the bounding force for each frame is calculated first. The frame bounding force is taken as the maximum of the frame forces from the linear compression and tension models. The yield force for each frame is then obtained by dividing the bounding force by a response modification factor (R_y). The Caltrans Z factors are not considered as studies have shown them to be incorrect (Miranda and Bertero, 1994). Hence, the period-independent AASHTO response modification factors (R-Factors) are used for all frames. The recommended R-factor for single columns is 3. Thus, $R_y = 3$ is chosen in order to obtain a target ductility of $\mu = 3$

for each frame. The frame yield forces are then utilized in the nonlinear pounding model to ascertain if the desired ductility demands are reached.
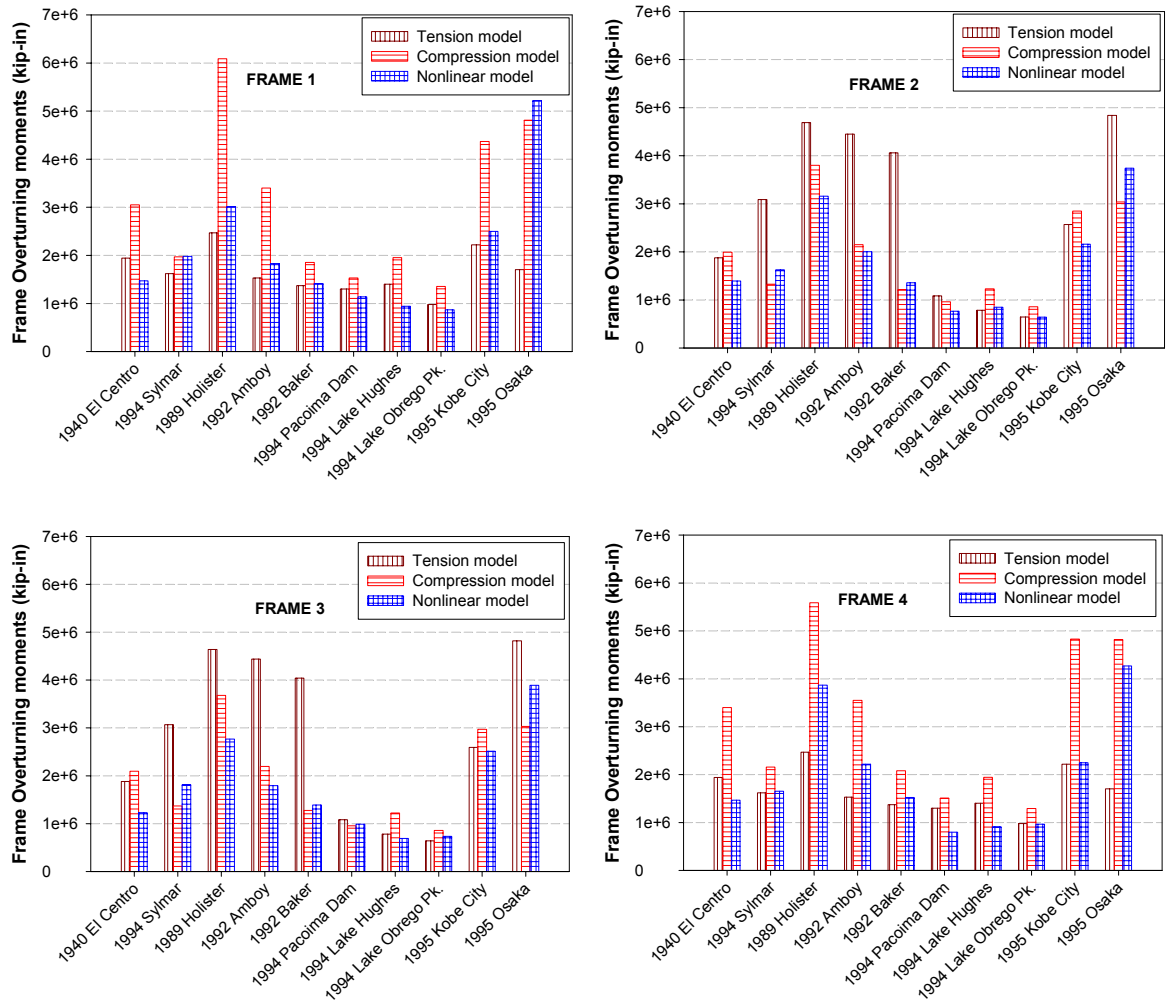
Figure 7.9: Comparison of elastic frame forces between various models

To calculate the ductility demand on each frame, a target node is defined at the center of mass of each frame. The ductility demand is then calculated as the ratio of absolute

maximum displacement at the target node to its yield displacement. The yield displacement is taken as the target node displacement corresponding to the time at which yielding is first observed in the columns. The frame displacement demands from the nonlinear analytical model using yield forces derived from the bounding models are shown in Figure 7.11.
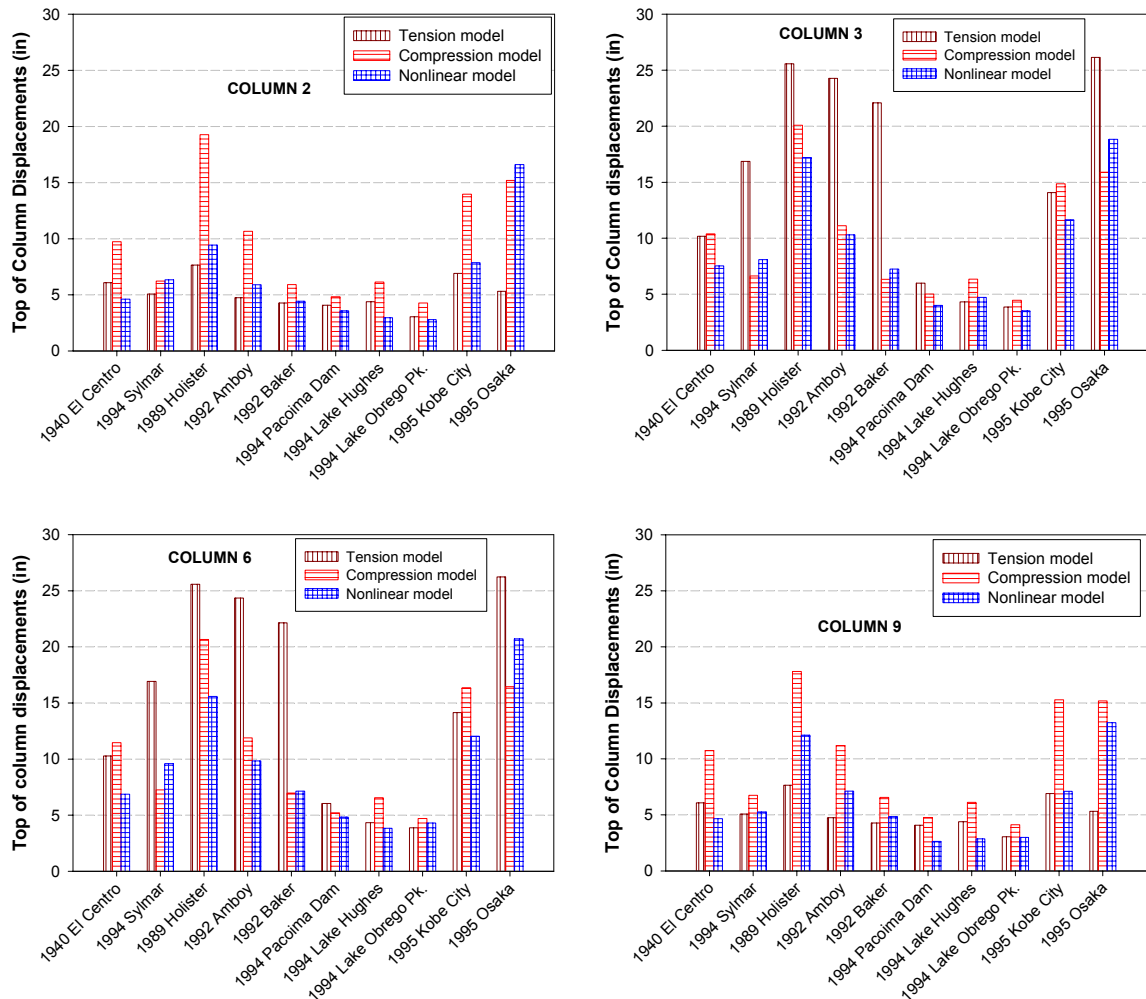
Figure 7.10: Comparison of top of column displacements between various models
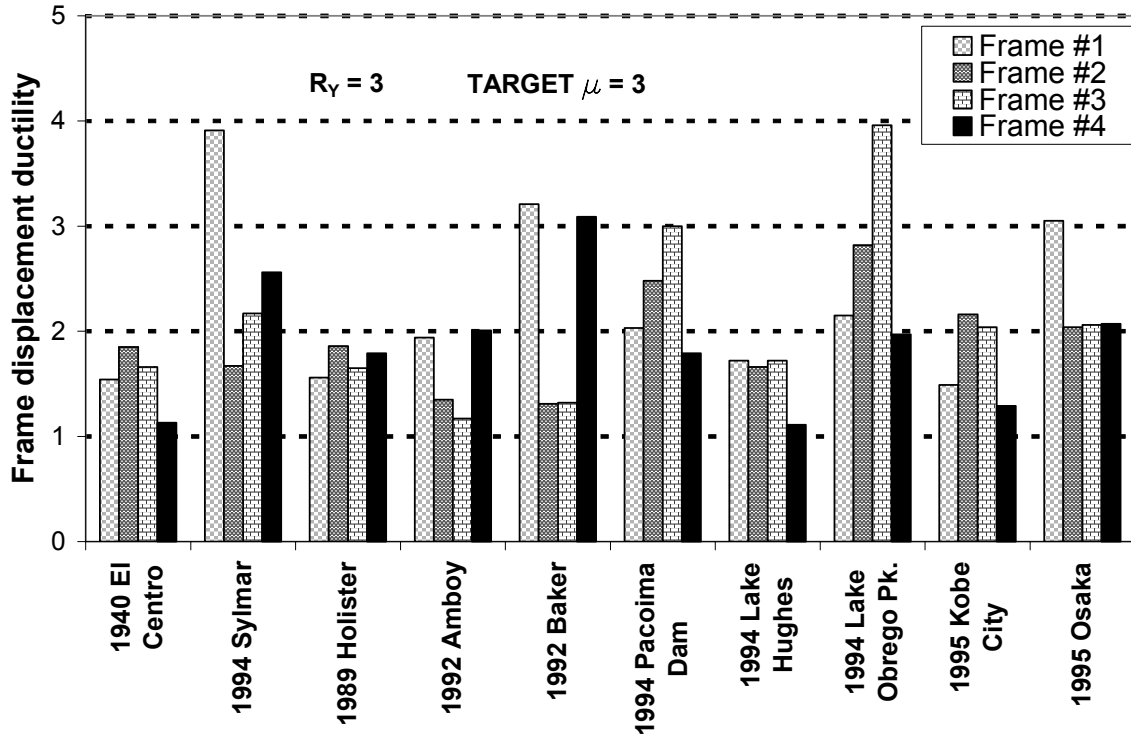
Figure 7.11: Frame ductility demands from the nonlinear model using a constant

reduction factor ($R_y = 3$) to obtain the yield forces.

At first glance, it can be observed that the design procedure performs a reasonable

job in limiting most frame demands under the target ductility demand ($\mu = 3$). The frame

demands from the 1994 Sylmar, 1992 Baker, 1994 Lake Obrego and 1995 Osaka records

are greater than the target demand ($\mu = 3$). The stand-alone periods of the stiff and

flexible frames in the bridge are 0.66 sec and 1.68 sec, respectively. The corresponding

strength reduction factors from the Nassar and Krawinkler relation (Equations 7.3 and

7.4) are 3.11 and 3.23. Thus, using a constant reduction factor, $R_y = 3$ provides a

conservative estimate for the yield force, resulting in the reasonable performance of the

design procedure. However for lower frame periods, the requisite reduction factor will be less than 3. Hence, the use of the thumb rule, $R_y = \mu$, in combination with pounding can result in frame ductility demands greater than the target demands.

7.4. Modified design procedure

Results from the earlier section indicate that the current design procedure is adequate in providing bounds for the pounding response of the bridge when the frames are elastic. The use of bounding model forces in conjunction with AASHTO R-Factors had reasonable success in limiting the inelastic frame demands to target demands for the multiple-frame bridge chosen. However, some revisions are necessary at lower frame periods, where the thumb rule, $R_y = \mu$, is not applicable. Improperly chosen reduction factors combined with seismic pounding can result in frame demands well over the target ductility demand. Hence, some modifications are suggested herein, with the introduction of a *frame design period* and the utilization of period dependent reduction factors. The steps are outlined below:

Step 1: Determine the bounding force for each frame as the maximum of frame forces from the compression and tension models.

Step 2: Determine the frame yield force by applying a reduction factor to the bounding force for each frame. Select the reduction factor based on a *design period* and the desired target ductility for each frame. The *design period* is defined as the period of the frame in the governing bounding model. For example, the design period for the stiffer frame is the period of the compression model, since the compression model always controls for the stiff frame. The design period for the flexible frame is

either the stand-alone period of that frame in the tension model (if the tension model governs), or the period of the compression model (if the compression model governs). The reduction factors are best obtained using a relation that accounts for the frequency content of the ground motion, such as the revised Vidic et al. relation (2003).

Step 3: The frame yield forces obtained in Step 2 are expected to provide adequate bounds for the frame ductility demands.

The suggested method is now applied to the suite of ground motion records, listed in Table 7.4. The response modification factors for each record are calculated using the revised Vidic et al. relation, which incorporates the frequency content of ground motion in its relation. Table 7.5 illustrates the application of the procedure for selected earthquake records. Figure 7.12 presents the frame ductility demands from the nonlinear analytical model.

The proposed method does a reasonable job in limiting most frame demands well below the target demand ($\mu = 3$). In a few cases, the target ductility ratio is exceeded by 5-25% (Frame 1 - 1995 Osaka, Frame 3 - 1989 Pacoima Dam, Frame 3 - 1989 Lake Obrego). However, it should be noted that the bounding models could not capture the nonlinear hinge response for the 1995 Osaka record, even when the columns were elastic. In the case of the Pacoima Dam record, the actual reduction factors obtained through iteration are 2.85, 3.15, 3.15 and 2.85 for Frames 1 through 4. Equation 7.5 predicts 3.60, 3.60, 3.60 and 3.60 for the reduction factors, which will result in higher ductility demands for the frames.

Table 7.5: Application of modified design procedure (Target μ = 3.0) – 5 earthquake records shown

Earthquake	Frame	M_{ten} (k-in)	M_{comp} (k-in)	M_{bound} (k-in)	T_d (s)	R_y	M_y (k-in)	μ_{NL}
1940 El Centro	1 (stiff)	1.94E+06	**3.05E+06**	3.05E+06	0.97	3.52	8.67E+05	**1.74**
	2 (flexible)	1.88E+06	**1.99E+06**	1.99E+06	0.97	3.52	5.65E+05	**2.06**
	3 (flexible)	1.88E+06	**2.09E+06**	2.09E+06	0.97	3.52	5.94E+05	**1.91**
	4 (stiff)	1.94E+06	**3.40E+06**	3.40E+06	0.97	3.52	9.66E+05	**1.26**
1989 Holister	1 (stiff)	2.47E+06	**6.09E+06**	6.09E+06	0.97	3.45	1.77E+06	**1.82**
	2 (flexible)	**4.69E+06**	3.80E+06	4.69E+06	1.68	3.60	1.30E+06	**2.15**
	3 (flexible)	**4.64E+06**	3.68E+06	4.64E+06	1.68	3.60	1.29E+06	**2.24**
	4 (stiff)	2.47E+06	**5.59E+06**	5.59E+06	1.68	3.45	1.62E+06	**1.92**
1992 Baker	1 (stiff)	1.37E+06	**1.85E+06**	1.85E+06	0.97	2.48	7.46E+05	**2.04**
	2 (flexible)	**4.06E+06**	1.21E+06	4.06E+06	1.68	3.57	1.14E+06	**1.52**
	3 (flexible)	**4.04E+06**	1.28E+06	4.04E+06	1.68	3.57	1.13E+06	**1.23**
	4 (stiff)	1.37E+06	**2.08E+06**	2.08E+06	0.97	2.48	8.39E+05	**2.27**
1994 Lake Hughes	1 (stiff)	1.40E+06	**1.95E+06**	1.95E+06	0.97	3.60	5.42E+05	**2.07**
	2 (flexible)	0.79E+06	**1.23E+06**	1.23E+06	0.97	3.60	3.42E+05	**1.82**
	3 (flexible)	0.78E+06	**1.22E+06**	1.22E+06	0.97	3.60	3.39E+05	**2.21**
	4 (stiff)	1.40E+06	**1.95E+06**	1.95E+06	0.97	3.60	5.42E+05	**1.47**
1940 Osaka	1 (stiff)	1.70E+06	**4.81E+06**	4.81E+06	0.97	3.60	1.34E+06	**3.22**
	2 (flexible)	**4.84E+06**	3.04E+06	4.84E+06	1.68	3.60	1.34E+06	**2.43**
	3 (flexible)	**4.82E+06**	3.03E+06	4.82E+06	1.68	3.60	1.34E+06	**2.53**
	4 (stiff)	1.70E+06	**4.82E+06**	4.82E+06	0.97	3.60	1.34E+06	**2.00**

M_{ten} – maximum frame overturning moment (tension model); M_{comp} – maximum frame overturning moment (compression model); M_{bound} – frame bounding moment; T_d – design period; R_y – reduction factor obtained using revised Vidic et al relation (2003); M_y – frame yield moment; μ_{NL} – Frame displacement ductility (nonlinear model).

171
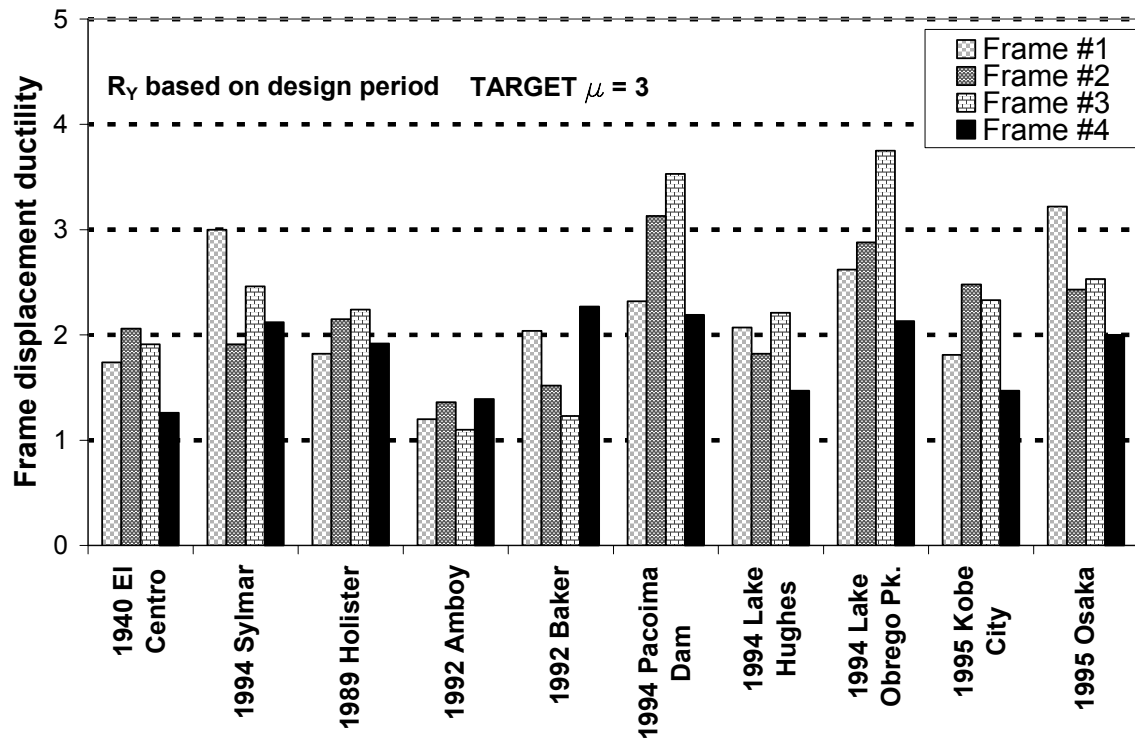
Figure 7.12: Frame ductility demands using the proposed method

7.5. Conclusions

The advent of an earthquake can induce seismic pounding of the bridge decks due to the interaction of adjacent frames in a multiple-frame bridge. The impact forces from pounding can increase the frame displacement demands, beyond what is typically assumed in design. While past research has concentrated on examining the causes and effects of seismic pounding, no effort has been made in reviewing the existing design procedures that account for dynamic impact.

This chapter examines the adequacy of current design procedures in accounting for

pounding. A nonlinear analytical model of a typical multiple-frame bridge including the effects of friction, abutments and pounding is developed for this purpose. The stand-alone periods of the stiff and flexible bridge frames are 0.66 s and 1.68 s respectively. An investigation reveals that the code-suggested linear compression and tension models adequately capture the nonlinear hinge response, when the columns remain elastic. For inelastic situations, the use of a constant, period independent reduction factor for all frames, as per AASHTO recommendations works reasonably well in limiting most frame demands below the target demands. However, the linear models may not perform adequately when applied to bridge frames having lower periods.

Hence, the current design procedure is revised by adopting period dependent reduction factors based on the calculation of a design period from the governing bounding model. The response modification factors are obtained using the revised Vidic et al. relation, which includes the frequency content of ground motion in its relation. The modified procedure is shown to work reasonably well for the multiple-frame bridge chosen. Application of the revised guideline is expected to limit frame demands to target demands with reasonable success, for all ranges of bridge frame periods.

CHAPTER 8

SIMPLIFIED CONTACT MODELS WITH ENERGY DISSIPATION FOR POUNDING SIMULATION

The analytical models available for the simulation of seismic pounding include contact force-based models such as the linear spring, Kelvin and Hertz models, and a momentum-based stereomechanical approach that uses a coefficient of restitution to account for energy dissipation during impact. Chapter 5 addressed the limitations of the existing impact models and introduced a Hertz contact model with hysteresis damping (Hertzdamp model) for simulating impact. A comparison of the various impact models revealed that the models without energy dissipation such as the linear spring and Hertz models overestimated the system responses due to impact. Furthermore, the Hertzdamp model was identified as the most effective contact-based model.

Most commercial software packages provide the linear spring element with a gap to model impact. The nonlinear Hertz spring can be approximated using a multi-linear spring with a gap. However, it is difficult to implement the energy dissipating impact models. The Kelvin model requires a damping element with a gap, which may not be available in several packages. The stereomechanical approach is also not favored, since it involves the modification of the velocities of the colliding bodies at the instant of impact. Thus, there is a need to develop a contact-based model which accounts for the impact energy loss in a rational manner, and which can be easily implemented in commercial structural software.

In this chapter, two simplified contact force-based models are developed for implementation in existing analysis programs. One idealization is an inelastic truss element with a gap and the other is an inelastic truss in parallel with a linear link element. Both models are based on the Hertzdamp contact model and are implemented in DRAIN-2DX. The model parameters such as the stiffness properties and the yield deformation are calculated by assuming an effective stiffness based on the Hertz contact law, and by equating the element hysteresis area to the energy dissipated during impact. A case study is then conducted to determine the most effective contact model. Finally, the simplified contact model is used to simulate pounding in a multiple-frame bridge subjected to ten ground motion records. The differences in the bridge responses when considering energy dissipation during impact, as opposed to using a linear impact spring are highlighted.

8.1. Simplified impact models

This section presents the development of simplified analytical models that account for the energy loss during seismic pounding. Two contact force-based models are proposed - a bilinear truss element with a gap, and a bilinear truss in combination with a linear link element. In order to determine the model parameters such as initial stiffness, yield force and strain hardening stiffness, an expression for the energy dissipated during impact needs to be developed first.

Using the stereoemechanical approach, the energy loss during impact (ΔE) can be expressed as follows:

$$\Delta E = \frac{1}{2} \frac{m_1 m_2}{m_1 + m_2} \left(1 - e^2\right)\left(v_1 - v_2\right)^2 \qquad (8.1)$$

where m_1, m_2 are the masses of the colliding bodies, e is the coefficient of restitution and v_1, v_2 are the approaching velocities of the masses. In Chapter 5, during the development of the damping coefficient for the Hertzdamp model, it was shown that relative velocity at the onset of impact (v_1-v_2) can be related to the maximum penetration (δ_m) during impact, as shown below:

$$\left(v_1 - v_2\right)^2 = \left[\frac{2\left(m_1 + m_2\right)}{m_1 m_2}\right]\left[\frac{k_h \delta_m^{n+1}}{n+1}\right] \tag{8.2}$$

where k_h is the impact stiffness parameter used in the Hertz model and n is the Hertz coefficient, typical taken as 3/2. Substituting (8.2) into (8.1), the energy dissipated during impact (ΔE) can be simplified to:

$$\Delta E = \frac{k_h \delta_m^{n+1}\left(1 - e^2\right)}{n+1} \tag{8.3}$$

Further discussion on the development of each analytical model is presented in the following subsections.

8.1.1. Inelastic truss element with a gap

A bilinear truss contact model is considered for representing impact between closely spaced adjacent structures, as illustrated in Figure 8.1. The desired force-deformation relation from the truss model is shown superimposed over the force-deformation curve resulting from the Hertzdamp model. The parameters of the truss contact element are the initial stiffness, K_{t1}, strain hardening stiffness, K_{t2}, and yield deformation δ_y. The above mentioned parameters need to be determined such that impact responses of the

participating systems using the truss element matches the impact responses obtained from the Hertzdamp model.
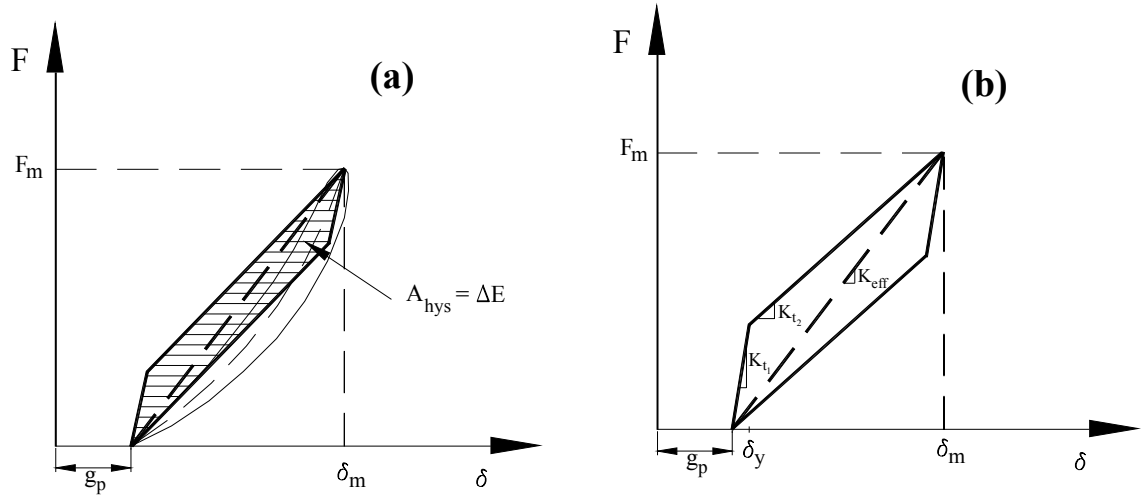
Figure 8.1 (a) Inelastic truss contact element for impact simulation; (b) Parameters of the inelastic truss model

Equating the maximum impact force (F_m) from the truss and Herzdamp models, the effective stiffness of the truss element, K_{eff}, can be obtained as:

$$K_{eff} = K_h \sqrt{\delta_m} \tag{8.4}$$

where K_h is the impact stiffness parameter from the Hertz model and δ_m is the maximum penetration observed during impact. The effective stiffness, K_{eff}, can be related to K_{t1} and K_{t2}, as shown below.

$$K_{eff} \delta_m = K_{t_1} \delta_y + K_{t_2} \left(\delta_m - \delta_y \right) \tag{8.5}$$

The area under the force-deformation relation for the truss model (A_{hys}) can be expressed in terms of the initial stiffness (K_{t1}), strain hardening stiffness (K_{t2}), yield deformation (δ_y) and maximum penetration (δ_m), as given by (8.6)

$$A_{hys} = \left(K_{t_1} - K_{t_2}\right)\delta_y\left(\delta_m - \delta_y\right)$$ (8.6)

Assuming that the area under the truss force-deformation relation, A_{hys}, equals the energy dissipated during impact, ΔE, and relating the yield deformation (δ_y) to the maximum penetration (δ_m) by (8.7), the stiffness parameters for the inelastic truss element can be obtained as follows:

$$\delta_y = a\delta_m$$ (8.7)

$$K_{t_1} = K_{eff} + \frac{\Delta E}{a\delta_m^2}$$ (8.8)

$$K_{t_2} = K_{eff} - \frac{\Delta E}{(1-a)\delta_m^2}$$ (8.9)

where ΔE is the energy loss during impact given by (8.3) and K_{eff} is the effective stiffness as specified in (8.4). For the strain hardening stiffness (K_{t2}) to be greater than zero, the yield parameter (a) must satisfy the following relation:

$$a < 1 - \frac{2}{5}\left(1 - e^2\right)$$ (8.10)

where e is the coefficient of restitution. For the values of e considered in this study – 0.6, 0.8, the yield parameter (a) should be less than 0.744. Thus, given the Hertz stiffness (K_h), the maximum penetration (δ_m) and the yield parameter (a), the properties of the bilinear truss model can be obtained using equations (8.3), (8.4) and (8.7)-(8.9).

To evaluate the performance of the simplified contact model, the inelastic truss element is used to simulate impact between two single degree-of-freedom oscillators, as

shown in Figure 8.2. The model is developed in DRAIN-2DX, using zero-length (Type 4) elastic elements for the participating systems. The impact element is modeled using a rigid link (Type 9) in series with a zero-length inelastic truss (Type 4) having a near zero yield strength in tension. The rigid link is activated only after the gap between the adjacent bodies close. The model is subjected to the 1940 El Centro record, which has a Peak Ground Acceleration (PGA) of 0.35g. The properties of the oscillators and impact element are listed in Table 8.1. The impact element properties are calculated by assuming the Hertz impact parameter, K_h = 25,000 kip-in$^{-3/2}$, and the yield parameter, a = 0.1. The maximum penetration (δ_m) during impact is equated to the maximum overlap obtained when the MATLAB-based Hertzdamp model is used to simulate impact for the same set of conditions.
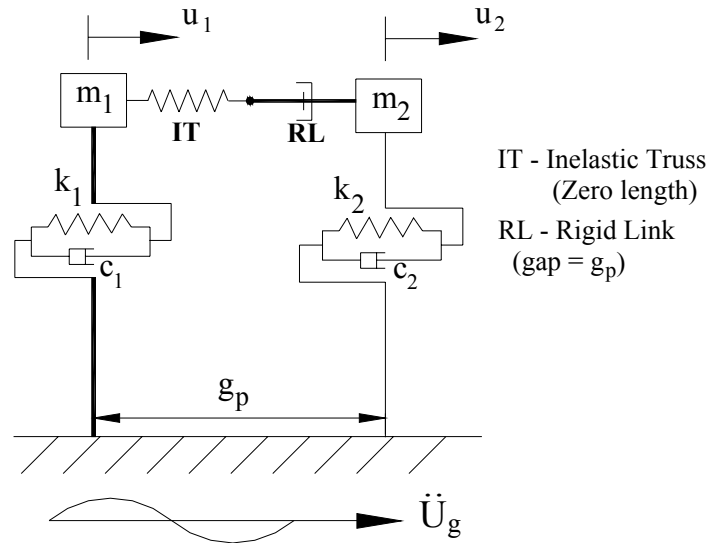
Figure 8.2: Two degree-of-freedom model in DRAIN-2DX – inelastic truss element with a gap used for impact.

Table 8.1: Properties of DRAIN-2DX model used to test the truss impact element

Property	Value
System periods, T_1, T_2	0.47 s, 1.12 s
System damping, c_1, c_2	based on 5% damping ratio
System force-deformation	Elastic
Hinge gap, g_p	0.5 inch
k_h	25000 kipin$^{-3/2}$
E	0.8
δ_m (from Hertzdamp model)	0.63 inches
K_{t1}	48030 kip/in
K_{t2}	16535 kip/in
A	0.1

Figure 8.3 compares the system displacements from the inelastic truss contact model with those obtained from using the Hertzdamp model for impact. The hysteresis loops during impact are shown in Figure 8.4. The system displacements from the two impact models are very similar, with a 2% difference in the maximum displacement of the stiff frame and a 10% difference in the maximum response of the flexible frame. The area under the truss element reasonably matches the energy loss from the Hertzdamp model, even though the force levels are different. Selecting a low value for the yield parameter (a) allows energy dissipation even for small overlaps, consistent with the Hertzdamp element behavior.
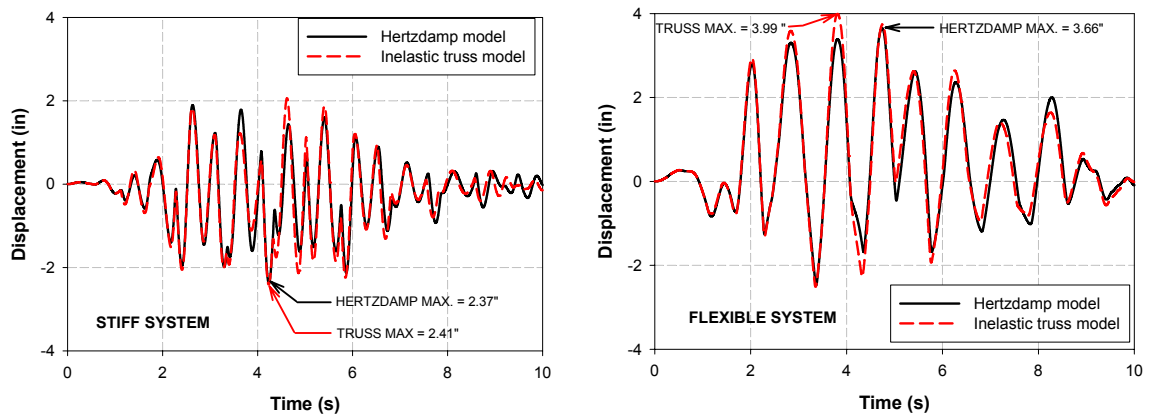
Figure 8.3: Comparison of system displacement responses when using the inelastic truss

contact model as opposed to the Hertzdamp model for pounding simulation
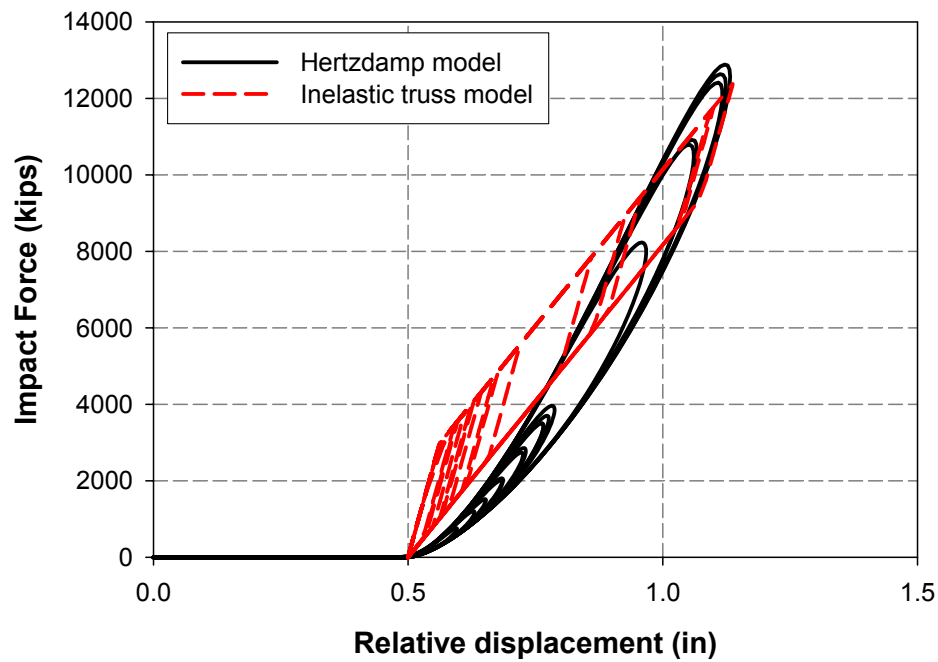
Figure 8.4: Impact force vs. relative displacement hysteresis loops for the MATLAB-

based Hertzdamp model and the DRAIN-based inelastic truss model.

However, further study is required to determine the most effective value for the yield parameter (a).

8.1.2. Inelastic truss with a gap in parallel with an elastic link element

The truss model considered earlier has a linear effective stiffness (K_{eff}) with two branches for loading (K_{t1}, K_{t2}) and two branches for unloading (K_{t1}, K_{t2}). In order to better approximate the nonlinear hysteresis from the Hertzdamp model, a higher order model is considered, as shown in Figure 8.5, with two loading branches (K_{L1}, K_{L2}) and three unloading branches (K_{UL1}, K_{UL2}, K_{UL3}). A truss element with a gap is combined in parallel with an elastic link element, as shown in Figure 8.6, to obtain the required hysteresis loop. The parameters of the higher order model (truss-link model) are the truss element initial stiffness, K_T, strain hardening stiffness, K_{TH}, the truss yield deformation δ_y and the link element stiffness, K_L.

The area under the force-deformation relation for the higher order element (A_{hys}) can be expressed in terms of the stiffness parameters, K_{L1}, K_{L2}, K_{UL1}, K_{UL2}, K_{UL3}, and the deformation parameters, δ_y and δ_m, as shown below.

$$A_{hys} = \left(-K_{L_1} + K_{L_2} - K_{UL_1} + K_{UL_3}\right)\frac{\delta_y^2}{2} + \delta_y \delta_m \left(K_{L_1} - K_{UL_3}\right) \tag{8.11}$$

While deriving the above expression, it has been assumed that $K_{L2} = K_{UL2}$. The yield deformation (δ_y) can be related to the maximum penetration (δ_m) through the yield parameter, a, as follows:

$$\delta_y = a\delta_m \tag{8.12}$$

182
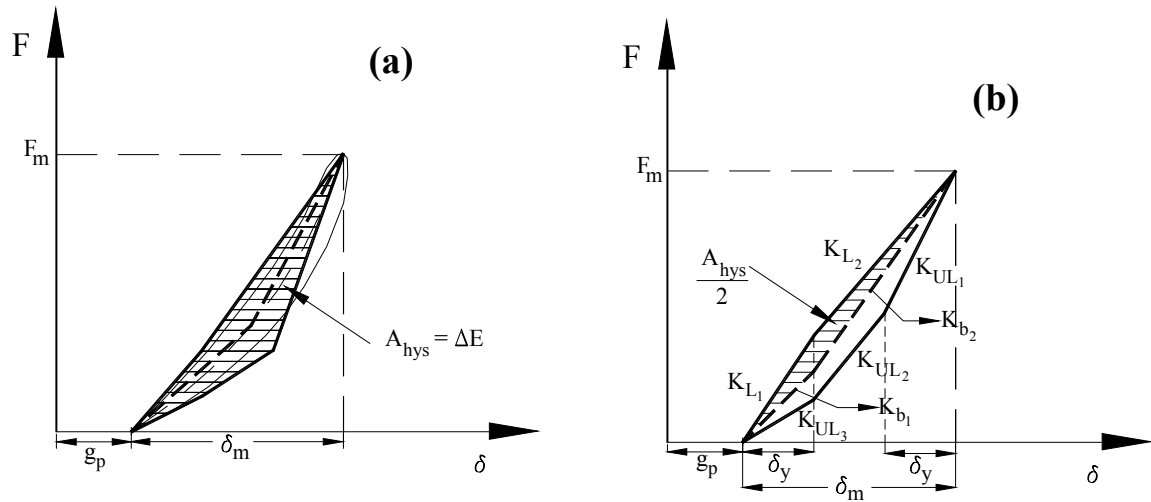
Figure 8.5 (a) Higher order contact element for impact simulation; (b) Parameters of the truss-link model
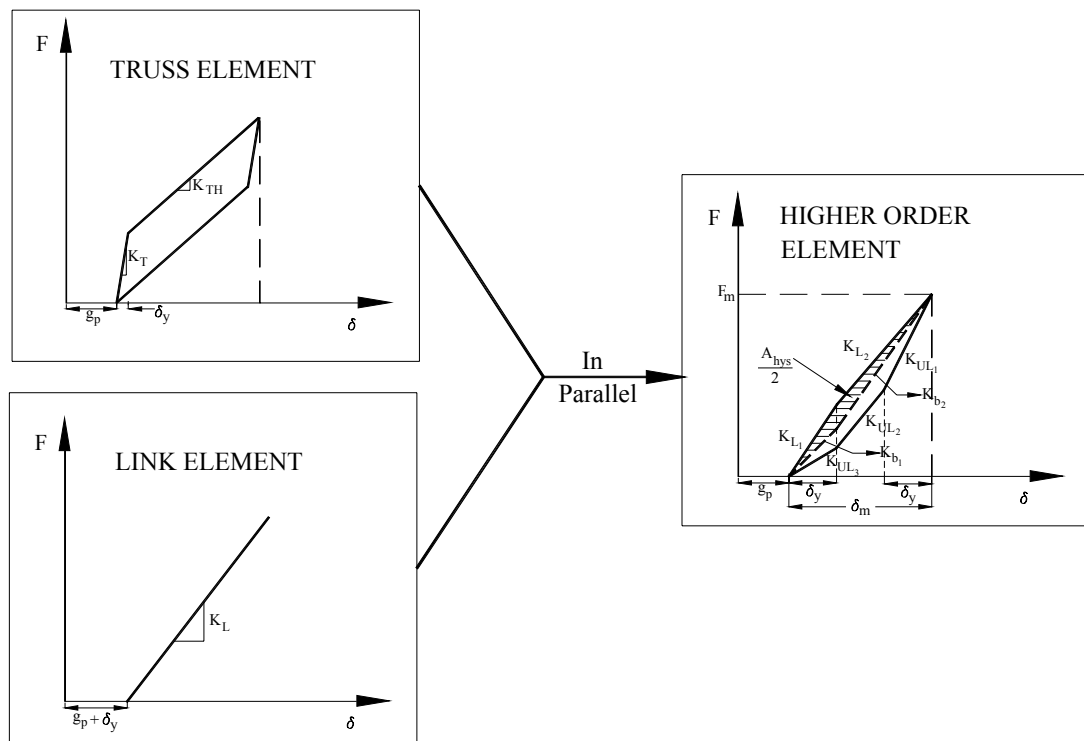
Figure 8.6: Higher order model using a combination of elements in DRAIN-2DX

The maximum impact force (F_m) can be expressed in terms of the loading stiffness parameters, K_{L1}, K_{L2}, as given below.

$$F_m = K_{L_1}\delta_y + K_{L_2}\left(\delta_m - \delta_y\right) \tag{8.13}$$

Equation (8.14) relates the maximum impact force to the unloading stiffness parameters, assuming that $K_{L2} = K_{UL2}$.

$$F_m = K_{UL_3}\delta_y + K_{L_2}\left(\delta_m - 2\delta_y\right) + K_{UL_1}\delta_y \tag{8.14}$$

Equating (8.13) and (8.14) results in:

$$K_{L_1} + K_{L_2} = K_{UL_1} + K_{UL_3} \tag{8.15}$$

Substituting (8.12) and (8.15) into (8.11), the expression for the hysteresis area can be simplified to:

$$A_{hys} = a\left(1-a\right)\left(K_{L_1} - K_{UL_3}\right)\delta_m^2 \tag{8.16}$$

Assuming the shaded area in Figure 8.5(b) equals half the hysteresis area (A_{hys}), K_{L1} can be related to the backbone stiffness K_{b1} as follows:

$$K_{L_1} = K_{b_1} + \frac{A_{hys}}{a\delta_m^2} \tag{8.17}$$

The loading stiffness (K_{L2}) can be related to the backbone stiffness (K_{b2}) by equating the maximum impact force levels and using (8.17) for K_{L1}, as given below.

$$K_{L_2} = K_{b_2} - \frac{A_{hys}}{\left(1-a\right)\delta_m^2} \tag{8.18}$$

The unloading stiffness (K_{UL3}) can then be obtained by substituting (8.17) into (8.16).

$$K_{UL_3} = K_{b_1} - \frac{A_{hys}}{\left(1-a\right)\delta_m^2} \tag{8.19}$$

Using (8.15), the unloading stiffness K_{UL1} can be expressed as:

$$K_{UL_1} = K_{b_2} + \frac{A_{hys}}{a\delta_m^2} \tag{8.20}$$

Now, the parameters of the truss and link elements can be related to stiffness parameters, $K_{L1}, K_{L2}, K_{UL1}, K_{UL2}, K_{UL3}$, through equations (8.21) – (8.25)

$$K_T = K_{L_1} \tag{8.21}$$

$$K_{TH} + K_L = K_{L_2} \tag{8.22}$$

$$K_T + K_L = K_{UL_1} \tag{8.23}$$

$$K_{TH} + K_L = K_{UL_2} = K_{L_2} \tag{8.24}$$

$$K_{TH} = K_{UL_3} \tag{8.25}$$

The backbone stiffness terms, K_{b1}, K_{b2} can be related to the Hertz stiffness parameter, K_h, the yield parameter, a, and the maximum penetration, δ_m, as follows:

$$K_{b_1} = K_h\sqrt{a\delta_m} \tag{8.26}$$

$$K_{b_2} = K_h \frac{\left(1 - a^{3/2}\right)}{1 - a}\sqrt{\delta_m} \tag{8.27}$$

Equating hysteresis area (A_{hys}) to the energy dissipated during impact, ΔE, the properties of the truss and link elements can be obtained using the equations below:

$$K_T = K_h\sqrt{a\delta_m} + \frac{\Delta E}{a\delta_m^2} \tag{8.28}$$

$$K_{TH} = K_h\sqrt{a\delta_m} - \frac{\Delta E}{(1 - a)\delta_m^2} \tag{8.29}$$

$$K_L = \frac{K_h\sqrt{\delta_m}}{1 + \sqrt{a}} \tag{8.30}$$

where ΔE is the energy loss during impact given by (8.3).

For the strain hardening stiffness (K_{TH}) to be greater than zero, the following condition must be satisfied:

$$e > \sqrt{1 - 2.5\sqrt{a}\,(1-a)} \qquad (8.31)$$

Thus, for values of the yield parameter (a) ranging from 0.1 – 0.5, the coefficient of restitution should be greater than 0.54. The range of e considered in this study is 0.6 – 1.0, satisfying the above constraint.

The higher order model is then used to simulate pounding between two single degree-of-freedom oscillators in DRAIN-2DX. The analytical model sketched in Figure 8.7 is developed using zero-length (Type 4) linear elements for the participating systems. The impact element is modeled using a combination of an elastic link (Type 9) in parallel with a finite-length inelastic truss (Type 1) having a near zero yield strength in tension. The combination is then connected in series with a rigid link, which is activated only after the gap between the adjacent bodies closes. The oscillator properties used in the earlier subsection are retained, herein.

Based on a Hertz impact stiffness, K_h = 25,000 kip-in$^{-3/2}$, the yield parameter, a = 0.1, and a maximum expected penetration, δ_m = 0.62 inches (obtained from the Hertzdamp model), the properties of the truss and link elements can be calculated using equations (8.28)-(8.30) as: K_T = 34571 kips/in; K_{TH} = 3075 kips/in; δ_y = 0.062 inches; K_L = 14956 kips/in. The responses of the DRAIN-2DX model with the truss-link impact element are matched with those from MATLAB, which uses the Hertzdamp impact model, as shown in Figures 8.8 and 8.9.

Clearly, the higher order truss-link model closely represents the impact response from the Hertzdamp model. The system displacements from the two impact models are nearly

identical, with only a 3% difference in the maximum response of the stiff system. The

maximum flexible system displacements are identical (3.65 inches). The hysteresis area

under the truss-link element closely matches the energy loss from the Hertzdamp model.

Thus, the higher order model shows improved performance over the earlier used truss

model. However as mentioned earlier, the most effective value for the yield parameter (a)

needs to be selected before deciding on which simplified contact model to use.
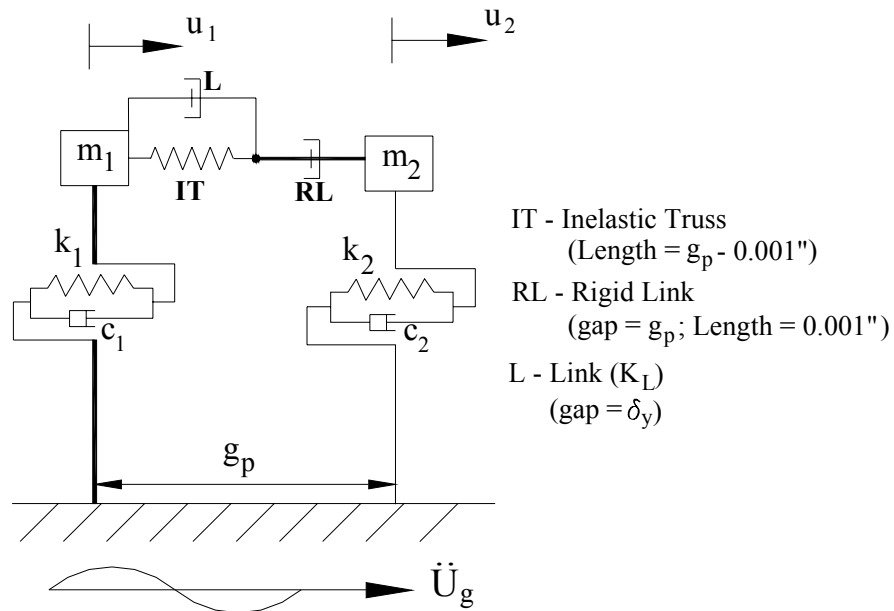
Figure 8.7: Two degree-of-freedom model in DRAIN-2DX – inelastic truss element with

a gap in combination with an elastic link to model impact.
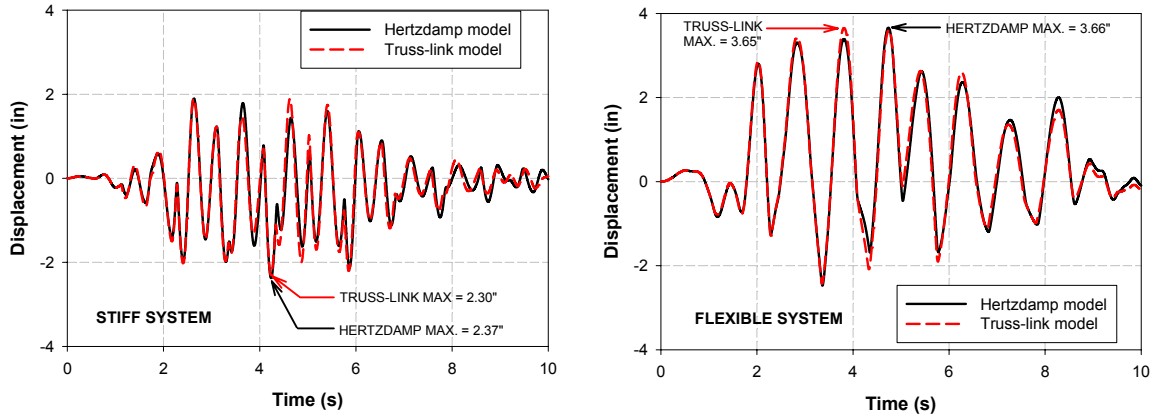
Figure 8.8: Comparison of system displacement responses – Truss-link impact model vs.

the Hertzdamp model
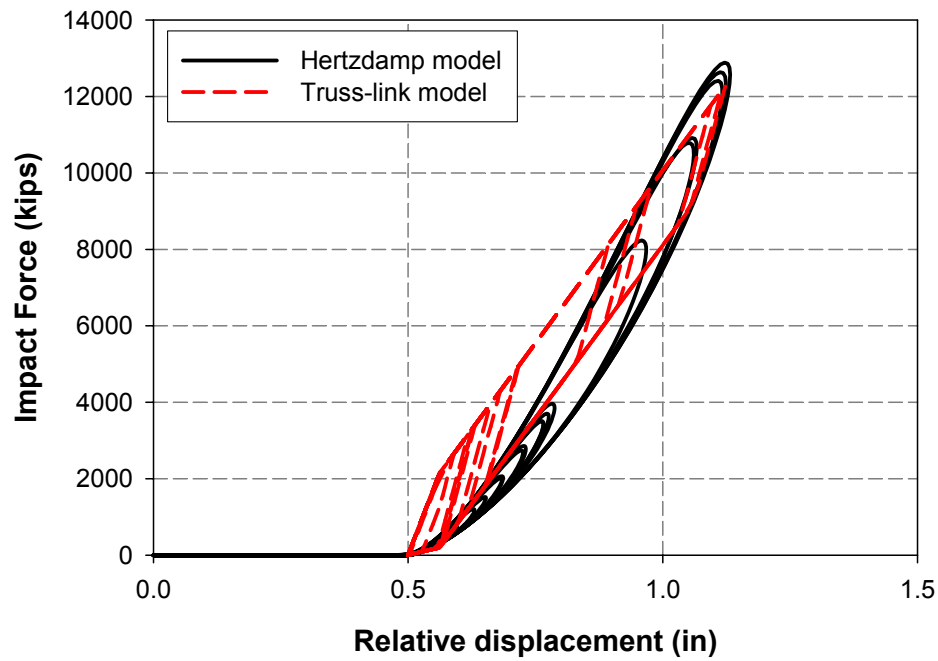
Figure 8.9: Impact force vs. relative displacement hysteresis loops for the MATLAB-

based Hertzdamp model and the DRAIN-based inelastic truss-link model.

8.1.3. Selection of effective contact model

This subsection identifies the simplified contact model that better represents energy dissipation during impact. Both the truss and truss-link models have a yield parameter (a) which relates the yield deformation of the truss element to the expected maximum penetration during impact. During the determination of the various truss model properties, the yield parameter (a) was constrained to be less than 0.74. For the truss-link model, the yield parameter was limited between 0.1 and 0.5, for e = 0.6, 0.8. A parameter study is conducted with the two degree-of-freedom system shown in Figure 8.10, to determine the best value for the yield parameter. Impact is modeled by both the truss and truss-link models. The maximum expected penetration is determined from the impact response of the Hertzdamp model, for the same set of conditions.
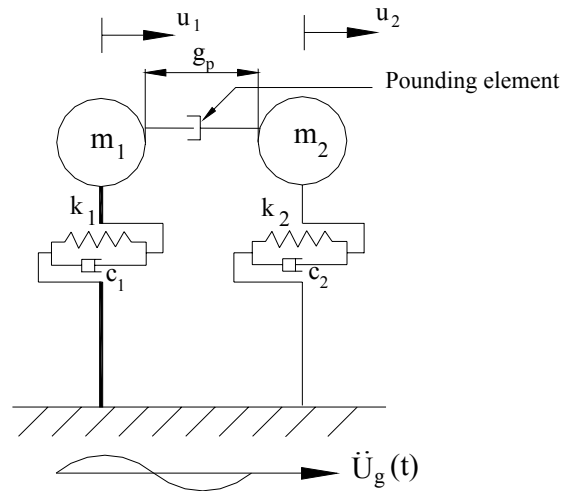
Figure 8.10: Two degree-of-freedom model used to evaluate the simplified contact models

The system response is assumed elastic and the oscillator periods are 0.18 and 0.60 seconds, which results in a period ratio, $T_1/T_2 = 0.3$. The hinge gap is taken as ½ inch. Two values for the coefficient of restitution are considered namely, e = 0.6 and 0.8. Only Zone I ($T_2/T_g < 1$) responses are considered, where the stiff system response is amplified and the flexible system response is de-amplified, as a result of pounding. A suite of ten ground motion records listed in Table 8.2 is used for analysis, with all records being scaled to 0.5 g PGA. The Hertz impact stiffness (K_h) is taken as 25,000 kip-in$^{-3/2}$. The yield parameter (a) is varied from 0.1 to 0.5, for both the simplified models.

Table 8.2: Ten ground motion records used in study evaluating simplified contact models

No	Earthquake	Station	Φ°	PGA (g)	T_g (s)
1	Whittier Narrows, 1987	E Grand Avenue	180	0.30	0.70
2	Landers, 1992	Joshua Tree	090	0.28	0.70
3	Morgan Hill, 1984	Gilroy Array #6	090	0.29	1.20
4	Loma Prieta, 1989	WAHO	000	0.37	0.85
5	Northridge, 1994	Mulhol	009	0.42	0.85
6	Cape Mendocino, 1992	Rio Dell Overpass	270	0.39	0.65
7	Northridge, 1994	Old Ridge Route	360	0.51	0.95
8	Loma Prieta, 1989	Coyote Lake Dam	285	0.48	0.65
9	Northridge, 1994	W Lost Cany	270	0.48	0.70
10	Loma Prieta, 1989	Saratoga – Aloha Avenue	000	0.51	1.80

Φ° - Component; PGA – Peak Ground Acceleration; T_g – Characteristic period

The impact responses from the simplified contact models are normalized with those from the Hertzdamp model. Figures 8.11 and 8.12 present the results for the truss model and the responses from the truss-link model are shown in Figures 8.13 and 8.14. The responses from the simplified models show smaller deviation from the Hertzdamp model responses for lower values of the yield parameter (a). This is understandable, as smaller yield parameter values allow for energy dissipation even during small overlaps, consistent with the behavior of the Hertzdamp model. For the truss model, a = 0.1 yields the best results, with the differences in model responses being under 10% for both values of e. The percent difference in responses between the truss-link and Hertzdamp models is under 5%, for a = 0.1.

Thus, it can be concluded that both the simplified models predict the impact response from the Hertzdamp model with reasonable accuracy, for a = 0.1. The inelastic truss model, with yield parameter, a = 0.1 is proposed for implementation in bridge analysis programs, as it is the simpler of the two models. An estimate of the maximum penetration (δ_m) can be obtained by observing the amount of overlap allowed by the linear impact spring under the same conditions.
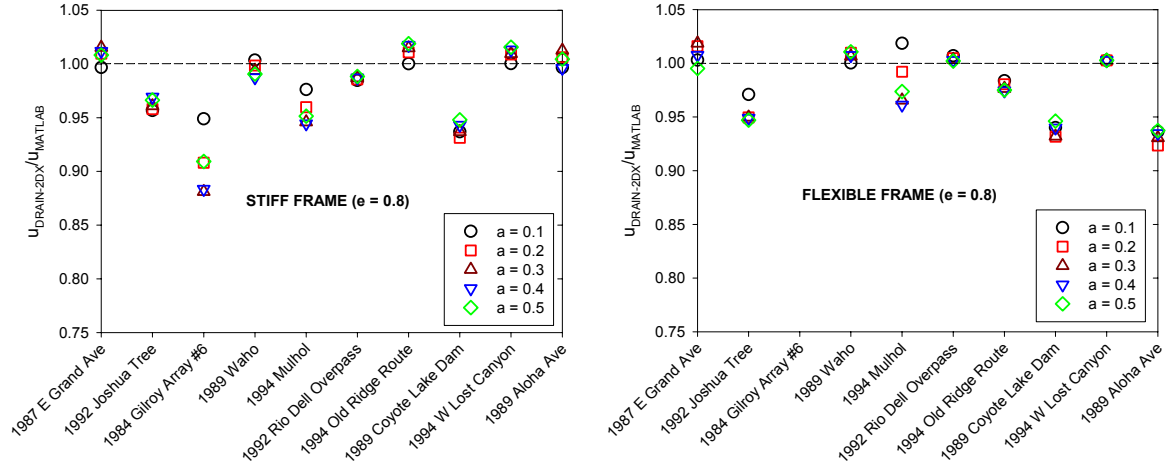
Figure 8.11: Ratio of maximum frame displacement responses between DRAIN-2DX (truss impact element) and MATLAB (Hertzdamp model) for different yield parameter (*a*) values - 2 DOF linear system ($T_1/T_2 = 0.3$; e = 0.8); 10 records scaled to 0.5 g.
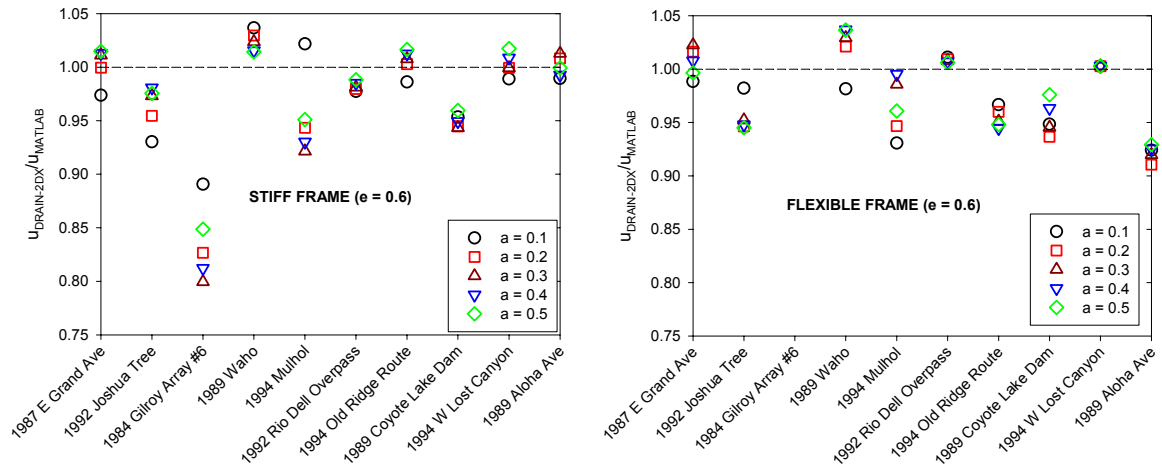
Figure 8.12: Ratio of maximum frame displacement responses between DRAIN-2DX (truss impact element) and MATLAB (Hertzdamp model) for different yield parameter (*a*) values - 2 DOF linear system ($T_1/T_2 = 0.3$; e = 0.6); 10 records scaled to 0.5 g.
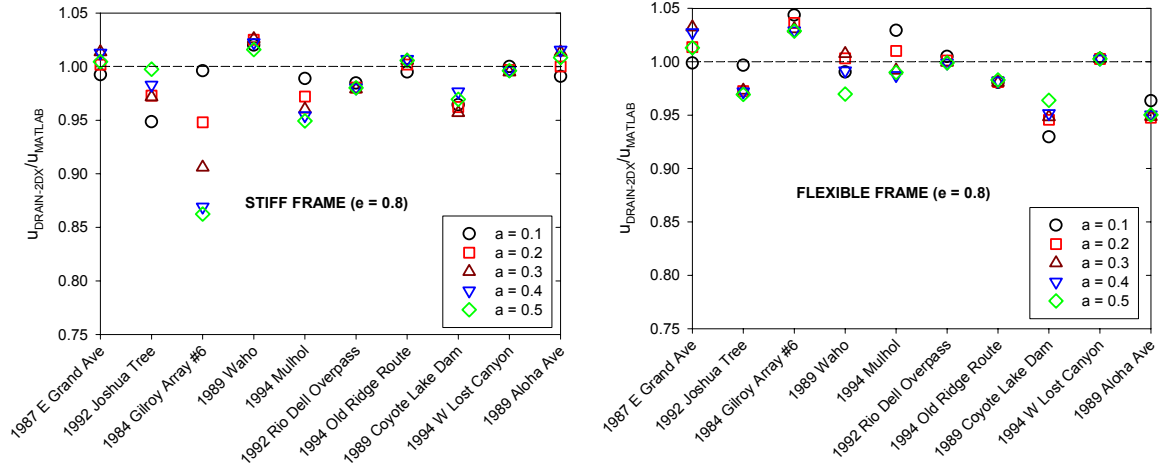
Figure 8.13: Ratio of maximum frame displacement responses between DRAIN-2DX (truss-link element) and MATLAB (Hertzdamp model) for different yield parameter (*a*) values - 2 DOF linear system ($T_1/T_2 = 0.3$; e = 0.8); 10 records scaled to 0.5 g.
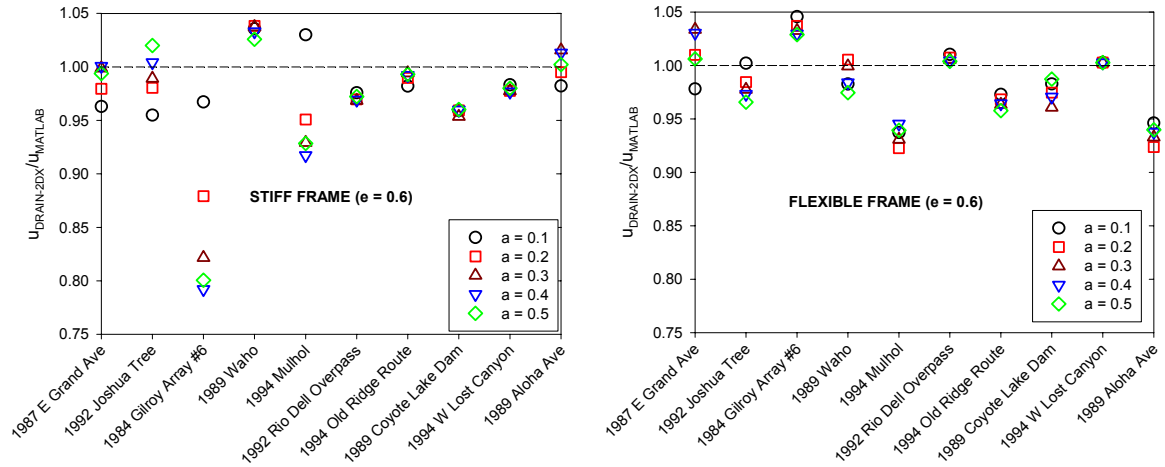
Figure 8.14: Ratio of maximum frame displacement responses between DRAIN-2DX (truss-link element) and MATLAB (Hertzdamp model) for different yield parameter (*a*) values - 2 DOF linear system ($T_1/T_2 = 0.3$; e = 0.6); 10 records scaled to 0.5 g.

8.2. Implementation of the inelastic truss element for pounding simulation in a multiple-frame bridge

The simplified contact model is now adopted to simulate pounding in multiple-frame bridges. The DRAIN-2DX nonlinear analytical bridge model developed in the previous chapter (bounding model study) is considered, as shown in Figure 8.15. The properties of the bridge are assumed the same as earlier. Cable restrainers are now modeled at the intermediate hinge locations with the properties specified in Table 8.3. The yield moments for the columns are calculated based on a moment-curvature analysis of the column cross sections. The yield moments for columns in Frame 1 (C_1, C_2) and Frame 4 (C_9, C_{10}) are taken as 3.59E+05 kip-in. The yield moments for columns in Frame 2 (C_3-C_5) and Frame 3 (C_6-C_8) are taken as 3.10E+05 kip-in. The suite of ground motion records listed in Table 8.2 is used for analysis, with all records scaled to 0.5 g PGA.

To illustrate the effect of energy loss during impact, two cases are considered – Case 1, where pounding is modeled using a linear spring of stiffness, K_L = 25000 kip/in, and Case 2, where the inelastic truss element with a gap is used with a Hertz stiffness parameter, K_h = 25000 kipin$^{-3/2}$ and e = 0.6. The maximum penetration (δ_m) allowed by the linear spring model at each impact location is utilized to calculate the stiffness properties of the simplified contact element. The yield parameter (a) is taken as 0.1. Figure 8.16 compares the frame impact responses for both Case1 and Case 2.

The results indicate that the linear spring element overestimates the impact responses, when compared to the inelastic truss element. The effects are more pronounced for the stiffer Frame 1. The linear spring element overestimates the displacement response of Frame 1 by as much as 18% when compared with the inelastic

194
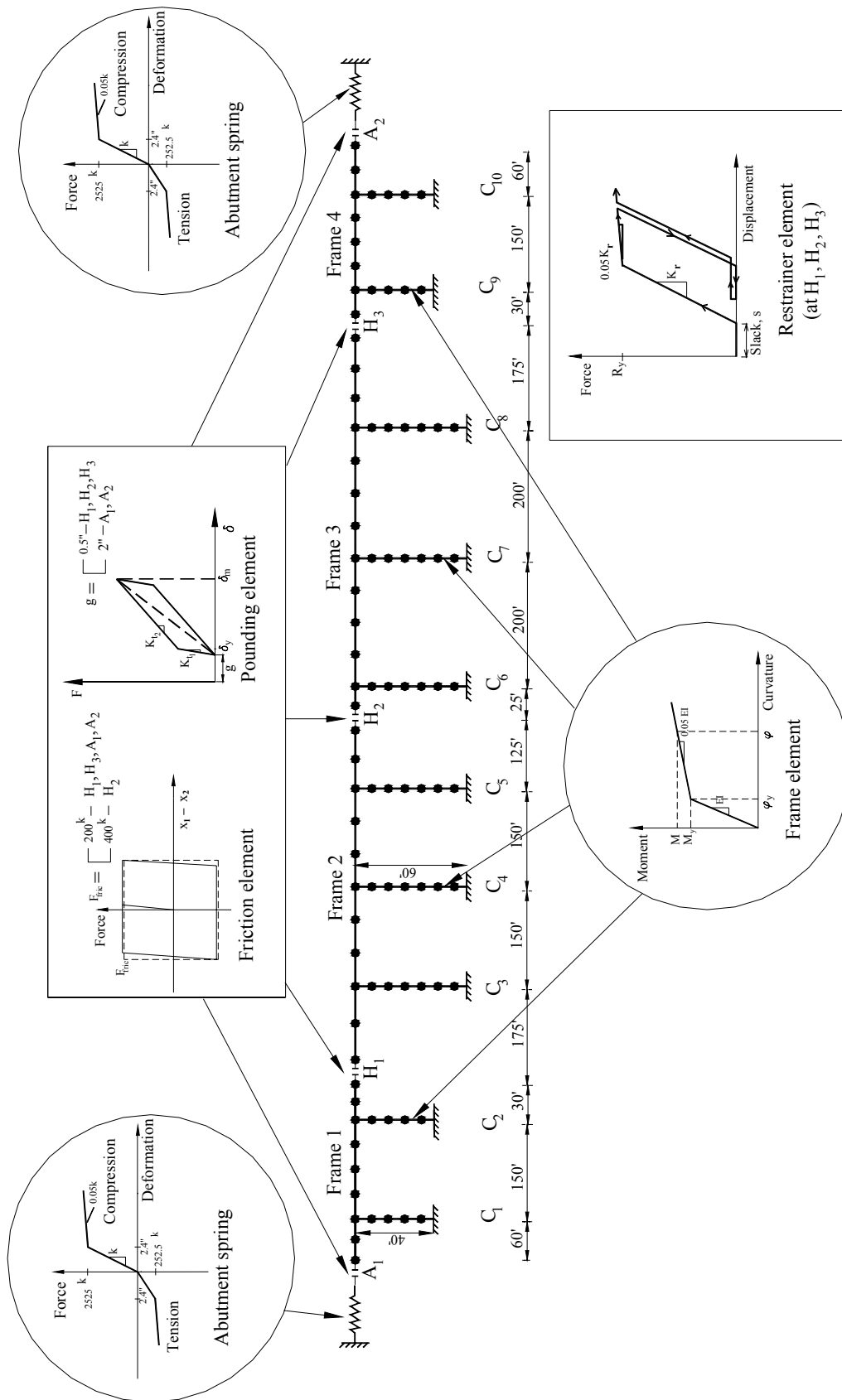
Figure 8.15: Multiple-frame bridge model developed in DRAIN-2DX with inelastic truss contact elements for pounding simulation

195

Table 8.3: Properties of cable restrainers used at the intermediate hinges

Location	Initial stiffness (kips/in)	Yield strength (kips)	Strain hardening (%)
H_1, H_3	200	840	5
H_2	100	420	5
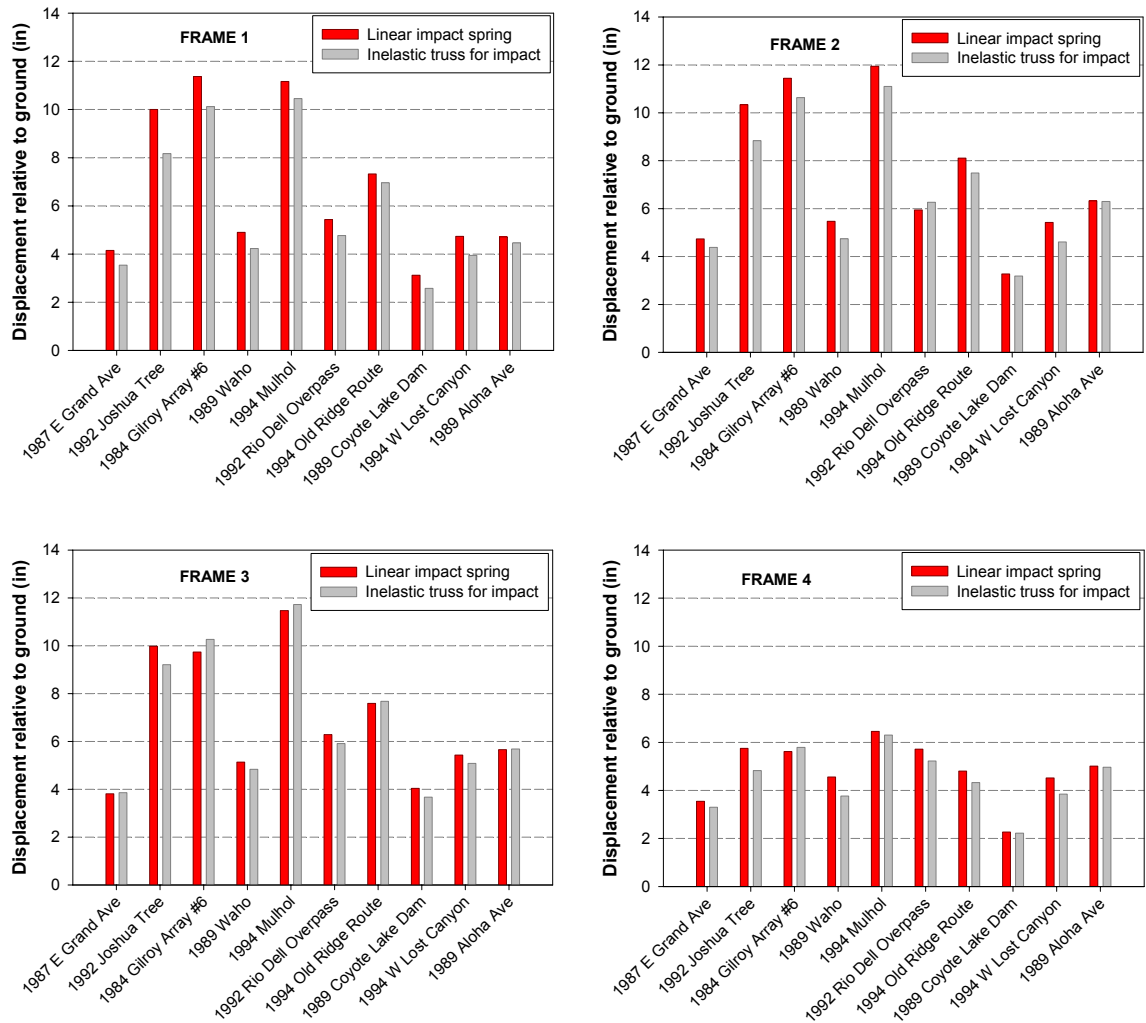
Figure 8.16: Comparison of frame displacements when using linear spring for impact as opposed to the inelastic truss contact element (10 earthquake records scaled to 0.5 g).

truss element for the 1992 Joshua tree record. On the average, neglecting energy dissipation during impact overestimates the frame displacements by 12%, 7%, 2% and 8% for Frames 1 through 4, respectively.

8.3. Conclusions

Most commercial structural software programs provide the linear spring element with a gap to model seismic pounding. Implementation of energy dissipating impact models, such as the Kelvin model and stereomechanical approach is often difficult. This chapter presents the development of a simplified contact model that accounts for energy dissipation during impact, and which can be readily implemented in commercial structural software. Two simplified contact force-based models for pounding simulation are proposed. The first model is a bilinear truss element with a gap and the second is an inelastic truss in parallel with a linear link element (truss-link model). Both models are based on the Hertzdamp contact model. The model parameters such as the stiffness properties and the yield deformation of the truss element and the stiffness of the linear link are determined using the Hertz contact law for the effective stiffness and by equating the element hysteresis area to the energy dissipated during impact.

A case study conducted with a two DOF system in DRAIN-2DX reveals that both the models capture the impact performance with reasonable accuracy, when compared to the Hertzdamp model. The truss-link model is the more accurate of the two, with only 5% differences in the system displacements, whereas the truss model shows differences up to 10%. The inelastic truss model being the simpler of the two models is then proposed as

the simplified model. The maximum expected penetration can be obtained by observing the amount of overlap allowed by the linear impact spring for the same set of conditions.

Finally, the simplified contact model is used to simulate pounding in a four-frame bridge model developed in DRAIN-2DX and subjected to ten ground motion records. On the average, energy dissipation during impact is found to reduce the frame responses by 12%, 7%, 2% and 8% for Frames 1 through 4 respectively.

CHAPTER 9

CONCLUSIONS AND RECOMMENDATIONS

Seismic pounding between adjacent frames in multiple-frame bridges and girder ends in multi-span simply supported bridges has been observed in several recent earthquakes. Pounding results in high magnitude and short duration acceleration pulses that can induce local crushing and spalling of concrete at the impact locations. More importantly, pounding can amplify the bridge displacement demands beyond those typically assumed in design. Past earthquakes have illustrated that the consequences of pounding include damage to column bents, abutments, shear keys, bearing pads and restrainers, and possible collapse of deck spans.

The objectives of this research were to identify the bridge parameters controlling impact, determine effective ways to model impact, and evaluate the adequacy of code specifications in representing the distribution of forces and deformations due to bridge deck impact. The multiple-frame bridge is considered as the representative bridge structure. A simplified nonlinear analytical model is developed in MATLAB to study the response of an *n*-frame bridge subject to longitudinal ground motion. The opening and closing of intermediate hinges, yielding of bridge frames and the engaging of cable restrainers, bearings and abutments are considered.

Several hysteretic models are chosen for the frame response including bilinear, stiffness degrading (Q-Hyst) and strength degrading (pivot hysteresis) models. Seismic pounding is represented using contact force-based models such as the linear spring, Kelvin and Hertz elements, and a stereomechanical approach which uses momentum

balance and a coefficient of restitution for energy loss. The equations of motion for the bridge system subjected to horizontal earthquake input are assembled and numerically solved using the 4th order Runge-Kutta method.

In order to mitigate the pounding damage in bridges, the factors affecting the pounding response are determined first. Previous research into the effects of seismic pounding on the bridge response has shown conflicting results. While some studies have shown that the forces acting on the piers and deck deformations increase as a result of pounding, others have suggested that pounding generally reduces the response of the bridge frames because of the energy dissipated during pounding, and because pounding disrupts the buildup of resonance.

The equations of motion for the longitudinal response of two adjacent frames subjected to earthquake ground motion are first expressed in a non-dimensional form. Subsequently, the primary factors affecting the pounding response are identified as the frame stiffness ratio (K_1/K_2) or period ratio (T_1/T_2), ground motion effective period ratio (T_{2eff}/T_g), restrainer stiffness ratio, κ, and the frame ductility ratio, μ. Unlike earlier studies which only accounted for the system period ratio in studying the pounding response, this is the first study that identifies T_{2eff}/T_g as an important pounding parameter.

Parametric studies using simplified 2-DOF models and a stereomechanical approach (e = 0.8) show that pounding is most critical for highly out-of-phase frames. Pounding reduces the frame response when vibrating near the characteristic period of the ground motion (T_g). The amplification in frame response as a function of T_{2eff}/T_g, and T_1/T_2 falls into three regions. In Zone I ($T_{2eff}/T_g < 1$), the stiff frame demand increases and the flexible frame demand decreases due to pounding. In Zone III ($T_{1eff}/T_g > 1$), the flexible

frame pounding response is increased while the stiff frame pounding response is reduced. In Zone II ($T_{1eff}/T_g < 1$ & $T_{2eff}/T_g > 1$), pounding slightly increases both frame responses.

Inelastic behavior (frame design ductility, $\mu = 4$) shows greater stiff frame amplification in Zone I when compared to the linear case. The yielding of frames also results in smaller response amplification for the flexible frame in Zone III, when compared to elastic behavior. It can be concluded that the response of bridge frames due to pounding is much less pronounced for $K_1/K_2 = 2.0$ ($T_1/T_2 = 0.71$), irrespective of the ground motion period ratio. This supports the Caltrans design recommendation that the period ratio of adjacent frames be greater than 0.7 to mitigate the effects of pounding. The effect of restrainers on the pounding response of bridge frames is also evaluated, for inelastic frames. The results show that restrainers have very little effect on the demands on bridge frames compared with pounding.

The cogency of various impact models in representing the pounding response of closely spaced structures is then investigated. In addition to the existing impact models, a contact model based on the Hertz law and using a nonlinear hysteresis damper (Hertzdamp model) is introduced for pounding simulation. A suite of thirty ground motion records, with PGAs varying from 0.1g to 1.0g is selected for analysis.

Parameter studies conducted using two degree-of-freedom oscillators with varying system period ratios ($T_1/T_2 = 0.3, 0.5, 0.7$), and coefficients of restitution ($e = 0.6, 1.0$) reveal that the displacement responses from the stereomechanical and contact force-based models are similar, even though they use different methodologies to represent impact. For linear systems, the differences in displacement amplifications between various impact

models are larger (up to 20%) for highly out-of-phase frames. Smaller differences (up to 10%) are exhibited for nonlinear frames.

Impact models without energy dissipation overestimate the displacement and acceleration amplifications due to impact. For linear systems with $T_1/T_2 = 0.3$ and PGA = 0.7g, the stiff frame displacement amplification is reduced by 50% for the stereomechanical model and 25% for the Kelvin model, when e changes from 1.0 to 0.6. The corresponding reduction in acceleration amplifications is around 60% for both models.

The Hertzdamp model appears to be the most effective contact-based model as it shows the least variation due to changes in e and also provides the lowest acceleration amplification and impact force, for both linear and nonlinear systems. Energy loss during pounding is found to be insignificant for in-phase systems ($T_1/T_2 = 0.7$). The responses of a four-frame bridge system with pounding implemented using various impact models show good agreement with the findings from the parameter study.

The effect of column hysteretic characteristics, such as stiffness degradation, strength deterioration and pinching on the impact response of adjacent frames is also studied in this research. Traditional analytical models such as the elasto-plastic and bilinear models, and more sophisticated models such as the Q-Hyst and pivot models are considered. The hysteretic parameters of the Q-Hyst and pivot model without strength degradation are adjusted such that the maximum displacement responses from both the models are similar.

Parameter studies conducted on two degree-of-freedom systems subjected to ten far field earthquake records show that the traditional models underestimate the stiff system

amplification and overestimate the flexible system amplification due to impact, when compared with the sophisticated models, for moderate to highly out-of-phase systems. At $T_1/T_2 = 0.3$, the traditional models under predict the stiff system pounding response by 30% and overestimate the flexible system response by 20%. The effect of various hysteresis models is not significant for in-phase frames ($T_1/T_2 = 0.7$).

Strength degradation increases the stiff frame displacement demand by 125% when compared to stiffness-degrading only systems, for highly out-of-phase systems, in the presence of near field records. For far field ground motions, the strength degradation effect imposes no additional demands on the pounding response as long as stiffness degradation is modeled. Furthermore, at $T_1/T_2 = 0.7$, the system amplifications show greater discrepancy from unity for near field ground motions, with a stiff frame amplification of 1.3 and a flexible frame de-amplification of 0.85.

A case study conducted on a four-frame bridge indicates that strength degradation in bridge columns combined with pounding can increase the stiff frame displacement by 50%, when compared with other hysteresis models. The pounding responses of the stiff frame using the traditional models are smaller than those from the more complex models, in good agreement with the findings from the parameter study using a two degree-of-freedom system.

While past research has concentrated on examining the causes and effects of seismic pounding, no effort has been made in reviewing the existing design procedures that account for dynamic impact. Hence, the adequacy of code-specified linear bounding models in capturing the nonlinear pounding response is explored. A nonlinear analytical model of a typical multiple-frame bridge including the effects of friction, abutments and

pounding is developed in DRAIN-2DX, and used as the benchmark. The individual periods of the stiff and flexible bridge frames are 0.66 s and 1.68 s, respectively. An investigation reveals that the code-suggested linear compression and tension models adequately capture the nonlinear hinge response, when the columns remain elastic. For inelastic situations, the use of a constant, period independent reduction factor for all frames, as per AASHTO recommendations works reasonably well in limiting most frame demands below the target demands. However, the linear models may not perform adequately when applied to bridge frames having lower periods.

Hence, the current design procedure is revised by adopting period dependent reduction factors based on the calculation of a design period from the governing bounding model. The response modification factors are obtained using the revised Vidic et al. relation, which includes the frequency content of ground motion. The modified procedure is shown to work reasonably well for the multiple-frame bridge chosen. Application of the revised guideline is expected to limit frame demands to target demands with reasonable success, for all ranges of bridge frame periods.

Most commercial structural software programs provide the linear spring element with a gap to model seismic pounding. Implementation of energy dissipating impact models, such as the Kelvin model and stereomechanical approach is often difficult. Hence, two simplified contact force-based models accounting for impact energy dissipation are proposed. The first model is a bilinear truss element with a gap and the second is an inelastic truss in parallel with a linear link element (truss-link model). Both models are based on the Hertzdamp contact model. The model parameters such as the stiffness properties and the yield deformation of the truss element and the stiffness of the linear

link are determined using the Hertz contact law for the effective stiffness and by equating the element hysteresis area to the energy dissipated during impact.

A case study conducted with a two DOF system in DRAIN-2DX reveals that both the models capture the impact performances with reasonable accuracy, when compared to the Hertzdamp model. The truss-link model is the more accurate of the two, with only 5% differences in the system displacements, whereas the truss model shows differences up to 10%. The inelastic truss model being the simpler of the two models is then proposed as the simplified contact model.

Finally, the simplified contact model is used to simulate pounding in a four-frame bridge subjected to ten ground motion records. The maximum expected penetration is obtained by observing the amount of overlap allowed by the linear impact spring for the same set of conditions. On the average, energy dissipation during impact is found to reduce the frame responses by 12%, 7%, 2% and 8% for Frames 1 through 4 respectively.

9.1. Recommendations for further study

The present study could be complemented with additional research in the following areas:

➢ Experimental shake-table testing of scaled bridge models to study the effects of pounding. These tests will validate the effectiveness of the Hertzdamp impact model. In addition, dynamic testing will help in identifying the values of impact spring stiffness and coefficient of restitution to be used in analysis.

- ➢ Effects of torsion due to curvilinear bridge geometry need investigation. Seismic pounding at skewed hinges can increase the lateral displacement and rotation of bridge girders, thereby increasing the potential for unseating.

- ➢ Spatial variability in ground motion input, non-uniform support motion and traveling wave effects on the pounding response of long multi-span bridges need to be studied using a spectral or random vibration approach. Pounding between adjacent frames of similar dynamic characteristics can occur under such conditions.

- ➢ The relevance of soil-structure interaction on the pounding response of inelastic bridge piers needs introspection. This will help in evaluating the degree of approximation inherent in studies which neglect the effects of soil flexibility.

- ➢ Further investigation is required to determine the effect of large acceleration pulses in forward-directivity near field ground motions on the pounding trends of closely spaced adjacent structures.

- ➢ The efficacy of pounding reduction devices such as shock absorbers and additional dampers between superstructure segments needs to be examined using analytical methods and validated using experimental techniques.

REFERENCES

AASHTO-83 (1988). "Guide Specification for the Seismic Design of Highway Bridges," American Association of State Highway and Transportation Officials, Washington, D.C.

AASHTO (1995). "Standard Specifications for Highway Bridges," 16th edition, American Association of State Highway and Transportation Officials, Washington, D.C.

Anagnostopoulos, S.A. (1988). "Pounding of Buildings in Series during Earthquakes," *Earthquake Engineering and Structural Dynamics*, Vol. 16:pp. 443 – 456.

Anagnostopoulos, S.A., and Spiliopoulos, K.V. (1992). "An Investigation of Earthquake Induced Pounding Between Adjacent Buildings," *Earthquake Engineering and Structural Dynamics*, Vol. 21:pp. 289 – 302.

Athanassiadou, C.J., Penelis, G.G., and Kappos A.J. (1994). "Seismic Response of Adjacent Buildings with Similar or Different Dynamic Characteristics," *Earthquake Spectra*, Vol. 10 (No. 2):pp. 293 – 317.

Bertero, V. V. (1987). "Observations on Structural Pounding," *Proceedings International Conference on Mexico Earthquakes*, ASCE:pp. 264-278.

Caltrans (1990). "Bridge Design Specifications Manual," California Department of Transportation, Sacramento, CA.

Caltrans (1993). "Bridge Design Specifications Manual," California Department of Transportation, Sacramento, CA.

Caltrans (1999). "Seismic Design Criteria - version 1.1," California Department of Transportation, Sacramento, CA.

Chau, K. T., and Wei X. X. (2001). "Pounding of Structures Modeled as Non-linear Impacts of Two Oscillators," *Earthquake Engineering and Structural Dynamics*, Vol. 30:pp. 633 - 651.

Chau, K. T., Wei, X. X., Guo, X., and Shen, C. Y. (2003). "Experimental and Theoretical Simulations of Seismic Poundings between Two Adjacent Structures," *Earthquake Engineering and Structural Dynamics*, Vol. 32:pp. 537 - 554.

Chopra, A.K. (2000). *Dynamics of Structures – Theory and Applications to Earthquake Engineering*, 2nd edition, Prentice Hall, New Jersey.

Clough, R.W., and Johnston, S.B. (1966). "Effect of Stiffness Degradation on Earthquake Ductility Requirements," *Proceedings, Japan Earthquake Engineering Symposium*, Tokyo, Japan:pp. 195-198.

Cuesta, I., Aschheim, M.A., and Fajfar, P. (2003). "Simplified R-Factor Relationships for Strong Ground Motions," *Earthquake* Spectra, Vol. 19(No. 1):pp. 25-45.

Davis, R.O. (1992). "Pounding of Buildings Modeled by Impact Oscillator," *Earthquake Engineering and Structural Dynamics*, Vol. 21:pp. 253-274.

DesRoches, R. and Fenves, G.L. (1997a), "New Design and Analysis Procedures for Intermediate Hinges in Multiple Frame Bridges," *Report No. UCB/EERC-97/12*, Earthquake Engineering Research Center, University of California, Berkeley.

DesRoches, R., and Fenves, G.L. (1997b). "Evaluation of Recorded Earthquake Response of a Curved Highway Bridge," *Earthquake* Spectra, Vol. 13(No. 3):pp. 363-386.

DesRoches, R., and Fenves, G.L. (2001). "Simplified Restrainer Design Procedure for Multiple-Frame Bridges," *Earthquake Spectra*, Vol. 17(No.4):pp. 551-567.

Dowell, R.K., Seible, F., and Wilson, E.L. (1998). "Pivot Hysteresis Model for Reinforced Concrete Members," *ACI Structural Journal*, Vol. 95(No. 5):pp. 607-617.

Earthquake Engineering Research Institute (EERI) (1990). "Loma Prieta Earthquake Reconnaissance Report," *Rep. No. 90-01*, Benuska, L., ed., EERI, Oakland, CA.

Earthquake Engineering Research Institute (EERI) (1995a). "Northridge Earthquake of January 17, 1994 - Reconnaissance Report, Vol. 1," *Rep. No. 95-03*, J.F.Hall, ed., EERI, Oakland, CA.

Earthquake Engineering Research Institute (EERI) (1995b). "The Hyogo-Ken Nanbu Earthquake Reconnaissance Report," *Rep. No. 95-04*, C.D.Comartin, M.Greene, and S.K.Tubbesing, eds., EERI, Oakland, CA.

Earthquake Engineering Research Institute (EERI) (2000). "Kocaeli, Turkey, Earthquake of August 17, 1999 Reconnaissance Report," *Publ. No. 00-03*, Youd, T. L., Bardet, J-P., Bray, J. D., ed., EERI, Oakland, CA.

Earthquake Engineering Research Institute (EERI) (2001a). "Chi-Chi, Taiwan, Earthquake of September 21, 1999 - Reconnaissance Report," *Publ. No. 01-02*, J. Uzarski, C. Arnold, eds., EERI, Oakland, CA.

Earthquake Engineering Research Institute (EERI) (2001b). "The Nisqually, Washington, Earthquake of February 28, 2001- Preliminary Reconnaissance Report," EERI, Oakland, CA.

Earthquake Engineering Research Institute (EERI) (2002). "Bhuj, India Earthquake of January 26, 2001 Reconnaissance Report." *Publ. No 02-01*, Jain, S.K., Lettis, W.R., Murty, C.V.R., and Bardet, J.P. (Eds), EERI, Oakland, CA.

Federal Highway Administration (FHWA) (1995). "Seismic Retrofitting Manual for Highway Bridges," *Publication No. FHWA-RD-94-052*, Mclean, VA.

Filiatrault, A., and Wagner, P. (1995). "Analytical Prediction of Experimental Building Pounding," *Earthquake Engineering and Structural Dynamics*, Vol. 24:pp. 1131-1154.

GoldSmith, W. (1960). *Impact: the Theory and Physical Behaviour of Colliding Solids*, Edward Arnold, London, England.

Hidalgo, P.A., and Arias, A. (1990). "New Chilean Code for Earthquake-Resistant Design of Buildings," *Proceedings 4th U.S. National Conference on Earthquake Engineering*, Palm Springs, California, Vol. 2:pp. 927-936.

Hunt, K.H., and Crossley, F.R.E. (1975). "Coefficient of Restitution Interpreted As Damping in Vibroimpact," *ASME Journal of Applied Mechanics*, Vol. 42:pp. 440-445.

Jankowski, R., Wilde, K., Fuzino, Y. (1998). "Pounding of Superstructure Segments in Isolated Elevated Bridge During Earthquakes," *Earthquake Engineering and Structural Dynamics*, Vol. 27:pp. 487 – 502.

Jankowski, R., Wilde, K., and Fuzino, Y. (1999). "Reduction of Earthquake Induced Effects of Pounding in Elevated Bridges," *Proceedings of the Second World Conference on Structural Control*, John Wiley & Sons, New York, Vol. 2:pp. 933 – 939.

Jennings, P. C. (1971). "Engineering Features of the San Fernando Earthquake of February 9, 1971," *Report No. EERL-71-02*, Earthquake Engineering Research Laboratory, California Institute of Technology, Pasadena.

Jing, H.-S., and Young, M. (1991). "Impact Interactions between Two Vibration Systems under Random Excitation," *Earthquake Engineering and Structural Dynamics*, Vol. 20:pp. 667-681.

Kajita, Y. (2000) "Fundamental Study on Aseismic Evaluation of Elevated Bridge Systems with Consideration of Pounding of Girders," PhD Thesis, Kyoto University, Japan.

Kawashima, K., and Shoji, G. (2000). "Effect of Shock Absorber to Mitigate Pounding Effect between Bridge Decks," *Proceedings, International Workshop on Mitigation of Seismic Effects on Transportation Structures*, National Center for Research on Earthquake Engineering, Taipei, Taiwan, R.O.C:pp. 207-218.

Kawashima, K., and Yabe, M. (1996). "Effectiveness of Unseating Prevention Device with Energy Dissipation," *Proceedings of the Fourth U.S.-Japan Workshop on Earthquake Protective System for Bridges*, December 9 and 10, 1996, Public Works Research Institute, Tsukuba-shi, Japan:pp. 285-307.

Kim, S.H., Lee, S.W., Won, J.H., Mha, H.S. (2000). "Dynamic Behaviors of Bridges Under Seismic Excitations With Pounding Between Adjacent Girders," *Proceedings, 12th World Conference on Earthquake Engineering*, Auckland, NZ.

Krawinkler, H., and Nassar, A. A. (1992). "Seismic Design Based on Ductility and Cumulative Damage Demands and Capacities," *Nonlinear Seismic Analysis and Design of Reinforced Concrete Buildings*, Fajfar, P. and Krawinkler, H., Eds., Elsevier Applied Science, New York.

Kunnath, S.K., Reinhorn, A.M., and Park, Y.J. (1990). "Analytical Modeling of Inelastic Seismic Response of R/C Structures," *Journal of Structural Engineering*, ASCE, Vol. 116(No. 4):pp. 996-1017.

Lai, S.-P., and Biggs, J.M. (1980). "Inelastic Response Spectra for Aseismic Building Design," *Journal of Structural Division*, ASCE, Vol. 106(No. ST6):pp. 1295-1310.

Lankarani, H.M., and Nikravesh, P.E. (1990). "A Contact Force Model with Hysteresis Damping for Impact Analysis of Multibody Systems," *Journal of Mechanical Design* ASME, Vol. 112:pp. 369-376.

Mahin, S. A., Bertero, V. V., Chopra, A. K., and Collins, R.G. (1976). "Response of the Olive View Hospital Main Building during the San Fernando earthquake," *Report No. EERC 76-22*, University of California, Berkeley.

Maison, B. F. (1992). "PC-ANSR: A Computer Program for Nonlinear Structural Analysis," *National Information Service for Earthquake Engineering*, University of California, Berkeley.

Maison, B. F., and Kasai, K. (1990a). "Analysis for Type of Structural Pounding," *Journal of Structural Engineering*, ASCE, Vol. 116(No. 4):pp. 957 - 975.

Maison, B. F., and Kasai, K. (1990b). "SLAM-2: A Computer Program for the Analysis of Structural Pounding," *National Information Service for Earthquake Engineering*, University of California, Berkeley.

Maison, B. F., and Kasai, K. (1992). "Dynamics of Pounding when Two Buildings Collide," *Earthquake Engineering and Structural Dynamics*, Vol. 21:pp. 771 - 786.

Malhotra, P. K. (1998). "Dynamics of Seismic Pounding at Expansion Joints of Concrete Bridges," *Journal of Engineering Mechanics*, ASCE, Vol. 124(No. 7):pp. 794 – 802.

Maragakis, E., Douglas, B., and Vrontinos, S. (1991). "Classical Formulation of the Impact between Bridge Deck and Abutments during Strong Earthquakes," *Proceedings of the 6th Canadian Conference on Earthquake Engineering*, Toronto, Canada:pp. 205 – 212.

Marhefka D.W., and Orin, D.E. (1999). "A Compliant Contact Model with Nonlinear Damping for Simulation of Robotic Systems," *IEEE Transactions on Systems, Man, and Cybernetics – Part A: Systems and Humans*, Vol. 29:pp. 566-572.

Miranda, E., and Bertero, V.V. (1994). "Evaluation of Strength Reduction Factors for Earthquake-Resistant Design," *Earthquake Spectra*, Vol. 10(No. 2):pp. 357-379.

Miranda, E. (2000). "Inelastic Displacement Ratios for Structures on Firm Sites," *Journal of Structural Engineering*, ASCE, Vol. 126 (No. 10):pp 1150-1159.

Murphy, L. (1973). "San Fernando, California Earthquake of February 9, 1971, Volume II," Supt. of Doc,. U.S. Government Printing Office, Washington D.C.:pp. 201- 233.

Naeim, F., and Kelly, J.M. (1999). *Design of Seismic Isolated Structures: From Theory to Practice*, John Wiley & Sons, Inc., New York.

National Academy of Sciences (1964). "The Great Alaska Earthquake of 1964," Engineering NAS Publication 1606, Washington, D.C.

Newmark, N. M. (1959). "A Method of Computation for Structural Dynamics," *Journal of Engineering Mechanics*, ASCE, Vol. 85:pp 67-94.

Pantelides. C. P., and Ma, X. (1998). "Linear and Nonlinear Pounding of Structural Systems," *Computers & Structures*, Vol. 66(No. 1):pp. 79 – 92.

Papadrakakis, M., Mouzakis, H., Plevris, N., and Bitzarakis, S. (1991). "A Lagrange Multiplier Solution Method for Pounding of Buildings During Earthquakes," *Earthquake Engineering and Structural Dynamics*, Vol. 20:pp. 981 – 998.

Papadrakakis, M., and Mouzakis, H.P. (1995). "Earthquake Simulator Testing of Pounding between Adjacent Buildings", *Earthquake Engineering and Structural Dynamics*, Vol. 24:pp. 811-834.

Papadrakakis, M., Apostolopoulou, C., Zacharopoulos, A., and Bitzarakis, S. (1996). "Three-Dimensional Simulation of Structural Pounding during Earthquakes," *Journal of Engineering Mechanics*, ASCE, Vol. 122(No. 5):pp. 423 - 431.

Prakash, V., Powell, G.H., Campbell, S.D., and Filippou, F.C. (1992). "DRAIN-2DX User Guide," Department of Civil Engineering, University of California, Berkeley.

Priestly, M. J. N., Seible, F., and Calvi, G. M. (1995). *Seismic Design and Retrofit of Bridges*, Wiley-Interscience, New York, New York.

Riddell, R., and Newmark, N.M. (1979). "Statistical Analysis of the Response of Nonlinear Systems Subjected to Earthquakes," *Structural Research Series No. 468*, Dept. of Civil Engineering, University of Illinois, Urbana.

Roeder, C.W., Stanton, J.F., and Taylor, A.W. (1987). "Performance of Elastomeric Bearings," *National Cooperative Highway Research Program Report 298*, Transportation Research Board, National Research Council, Washington, D.C.

Roeder, C.W., Stanton, J.F., and Feller, T. (1990). "Low-Temperature Performance of Elastomeric Bearings," *Journal of Cold Regions Engineering*, Vol. 4(No. 3):pp. 113-132.

Roeder, C.W., Stanton, J.F. (1991). "State-of-the-Art Elastomeric Bridge Bearing Design," *ACI Structural Journal*, Vol. 88(No. 1):pp. 31-41.

Ruangrassamee, A., and Kawashima, K. (2001). "Relative Displacement Response Spectra with Pounding Effect," *Earthquake Engineering and Structural Dynamics*, Vol. 30:pp. 1511-1538.

Saatcioglu, M., and Ozcebe, G. (1989). "Response of Reinforced Concrete Columns to Simulated Seismic Loading," *ACI Structural Journal*, Vol. 86(No. 1):pp. 3-12.

Saiidi, M., and Sozen, M.A. (1979). "Simple and Complex Models for Nonlinear Seismic Response of Reinforced Concrete Structures," *Rep. No. UILU-ENG-79-2013*, Struct. Res. Series No. 465, University of Illinois, Urbana.

Scalzi, J., and McGrath, W. (1971). "Mechanical Properties of Structural Cables," *Journal of Structural Engineering*, ASCE, Vol. 97(No. 12):pp. 2837 - 2844.

Schiff, A.J. (1995). "Northridge Earthquake Lifeline Performance and Post-earthquake Response," *Technical Council on Lifeline Earthquake Engineering, Monograph No. 8*, ASCE, New York.

Standard Specifications (1981). *Section 83-2.02A Cable Barrier*, California Department of Transportation, Sacramento, California.

Takeda, T., Sozen, M., and Nielsen, N. (1970). "Reinforced Concrete Response to Simulated Earthquake," *Journal of the Structural Division*, *ASCE*, Vol. 96(No. 12):pp. 55-61.

Tonias, D.E. (1995). *Bridge Engineering: Design, Rehabilitation, and Maintenance of Modern Highway Bridges*, McGraw-Hill, Inc., New York.

Trochalakis, P., Eberhard, M. and Stanton, J. (1997). "Evaluation and Design of Seismic Restrainers for In-Span Hinges," *Journal of Structural Engineering*, ASCE, Vol. 123(No. 4):pp. 103 – 113.

Valles, R. E., and Reinhorn, A. M. (1997). "Evaluation, Prevention and Mitigation of Pounding Effects in Building Structures," *Technical Report NCEER-97-0001*, State University of New York, Buffalo.

Van Mier, J.G.M., Pruijssers, A.F., Reinhardt, H.W., and Monnier, T. (1991). "Load-Time Response of Colliding Concrete Bodies," *Journal of Structural Engineering*, ASCE, Vol. 117(No. 2):pp. 354-374.

Vidic, T., Fajfar, P., and Fischinger, M. (1994). "Consistent Inelastic Design Spectra: Strength and Displacement," *Earthquake Engineering and Structural Dynamics*, Vol. 23:pp. 507-521.

Wolf, J.P., and Skrikerud, P.E. (1980). "Mutual Pounding of Adjacent Structures During Earthquakes," *Nuclear Engineering and Design*, Vol. 57:pp. 253-275.

Xanthakos, P.P. (1996). *Bridge Strengthening and Rehabilitation*, Prentice Hall, Inc., Upper Saddle River, NJ.

Yang, J.N., and Agrawal, A.K. (2002). "Semi-Active Hybrid Control Systems for Nonlinear Buildings Against Near-Field Earthquakes," *Engineering Structures*, Vol. 24:pp. 271-280.

Yashinsky, M. (1992). "Caltrans Bridge Restrainer Retrofit Program," California Department of Transportation.

Zhu, P., Abe, M., and Fuzino, Y. (2002). "Modelling Three-dimensional Non-linear Seismic Performance of Elevated Bridges with Emphasis on Pounding of Girders", *Earthquake Engineering and Structural Dynamics*, Vol. 31:pp. 1891-1913.

VITA

Susendar Muthukumar was born on January 22, 1977 in Madras, India. After appearing for the All India Joint Entrance Examination, he gained admission to the Indian Institute of Technology, Madras in 1994. He graduated with a Bachelor of Technology in Civil Engineering in 1998. He then entered the Georgia Institute of Technology in September 1998 to pursue graduate study in the School of Civil and Environmental Engineering. After receiving his Master of Science in Civil Engineering in the summer of 2000, he continued to pursue a doctoral degree.